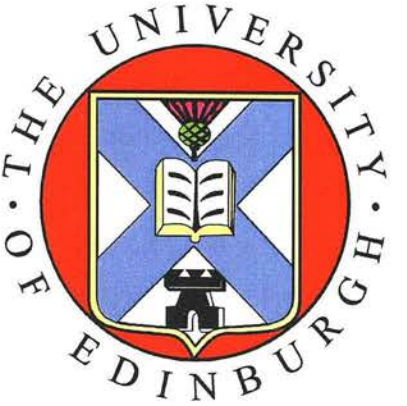

An Exploration of Polymorphism in Pharmaceutical Compounds Using High Pressure

Nasir Abbas

A thesis submitted in fulfilment of the requirements for the degree of Doctor of Philosophy to the School of Chemistry, the University of Edinburgh

February 2010

Abstract

The effects of high pressure on a selection of organic compounds have been studied. Crystallisation at high pressure has been successfully used to grow a single crystal of an elusive polymorph (form II) of mefenamic acid. Milling experiments revealed that form I can be converted to form II by milling at both ambient temperature and at -78 °C. Direct compression of powder samples of form I at 1.5 GPa using methanol:ethanol as a pressure-transmitting medium resulted in the formation of a new high-pressure form III and this new form is recoverable to ambient pressure. Compression of powder samples of forms I and II using Fluorinert-FC77 as a pressure-transmitting medium resulted in a reversible phase transition to a new high-pressure form IV.

High-pressure crystallisation of N,N'-dimethylurea resulted in the formation of two new high-pressure polymorphs designated as forms III and IV. Crystal structures of these forms are reported here. Form III was also produced by compression of a powder samples of form I and decompression studies showed that it can be recovered to ambient pressure, but it was metastable compared to form I. Form II was produced through compression of form I using Fluorinert FC-77 as a pressure-transmitting medium. Form IV was produced by heating a mixture of form II and III to 150 °C at 1.75 GPa. Decompression of form IV resulted in formation of a new form, which was recoverable at ambient pressure. The experimental results have been compared with crystal structure prediction calculations.

High-pressure techniques have been used to study polymorphism of GSK developmental compounds A and B. New polymorphs for these compounds have been obtained at high pressure. Of particular importance are forms III and VI of compounds A and B, respectively, where recrystallisation at high pressure resulted in production of these forms and decompression studies have shown that they can be recovered to ambient pressure. From the compression studies performed on the powder samples of compound A, two new high-pressure forms designated as forms V and VI were obtained at 0.9 and 1.4 GPa, respectively. New polymorphs for these compounds were also produced from recrystallisation at ambient pressure.

Declaration

I declare that this thesis was written by myself and that the work detailed in this thesis is my own, or I have contributed substantially to such work, except where specific reference is made to the work of another.

Nasir Abbas

Acknowledgements

I would like to thank everyone who helped me in the course of this PhD. I am heartily thankful to my supervisor, Prof. Colin Pulham, who provided encouragement, invaluable assistance, support and guidance throughout the course of the project. I would like to thank my industrial supervisor Dr. Clare Anderton for her support and advice, and the opportunity to work briefly at GSK.

Special thanks are due to Dr. Iain Oswald for his valuable help with crystallography and his useful input during the course of my PhD. I would like to thank all members of the Pulham group and CSEC for a pleasant working environment.

I would like to thank Dr. Graeme Day for the crystal structure prediction calculations on DMU and Prof. Alastair Florence for solving the structure of form II of compound B. I thank the crystallography service at The University of Edinburgh for recording data. I would like to thank Dr Alistair Lennie, Dr. Timothy Prior, Dr. John Warren and Dr. Annette Kleppe for all their help with experiments at Daresbury and the Diamond Light Source.

I would like to thank the University of Edinburgh, GlaxoSmithKline and EaStCHEM for jointly funding this PhD.

This research project would not have been possible without the encouragement and love of my family back home in Pakistan, especially my wife, Saba, for her understanding and love.

This thesis is dedicated to my parents, who are my lasting source of love and inspiration.

Contents

Chapter 3

Chapter 4

Chapter 5

Chapter 6

Chapter 1

Introduction

Chapter 1: Introduction

1.1. Polymorphism

Polymorphism (from the Greek meaning "having multiple forms") is a term used in many disciplines. According to the Oxford English Dictionary, the term first emerged in 1656 to express changes in fashion. In chemistry, polymorphism is the ability of a solid substance to crystallise with more than one crystal structure; these different crystalline forms are termed polymorphs. Polymorphs of a compound have the same chemical formulae, but different three dimensional arrangements and/or conformations of molecules within the unit cell. These different arrangements can have profound effects on the physical and chemical properties of the material. Examples include melting point, sublimation temperature, heat capacity, conductivity, solubility, density, dissolution rate, stability, hygroscopicity, and solid-state chemistry [1, 2].

The term *pseudo-polymorphism* is sometimes applied to hydrates and solvates and is widely found in older literature. This notation has now been discouraged due to its rather confusing nature. The term allotrope is more commonly used when the substance under consideration is an element. The classic example of allotropy in nature is represented by carbon and three of its main allotropes, diamond, graphite and C_{60} (Buckminsterfullerene). Each of these forms display markedly different structures and properties (Figure 1.1). For example, graphite is a black, soft, electrically conducting and chemically reactive material. Diamond is optically transparent, hard, electrically insulating, and chemically rather inert. C_{60} is quite different from both and its structure comprises hexagons and pentagons of carbon atoms in a closed shell. It is soluble in aromatic solvents and can be vaporised at relatively low temperatures.

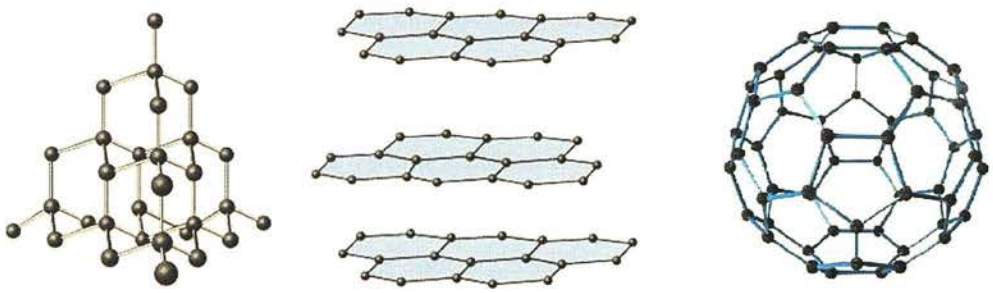

Figure 1.1: Structures of (a) diamond, (b) graphite, and (c) C_{60}

The first observation of polymorphism in organic materials is attributed to Friedrich Wohler and Justus Von Liebig in 1832 when they examined a boiling solution of benzamide. On cooling the benzamide initially crystallised as silky needles, but on standing these were slowly replaced by rhombic crystals [3].

1.1.1. Occurrence of polymorphism

Walter McCrone stated that *"every compound has different polymorphic forms, and that, in general, the number of forms known for a given compound is proportional to the time and money spent in research on that compound"* [4]. Buerger and Bloom in 1937 stated that *"polymorphism is an inherent property of the solid state and that it fails to appear only under special condition"* [5]. However, according to Bernstein [2] this statement should be used with caution because some very common materials, such as sucrose and naphthalene, which have been crystallised many times, have not been reported to be polymorphic.

Despite its potential implications, polymorphism is not always well understood. Crystallisation is determined by the complex interplay between kinetics and thermodynamics. Thermodynamics governs the order of stability of each form, whilst kinetic factors influence the appearance of thermodynamically less stable forms. The metastable form ultimately converts to the stable form, but in some cases

metastable forms are known to exhibit apparent stability for years, depending upon the environment surrounding the crystal (temperature, humidity, solvation, *etc.*).

Ostwald's rule of stages [6] is often applied in polymorphism involving molecular compounds. It states that, in general, it is not the most stable, but the least stable polymorph that crystallises first, which shows the dominance of kinetic factors upon crystallisation. With time, the metastable form is transformed to a more stable form (depending upon the thermodynamic energy difference between these forms). In terms of thermodynamics, there are two types of polymorphism [2]. For a monotropic system, plots of the free energies of two polymorphs against temperature do not cross before the two polymorphs melt (Figure 1.2), *i.e.* any transition from one polymorph to another will be irreversible. For an enantiotropic system, plots of the free energy against temperature show a crossing point before the two melting points, and it is possible to convert reversibly between the two polymorphs on heating and cooling.

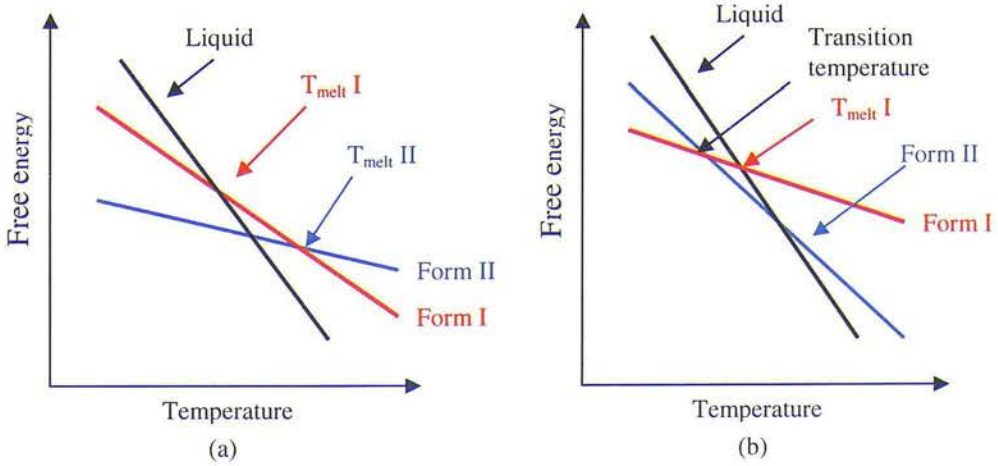

Figure 1.2: Free energy/temperature diagram for monotropic (a) and enantiotropic (b) polymorphs [7].

1.1.2 Implications of polymorphism

The phenomenon of polymorphism in the crystallisation of compounds is of fundamental interest to experimental and theoretical chemists, and is also of crucial importance to industry for a wide range of materials that includes pharmaceuticals,

pigments, explosives (energetic materials), food products and proteins [2]. Examples of polymorphism for various classes of compounds are given in the following sections.

1.1.2.1. Pigments

The pigment and dye industry has been a significant commercial enterprise since the discovery of the dye indigo, which is the source of colour for the ubiquitous blue jeans [2]. One of the best examples of a pigment displaying polymorphism is copper phthalocyanine (Figure 1.3). At least five polymorphs are known, designated α, β, γ, δ, ε, and at least four more are claimed in the literature. All these forms exhibit different solubilities.

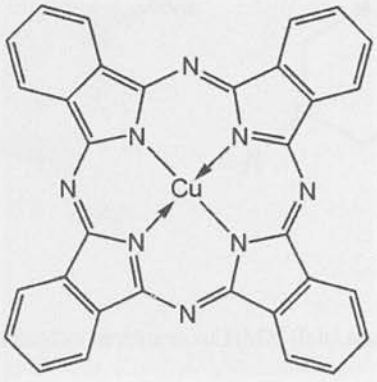

Figure 1.3: Molecular structure of copper phthalocyanine

These different polymorphs also have different shades of blue. The β-form is used as the standard letter press printing ink, and the ε-form is used as a colour filter for liquid crystal displays [2].

1.1.2.2. Energetic materials

Energetic materials are defined as those that generate large amounts of heat and generally a large amount of gas upon stimulus by heat, impact, shock, spark, *etc* [8]. They can be broadly classified as explosives, propellants, gas generators, and pyrotechnics. Polymorphism can alter the sensitivity and performance of these

energetic materials. For example, different polymorphs may have different densities that can affect the detonation velocity of an explosive. The widely used explosive HMX (1, 3, 5, 7-tetranitro-1, 3, 5, 7-tetrazocane) (Figure 1.4) can exist as four crystalline forms (the γ-form is actually a hydrated form rather than a true polymorph) and the sensitivity to impact is in the order $\delta > \gamma > \alpha > \beta$ [8]. RDX (1, 3, 5-trinitrohexahydro-1, 3, 5-triazine) (Figure 1.4) is another example of a widely used military explosive which shows polymorphic behaviour. RDX exists as three crystalline forms; the α- and β-forms can be obtained at ambient pressure, and the γ-form can be obtained at high pressure [9].

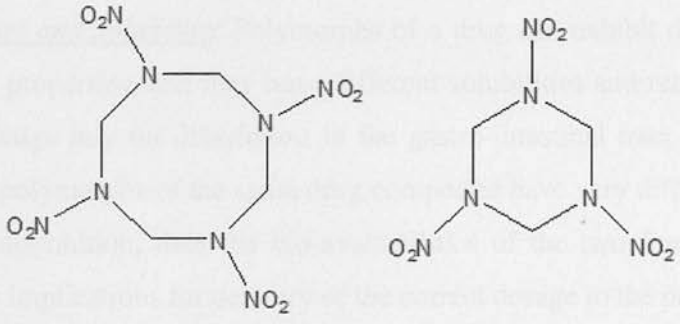

Figure 1.4: Molecular structures of HMX (left) and RDX (right).

1.1.2.3. Amino acids and proteins

Glycine is the simplest amino acid and its polymorphism has been widely studied at both ambient and elevated pressures [10]. It has three polymorphs under ambient conditions (termed α, β and γ) and a further two at high pressure (termed δ and ε). δ-glycine was produced by direct compression of β-glycine, whilst ε-glycine was produced by compression of γ-glycine [10].

The most well known example of polymorphism in proteins is the complex polymorphism of lysozyme, a small enzyme that attacks the protective cell wall of bacteria. At least six different modifications are known [2] depending on the cystallisation conditions.

1.1.3. Polymorphism in the pharmaceutical industry

Although new routes of administration for pharmaceutical active therapeutic agents are continuing to develop, solid dosage forms are still the fundamental and most preferred route of administration [11]. As with most compounds, the solid pharmaceutical agent can exist as an amorphous and/or crystalline form. The crystalline form is preferred because the crystals are relatively easy to isolate and minimise the risk of impurities [12]. The phenomenon of polymorphism (and solvate formation) in the pharmaceutical industry is particularly important for the following reasons:

Bio-availability and solubility: Polymorphs of a drug can exhibit different physical and chemical properties, and may have different solubilities and rates of dissolution [13]. Many drugs rely on dissolution in the gastro-intestinal tract for their action. Hence if two polymorphs of the same drug compound have very different solubilities and rates of dissolution, then the bio-availabilities of the two forms may be very different with implications for delivery of the correct dosage to the patient.

Processibility and storage: Drug materials go through several stages of processing before being finally incorporated into dosage form. These may include crystallisation, milling, freeze drying, wet granulation, mixing with excipients, and tabletting. Different polymorphs may respond very differently to these processes and so polymorph selection and control is crucial [13]. The conditions under which polymorphs interconvert is of critical importance, particularly as pharmaceuticals may be exposed to a wide range of temperatures and relative humidities during storage. It is important to know if any phase transitions are possible in order to control the properties of drugs selectively and consistently.

Regulatory authorities: On account of the potential risks to patients, regulatory authorities such as the US Food and Drug Administration (FDA) now demand detailed information about drug polymorphs (polymorph types, reproducibility of manufacturing, and purity levels) before granting licenses for product distribution.

Intellectual property: Different polymorphs of a drug compound can be patented, and so intellectual property can also become an issue for the pharmaceutical companies who develop and market new drug products. Challenges to patents on the basis of polymorphism are therefore becoming increasingly frequent and are very expensive [2].

For all these reasons, an understanding of the solid-state properties of a drug compound, including the identification of all possible forms and thorough characterisation of the observed forms, is of prime importance within the pharmaceutical industry. Establishing the polymorphic behaviour of a drug molecule early in development minimises the number of unsuitable candidates progressed and reduces the risk of encountering later issues that may have major financial impact [14].

The most striking example of the impact of polymorphism in the pharmaceutical industry to date is represented by the case of Ritonavir. Ritonavir is a protease inhibitor used in the treatment of HIV and is currently marketed as Norvir [15]. It was discovered in 1992 and brought to the market in 1996 as a semi-solid capsule by Abbott Laboratories. However, after about two years of production many final product lots failed a dissolution test. This was subsequently revealed as being due to the appearance of a new, much more stable and hence less soluble polymorph. This transformation of the polymorphic form caused major problems for processing and for the bioavailability of the drug in capsule form. A new formulation to accommodate the new form was designed and a controlled process was established to generate the initial form consistently. Abbott Laboratories lost an estimated $250 million in sales because of the withdrawal of all of its batches from the market.

The case of ranitidine hydrochloride (Zantac), the largest selling anti-ulcer drug from GlaxoSmithKline (GSK), provides an example of the importance of polymorphism in patent litigation. Ranitidine hydrochloride exists in two polymorphic forms (I and II). In the mid-1990s, the patent on form I was about to expire and the patent on form II was still in force. Many pharmaceutical companies

were interested in manufacturing and selling form I, but the problem of making form I is that it is always contaminated by form II. Novopharm, was repeatedly sued by GSK for manufacturing and selling mixtures of form I and form II. However, after several court cases and appeals, Novopharm was allowed to market its formulation and GSK lost large amounts of revenue.

Cefdinir is a broad-spectrum antibiotic which appears in 11 patents from 5 pharmaceutical companies in which a total of 5 different polymorphs are described. The original inventor Fujisawa (now Astellas) extended the original patent covering a suspension with a new anhydrous formulation. Competitors in turn patented hydrates of the drug with varying water content [16].

The cases of Ritonavir, Ranitidine and Cefdinir emphasise the need for an effective and rapid means of identification, characterisation and mapping of drug polymorphs in the lengthy and expensive process of drug development. Nowadays pharmaceutical companies deploy substantial effort and resources in the screening of polymorphs and solvates of drugs, often in the early stages of development.

1.1.4. Polymorph screening

Physical form screening (or polymorph screening) includes systematic searches by applying a wide range of variables. The objectives of this screening process are to characterise the relationships between all forms, to identify the most thermodynamically stable form, and to optimise key physical properties, particularly solubility, dissolution rate and hygroscopicity. The key to successful product development is the early selection of the most appropriate solid-state form of the active ingredient to be used in the final product. Screening methodologies depend upon systematically fingerprinting samples, recrystallised under a wide range of conditions using spectroscopic, calorimetric and diffraction techniques [17]. The conventional method of polymorph screening is described in the flow sheet diagram below (Figure 1.5).

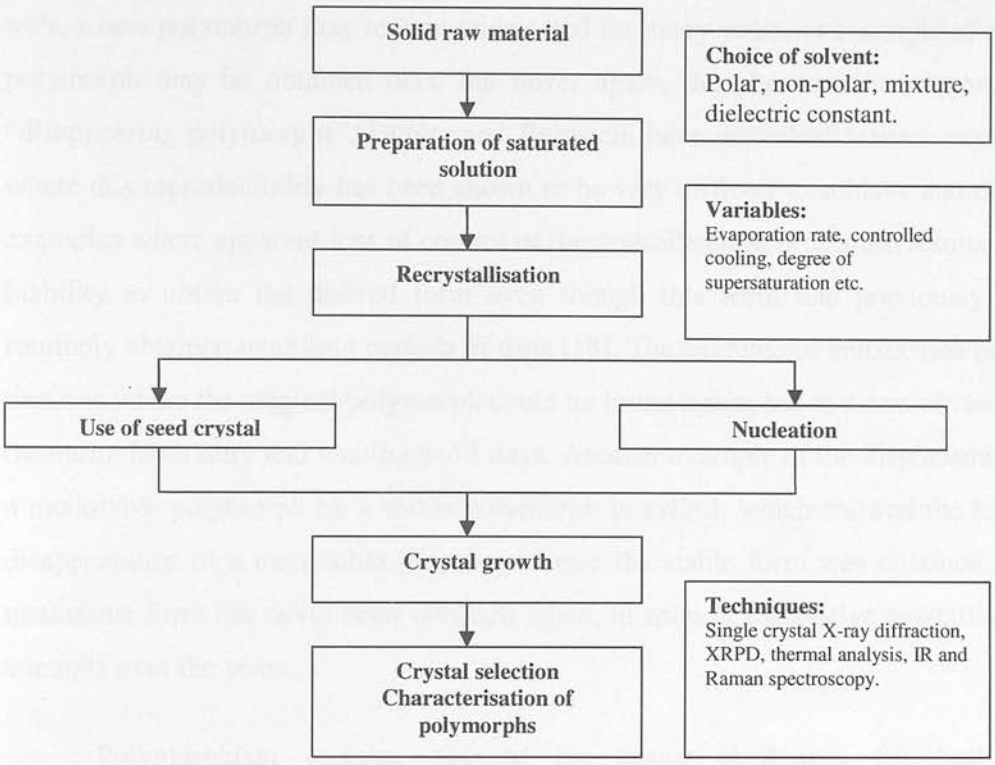

Figure 1.5: Flow sheet diagram for polymorph screening, outlining different steps

A wide range of variables can be employed and some examples are tabulated in Table 1.1

Thermal	Anti Solvent	Evaporation	Slurry Conversion	Other Variables
Heating rate	Anti-solvent type	Rate of evaporation	Solvent type	Mixing rate
Cooling rate	Rate of anti-solvent addition	Evaporation time	Incubation temperature	Impeller design
Maximum temperature	Temperature of anti-solvent addition	Carrier gas	Incubation time	Crystallisation vessel design
Minimum temperature	Time of anti-solvent addition	Surface:volume ratio	Thermal cycling and gradient	

Table1.1 Different variables used in polymorph screening

In recent years considerable effort has been put into developing high-throughput, automated approaches to both salt and polymorph screening. The main aim is to develop methods that are capable of producing and identifying large numbers of samples in a relatively short period of time. Even after these exhaustive

tests, a new polymorph may remain undetected for many years, or a sample of a new polymorph may be obtained once but never again, the phenomenon of so-called "disappearing polymorphs". Dunitz and Bernstein have described several examples where this reproducibility has been shown to be very difficult to achieve and quoted examples where apparent loss of control of the crystallisation procedure results in an inability to obtain the desired form even though this form had previously been routinely obtained over long periods of time [18]. The example of benzocaine picrate was one where the original polymorph could be found again, but at a cost of cleaning the entire laboratory and waiting 8–12 days. Another example of the displacement of a metastable polymorph by a stable polymorph is xylitol, which showed the loss or disappearance of a metastable polymorph once the stable form was obtained. This metastable form has never been obtained again, in spite of exhaustive crystallisation attempts over the years.

Polymorphism remains one of the major challenges for both the pharmaceutical and academic sectors. The development of complementary methods for efficient polymorph and solvate formation, and more importantly the understanding of factors that result in different packing arrangements of organic molecule in the solid state would therefore be highly desirable. Within the pharmaceutical industry better control of polymorphism could ultimately improve the preparation and control of dosage form.

1.1.5. Crystal structure prediction

The prediction of crystal structures from nothing more than connectivity of atoms within a molecule has greatly improved in recent years. To date, several groups active in this field have performed four separate blind tests in the years 1999, 2001, 2005 and 2009 [19-22]. The aim of these blind tests was to evaluate how well currently available methods of crystal structure prediction perform when given only the molecular formula for an organic compound. The most recent fourth blind test has shown important improvements in the modelling methods and suggests that, at least for small rigid molecules [22], such calculations can be successfully applied to

understand crystallisation and polymorphism of organic molecules. Calculations usually locate many more potential structures than are likely to be observed within a reasonable energy range and the energy differences between structures are typically in the order of 0.1-1 kJ mol^{-1}. It is highly likely that some of the previously unobserved structures from these studies should be accessible through changes in growth conditions *e.g.* denser structure can be generated by high-pressure conditions. Due to the latest advances in methodology, CSP (crystal structure prediction) has potentially important applications in polymorph prediction within the pharmaceutical industry [23], although there remain significant challenges with the complexity and degree of conformational freedom associated with typical pharmaceutical molecules.

1.2. High-pressure research

1.2.1. General concept

The field of high-pressure research has attracted significant scientific interest over the last hundred years. P. W. Bridgman was a pioneer in high-pressure research and developed an opposed-anvil device for compressing solids up to pressures of 100,000 atmospheres (*ca.* 10 GPa) [24]. Bridgman made many improvements to his high-pressure apparatus over the years, and attempted the synthesis of diamond many times. In his volumetric experiments conducted up to 10 GPa, he carried out extensive investigations on the properties of matter, including a study of compressibility, electrical and thermal conductivity, tensile strength and viscosity of more than 100 different compounds [24]. Bridgman received a Nobel Prize in 1946 for his pioneering work in this field. Since then researchers have continued to study a wide range of materials under conditions of high pressure.

In high-pressure research, several units of pressure are often used. The unit of gigapascals (GPa) will be employed in this work. The relationship between the three most common units are as follows:

9869.2 atm =10 kbar = 1 GPa

Until recently, high-pressure research has mainly been focused within the Physics and Geosciences communities, where the use of pressure has been shown to be very effective for inducing phase transitions and substantial changes in electrical, optical, or magnetic properties in elements, ices, semiconductors, minerals, and ceramics. An entire volume of *Reviews in Mineralogy & Geochemistry* (volume 41) is dedicated to high-pressure and high-temperature crystal chemistry [25]. The first part of this volume comprises numerous excellent reviews on the variation of structures with temperature and pressure. Minerals, framework structures, silicate structures, hydrous phases and molecular crystals are covered in part II of this volume. This volume also includes excellent reviews on experimental and analytical techniques for high-pressure crystallography. In the following section high-pressure research in molecular organic compounds is reviewed. Reviews on high-pressure work in other areas *e.g.* simple metals, condensed gases, and proteins *etc.* can also be found [25-27].

1.2.2. High-pressure studies of molecular organic compounds

The use of pressure as a variable for studying the structural chemistry of the organic solid state is relatively recent. In the last two decades, the number of publications dealing with the effects of pressure on molecular compounds has started to grow rapidly. This is due to several factors that include progress achieved in the design of diamond-anvil cells (*e.g.* larger apertures of high-pressure cells), the procedures used for data collection and reduction, and more reliable measurement of the intensities of reflections. Two-dimensional detectors, brighter laboratory sources of X-rays, and easier access to synchrotron radiation have also enabled *in situ* high-pressure studies of samples contained in diamond-anvil cell. The study of relatively weakly diffracting crystals with low (monoclinic and even triclinic) symmetry is also now possible. Some of these technical developments are summarised in reviews by Miletich *et al.* [28] and Katrusiak [29].

High-pressure studies on molecular organic compounds can be broadly divided into two main categories; direct compression of the solids, and high-pressure

crystallisation from solution or from liquid. Studies can also be further categorised depending on the physical nature of the sample at ambient conditions *i.e.* gases, liquids and solids. High-pressure studies on samples that are gases at ambient pressure require more specialised loading and are not reported here.

1.2.2.1. Studies of the effect of pressure on solids immersed in hydrostatic liquids (compression studies).

Samples for compression studies are usually loaded as powders or single crystals. The evolution of structural changes can then be followed as a function of pressure. These studies are of fundamental importance and provide insight into the nature of intra- and inter-molecular interactions in molecular solids. Intermolecular interactions are strongly distance dependent and so pressure is a very useful tool for investigating these interactions. Compression of molecular crystals (to <10 GPa) affects the weaker, longer interactions between the constituent molecules (*e.g.* hydrogen bonds, C-H...π interaction, and van der Waals interactions), but the conformations of molecules themselves can also be modified. Since organic molecules are usually not spherically symmetric, their orientation in the structure and the changes in the angles between the planes and axes of the molecules in the structure increase the number of possible variants of pressure-induced structural changes [30]. As a result, one can observe either a structural reconstruction (a phase transition), or a continuous anisotropic distortion within the limits of stability of the same phase.

Effect of hydrostatic pressure on organic crystals (usually in the range 0.1–10 GPa) has been reviewed in the literature by Hemley & Dera [31] and Boldyreva [32, 33]. It is generally accepted that the effect of increasing pressure is comparable and correlated to that of decreasing temperature [27]. However, this is strictly true only for isotropic distortion in cubic systems and for crystal systems of lower symmetry the distortion is usually anisotropic. Paracetamol is one of the many examples that shows that the response can be qualitatively and quantitatively quite different [34].

Systematic studies of the compressibility of various hydrogen bonded organic compounds have been described by Katrusiak [35-38]. The compressibility of hydrogen bonds in these compounds depends on the type of intermolecular motif within the crystal structure. For example, the compressibility of the OH...O hydrogen bonds, linking molecules into chains in the structures of 1,3-cyclohexanedione (Figure 1.6) is significantly less than for the OH...O bonds linking the molecules of dimedone (5,5-dimethyl-1,3-cyclopentanedione) into helices [36, 37]. Amino acids represent another class of hydrogen bonded organic compounds that have been studies in compression experiments. Comprehensive reviews on the effect of pressure on amino acids can be found in literature by Freire [39], Boldyreva [32] and Moggach *et al.* [10]. General phenomena that have been observed on compression of these compounds include the collapse of structural voids and changes in the conformations of molecules. Analysis of the structures of these compounds reveals the directions in which the structure is rigid and the directions in which it is more compressible. For structures in which molecules form hydrogen-bonded chains or two-dimensional layers, linear strain can be considered in relation to the orientation of hydrogen bonded chains and layers [30]. For example, most of the amino acids are most rigid in the directions of the head-to-tail chains *e.g.* the structures of γ-glycine and DL-serine are less compressible along the head-to-tail chains of the zwitterions than in the plane normal to these chains [40-42].

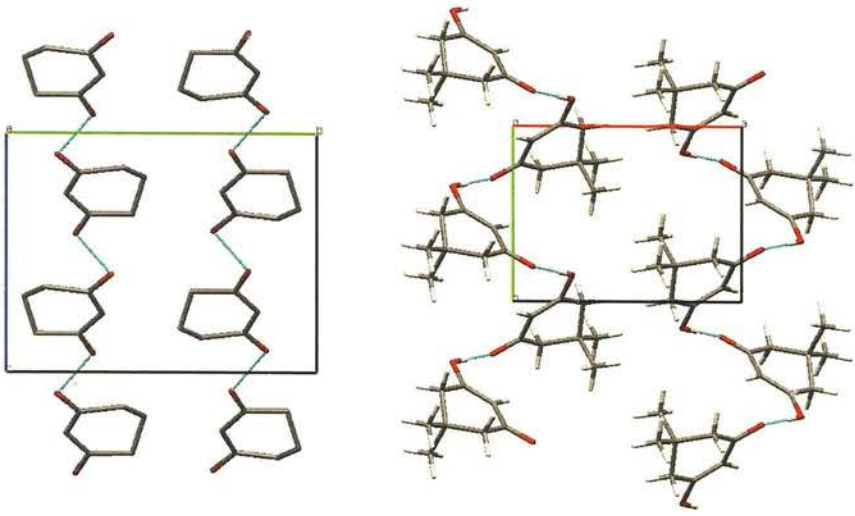

Figure 1.6: Crystal packing diagrams of 1,3-cyclohexanedione viewed along a-axis (left) and dimedone viewed along c-axis (right).

From these and other examples it has been possible to make some generalisations about the effects of pressure on the structures of these molecular compounds. For example, many structures are more compressible in the direction normal to the molecular layers. However, there are also some exceptions *e.g.* α-glycine is about 1.2 times more compressible along the direction of the hydrogen bonds [41, 43]. Other examples which shows this type of behaviour include benzoquinone [34] and dimedone [37].

Compression of an organic compound can also induce phase transitions and some examples have been recently reviewed by Moggach *et al.* [10] and Boldyreva [32, 44]. Many of the pressure-induced polymorphic transitions are isosymmetric and the structures of the ambient-pressure and the high-pressure phases are often related, especially if the compression is performed on the single crystal. Such transformations are often reversible and give metastable forms although on occasions metastable forms can be recovered. The kinetic and thermodynamic aspects of these transitions are discussed in a recent review by Boldyreva [44]. The occurrence of phase transitions can also depend on the starting polymorph. An example is provided by glycine. The structure of α-glycine is stable at least up to 23 GPa [45], but β-glycine undergoes a reversible single-crystal-to-single-crystal phase transition at 0.76

GPa [43], whereas γ-glycine transforms irreversibly into δ-glycine at a pressure of *ca.* 3.5 GPa [41], and then converts into the ζ-form on decompression down to 0.6 GPa. The phase transformation can also be sensitive to the choice of the pressure-transmitting liquid and an example is provided by a Co(III)-coordination compound ($[Co(NH_3)_5NO_2]I_2$), where no polymorphic transition was observed in fluorinated oil, but was observed in a methanol:ethanol:water mixture [46].

1.2.2.2. High-pressure crystallisation

High-pressure crystallisation techniques can further be divided into two categories, depending on the physical nature of the sample at ambient conditions.

Crystallisation of liquids at high pressure

Crystallisation of liquids by the application of pressure has been known as an alternative to crystallisation by cooling since the time of Bridgman [24]. Liquid samples are generally straightforward to load and crystallisation can be induced by the application of pressure. The loading procedure involves placing a small drop of liquid on the edge of the gasket hole. The diamond-anvil cell is then rapidly assembled and the pressure is applied to induce crystallisation. This results in the formation of a polycrystalline solid. A single crystal is then grown by heating the sample, thereby reducing the number of crystallites, until a single crystal remains. The sample is then allowed to cool and this results in the growth of a single crystal that ideally fills the entire gasket hole. This single crystal can be studied by a range of techniques including single crystal X-ray diffraction.

Many examples of high-pressure studies of simple organic compounds that are liquid at ambient pressure have been published [47-60]. In most of these studies pressures in the range of 0.1-10.0 GPa have been used to investigate any structural changes. Almost all of the compounds studied have undergone one or more phase changes to give high-pressure polymorphs. On occasions, high-pressure forms have been found to be the same as the forms produced by crystallisation on cooling. Examples include 1,2-dichloromethane [47], carbon disulfide [48], 3-fluorophenol

and 3-chlorophenol [49]. More often, though, the high-pressure and the low-temperature polymorphs differ. Benzene [50-52], cyclohexane [53], acetone [54], simple alcohols [54-57], acetic acid [54], sulfuric acid [56], water [58], 1,2-diaminoethane [59], 2-chlorophenol, 2-fluorophenol and 4-fluorophenol [49] are just some examples of compounds that are liquid at ambient conditions and for which the high-pressure polymorphs are different from the forms obtained on cooling at ambient pressure.

Low-temperature and high-pressure polymorphs may differ in the conformations of the molecules as they pack together in the crystal structure. Formic acid [60] and propionic acid [61] are examples of monocarboxylic acids where low-temperature and high-pressure forms differ in the conformations adopted by molecules in their respective crystal structures. On many occasions, the main structural differences between high-pressure and low-temperature forms are related to the orientation of the molecules with respect to each other *e.g.* in acetic acid the hydrogen bonded molecular chains found in the high-pressure polymorph [54] at 0.2 GPa are identical to those of the low-temperature phase [62], but the relative orientations of the chains are noticeable different.

Sometimes it is found that the low-temperature structure is disordered, but the high-pressure form is completely ordered *e.g.* 1, 3-cyclohexanedione (CHD) [36]. When subjected to pressure of *ca.* 0.1 GPa a crystal of CHD was observed to undergo a structural transformation which significantly changed the arrangement of the molecules and resulted in ordering of the methylene groups, but maintained the space group ($P2_1/c$).

Compression without temperature variation can give forms different from those obtained by the combination of compression and temperature cycling [44]. Katrusiak *et al.* have applied this technique to obtain high-pressure polymorphs for many halogenated compounds *e.g.* dichloromethane and dibromomethane [63].

Crystallisation of solids at high pressure

It is clear from the above examples that that pressure-induced crystallisation of liquids is a very powerful method for accessing new polymorphs of these compounds. Solid samples with low melting points (typically < 323 K) can be gently heated until molten and then loaded into the DAC using the same procedure described in the previous section. For samples that crystallise rapidly, gentle heating of the cell components is required to ensure that the sample remains liquid. It is important to ensure that the crystallisation is achieved by the application of pressure rather than cooling at ambient pressure.

However, when we deal with larger organic molecules such as pharmaceuticals that typically have melting points significantly higher than ambient temperature, crystallisation from the melt is less applicable. The problem is made more difficult by the substantial increase in melting point induced in most substances by the application of pressure. Generally, chemical decomposition or some undesirable chemical reaction takes place before the pressure-elevated melting point is reached. Furthermore, there is often a substantial kinetic barrier to be overcome before the molecules can rearrange. A way to tackle these problems is by growing single crystals or polycrystalline powder from solution at high pressure. This removes the need for excessively high temperatures, and overcomes the barrier to molecular rearrangement in the solid, as the lattice energy is now overcome by the solvation energy. In this method, a diamond-anvil cell is first loaded with a solution of the compound and then is pressurised. This usually causes a decrease in the solubility of the compound and results in precipitation of the polycrystalline material, often as a high-pressure form. This powder can then be studied *in situ* by spectroscopic methods and by powder X-ray diffraction. Alternatively, by carefully cycling the temperature of the sample it is often possible to dissolve all but one of the crystallites, which on subsequent cooling grows to a large single crystal suitable for single-crystal X-ray diffraction. The technique is described in more detail in chapter 2.

Crystallisation from solution at high pressure has been known for a long time and has been widely applied in hydrothermal growth of inorganic materials such as quartz [64], but its systematic application for organic compounds started only recently at the University of Edinburgh [65]. This technique is increasingly being used to explore polymorphism in molecular crystals at high pressure. Examples include a new polymorph of phenanthrene crystallised from dichloromethane solution at 0.35 GPa [66], a new polymorph of pyrene (form III) crystallised from dichloromethane solution at 0.3 and 0.7 GPa [67], and a new polymorph of acetamide crystallised from water at 0.8 GPa [68].

The high-pressure crystallisation technique also provides an opportunity to study crystallisation from different solvent systems. This has important implications for polymorph screening of pharmaceuticals where a range of solvents is used to discover new polymorphs. Furthermore, this technique also provides an opportunity for the formation of new solvates of these compounds. Paracetamol gives an example where high-pressure recrystallisation from solution has resulted in the formation of a new hydrate and a solvate. High-pressure recrystallisation of paracetamol from water at 1.1 GPa and methanol at 0.6 GPa gives a dihydrate and a 1:1 methanol solvate, respectively [69].

This technique has also been employed recently for high-pressure co-crystallisation of solid compounds [70]. Crystallisation of paracetamol and piperazine from ethanol at a pressure of 0.57 GPa produced an ethanol solvate of a 2:1 co-crystal of paracetamol:piperazine. This contrasts with crystallisation from ethanol at ambient pressure for which only an unsolvated 2:1 co-crystal of paracetamol:piperazine has been obtained.

1.2.3. High-pressure studies of pharmaceuticals

One of the areas that has until recently been unexplored is the use of high pressure to study polymorphism in more complex organic compounds *e.g.* pharmaceuticals. The effect of pressure on the solid-state properties of

pharmaceuticals is currently of great interest and there are many reasons for this. Firstly, many solid drugs are subjected to pressure during processing, *e.g.* milling (or mechanical grinding) and tabletting. Milling is used to reduce particle size and to ensure homogeneity of the formulation. Under these conditions the material can experience significant localised compression and shear stress, in addition to localised heating. Milling results not only in an increase in surface area, but can also lead to the formation of various defects in the crystals and this can lead ultimately to the disappearance of long range order and crystallinity, *i.e.* the material becomes amorphous. Examples include cephalexine, cephalotine, and clonidine [71]. Furthermore, milling and grinding can also induce phase transitions to different polymorphic forms. Phenylbutazone, sulfathiazole, caffeine, cimetidine represent a few of the many such examples that have been reported [72-74].

Tabletting is another process that involves the direct compression of the pharmaceutical substance with other excipients (*e.g.* starch, lactose, magnesium stearate). Tabletting generally produce pressures in the range 40–200 MPa (0.02-02 GPa) and these are applied for relatively short times (typically <1 second). Some pharmaceutical substances have been shown to undergo changes in phase composition under these compression conditions. Some examples include indomethacin, carbamazepine dihydrate and chlorpropamide [71, 73]. A study by Chan and Doelker showed that out of 32 selected pharmaceutical substances known to be polymorphic, 11 were transformed either completely or partially into other polymorphs during tabletting [75].

Recent advances in the field of high pressure have enabled high-pressure studies of pharmaceuticals. The high-pressure crystallisation technique is proving to be especially effective at producing new polymorphs and solvates of these compounds. High-pressure studies performed on some of the pharmaceuticals are summarised below.

Paracetamol: Paracetamol (acetaminophen) is one of the examples of a pharmaceutical which has been studied by high-pressure techniques. Its molecular

structure is shown in Figure 1.7. It is a widely used analgesic and has been extensively studied using a range of techniques. Under ambient conditions the monoclinic form I is thermodynamically stable and a metastable orthorhombic form II has been prepared. An elusive third form (form III) has also been observed [76, 77], and its crystal structure has recently been solved from X-ray powder diffraction data [78]. In forms I and II, molecular packing in crystal structure is dominated by the formation of N-H...OH and O-H...O=C hydrogen bonds that give rise to a layered 2-D networks. In form I, the hydrogen-bonded layers are arranged parallel to the (010) planes: these give rise to polar layers, where all the molecules have the methyl group on the same side (Figure 1.8). In form II, methyl groups lie on the left- and right-hand sides of the molecules to form non-polar layers (Figure 1.8). Despite these structural differences, compression studies performed on forms I and II have shown that both polymorphs have very similar bulk compressibilities (*i.e.* the relative volume decrease as a function of pressure) leading to a *ca.* 20% decrease in volume from ambient pressure to 4.0 GPa [79]. Boldyreva *et al.* also demonstrated that the application of pressures in excess of 4 GPa to powdered samples of paracetamol resulted in conversion of form I into form II, but for kinetic reasons the conversion was incomplete and poorly reproducible. No conversion was observed in a single crystal. Such a transition would require reorientation of every other chain in a layer and hence the breaking/reforming of many intermolecular hydrogen bonds, leading to a high activation energy. The application of pressure alone was not sufficient to induce a phase transition to form II. As described earlier, recrystallisation from solution at high pressure is an alternative to overcome this problem. Direct crystallisation of paracetamol from ethanol solution at 1.1 GPa gave form II [66].

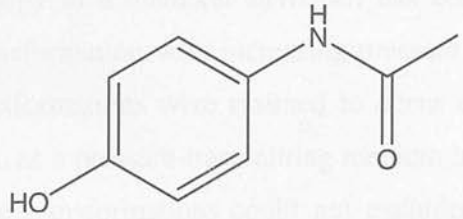

Figure 1.7: Molecular structure of paracetamol.

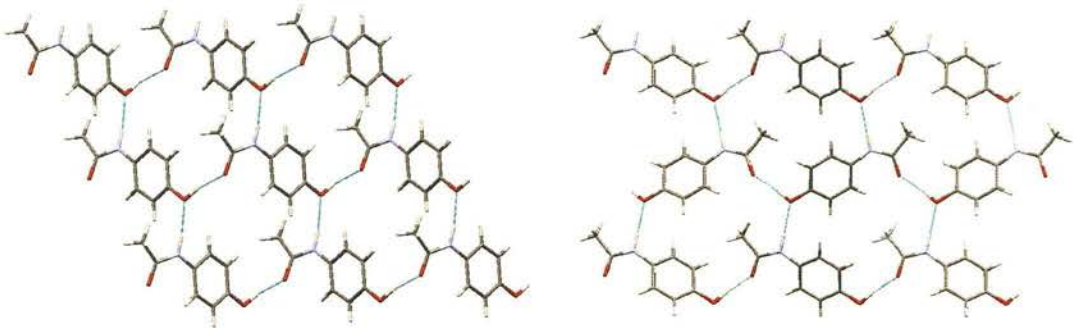

Figure 1.8: Hydrogen-bonded layers in (left) monoclinic paracetamol (form I) viewed along the *b*-axis and (right) orthorhombic paracetamol (form II) viewed along the *c*-axis.

Chlorpropamide: Chlorpropamide is a member of the sulfonylurea group of compounds, and is widely used as an oral antidiabetic agent [80]. Its molecular structure is shown in Figure 1.9. Seven polymorphs and a benzene solvate have been described in the literature [81]. Form-A is known to be the thermodynamically stable form and is the commercially available one. Chlorpropamide can be considered as a model compound to study polymorphic transformations on tabletting [82]. On tabletting, form-A has been reported to transform partially into another polymorph, form-C. Otsuka *et al.* have shown that when chlorpropamide is compacted at *ca.* 200 MPa (0.2 GPa), form-A transformed to form-C [83]. Form-C is also known to be formed from form-A on heating up to *ca.* 115 °C [84]. Wildfong *et al.* have described a method for quantitative determination of polymorphic composition of chlorpropamide in intact compacts by parallel-beam X-ray powder diffractometry [85]. They demonstrated that the minimum pressure for "A-to-C" is *ca.* 10.5 MPa (0.01 GPa). In a study by Boldyreva *et al.* the effect of hydrostatic pressure on form-A by Raman spectroscopy in a diamond anvil cell has been studied [86]. In this study, no "A-to-C" transformation with increasing pressure was observed, but two other polymorphic transformations were claimed to occur at *ca.* 0.9 and 2.0 GPa. Since they used ethanol, as a pressure-transmitting medium in these experiments, the role of ethanol in these transformations could not excluded. Compression studies performed on powder samples of chlorpropamide have shown that in the absence of a pressure-transmitting liquid, no "A-to-C" polymorphic transformation was observed

[86]. Therefore, the polymorphic transformation of form-A to form-C, which was reported during tabletting, is probably due to local heating effects. However, the pressure-induced phase transitions of form-A at 0.9 and 2.0 GPa may be solvent mediated. This was confirmed by high-pressure X-ray diffraction studies performed on samples of chlorpropamide compressed in the saturated ethanol solution [87].

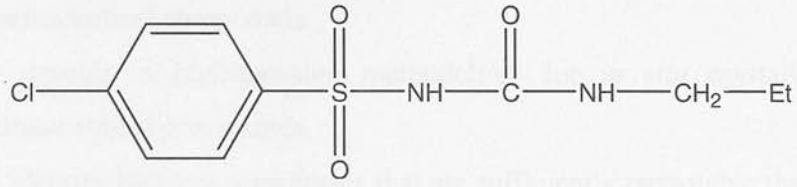

Figure 1.9: Molecular structure of Chlorpropamide.

The example of chlorpropamide shows that the choice of pressure-transmitting medium may have an effect on the polymorphic transformations during compression. Indomethacin, a non-steroidal anti-inflammatory drug, gives another example where no phase transitions were observed on compressing dry intact powder, but occurred when an ethanol slurry was compressed [88].

Piracetam: Piracetam, a nootropic agent used to treat disorders of nervous system, is another drug that has been studied using high-pressure techniques [89, 90]. High-pressure recrystallisation of aqueous and methanolic solutions of piracetam at pressures of 0.07-0.4 GPa resulted in the formation of a new high-pressure polymorph, form IV. Compression of form II resulted in a reversible, single to single crystal transition to a new polymorph, form V, between pressures of 0.45-0.7 GPa. Crystallisation from aqueous solution at pressure of 0.6 GPa resulted in the formation of a previously unreported dihydrate.

1.3. General aims and outline of research

The aims of this work are as follows:

- To explore the extent to which high pressure can affect the polymorphic behaviour of different compounds with a particular emphasis on pharmaceutical compounds.
- To develop a high-pressure methodology for *in situ* crystallisation of pharmaceutical compounds.
- To identify high-pressure forms that are sufficiently metastable that they can be recovered to ambient pressure.
- To develop methodologies for polymorph/solvate screening at high pressure.

The principles of high-pressure techniques employed in this PhD and experimental procedures for sample preparation and structural characterisation are illustrated in Chapter 2. Chapter 3 describes the high-pressure studies of a non-steroidal anti-inflammatory agent, mefenamic acid. The structure of new high-pressure polymorphs of N,N'-dimethylurea are presented in Chapter 4 alongside crystal structure prediction results. High-pressure and ambient-pressure studies of GSK developmental compound (Compound A) are described in Chapter 5. Chapter 6 describes high-pressure studies performed on a second GSK compound (compound B). Conclusions and future directions are described in Chapter 7.

1.4. References

1. D. Giron, *Pharmaceutical Science & Technology Today*, 1998, **1**, 191.
2. J. Bernstein, *Polymorphism in molecular crystals*, Clarendon Press, Oxford, UK, 2002.
3. Wöhler and Liebig, *Annalen der Pharmacie*, 1832, **3**, 249-282.
4. W. C. McCrone, *Physics and Chemistry of the Organic Solid State*, 1965, 725-767.
5. M. J. Buerger and M. C. Bloom, *Zeitschrift fuer Kristallographie, Kristallgeometrie, Kristallphysik, Kristallchemie*, 1937, **96**, 182-200.
6. W. Ostwald, *Z. Physik. Ch.*, 1897, **22**, 289-330.
7. R. A. Carlton, *Microscopy and Microanalysis*, 2004, **10**, 1346-1347.

8. J. Akhavan, In *The Chemistry of Explosives,* The Royal Society of Chemistry, Cambridge, UK, 2nd edn., 2004.
9. A. J. Davidson, I. D. H. Oswald, D. J. Francis, A. R. Lennie, W. G. Marshall, D. I. A. Millar, C. R. Pulham, J. E. Warren and A. S. Cumming, *CrystEngComm*, 2008, **10**, 162-165.
10. S. A. Moggach, S. Parsons and P. A. Wood, *Crystallogr. Rev.*, 2008, **14**, 143-184.
11. H. G. Brittain, *J. Pharm. Sci.*, 1997, **86**, 405-412.
12. S. R. Vippagunta, H. G. Brittain and D. J. W. Grant, *Adv. Drug Delivery Rev.*, 2001, **48**, 3-26.
13. H. G. Brittain, *Polymorphism in Pharmaceutical Solids,* Marcel Dekker Inc., New York, USA, 1999.
14. E. H. Kerns, *J. Pharm. Sci.*, 2001, **90**, 1838-1858.
15. S. R. Chemburkar, J. Bauer, K. Deming, H. Spiwek, K. Patel, J. Morris, R. Henry, S. Spanton, W. Dziki, W. Porter, J. Quick, P. Bauer, J. Donaubauer, B. A. Narayanan, M. Soldani, D. Riley and K. McFarland, *Org. Process Res. Dev.*, 2000, **4**, 413-417.
16. W. Cabri, P. Ghetti, G. Pozzi and M. Alpegiani, *Org. Process Res. Dev.*, 2006, **11**, 64.
17. C. Anderton, *American Pharmaceutical Review*, 2007, **10**, 34, 36-40.
18. J. D. Dunitz and J. Bernstein, *Acc. Chem. Res.*, 1995, **28**, 193-200.
19. J. P. M. Lommerse, W. D. S. Motherwell, H. L. Ammon, J. D. Dunitz, A. Gavezzotti, D. W. M. Hofmann, F. J. J. Leusen, W. T. M. Mooij, S. L. Price, B. Schweizer, M. U. Schmidt, B. P. van Eijck, P. Verwer and D. E. Williams, *Acta Crystallogr., Sect. B: Struct. Sci.*, 2000, **56**, 697-714.
20. W. D. S. Motherwell, H. L. Ammon, J. D. Dunitz, A. Dzyabchenko, P. Erk, A. Gavezzotti, D. W. M. Hofmann, F. J. J. Leusen, J. P. M. Lommerse, W. T. M. Mooij, S. L. Price, H. Scheraga, B. Schweizer, M. U. Schmidt, B. P. van Eijck, P. Verwer and D. E. Williams, *Acta Crystallogr., Sect. B: Struct. Sci.,* 2002, **58**, 647-661.
21. G. M. Day, W. D. S. Motherwell, H. L. Ammon, S. X. M. Boerrigter, R. G. Della Valle, E. Venuti, A. Dzyabchenko, J. D. Dunitz, B. Schweizer, B. P. van Eijck, P. Erk, J. C. Facelli, V. E. Bazterra, M. B. Ferraro, D. W. M. Hofmann, F. J. J. Leusen, C. Liang, C. C. Pantelides, P. G. Karamertzanis, S. L. Price, T. C. Lewis, H. Nowell, A. Torrisi, H. A. Scheraga, Y. A. Arnautova, M. U. Schmidt and P. Verwer, *Acta Crystallogr., Sect. B: Struct. Sci.,* 2005, **61**, 511-527.
22. G. M. Day, T. G. Cooper, A. J. Cruz-Cabeza, K. E. Hejczyk, H. L. Ammon, S. X. M. Boerrigter, J. S. Tan, R. G. Della Valle, E. Venuti, J. Jose, S. R. Gadre, G. R. Desiraju, T. S. Thakur, B. P. van Eijck, J. C. Facelli, V. E. Bazterra, M. B. Ferraro, D. W. M. Hofmann, M. A. Neumann, F. J. J. Leusen, J. Kendrick, S. L. Price, A. J. Misquitta, P. G. Karamertzanis, G. W. A. Welch, H. A. Scheraga, Y. A. Arnautova, M. U. Schmidt, J. van de Streek, A. K. Wolf and B. Schweizer, *Acta Crystallogr., Sect. B: Struct. Sci.,*2009, **65**, 107-125.
23. S. L. Price, *Acc. Chem. Res.*, 2008, **42**, 117-126.
24. P. W. Bridgman, *Rev. Mod. Phys.*, 1946, **18**, 1-93.

25. T. B. Ballaran, *Rev. Mineral. Geochem., High-Temperature and High-pressure Crystal Chemistry, edited by R. M. Hazen and R. T. Downs*, 2003, **41,** 1-595.
26. L. Smeller, H. Roemich and R. Lange, *Biochim. Biophys. Acta, Proteins Proteomics,* 2006, **1764**, 329.
27. R. M. Hazen and L. W. Finger, In *Comparative Crystal Chemistry: Temperature, Pressure, Composition and the Variation of Crystal Structure*, John Wiley & Sons Inc., London, UK.1982.
28. R. Miletich, D. R. Allan and W. F. Kuhs, *Rev. Mineral. Geochem.*, 2001, **41**, 445-519.
29. A. Katrusiak, *Acta Crystallogr., Sect. A: Found. Crystallogr.,* 2008, **64**, 135-148.
30. E. V. Boldyreva, *Cryst. Eng.*, 2004, **6**, 235-254.
31. R. J. Hemley and P. Dera, *Rev. Mineral. Geochem.*, 2001, **41**, 335-419.
32. E. V. Boldyreva, *Acta Crystallogr., Sect. A: Found. Crystallogr.*, 2008, **A64**, 218-231.
33. E. V. Boldyreva, *J. Mol. Struct.*, 2004, **700**, 151-155.
34. E. V. Boldyreva, *J. Mol. Struct.*, 2003, **647**, 159-179.
35. A. Katrusiak, *Cryst. Res. Technol.*, 1991, **26**, 523-531.
36. A. Katrusiak, *Acta Crystallogr., Sect. B: Struct. Sci.*, 1990, **B46**, 246-256.
37. A. Katrusiak, *High Pressure Res.*, 1991, **6**, 265 - 275.
38. A. Katrusiak, *High Pressure Res.*, 1991, **6**, 155 - 167.
39. P. T. C. Freire, *International School of Crystallography*, Erice, Italy, 2009.
40. E. V. Boldyreva, T. N. Drebushchak and E. S. Shutova, *Z. Kristallogr.*, 2003, **218**, 366-376.
41. E. V. Boldyreva, H. Ahsbahs and H. P. Weber, *Z. Kristallogr.*, 2003, **218**, 231-236.
42. E. V. Boldyreva, E. N. Kolesnik, T. N. Drebushchak, H. Sowa, H. Ahsbahs and Y. V. Seryotkin, *Z. Kristallogr.*, 2006, **221**, 150-161.
43. A. Dawson, D. R. Allan, S. A. Belmonte, S. J. Clark, W. I. F. David, P. A. McGregor, S. Parsons, C. R. Pulham and L. Sawyer, *Cryst. Growth Des.*, **5**, 2005, 1415-1427.
44. E. V. Boldyreva, *Cryst. Growth Des.*, 2007, **7**, 1662-1668.
45. C. Murli, S. M. Sharma, S. Karmakar and S. K. Sikka, *Physica B: Condensed Matter*, 2003, **339**, 23-30.
46. E. V. Boldyreva, H. Ahsbahs, H. Uchtmann and N. Kashcheeva, *High Pressure Res.*, 2000, **17**, 79 - 99.
47. M. Podsiadlo, K. Dziubek and A. Katrusiak, *Acta Crystallogr., Sect. B: Struct. Sci.*, 2005, **B61**, 595-600.
48. K. F. Dziubek and A. Katrusiak, *J. Phys. Chem. B*, 2004, **108**, 19089-19092.
49. I. D. H. Oswald, D. R. Allan, W. D. S. Motherwell and S. Parsons, *Acta Crystallogr., Sect. B: Struct. Sci.*, 2005, **B61**, 69-79.
50. I. D. H. Oswald, D. R. Allan, G. M. Day, W. D. S. Motherwell and S. Parsons, *Cryst. Growth Des.*, 2005, **5**, 1055-1071.
51. G. J. Piermarini, A. D. Mighell, C. E. Weir and S. Block, *Science*, 1969, **165**, 1250-1255.

52. C. E. Weir, G. J. Piermarini and S. Block, *J. Chem. Phys.*, 1969, **50**, 2089-2093.
53. N. B. Wilding, P. D. Hatton and G. S. Pawley, *Acta Crystallogr., Sect. A: Found. Crystallogr.*, 1991, **47**, 797-806.
54. D. R. Allan and S. J. Clark, *Phys. Rev. B: Condens. Matter*, 1999, **60**, 6328-6334.
55. D. R. Allan, S. J. Clark, M. J. P. Brugmans, G. J. Ackland and W. L. Vos, *Phys. Rev. B: Condens. Matter*, 1998, **58**, R11809-R11812.
56. D. R. Allan, S. J. Clark, A. Dawson, P. A. McGregor and S. Parsons, *Acta Crystallogr., Sect. B: Struct. Sci.*, 2002, **B58**, 1018-1024.
57. D. R. Allan, S. Parsons and S. J. Teat, *J. Synchrotron Radiat.*, 2001, **8**, 10-17.
58. A. D. Fortes, I. G. Wood, M. Alfredsson, L. Vocadlo and K. S. Knight, *J. Appl. Crystallogr.*, 2005, **38**, 612-618.
59. A. Budzianowski, A. Olejniczak and A. Katrusiak, *Acta Crystallogr., Sect. B: Struct. Sci.*, 2006, **B62**, 1078-1089.
60. D. R. Allan and S. J. Clark, *Phys. Rev. Lett.*, 1999, **82**, 3464-3467.
61. D. R. Allan, S. J. Clark, S. Parsons and M. Ruf, *J. Phys.: Condens. Matter*, 2000, **12**, L613-L620.
62. I. Nahringbauer, *Acta Chem. Scand.*, 1970, **24**, 453-462.
63. A. Katrusiak, R. Gajda, A. Olejniczak and M. Podsiadlo, *Acta Crystallogr., Sect. A: Found. Crystallogr.*, 2007, **63**, s68-s69.
64. K. Suito, M. Miyoshi and A. Onodera, *High Pressure Res.*, 1999, **16**, 217 - 232.
65. F. P. A. Fabbiani, Ph.D. Thesis, University of Edinburgh, 2005.
66. F. P. A. Fabbiani, D. R. Allan, W. I. F. David, S. A. Moggach, S. Parsons and C. R. Pulham, *CrystEngComm*, 2004, **6**, 504-511.
67. F. P. A. Fabbiani, D. R. Allan, S. Parsons and C. R. Pulham, *Acta Crystallogr., Sect. B: Struct. Sci.*, 2006, **B62**, 826-842.
68. F. P. A. Fabbiani, D. R. Allan, W. G. Marshall, S. Parsons, C. R. Pulham and R. I. Smith, *J. Cryst. Growth*, 2005, **275**, 185-192.
69. F. P. A. Fabbiani, D. R. Allan, A. Dawson, W. I. F. David, P. A. McGregor, I. D. H. Oswald, S. Parsons and C. R. Pulham, *Chem. Comun.*, 2003, 3004-3005.
70. I. D. H. Oswald and C. R. Pulham, *CrystEngComm*, 2008, **10**, 1114-1116.
71. V. V. Boldyrev, *J. Mater. Sci.*, 2004, **39**, 5117.
72. T. Matsumoto, J. Ichikawa, N. Kaneniwa and M. Otsuka, *Chem. Pharm. Bull.*, 1988, **36**, 1074-1085.
73. G. B. Harry, *J. Pharm. Sci.*, 2002, **91**, 1573-1580.
74. T. P. Shakhtshneider and V. V. Boldyrev, *Drug Dev. Ind. Pharm.*, 1993, **19**, 2055-2067.
75. H. K. Chan and E. Doelker, *Drug Dev. Ind. Pharm.*, 1985, **11**, 315-332.
76. P. Di Martino, P. Conflant, M. Drache, J. P. Huvenne and A. M. Guyot-Hermann, *J. Therm. Anal.*, 1997, **48**, 447-458.
77. J. C. Burley, M. J. Duer, R. S. Stein and R. M. Vrcelj, *Eur. J. Pharm. Sci.*, 2007, **31**, 271-276.
78. M. A. Perrin, M. A. Neumann, H. Elmaleh and L. Zaske, *Chem. Comun.*, 2009, 3181-3183.

79. E. V. Boldyreva, T. P. Shakhtshneider, H. Ahsbahs, H. Sowa and H. Uchtmann, *Journal. Therm. Anal. Calorim.*, 2002, **68**, 437-452.
80. R. R. Koski, *J. Pharm. Pract.*, 2004, **17**, 39-48.
81. T. N. Drebushchak, N. V. Chukanov and E. V. Boldyreva, *Acta Crystallogr., Sect. C: Cryst. Struct. Commun.*, 2007, **C63**, o355-o357.
82. M. Otsuka, T. Matsumoto and N. Kaneniwa, *J. Pharm. Pharmacol.*, 1989, **41**, 665-669.
83. M. Otsuka, T. Matsumoto, S. Higuchi, K. Otsuka and N. Kaneniwa, *J. Pharm. Sci.*, 1995, **84**, 614-618.
84. S. S. Al-Saieq and G. S. Riley, *Pharm. Acta Helv.*, 1982, **57**, 8-11.
85. P. L. D. Wildfong, N. A. Morley, M. D. Moore and K. R. Morris, *J. Pharm. Biomed. Anal.*, 2005, **39**, 1.
86. E. V. Boldyreva, V. Dmitriev and B. C. Hancock, *Int. J. Pharm.*, 2006, **327**, 51-57.
87. E. V. Boldyreva, H. Sowa, H. Ahsbahs, S. V. Goryainov, V. V. Chernyshev, V. P. Dmitriev, Y. V. Seryotkin, E. N. Kolesnik, T. P. Shakhtshneider, S. N. Ivashevskaya and T. N. Drebushchak, *J. Phys.: Conf. Ser.*, 2008, **121**, 1-11.
88. T. Okumura, M. Ishida, K. Takayama and M. Otsuka, *J. Pharm. Sci.*, 2006, **95**, 689-700.
89. F. P. A. Fabbiani, D. R. Allan, W. I. F. David, A. J. Davidson, A. R. Lennie, S. Parsons, C. R. Pulham and J. E. Warren, *Cryst. Growth Des.*, 2007, **7**, 1115-1124.
90. F. P. A. Fabbiani, D. R. Allan, S. Parsons and C. R. Pulham, *CrystEngComm*, 2005, **7**, 179-186.

Chapter 2

Experimental Techniques

Chapter 2: Experimental Techniques

2.1. The Merrill-Bassett diamond-anvil cell

The development of high-pressure apparatus continues to be a very active area of research. From the pioneering work by Bridgman until the 1960s, hydraulically driven anvils and piston-cylinder devices dominated high-pressure science [1]. These devices were massive, and required specialised laboratories for operation. With the advent of the gasketed diamond-anvil cell in the mid 1960s, high-pressure research became less technically demanding and more accessible to non-specialised laboratories [2, 3]. The assembly of the gasketed diamond-anvil cell (DAC) is illustrated in the Figure 2.1.

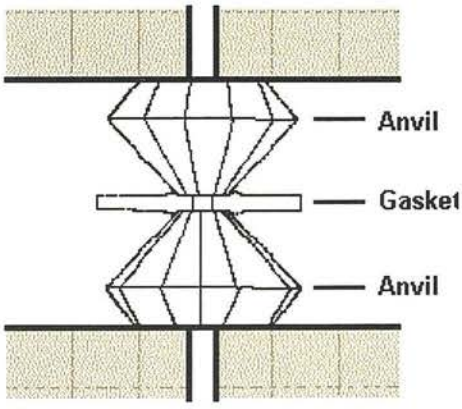

Figure 2.1: Assembly of the gasketed diamond-anvil cell

The basic principle of the DAC is relatively simple. A sample is placed between two flat parallel diamond faces and the sample is subjected to conditions of high pressure when a force pushes the opposed anvils together. Due to the fact that diamond is transparent to a wide range of electromagnetic radiation, DACs have been utilised for both X-ray diffraction and spectroscopic studies.

Much of the work undertaken in this thesis was performed using a Merrill-Bassett DAC [4]. A schematic representation is shown in Figure 2.2.

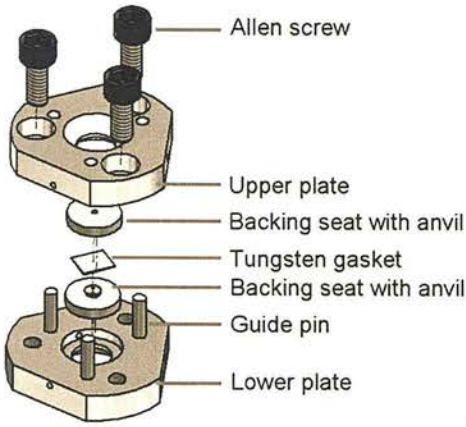

Figure 2.2: Cross-section view of Merrill-Bassett diamond-anvil cell [4].

The choice of material, the preparation of the various cell components and their functions have been described in detail by Miletich *et al.* [5]. The DAC is *ca.* 5 cm in diameter and comprises two gem-quality diamonds mounted on two beryllium backing discs. The backing discs are not only used to support the diamonds but also act as X-ray windows. These backing plates have confocal holes drilled through them to allow optical alignment of the diamonds and act as windows for electromagnetic radiation and sample viewing. The backing discs are held in a stainless steel casing by small screws to allow alignment of the diamond anvils. With the design of the DAC used at The University of Edinburgh the culet can be corrected for lateral but not for parallel alignment; parallelism can only be corrected during the mounting of the diamonds on the backing plates with glue. Diamond alignment is a crucial step in the cell preparation and misalignment is the most common reason for diamond failure. Type I diamonds were used for most of the experiments presented in this thesis, with the exception of experiments which involved Raman spectroscopic measurements, for which type II diamonds (low fluorescence) were used. The culet size of the diamonds that are used in the DAC play a big part in determining the pressure which can be reached. The diamond culets used in this work varied between 400 and 600 μm.

Beryllium is a material often used for the backing plates. Due to its low atomic number, Be has a small absorption coefficient for X-rays ($\lambda \leq 0.7$ Å).

Beryllium also has a high tensile strength and so can be used to reach pressures in excess of 20 GPa. Although Be is transparent to X-rays, it is polycrystalline and produces a powder pattern that contaminates the diffraction pattern. Furthermore, Be is toxic, and so its handling requires care. Conically ground tungsten carbide (WC) backing discs can overcome this problem; however they provide little support for the diamonds of the type usually used in Merrill-Bassett cells. Boehler-Almax cut diamonds have recently become available [6], and these can be embedded in the WC backing plates, retaining the typical 80° opening angle and providing support for the diamonds. Figure 2.3 shows two DAC types with their backing disc design. DAC with WC backing discs were also used in some experiments described in this thesis.

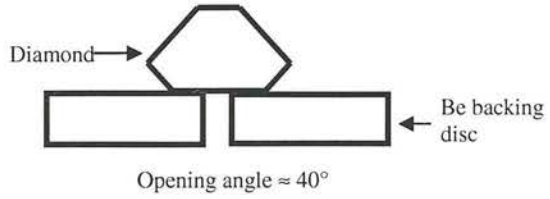

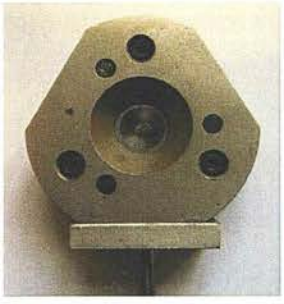

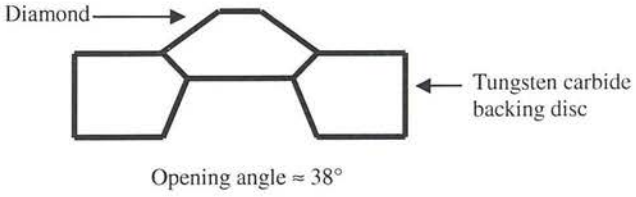

Figure 2.3: Backing seat and anvil design for (*top*) a beryllium backing seat with a modified brilliant-cut diamond anvil, (*bottom*) a WC backing seat with a conical Boehler-Almax diamond anvil.

The sample chamber was created by drilling a hole of 250 μm or 300 μm diameter through a pre-indented 250 μm thick tungsten gasket by spark erosion. This gasket was then placed in between the two diamonds by aligning the hole with the diamond's thrust axis. Pressure is then applied by tightening the three Allen screws attached to the steel casing. As the diamonds are pushed together, the gasket

extrudes outwards around the culets, sealing the sample chamber. In this arrangement, very high pressures can easily be reached because the force is applied to a very small area. The pressure limit of the cells used in Edinburgh is about 12 GPa, but can be substantially increased by reducing the size of the gasket hole and the diamond culets. This pressure range is modest compared to the pressure routinely employed in other areas of research (*e.g.* pressure in the 100 GPa range for study of planetary interiors), but more than sufficient for the high-pressure experiments presented in this thesis. In the case of high-pressure crystallisation experiments from solution, 12 GPa is well in excess of the working range, which rarely exceeds 2 GPa.

2.2. Sample loading

2.2.1. Direct compression experiments

The compression studies reported in this thesis were conducted using materials as either a single crystal or polycrystalline powder. For both types of experiment, the sample was loaded into the tungsten gasket chamber along with a ruby chip. Pressure was then applied gradually by tightening the screws of the DAC.

Most studies performed in this work have been performed under hydrostatic conditions. For this reason samples under study were loaded into a DAC together with a hydrostatic medium [7]. The use of a fluid as a pressure-transmitting medium generally fulfils this condition provided the fluid does not solidify in the pressure range under study. However, the selection of an appropriate pressure-transmitting medium is crucial, as non-hydrostatic media can cause several problems *e.g.* significant broadening and shifts in diffraction peaks may be observed. Such conditions can also promote or suppress phase transitions, and may also lead to crushing and amorphisation of the sample. In addition, they can modify the relative change of cell parameters with pressure and can cause problems in determining pressure using ruby fluorescence on account of broadening of the R_1 line (Section 2.3).

In much of the work presented in this thesis, a 4:1 mixture of methanol: ethanol by volume was used. This has been shown to be hydrostatic up to pressures of 10 GPa [7, 8]. However, a disadvantage of this mixture is that some samples may dissolve in these alcohols. For these compounds an alternative pressure-transmitting medium is Fluorinert-FC77, which is a fluorinated hydrocarbon and has shown to be hydrostatic up to 1.2 GPa [9].

2.2.2. Pressure induced crystallisation

The technique of pressure-induced crystallisation from the pure liquid or from the melt for the generation of new polymorphs was briefly discussed in the introductory chapter. These techniques are particularly effective when the compounds under study have normal melting points that lie below or close to room temperature. However, for more complex compounds *e.g.* pharmaceuticals that have higher melting points, these techniques have been less successful. This is because thermal decomposition of such compounds usually occurs long before the pressure-elevated melting temperature is reached. Furthermore, there is often a substantial kinetic barrier to be overcome before the molecules can rearrange.

To overcome these problems a technique that involves recrystallisation from solution at high-pressure has been employed. This technique not only removes the need for excessive high temperatures to overcome the kinetic barrier to molecular rearrangement and also provides an opportunity to study high-pressure crystallisation from different solvent systems. This has important implications for polymorph screening of pharmaceuticals where a range of solvents is used to discover new polymorphs. Previously at Edinburgh this technique has been successfully used to produce new polymorphs and solvates of pharmaceutical compounds [10-12]. A schematic procedure for the technique is summarised in Figure 2.4.

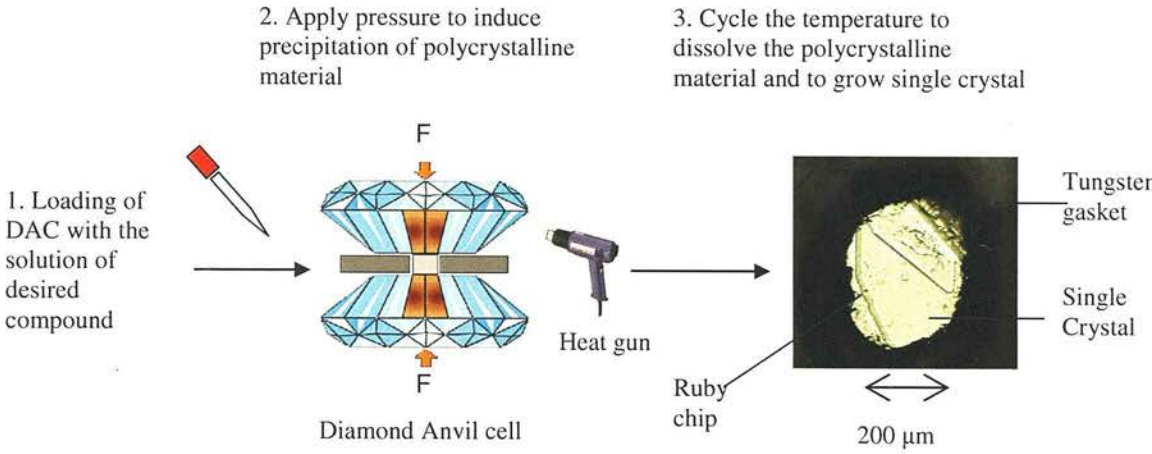

Figure 2.4: Schematic procedure for high-pressure recrystallisation

Cell loading and crystal growth are performed under an optical microscope. The procedure consists of the following: a small drop of the solution with solvent of choice was placed on the edge of the gasket hole. The cell was then rapidly assembled and then pressurised by tightening the screws. This normally caused a decrease in the solubility of the compound, and usually resulted in the precipitation of a polycrystalline material; this corresponds to the crystallisation step. This powder could then be studied by X-ray powder diffraction and/or spectroscopic methods. For the single crystal studies, the single crystal was grown by heating the cell with a hot-air gun, thereby reducing the number of crystallites, until a single crystal remains. A large single crystal could then be grown from this seed as the system was cooled, which ideally filled as much of the gasket hole as possible. Detailed descriptions of individual recrystallisations are given in the particular chapter.

Several variables can be controlled prior to and during a high-pressure crystallisation experiment and these are discussed in more detailed in the following sections.

2.2.2.1. Choice of solvent

The choice of solvent can be crucial for high-pressure crystallisation. The solvent is chosen so that the compound of interest has reasonable solubility. Solubility not only affects the pressure at which crystallisation can be achieved, but also ensures that the resulting crystal is of reasonable size for single crystal X-ray diffraction.

An important feature to be considered is the pressure at which the solvent crystallises. Ideally it should crystallise at reasonably high pressures > 0.5 GPa. This ensures a good working range for the high-pressure recrystallisation of the solute. The solvents that were used in the experiments described in this thesis were methanol, ethanol, isopropyl alcohol and methanol:ethanol mixture (4:1).

Another requirement for the choice of solvent is that it should not react with the solute under high-pressure conditions when the temperature is increased during heating. The possibility of a high-pressure reaction is an active area of high-pressure research, but has not been explored in this work [13].

Another important consideration is the viscosity of the solvent. It has been previously reported by Jenner [13] that viscosity is greatly affected by pressure; normally it increases with increasing pressure. This may hinder the crystallisation process by preventing nucleation. One way of dealing with this problem is by decreasing the pressure within the DAC and this can sometimes induce crystallisation. Alternatively, in the case of a solvent with a low freezing pressure, crystallisation (freezing) of the solvent with pressure can sometimes create nucleation points, thus resulting in precipitation of the solute.

2.2.2.2. Concentration

A second important factor to be considered is the concentration of the solute in the solvent system. Concentration plays a role in determining the size of crystal that can be grown in DAC. Secondly, concentration may influence whether an

unsolvated or a solvated species is crystallised. There are some examples in the literature where concentration has played a part in this respect [14]. Concentration also affects the pressure at which precipitation occurs; the higher the concentration, the lower the pressure, provided solubility decreases with increasing pressure. For this reason, in some experiments presented in this thesis, the DAC was loaded with the solution of the compound of interest together with a few crystallites of the compound. The pressure was then increased only very slightly to form a sealed system and the cell was then gently heated to dissolve all of the crystallites. This is a crucial step as all the seeds of an ambient-pressure polymorph should be dissolved to avoid crystallisation of this polymorph at high pressure. The pressure inside the cell was then increased while the cell was still warm; the cell was then allowed to cool to observe precipitation. The main advantage of this procedure is that on cooling a large single crystal can often be recovered at ambient pressure.

2.3. Pressure measurement

The pressure within the cell is usually measured using diffraction or fluorescence [15]. The ruby fluorescence (Cr^{3+} doped α-Al_2O_3) method was introduced in 1972 as a new way for calibrating the pressure in the DAC [16]. Prior to this, pressure was determined by internal pressure markers such as sodium chloride or silver where the known equation of state is applied to convert measured unit-cell volumes to pressure. Ruby fluorescence is characterised by an intense doublet, with a sharp band at approximately 694 nm [17]. Under compression the doublet shifts to higher wavelength, and this fluorescence shift has been calibrated up to 20 GPa.

A small chip of ruby was placed in the tungsten gasket together with the sample and a pressure-transmitting medium. Ruby fluorescence in this work was induced using the 632.8 nm line from a He-Ne laser, and was dispersed and detected by a Jobin-Yvon LabRam 300 spectrometer with a typical precision in the measurements of ± 0.05 GPa.

2.4. Raman spectroscopy

Raman spectroscopy has been less widely used than infrared spectroscopy (IR), but recent advances in instrument technologies have simplified the equipment, and so Raman spectroscopy is now relatively straightforward and ideally suited for high-pressure studies using DACs.

Raman spectroscopy involves shining an intense light source, *e.g.* a laser beam, on a sample and detecting the scattered light. When a beam of monochromatic light interacts with the sample, photons can be absorbed or scattered by the material. The vast majority of the scattered photons have exactly the same wavelength as the incident photons and this is known as Rayleigh scattering. However a tiny proportion about (1 in 10^7) of the scattered radiation is shifted to a different wavelength. This scattering is known as Raman scattering. The scattering of the light is demonstrated in Figure 2.5.

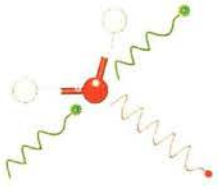

Figure 2.5: Light scattered from a molecule has several components - the Rayleigh scattering (red) and the Stokes and anti-Stokes Raman scattering (green).

Most of the Raman scattered photons are shifted to a longer wavelength (Stokes shift), but a small proportion is shifted to shorter wavelengths (anti-Stokes shifts) [18]. A simplified energy diagram that illustrates this concept is given in Figure 2.6.

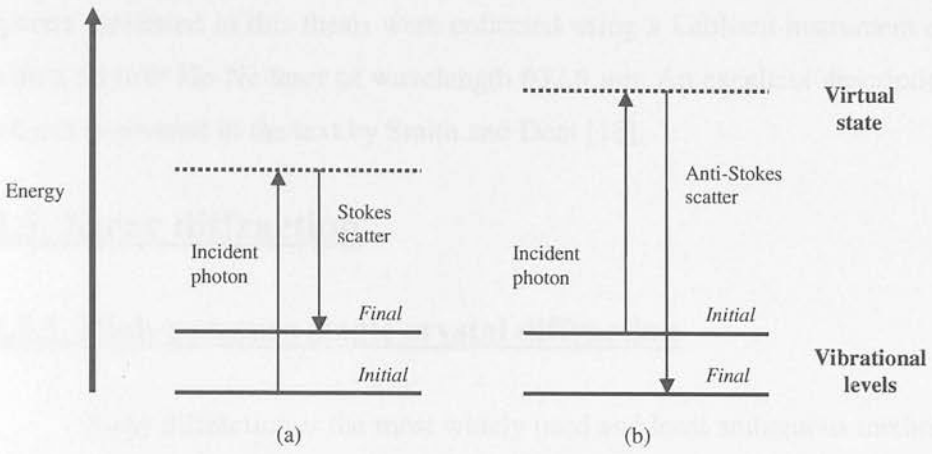

Figure 2.6: Energy level diagram for Raman scattering; (a) Stokes Raman scattering (b) Anti-Stokes Raman scattering.

A Raman spectrum is a plot of the intensity of Raman scattering as a function of its frequency difference from the incident radiation (usually in units of wave numbers, cm^{-1}). This difference is called Raman shift and is independent of the frequency of the incident radiation. Although Infrared and Raman spectroscopy both measure the vibrational energies of the molecule, each method relies on different selection rules. For a transition to be Raman active there must be change in polarisability. This is best pictured as the ease with which the electron cloud is distorted *i.e.* polarised.

Raman spectroscopy is a very useful technique for detecting phase transitions in the crystalline state because the active vibrational modes of molecules are dependent not only on molecular symmetry but also on site symmetry in the crystal. In particular, vibrational bands below 100 cm^{-1} are sensitive to changes in intermolecular potential. Raman spectroscopy is very effectively used in high-pressure studies; the appearance of new bands and shifts in wavenumber with increasing pressure are primarily due to changes in the environment, solvation and intramolecular interactions. If a phase transformation occurs with pressure, new spectral features characteristic of the new lattice may appear. Moreover, the position of some of the bands may change dramatically and a plot of wavenumber *vs.* pressure may exhibit changes in gradient thus indicating a potential phase transition. Raman

spectra presented in this thesis were collected using a LabRam instrument equipped with a 50 mW He-Ne laser of wavelength 632.8 nm. An excellent description of the subject is covered in the text by Smith and Dent [18].

2.5. X-ray diffraction

2.5.1. High-pressure single crystal diffraction

X-ray diffraction is the most widely used and least ambiguous method for the determination of positions of atoms in molecules and solids. X-ray diffraction occurs when a beam of X-rays interacts with electrons in a material and is elastically scattered. Distance between atoms or ions are typically in the order of few Å, which is comparable to X-ray wavelength produce by bombardment of metal by electrons (*e.g.* Mo-Kα radiation, $\lambda = 0.71073$ Å). In a crystal, regular arrays of atoms results in the interference of the scattered X-rays. According to Bragg Equation, $n\lambda = 2d\sin\theta$, constructive interference occurs when reflected rays are completely in phase *i.e.* their path difference ($2d\sin\theta$) must be a whole number of wavelengths ($n\lambda$) where d is the separation between the planes and λ is the wavelength of the X-rays. This gives a characteristic pattern of intensities. Figure 2.7 shows schematic diagram of X-rays scattering from a crystal lattice.

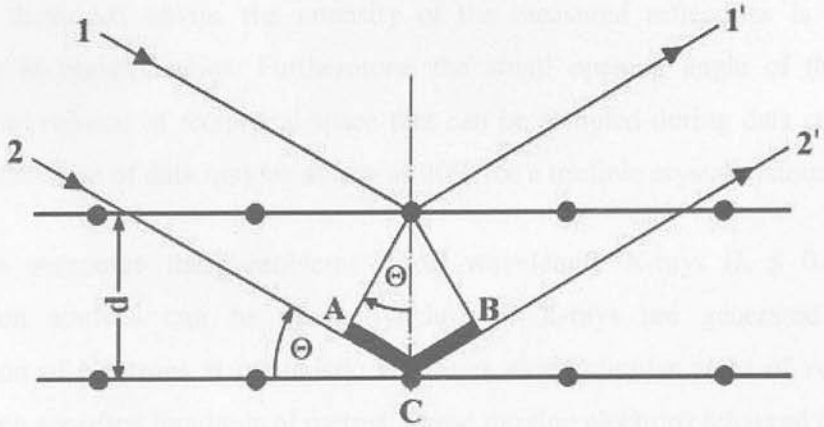

Figure 2.7: The Bragg construction for diffraction by two planes of atoms

Intensities are directly proportional to the square of the amplitude of the scattered radiation, but provide no knowledge about the phase of the wave, giving rise to the so-called phase problem. This is the one of the fundamental challenges in X-ray crystallography, since both the amplitude and the phase of the X-rays scattered by a crystal are required in order to obtain its molecular structure. The determination of approximate phases can be achieved by the development of the structural model by structure solution (Patterson, direct methods). Calculated phases can then be combined with observed intensities. Fourier transformation is then used to create a better model (and as such a new set of calculated phases). Missing atoms can then be located by a difference Fourier synthesis. Structure refinement is then performed, where the aim is to create the best agreement between observed and calculated amplitudes or intensities, leading to determination of the crystal structure. A comprehensive description of this subject is given in texts by W. Massa and C. Giacovazzo [19, 20].

2.5.1.1. Synchrotron sources

The small size of the pressure chamber and limited opening angle of the DAC, typically between 80-90°, gives rise to significant problems in data collection. The maximum size of the crystal loaded in the DAC is generally no larger than 100 × 100 × 50 μm. Due to this small size, together with the absorption from the backing disc and diamonds anvils, the intensity of the measured reflections is reduced, especially at higher angles. Furthermore, the small opening angle of the DAC, restricts the volume of reciprocal space that can be sampled during data collection. The completeness of data may be as low as 20% for a triclinic crystal system.

To overcome these problems, short wavelength X-rays ($\lambda \leq 0.6$ Å) at synchrotron sources can be used. Synchrotron X-rays are generated by the acceleration of electrons at relativistic velocities along circular paths of very large radii, which are often hundreds of metres. These moving electrons (charged particles) under the influence of an accelerating field emit electromagnetic radiation. This

radiation, which is emitted tangentially from the ring, has a continuous spectrum, from which a single wavelength of any value can be selected by monochromator.

With conventional sources, experiments are limited to specific wavelengths. Experiments conducted using synchrotron radiation do not suffer from this limitation and for high-pressure experiments short wavelengths are normally used. This increases the completeness of the data relative to laboratory sources by increasing the amount of reciprocal space sampled, while the higher flux of X-rays allows shorter data collection times for small samples.

2.5.1.2. Data collection

The majority of experiments presented in this thesis were performed at Edinburgh on a Bruker-Nonius APEX 2 CCD diffractometer using Mo-$K\alpha$ radiation, $\lambda = 0.71073$ Å at 293(2) K. Some work was done at the SRS Daresbury Laboratory, Warrington, UK, on Stations 9.8 and 16.2 with a Bruker APEX 2 CCD diffractometer at 293(2) K using synchrotron radiation with X-ray wavelengths of between 0.65 Å and 0.85 Å.

Data collection was performed according to an established procedure [21]. The DAC was attached to a stainless steel "table" (usually with superglue or some other adhesive), which has a vertical pin that can fit into the goniometer head. For the pressure cell to fit onto the goniometer, a short collimator was used to give enough clearance for the cell to be rotated whilst collecting data (Figure 2.8).

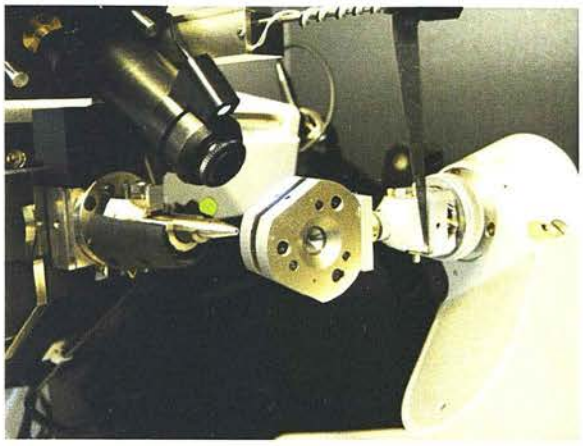

Figure 2.8: Experimental setup for collecting single crystal data from samples within a DAC.

2.5.1.3. Data processing

All single-crystal data were processed according to the procedure described by Dawson *et al.* [21] which are summarised here and described further in each chapter.

Processing of high-pressure data from CCD detector is non-trivial, because the images contain not only sample reflections, but also intense diamond reflections and powder lines from the backing seat and gasket material. Figure 2.9 shows a copy of a SMART CCD frame contaminated by an intense diamond reflection and by beryllium powder rings. The contamination of the diffraction pattern makes the whole process of indexing, integration and structure solution more challenging compared to ambient-pressure studies.

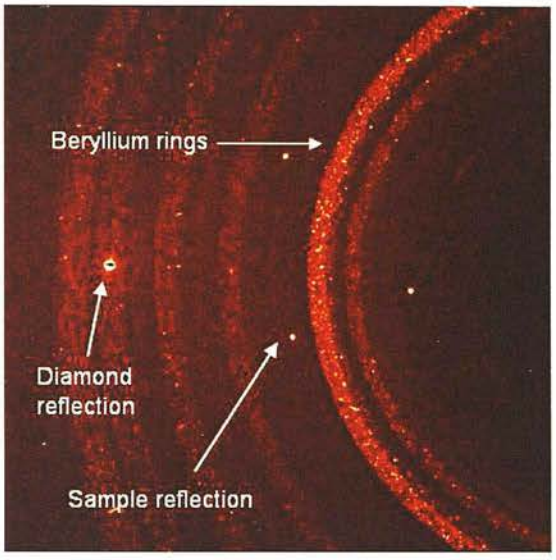

Figure 2.9: Bruker Smart CCD data frame taken for high-pressure sample contained in a DAC.

A thresholding algorithm in the *APEX* 2 program was used to harvest sample reflections [22]. In most cases, manual editing of the data set was required to remove spots arising from the DAC (Figure 2.10) and was performed by using a reciprocal lattice viewer (*e.g.* BrukerNonius *RLATT*). Orientation matrices and unit cell parameters were obtained using the same program unless otherwise specified. Data integration and global-cell refinement were performed using the program *SAINT* [23]. Dynamic masks were applied during integration to ensure that intensity data were not harvested from the regions of the detector that are shaded by the body of the DAC and areas of intense diffraction from beryllium. The use of dynamic masks during the data integration has been shown to improve significantly the results from such experiments.

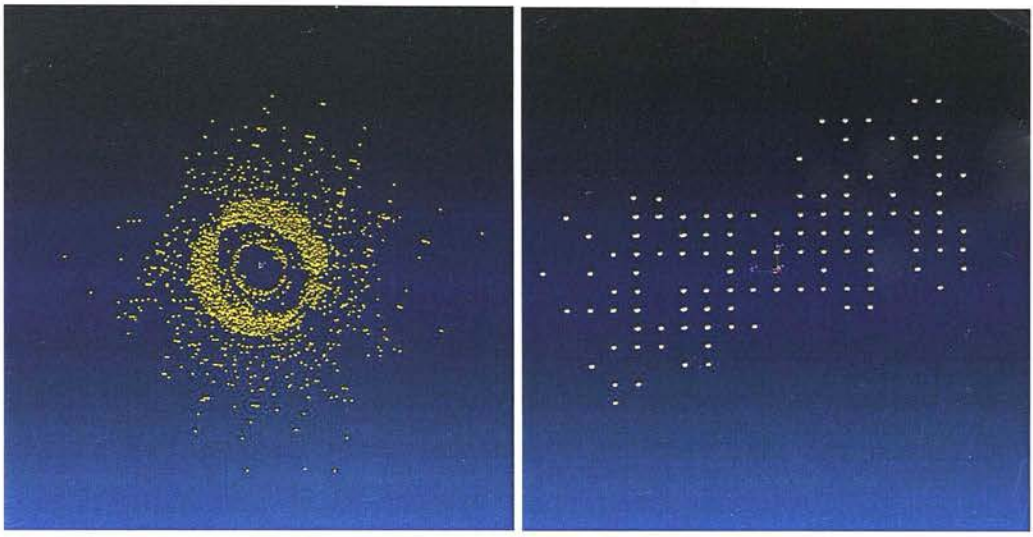

Figure 2.10: Pictures of diffraction spots taken from reciprocal space editor (BrukerNonius RLATT), unedited (left) and edited (right)

The quality of the data can be improved by applying various corrections as described by Dawson *et al.* [21]. An analytical absorption correction was performed using the program *SHADE* [24]. This rejects reflections that lie within 2° of the high-pressure cell opening angle (40°) and have poorly fitting profiles. In the next step, a multi-scan absorption correction was performed using the program *SADABS* [25], to correct for the differences in path lengths of X-rays through the crystals, which varied as the crystal orientation changed. The data were then merged using the program *SORTAV* [26] in the WinGX [27] suite of programs.

The structures reported in this thesis were solved by reciprocal-space methods (direct methods: *SHELXS* [28], *Sir*92 [29], *Sir*2002 [30]), as detailed in each chapter.

One of the main problems with the high-pressure data is caused by the limited opening angle of the DAC, which is generally between 80-90°. This restricts the volume of reciprocal space that can be accessed during data collection. This can be exacerbated by an unfortunate orientation of the crystal inside DAC. The low resolution of the data can cause further difficulties. Fortunately they may be overcome using direct-space methods which have previously been used for solution

of structures from powder diffraction data [31]. This particular area has developed significantly in the last few years, with the introduction of global optimisation methods for structure solution from powder samples. The success of these methods results from the fact that the problem of structure solution is reduced to determining only molecular position, orientation and internal conformation within the unit cell. However, these methods are only successful when the molecular contents of the crystal structure are known. Fortunately, for the high-pressure recrystallisation studies the main molecular contents are already known. These structure solution methods have successfully been used to solve structures from high-pressure single-crystal data sets collected on a range of small molecule structures [32].

Once a solution has been obtained, structure refinement was performed using the program *CRYSTALS* [33], which will be described in each relevant section. Various strategies were used during refinement (*e.g.* the use of restraints to increase the data to parameter ratio).

2.5.2. X-ray powder diffraction

Single crystal X-ray diffraction remains a benchmark technique. It provides direct information about covalent bond lengths, bond angles and molecular conformation and intermolecular interactions, such as hydrogen bonds. However, the technique requires sufficiently large crystals of good quality. When crystals of a suitable size/quality are not available for a single-crystal experiment, then powder diffraction can be a useful alternative.

The basic principle of X-ray powder diffraction is the same as single crystal X-ray diffraction, except that a small quantity of polycrystalline powder is used in the experiment. X-rays of known wavelength are passed through the powder, which consists of an essentially infinite number of tiny crystals, and this produces concentric rings for each reflection (Figure 2.11), with the radii determined by the Bragg equation. The resulting powder-pattern gives a number of sharp peaks of intensity versus diffraction angle (2θ). Each peak corresponds to one or more Bragg

planes. Identifying the plane(s) associated with each peak and the peaks angular position in 2θ gives the unit cell. The intensities of the peaks give information on the positions of the various atoms in the unit cell, but this is rarely straightforward because the intensity for each peak may be due to a number of overlapping Bragg reflections. Therefore, it is difficult to assign intensity to each without knowing the location of the atoms in the first place. By grinding up the crystalline material into a fine powder with randomly oriented grains much of the 3D spatial information from the diffraction pattern has been lost. Only the single dimension of the scattering angle remains, and this makes the problem of indexing and obtaining any specific intensity measurements rather difficult.

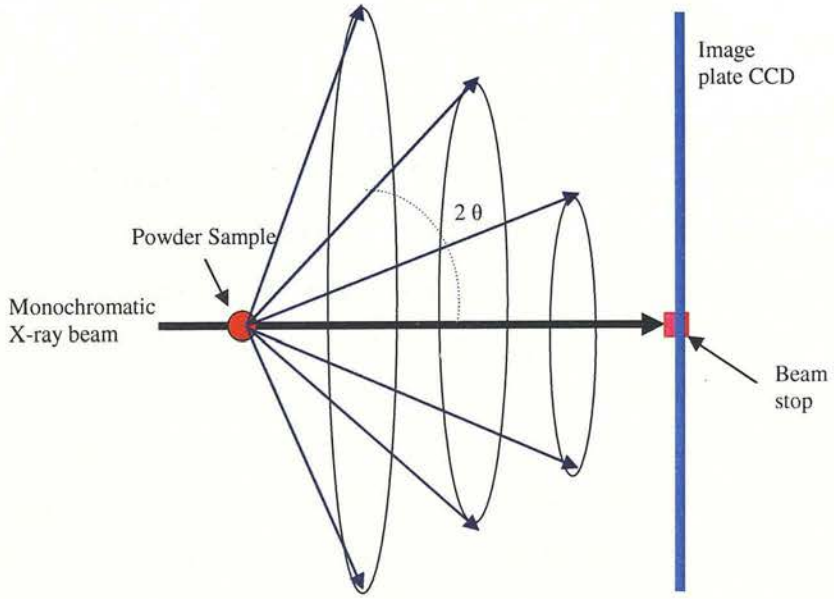

Figure 2.11: Schematic diagram of powder diffraction

The main advantage of powder diffraction is that it is far easier to obtain a powder of a sample as opposed to a single crystal, as in some cases it is difficult to grow a suitable crystal for single crystal X-ray diffraction. In addition, powder X-ray diffraction experiments are much quicker to perform than single-crystal X-ray diffraction experiments, and the technique is therefore an excellent method for phase identification.

X-ray powder diffraction is also proving a very powerful tool in high-pressure crystallography especially in identifying phase transitions caused by pressure. However, the sample volume in DAC suitable for X-ray powder diffraction studies is very small (≤100 μm across). The resulting low signal-to-noise ratio makes it very difficult to obtain useful results with monochromatic angle-dispersive techniques, and the alternative white beam energy-dispersive techniques have limited resolution and generally give unreliable peak intensities. Due to these reasons, all high-pressure powder studies are performed exclusively with synchrotron X-ray source where the introduction of the image-plate two-dimensional detector allows angle-dispersive methods to be used with a greatly increased signal and improved powder averaging. The detailed description of the technique is given by Nelmes and McMahon [34, 35].

The high-pressure X-ray diffraction experiments described in thesis were performed on Station 9.5 HPT (λ= 0.44397 Å) at the SRS Daresbury Laboratory, Warrington, UK and on Beamline I15 (λ= 0.444 Å) at the Diamond Light Source, Oxfordshire. A focusing monochromator using Laue geometry was used to provide the monochromatic beam at the desired wavelength [36]. This focused beam was used to probe the samples contained in a DAC. The scattered radiation was then collected on an image-plate area detector (Mar345). Any intense diffraction peaks due to diamonds were masked and the remaining two-dimensional pattern was then integrated to obtain a one dimensional powder-diffraction pattern with the help of *FIT2D* software for further processing [37]. The experimental set up on Station 9.5 is shown in Figure 2.12 and 2.13, with an example of a powder diffraction pattern detected on an image plate illustrated in Figure 2.14.

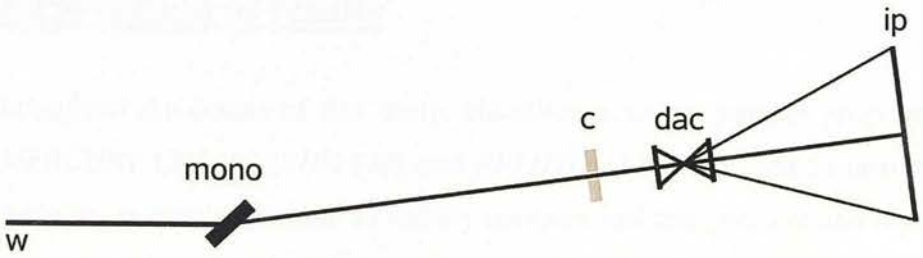

Figure 2.12: Schematic of Station 9.5.

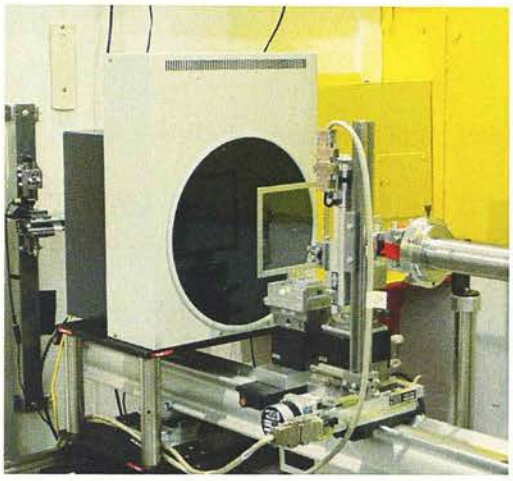

Figure 2.13: Experimental arrangement at Station 9.5 HPT.

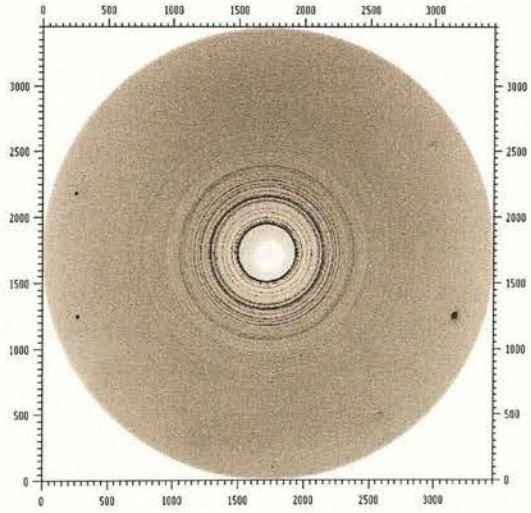

Figure 2.14: Powder pattern obtained from Station 9.5 HPT using an image-plate.

2.6. Interpretation of results

Throughout the course of this study, visualisation using graphics programs such as *MERCURY* [38], *PLATON* [39] and *RPLUTO* [40] were used to analyse results. These are particularly useful to rapidly compare ambient-pressure and high-pressure polymorphs, where packing and intermolecular interactions may be considerably different for each polymorph.

2.7. References

1. P. W. Bridgman, *The Physics of High-pressure*, Dover Publications, New York, USA, 1971.
2. A. V. Valkenburg Jr., *Rev. Sci. Instrum.*, 1962, **33**, 1462.
3. C. E. Weir, G. J. Piermarini and S. Block, *Trans. Am. Cryst. Assoc.*, 1969, **5**, 105-111.
4. L. Merrill and W. A. Bassett, *Rev. Sci. Instrum.*, 1974, **45**, 290-294.
5. R. Miletich, D. R. Allan and W. F. Kuhs, *Rev. Mineral. Geochem.*, 2001, **41**, 445-519.
6. S. A. Moggach, D. R. Allan, S. Parsons and J. E. Warren, *J. Appl. Crystallogr.*, 2008, **41**, 249-251.
7. R. J. Angel, M. Bujak, J. Zhao, G. D. Gatta and S. D. Jacobsen, *J. Appl. Crystallogr.*, 2007, **40**, 26-32.
8. G. J. Piermarini, S. Block and J. D. Barnett, *J. Appl. Phys.*, 1973, **44**, 5377-5382.
9. T. Varga, A. P. Wilkinson and R. J. Angel, *Rev. Sci. Instrum.*, 2003, **74**, 4564-4566.
10. I. D. H. Oswald, I. Chataigner, S. Elphick, F. P. A. Fabbiani, A. R. Lennie, J. Maddaluno, W. G. Marshall, T. J. Prior, C. R. Pulham and R. I. Smith, *CrystEngComm*, 2009, **11**, 359-366.
11. F. P. A. Fabbiani, D. R. Allan, W. I. F. David, A. J. Davidson, A. R. Lennie, S. Parsons, C. R. Pulham and J. E. Warren, *Cryst. Growth Des.*, 2007, **7**, 1115-1124.
12. F. P. A. Fabbiani and C. R. Pulham, *Chem. Soc. Rev.*, 2006, **35**, 932-942.
13. G. Jenner, *Mini-Rev. Org. Chem.*, 2004, **1**, 9-26.
14. F. P. A. Fabbiani, D. R. Allan, S. Parsons and C. R. Pulham, *CrystEngComm*, 2005, **7**, 179-186.
15. F. Datchi, A. Dewaele, P. Loubeyre, R. Letoullec, Y. Le Godec and B. Canny, *High Pressure Res.*, 2007, **27**, 447-463.
16. R. A. Forman, G. J. Piermarini, J. D. Barnett and S. Block, *Science*, 1972, **176**, 284-285.
17. G. J. Piermarini, S. Block, J. D. Barnett and R. A. Forman, *J. Appl. Phys.*, 1975, **46**, 2774-2780.

18. G. D. E. Smith, *Modern Raman Spectroscopy: A Modern Approach*, Wiley and Sons, Hoboken, USA, 2005.
19. W. Massa, *Crystal Structure Determination*, Springer-Verlag, Berlin, Germany, 2000.
20. H. L. M. Giacovazzo, D. Viterbo, F. Scordardi, G. Gilli, G. Zanotti, M. Catti, *Fundamentals of Crystallography*, Oxford Univeristy Press, Oxford, UK, 1992.
21. A. Dawson, D. R. Allan, S. Parsons and M. Ruf, *J. Appl. Crystallogr.*, 2004, **37**, 410-416.
22. B. AXS, *APEX 2*, Bruker-AXS, Madison, Wisconsin, USA, 2006.
23. B. AXS, *SAINT*, Bruker-AXS, Madison, Wisconsin, USA, 2003.
24. S. Parsons, *SHADE*, University of Edinburgh, Scotland, UK, 2004.
25. G. M. Sheldrick, *SADABS*, University of Göttingen, Germany, 2006.
26. R. Blessing, *Acta Crystallogr., Sect. A: Found. Crystallogr.*, 1995, **51**, 33-38.
27. Anon, *J. Appl. Crystallogr.*, 1999, **32**, 837-838.
28. G. M. Sheldrick, *SHELXS*, Bruker-AXS, Madison, Wisonsin, USA, 1997.
29. A. Altomare, G. Cascarano, C. Giacovazzo and A. Guagliardi, *J. Appl. Crystallogr.*, 1993, **26**, 343-350.
30. M. C. Burla, M. Camalli, B. Carrozzini, G. L. Cascarano, C. Giacovazzo, G. Polidori and R. Spagna, *J. Appl. Crystallogr.*, 2003, **36**, 1103.
31. K. S. W.I.F. David, L.B. McCusker, and C. Bärlocher, *Structure Determination from Powder Diffraction Data*, Oxford University press, Oxford, 2002.
32. F. P. A. Fabbiani, Ph.D Thesis, University of Edinburgh, 2005.
33. P. W. Betteridge, J. R. Carruthers, R. I. Cooper, K. Prout and D. J. Watkin, *J. Appl. Crystallogr.*, 2003, **36**, 1487.
34. R. J. Nelmes and M. I. McMahon, *J. Synchrotron Radiat.*, 1994, **1**, 69-73.
35. R. J. Nelmes and M. I. McMahon, *Adv. X-Ray Anal.*, 1994, **37**, 419-432.
36. A. R. Lennie, D. Laundy, M. A. Roberts and G. Bushnell-Wye, *J. Synchrotron Radiat.*, 2007, **14**, 433-438.
37. A. P. Hammersley, S. O. Svensson, M. H. and, A. N. Fitch and D. Hausermann, *High Pressure Res.*, 1996, **14**, 235-248.
38. C. F. Macrae, P. R. Edgington, P. McCabe, E. Pidcock, G. P. Shields, R. Taylor, M. Towler and J. van de Streek, *J. Appl. Crystallogr.*, 2006, **39**, 453-457.
39. A. L. Spek, *PLATON,* Utrecht University, Utrecht, Netherlands, 2008.
40. W. D. S. Motherwell, G. P. Shields and F. H. Allen, *Acta Crystallogr., Sect. B: Struct. Sci.*, 1999, **B55**, 1044-1056.

Chapter 3

High-Pressure Studies of Mefenamic acid

Chapter 3: High-Pressure Studies of Mefenamic acid

3.1. Background

Mefenamic acid (2-{(2, 3-dimethyl phenyl)-amino} benzoic acid), is a well known fenamate derivative showing potent analgesic effect [1] and is marketed as Ponstel®. It belongs to the group of medicines called non-steroidal anti-inflammatory drugs (NSAIDs), which are among the most frequently used medicinal drugs. They are utilised primarily as analgesics, anti-inflammatories and antipyretics, and their effects have been well studied [2]. They work by blocking the action of the enzyme cyclo-oxygenase that is involved in the production of prostaglandins in the body [3]. Prostaglandins are produced in response to injury or certain diseases and cause pain, swelling and inflammation. As mefenamic acid (MA) blocks the production of prostaglandins, it is effective in relieving various types of pain and inflammation, *e.g.* for pain related to menstrual disorders. The neuroprotective effects and improvement of cognitive impairment in Alzheimer's disease by the use of MA have recently been reported [4-6].

The molecular structure of MA with the numbering scheme used in this work is shown in Figure 3.1. It is structurally based on N-phenylanthranilic acid [7, 8]. The melting point of MA is *ca.* 231 °C [9, 10].

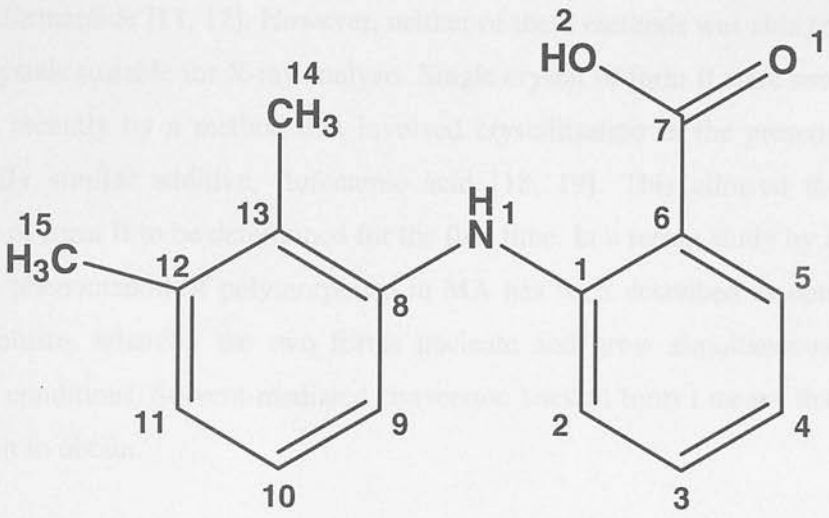

Figure 3.1: Mefenamic acid molecule, with numbering scheme used in this work.

MA is known to exist as two polymorphic forms, denoted as forms I and II, that are enantiotropically related. These polymorphs show different solubility and stability behaviour [11, 12]. Form I is the most stable form under ambient conditions, but form II is the stable form above 160 °C [13]. Gilpin and Zhou described an infrared method to study the thermal conversion of MA from form I to II [14], and observed that the rate of the conversion was dependent on the temperature. Form II rapidly transformed to form I in the presence of a solvent such as methanol and ethanol, even when its solubility is low [15]. The thermodynamic relationships involving the conversion between the two forms were studied by Anguiar and Zelmer [11]. They reported that the metastable form II of MA had a higher solubility than form I, but in the dissolution media form II was unstable and was completely converted to form I. The limiting step in the dissolution process was therefore attributed to the poor solubility of form I.

The crystal structure of form I was reported in 1976 [16]. NMR spectroscopy [17] and crystallographic and theoretical studies [7] have shown that form I has some conformational similarities with related fenamate compounds *e.g.* flufenamic acid, niflumic acid and maclofenamic acid. Until recently there were two known methods to obtain the metastable form II. These are (i) heating of form I above the transition temperature and (ii) rapid cooling of a supersaturated solution in *N,N*-

dimethylformamide [11, 12]. However, neither of these methods was able to produce single crystals suitable for X-ray analysis. Single crystal of form II were successfully obtained recently by a method that involved crystallisation in the presence of the structurally similar additive, flufenamic acid [18, 19]. This allowed the crystal structure of form II to be determined for the first time. In a recent study by Lee *et al.* [20], the phenomenon of polymorphism in MA has been described as concomitant polymorphism, whereby the two forms nucleate and grow simultaneously under identical conditions. Solvent-mediated conversion back to form I means that form II is difficult to obtain.

One of the problems for the delivery of MA to patients is its poor water-solubility and absorption characteristics. Significant effort has therefore been made to improve the dissolution behaviour in order to enhance the drug's bioavailability [9, 21, 22]. Form II exhibited higher solubility than form I in several solvent systems. The dissolution profile of form II showed initial super-saturation with respect to form I, but the solubility gradually decreased due to the transformation to form I. The dissolution profiles and solubilities of the two forms were examined in solvent mixtures of ethanol-water and ethyl acetate-ethanol by Romero *et al.* [9, 12]. Both forms showed high dissolution rates in the less polar mixture. Moreover, form II showed higher dissolution rates and solubility than form I. Park *et al.* presented a technique for determining the solubility of both stable and metastable polymorphs [9]. They used MA as a model compound along with carbamazepine and glycine. They showed that it is possible to measure the solubility of metastable forms using a DSC technique. Kato *et al.* [23] investigated the transformation kinetics of MA from form II to I in three different solvents under high humidity conditions. They showed that form II transformed to form I under all storage conditions and the rate of transformation depended on the nature of solvent. The nucleation and growth processes were significantly accelerated in ethanol compared with water. Furthermore, addition of seed crystals of the stable form I also reduced both nucleation and growth processes and resulted in an accelerated phase transition. Various strategies have been employed to overcome the problems arising from the low solubility of MA. These include production of a MA complex with cyclodextrins

and alkalonamids [24, 25]. Some complexes of MA with metal ions have also been reported [26, 27].

The compression behaviour of the two polymorphs has been studied in connection with the mechanical properties of the finished tablets, but very little attention has been paid to possible polymorphic transitions of the active ingredient under mechanical treatment [28]. All polymorph screening has been performed at ambient pressure [29]. The aim of the current investigation was therefore to explore whether high-pressure methods could be used to obtain the elusive form II, or other new forms.

3.2. Results and discussion

3.2.1. Direct compression of a single crystal of form I

High pressures for single-crystal X-ray diffraction studies were generated using a Merrill-Bassett diamond anvil cell (DAC) [30] equipped with 600 μm culet diamonds and a tungsten gasket. A single crystal of form I obtained from recrystallisation of a saturated solution of MA in THF (tetrahydrofuran) and a small ruby chip were loaded into the DAC. A methanol-ethanol (4:1) mixture was used as the pressure-transmitting medium [31]. The pressure applied to the sample was determined by the ruby fluorescence method [32] using a 632.8 nm excitation line from a He-Ne laser. The fluorescence was detected by a Jobin-Yvon LabRam 300. High-pressure data sets were collected using ω-scans in 12 settings of 2θ and φ with step size 0.3° for 1 second [33]. Diffraction data were collected on a Bruker-Nonius *APEX-II* diffractometer with silicon-monochromated synchrotron radiation on Station 16.2SMX (λ= 0.797 Å) at the SRS, Daresbury Laboratories.

The first data-set was collected at ambient pressure. Indexing of the reflections confirmed the known triclinic form I of MA. Diffraction data were then collected in incremental steps of pressure up to 2.5 GPa. Data indexing from all the data sets were performed using the indexing programme *CELL_NOW* [34]. Lattice

parameters at pressures up to 2.5 GPa are shown in Table 3.1. On raising the pressure to 3.0 GPa the crystal disintegrated.

Pressure	**ambient**	**0.18 GPa**	**0.49 GPa**	**0.90 GPa**	**1.67 GPa**	**2.50 GPa**
Crystal System	Triclinic	Triclinic	Triclinic	Triclinic	Triclinic	Triclinic
Space group	*P*-1	*P*-1	*P*-1	*P*-1	*P*-1	*P*-1
a **(Å)**	6.7582(14)	6.775(2)	6.7120(13)	6.6432(3)	6.5642(13)	6.5153(13)
b **(Å)**	7.3391(15)	7.288(2)	7.2369(14)	7.1516(6)	7.1406(14)	7.0188(14)
c **(Å)**	14.3127(29)	14.303(15)	14.0762(28)	13.7098(8)	13.4047(27)	13.1342(26)
α (°)	76.69(3)	76.72(5)	77.02(3)	77.724(6)	77.888(3)	78.38(26)
β (°)	79.83(3)	79.11(5)	79.43(3)	78.962(4)	77.426(3)	77.11(3)
γ (°)	65.70(3)	65.55(2)	65.72(3)	65.606(6)	63.846(3)	62.82(3)
V (Å^3)	626.94(31)	622.1(7)	604.1(31)	575.69(6)	545.78(2)	535.0(17)
Z	2	2	2	2	2	2
T (K)	293(2)	293(2)	293(2)	293(2)	293(2)	293(2)

Table 3.1: Lattice parameters for form I with increasing pressure up to 2.50 GPa.

All data sets up to 2.50 GPa were processed according to the procedure described in chapter 2. As a result of the limitations caused by shading from the steel body of the diamond-anvil cell, high-pressure data-sets are frequently incomplete compared with data-sets recorded at ambient pressure. These factors combined to make structural refinement particularly challenging and in this case resulted in poor structural refinement with high *R*-factors. Therefore, only lattice parameters are reported here. Figure 3.2 shows the variation of unit cell volume with increasing pressure. There was a *ca.* 14 % decrease in the unit cell volume over the studied pressure range. Within the limits of experimental errors, the volume decreases smoothly over this pressure range, indicating that there is no phase transition associated with direct compression of the single crystal.

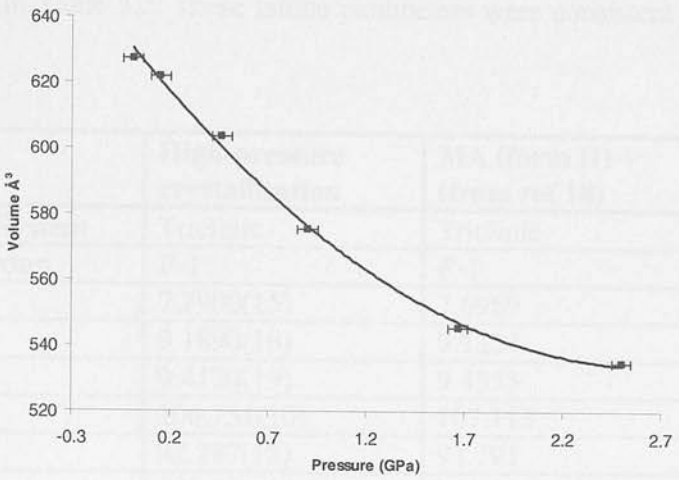

Figure 3.2: variation of unit cell volume of form I with pressure.

The observation that at 3.0 GPa the crystal disintegrated to give a polycrystalline powder, suggests reconstructive phase transition at this pressure. These observations prompted a study by recrystallisation from solution at high pressure.

3.2.2. Crystallisation from solution at high pressure

A *ca.* 1M solution of mefenamic acid was prepared in ethanol. The solution was then loaded along with a few crystallites of form I at 293(2) K into a DAC. A small piece of ruby was also added in order to allow the determination of the pressure by laser fluorescence spectroscopy [32]. The pressure was increased to a minimum in order to form a sealed system and the cell was then gently heated to dissolve all of the solid material. Pressure was then applied by tightening the screws of the DAC to induce precipitation. Crystallisation was achieved at *ca.* 0.6 GPa. The pressure was then reduced to 0.3 GPa in order to facilitate growth of a single crystal. The temperature was then cycled near 353 K in order to dissolve all but one of the crystallites. On slow cooling to 298 K a single crystal grew. Diffraction data were then collected on a Bruker *APEX II* CCD diffractometer by using ω-scans in 12 settings of 2θ and φ with step size 0.3° for 30 s. Data indexing was performed using the indexing programme *CELL_NOW* [34]. This gave a triclinic unit cell with lattice

parameters shown in Table 3.2. These lattice parameters were consistent with those of form II [18].

	High-pressure crystallisation	**MA (form II) (from ref 18)**
Crystal System	Triclinic	Triclinic
Space group	*P*-1	*P*-1
a **(Å)**	7.7900(15)	7.6969
b **(Å)**	9.1890(18)	9.1234
c **(Å)**	9.4120(19)	9.4535
α **(°)**	106.751(10)	107.113
β **(°)**	92.287(12)	91.791
γ **(°)**	101.337(11)	101.481
V **(Å^3)**	629.1(2)	618.89
Z	2	2
P/GPa	0.30(5)	0.0
T/K	293(2)	150(2)

Table 3.2: Lattice parameters for form II of MA.

Data processing was performed according to the procedure described by Dawson *et al.* (2004) [35] and detailed in chapter 2. Integration of data sets and global cell refinement were carried out using the program *SAINT* [36], in which 'dynamic masks' were used in order to prevent integration of areas of the detector shaded by the body of the DAC. An analytical correction for the absorption by the DAC component was then applied using *SHADE* [37] and an absorption correction for the crystal was applied using *SADABS* [38]. Known coordinates were taken from the literature [16]. Refinement was then performed using *CRYSTALS* [39]. All non-hydrogen atoms were refined isotropically and hydrogen atoms were placed in calculated positions. A completeness of only *ca.* 40 % was obtained for this dataset and this led to a rather high *R*-factor of 9.5 %. Nevertheless, this was sufficient to identify the main structural features of form II and make a comparison between the polymorphs. Full structural refinements details are shown in Appendix A. Crystallographic data in CIF format are available on the attached CD.

3.2.2.1. Decompression studies

On progressive decompression from 0.3 GPa at 293 K to ambient pressure, no colour change or destruction of the crystal was observed. This tiny crystal was then removed from gasket, placed on the goniometer and was successfully indexed as form II. However, owing to poor quality and the damage done during unloading from the gasket it was not possible to obtain sufficiently good data for full structure refinements. The crystal was also used as a seed in order to attempt the growth of single crystals of form II at ambient pressure, but this resulted in the production of form I instead. This suggests that presence of form I seeds in solution may dominate the crystallisation process.

In order to demonstrate reproducibility, repeated crystallisation at high pressure always resulted in form II. These results are of great significance as they demonstrate that form II can be prepared reproducibly at high pressure and recovered successfully to ambient pressure. Furthermore, unlike in the study by Lee *et al.*, [18] no additives were required. This may suggest that the form II is the more thermodynamically stable form at high pressure, mirroring the behaviour of paracetamol [40].

3.2.3. Comparison of the crystal structures of forms I and II

Crystallographic data for forms I and II are summarised in Table 4.3. The structures of forms I and II have been previously described by McConnell *et al.*, [16] and Lee *et al.*, [18] respectively .

parameter	MA II (high-pressure crystallisation)[a]	MA II (Lee, Byrn and Carvjal)[b]	MA I (CSD:XYANAC)[c]
Chemical formula	$C_{15}H_{15}NO_2$	$C_{15}H_{15}NO_2$	$C_{15}H_{15}NO_2$
Formula weight	241.29	241.29	241.29
Crystal system	*P*-1	*P*-1	*P*-1
Space group	Triclinic	Triclinic	Triclinic
a (Å)	7.7900(15)	7.6969	14.556
b (Å)	9.1890(18)	9.1234	6.811
c (Å)	9.4120(19)	9.4535	7.657
α (°)	106.751(10)	107.113	119.57
β (°)	92.287(12)	91.791	103.93
γ (°)	101.377(11)	101.481	91.30
V (Å^3)	629.1(2)	618.89	631.766
Z	2	2	2
T (K)	298(2)	150	298
$R(F_o)$	0.095	0.052	0.045
$Rw(F^2_o)$	0.095	0.134	
Programme used	CRYSTALS	SHELXTL	MULTAN

[a] this study [b] E. H. Lee *et al.* [18][c] McConnell *et al.*[16]

Table 3.3: Comparison of cell parameters for forms I and II.

The molecular structure of MA with numbering scheme used in this work is shown in Figure 3.3. The conformation of the molecule in the crystal structure can be described by three torsional angles (see Figure 3.3): θ_1 (O1-C7-C6-C1) *i.e.* twisting of the carboxylic group with respect to C6-C7 axis; θ_2 (C1-N1-C8-C13) *i.e.* twisting of the second phenyl group with respect to the N1-C8 axis; and θ_3 (C6-C1-N1-C8) *i.e.* twisting of bridging group relative to the C1-N2 axis. These torsional angles are shown by arrows in Figure 3.3 and are calculated by using the program *MERCURY* [41].

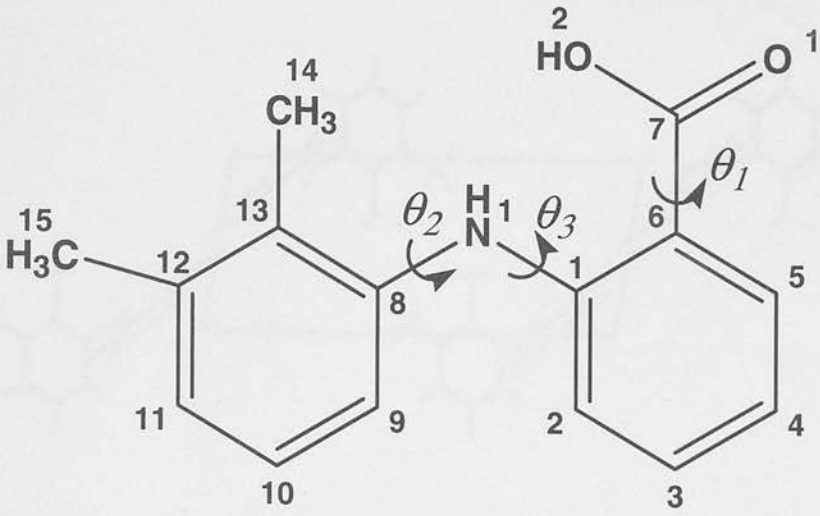

Figure 3.3: Mefenamic acid molecule, with numbering scheme used in this work. Definition of torsional angles: θ_1 is the angle involving O1-C7-C6-C1, θ_2 is the angle involving C1-N1-C8-C13 and θ_3 is the angle involving C6-C1-N1-C8.

3.2.3.1. Description of crystal structure of form I

The crystal packing diagram of form I is shown in Figure 3.4. There are two molecules in the unit cell. The phenyl ring bearing the carboxyl group is coplanar with the carboxyl- and bridging amino-groups. This coplanar conformation is stabilised by the resonance interaction and internal hydrogen bond between the amino- and carboxyl-groups [7]. The distance between the atoms (N1…O1) involved in this interaction is *ca.* 2.63 Å (Figure 3.5). The molecules pack as dimer units through an intermolecular hydrogen bond involving the carboxylic acid group (O2-H…O1) with an O2…O1 distance of 2.65 Å. Hydrogen bonding in form I can be best described with the aid of graph-set analysis. The graph-set notations are assigned by the method described by Bernstein *et al.* [42], and can be obtained from *PLUTO* [43] and *MERCURY* [41]. The description of the hydrogen-bond pattern in form II according to the graph-set notation at the first level graph set is N_1 = $S(6)R_2^2(8)$ where S and R motifs represents internal and external hydrogen bonds, respectively. The values for the three torsional angles θ_1, θ_2 and θ_3 are shown in Table 3.4.

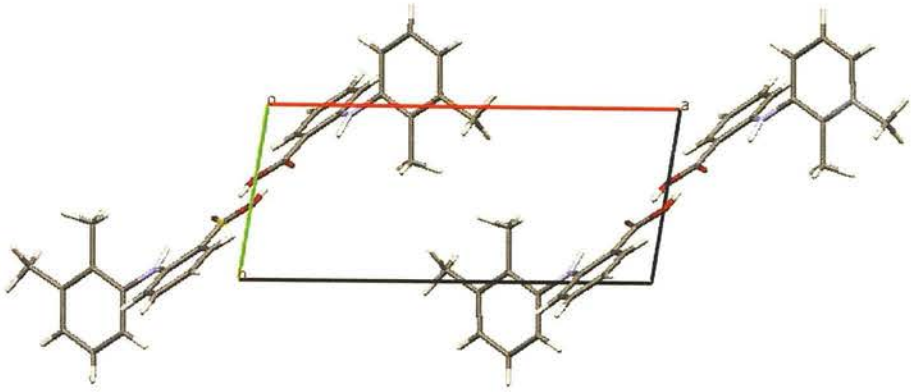

Figure 3.4: Crystal packing diagram of form I viewed down the *c*-axis.

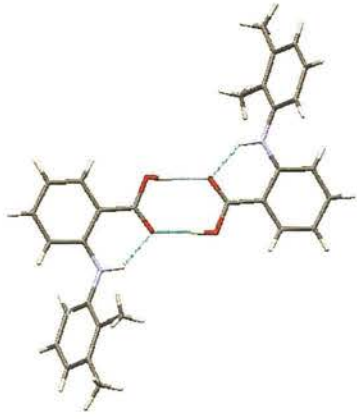

Figure 3.5: Dimer unit in form I.

3.2.3.2. Description of crystal structure of form II

The crystal packing diagram of form II is shown in Figure 3.6. Similar to form I the phenyl ring bearing the carboxyl-group is coplanar with the carboxylic acid group. There are two molecules in the unit cell which pack as dimer units by making two hydrogen bonds involving the carboxylic acid group. The distance between O2...O1 is *ca.* 2.65 Å, similar to that found in form I. An internal hydrogen bond with an N1...O1 distance of *ca.* 2.68 Å is also found in form II.

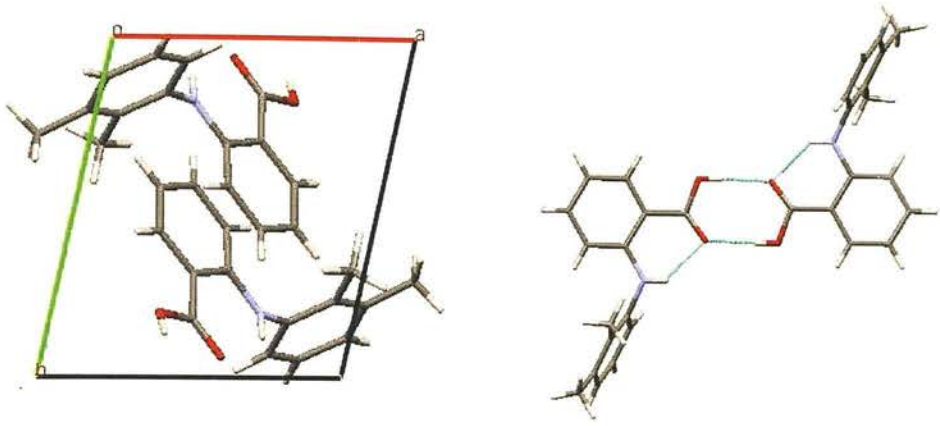

Figure 3.6: Crystal packing diagram of form II (left) and dimer packing unit of MA molecule as they pack in crystal structure of form II (right).

The comparison of space-filling diagrams (Figure 3.7) of forms I and II indicates more efficient packing of MA molecules in form II. The difference in the crystal packing between forms I and II arises from the torsional angle θ_2 (Table 3.4), where the values has changed significantly from -119.99° to -85.19°, whilst the deviation in the other two torsional angles, (θ_1 and θ_3) are very small. Due to changes in θ_2, the carboxylic acid group and the amino group are no longer coplanar in form II and as a result the length of the intramolecular hydrogen bond (N1...O1) increases slightly from 2.63 Å to 2.67 Å.

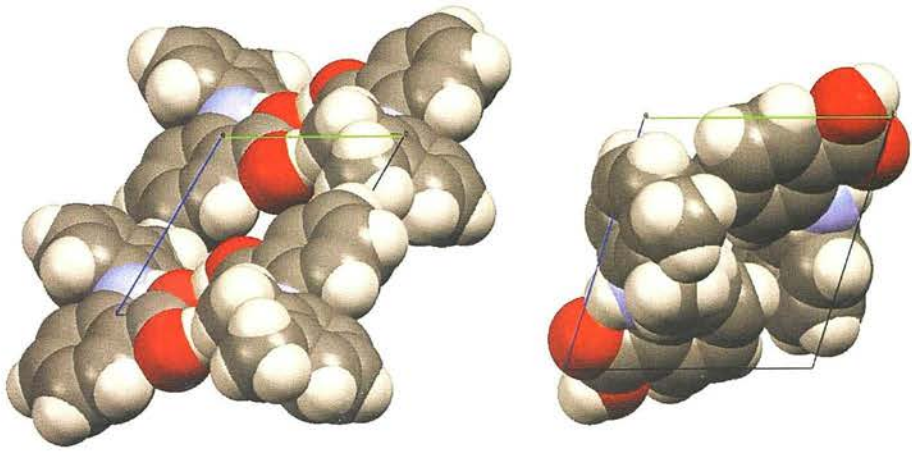

Figure 3.7: Space-filling diagrams for forms I (left) and II (right).

Torsional angle	MA I [16]	MA II [this study]
θ_1	-1.71	-5.30
θ_2	-119.99	-90.07
θ_3	-179.34	-171.56

Table 3.4: Comparison of torsional angles between forms I and II of MA.

3.2.4. Variable temperature X-ray powder diffraction

Variable temperature X-ray powder diffraction (XRPD) experiments were performed using an Anton Parr TTK450 heating and cooling stage (Figure 3.8) over the temperature range from 20 °C to 210 °C. About 1 g MA sample was presented as a flat pressed powder in a sample stage. XRPD data were collected on a Bruker AXS D8 diffractometer (operating at 40 kV, 40 mA), using Cu-$K\alpha$ radiation (λ = 1.5418 Å) with a position sensitive detector (PSD). Diffraction data were collected in the range 2θ = 2-30° with a step size of 0.02°.

Figure 3.8: Anton Parr TTK450 heating and cooling stage used for variable temperature XRPD.

The purpose of these experiments was to confirm that form II is the high-temperature form and to identify the transition temperature. Figure 3.9 shows the powder diffraction patterns of MA obtained at elevated temperature, starting from 50 °C up to 210 °C. The powder pattern at 50 °C represents pure form I, and characteristic Bragg peaks of form I were observed at 2θ values of 6.3, 21.3 and 26.3°. All peaks were consistent with the calculated powder pattern obtained from the crystal structure of form I. With increasing temperature up to 160 °C no changes except movement of peaks to lower 2θ value were observed. All patterns up to 160

°C were indexed as form I. At 170 °C a number of new peaks appeared in the pattern indicating transition to a new phase. These new peaks were observed at 2θ values of 11.8, 17.9, 23.8 and 25.6° and are characteristic of form II. Therefore the powder pattern at 170 °C represents a mixture of forms I and II. With increasing temperature, form I peaks gradually disappeared and the sample completely converted to form II. The pattern at 190 °C could be indexed as form II and represents pure form II. Further increase in temperature up to the melting point showed no further phase transitions. Optical observation showed a colour change from white to green-yellow on conversion to form II.

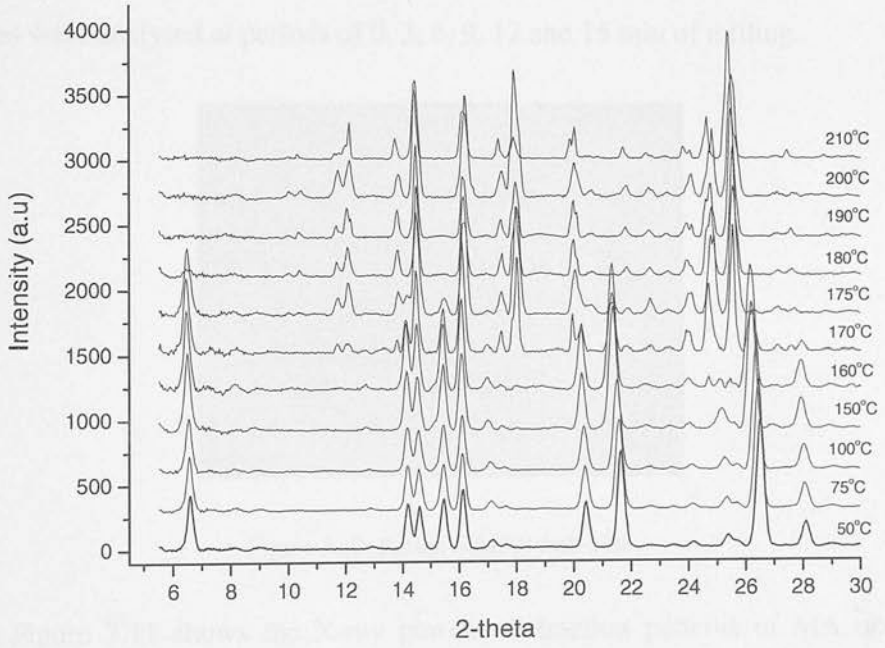

Figure 3.9: X-ray powder diffraction patterns of MA collected at temperature ranges 50 °C to 210 °C (λ = 1.5418 Å).

3.2.5. Dry grinding and milling experiments

Milling of MA was carried out in a Retsch MM301 Ball Mill, as shown in Figure 3.10. In a typical experiment, *ca.* 0.5 g of sample was loaded into the milling vessel along with a steel ball (mass *ca.* 30 g and diameter *ca.* 20 mm). The vessel was then shaken at 5 Hz for up to 15 min. XRPD and IR techniques were used to analyse powder samples after milling. XRPD data were collected on a Bruker D8 diffractometer using Cu-*K*α radiation (λ = 1.5418 Å) at 40 kV and 40 mA. Each sample was analysed between 2θ = 2-40° with a step size of 0.02°. Experimental powder patterns were compared to simulated powder patterns obtained from crystal structure. IR absorption spectra were collected in the ranges of 200-3500 cm^{-1}. Samples were analysed at periods of 0, 3, 6, 9, 12 and 15 min of milling.

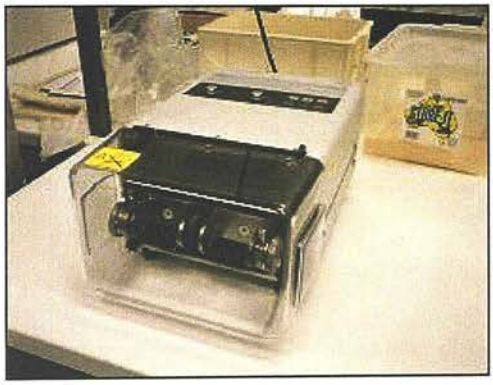

Figure 3.10: Retsch MM301 ball mill.

Figure 3.11 shows the X-ray powder diffraction patterns of MA obtained after different times of milling. Milling was initially performed in the absence of any solvent or liquid. The starting form was form I, represented by bottom pattern in Figure 3.11. No changes were observed in the pattern after 3 min of milling. In the pattern obtained after 6 min of milling, new peaks at values of 2θ = 12.1, 17.3 and 24.1 appeared. These peaks were attributable to form II and therefore this pattern represents a mixture of forms I and II. After 15 mins of milling, all of the sample had been converted to form II. It was also noticeable from the patterns that there was an increase in background intensity, and that the peaks became broader with increasing

time of milling. These changes can be attributed to both possible size reduction and partial amorphisation of the sample as grinding progressed. Thus, not only was the phase transition observed by milling but a decrease in crystallinity was also achieved, which may account for the increase in the dissolution rate of MA [28].

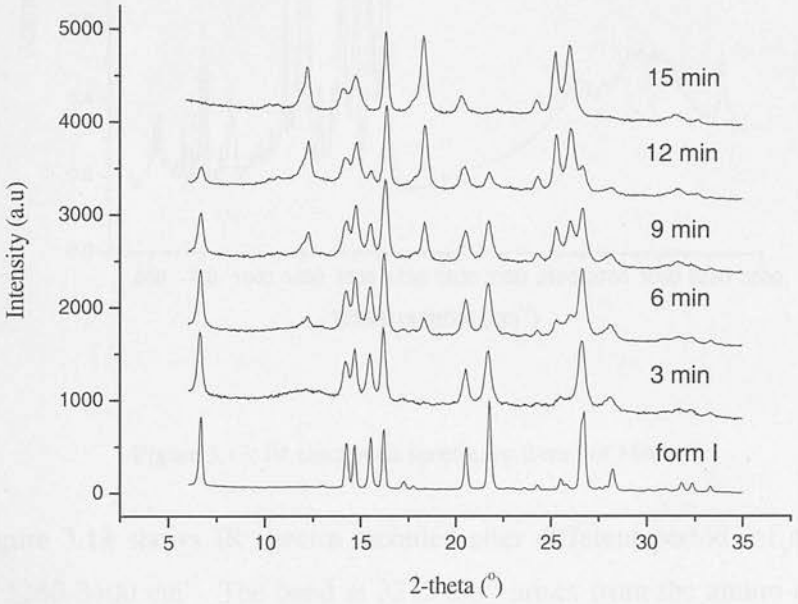

Figure 3.11: X-ray powder diffraction patterns of MA collected after different times of dry milling (λ = 1.5418 Å).

X-ray powder diffraction results are supported by IR spectroscopic measurements. Figure 3.12 shows the IR spectrum recorded as a KBr disc of a MA powder sample. The spectrum agrees with that previously published for form I [12]. An important spectral feature that can be used to distinguish between polymorphs of MA is the N-H stretching band that occurs in the range 3300-3350 cm^{-1}.

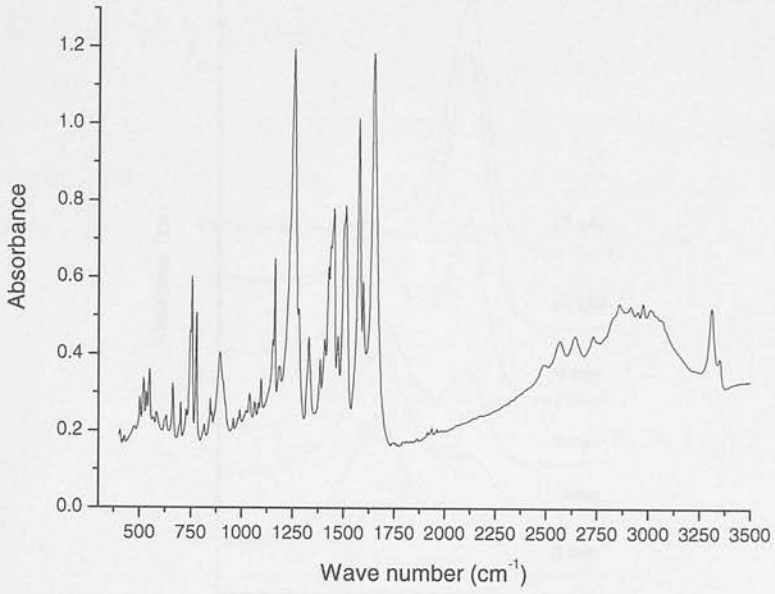

Figure 3.12: IR absorption spectra for form I of MA.

Figure 3.13 shows IR spectra recorded after different periods of milling, in the range 3250-3400 cm^{-1}. The band at 3312 cm^{-1} arises from the amino-group that forms an intramolecular hydrogen bond with the carboxyl-group (Figure 3.1) associated with form I. During milling, the intensity of this band decreases and a band at 3353 cm^{-1} begins to grow. This new band is significantly less broad than the initial band at 3312 cm^{-1}. Both of these observations can be interpreted by the transformation of form I to II. In form I, the N-H bond is involved in a relatively strong interaction with the carbonyl group (N...O distance is 2.63 Å). In form II, this distance increases to 2.67 Å, indicating a weaker interaction. This results in the N-H bond becoming stronger and hence shifting to higher energy. These spectral changes are consistent with the quantum mechanical calculations performed on the structure of MA [21, 44].

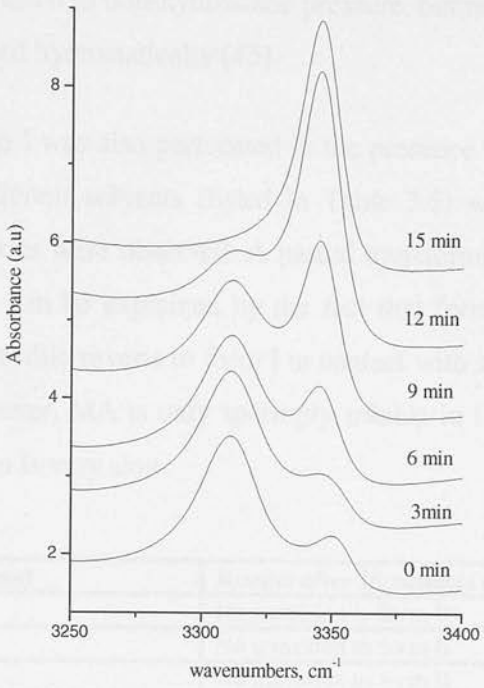

Figure 3.13: Comparison of IR absorption spectra (3250-3400 cm^{-1}) of MA recorded over short periods of milling.

In the milling process, not only are shear and stress forces applied, but a heating of the mill assembly (typically up to *ca.* 50 °C) occurs. This is a relatively modest temperature rise, and would be insufficient to transform form I to form II (transition temperature is *ca.* 170 °C). However, it is also necessary to consider the effect of *local* heating when the steel ball impacts on the wall of the mill. Hence the question arises as to whether the transformation induced by milling is caused by pressure or temperature. To answer this, an experiment was performed in which the sample was milled in the presence of an excess of dry ice at a temperature of -78 °C. The results showed that under these conditions, form I did indeed transform to form II, indicating that it is a localised pressure increase that may be responsible for the transformation. Of course, this pressure is significantly lower than the hydrostatic pressure experienced in the diamond-anvil cell, but this may reflect the fact that the pressure experienced during ball-milling will be highly non-hydrostatic. Such phenomena are well documented in other systems, *e.g.* ammonium nitrate undergoes

a phase transition subjected to non-hydrostatic pressure, but no transition is observed when pressure is applied hydrostatically [45].

Milling of form I was also performed in the presence of a small amount (*ca.* 1 ml) of solvent. Different solvents (listed in Table 3.5) were used. In all cases except one, no transitions were observed. A partial transformation was observed for Fluorinert-FC77. This can be explained by the fact that form II is metastable with respect to form I and readily reverts to form I in contact with solvents in which it has some solubility. However, MA is only sparingly soluble in Fluorinert-FC77 and so the back transformation is very slow.

Solvent used	**Results after 15 minutes of milling**
Methanol	No transition to form II
Ethanol	No transition to form II
THF	No transition to form II
Water	No transition to form II
DMF	No transition to form II
Fluorinert-FC77	Partial transition to form II
Methanol: ethanol (4:1)	No transition to form II
Isopropyl alcohol	No transition to form II
DMSO	No transition to form II
Acetone	No transition to form II
Acetonitrile	No transition to form II

Table 3.5: Results from wet milling of MA with different solvents.

3.2.6. High-pressure X-ray powder diffraction experiments

High-pressure X-ray powder diffraction experiments were performed using a Merrill-Bassett diamond-anvil cell (half-opening angle 40°) [30]. A pre-indented tungsten gasket of thickness 250 μm with a 300 μm diameter hole was used. To improve the uniformity of polycrystalline material, the powder was ground using a mortar and pestle prior to loading into the cell. The powder was loaded with a small ruby chip to measure pressure using the ruby fluorescence technique. The pressure-transmitting medium used in these experiments was either a methanol:ethanol (4:1) mixture or Fluorinert-FC77. Pressure was increased in small steps and after each

pressure adjustment the DAC was allowed to stand as such for 2-3 hours. This also allowed any slow phase transitions to occur.

Powder diffraction patterns were collected with synchrotron X-ray radiation using Station 9.5HPT (λ= 0.4439 Å) at the SRS, Daresbury Laboratory. To improve the uniformity of the cones of diffracted radiation, the sample was continuously rastered over a range of $\pm$100 μm transverse to the incident X-ray beam in order to illuminate as many individual crystallites as possible. The scattered radiation was then collected on an image-plate area detector (Mar345). Any intense diffraction peaks due to diamonds were masked and the remaining two-dimensional pattern was then integrated to obtain a one dimensional powder diffraction pattern with using *FIT2D* software [46]. Data were initially processed by Datlab and Powder cell [47] and then further analysed by Le Bail methods using *GSAS* [48] with an *EXPGUI* [49] interface to refine unit cell parameters.

3.2.6.1. Powder compression using methanol:ethanol (4:1) as a pressure-transmitting medium

Figure 3.14 shows the powder diffraction patterns of MA collected at pressures between ambient and 2.8 GPa. Methanol:ethanol (4:1) mixture was used as the pressure-transmitting medium. The pattern recorded at ambient pressure was indexed as form I. On increasing the pressure to 1.1 GPa no significant changes were observed in the powder patterns except for the movement of peaks towards higher 2θ values. All the powder patterns up to 1.1 GPa could be indexed as form I, and the lattice parameters are shown in Table 3.6.

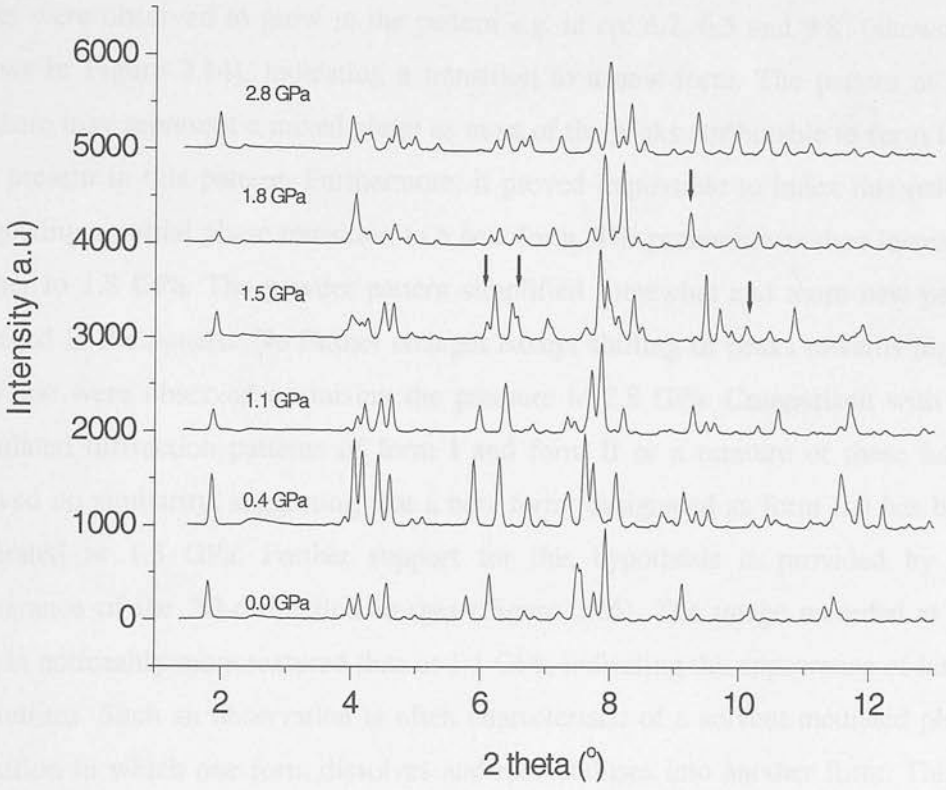

Figure 3.14: X-ray powder diffraction patterns of MA collected at pressure up to 2.8 GPa (λ = 0.4439 Å).

Pressure	**Ambient**	**0.45 GPa**	**1.1 GPa**
Crystal System	Triclinic	Triclinic	Triclinic
Space group	*P*-1	*P*-1	*P*-1
a **(Å)**	14.5668(9)	14.2918(15)	14.1320(11)
b **(Å)**	6.8138(6)	6.7251(7)	6.6688(5)
c **(Å)**	7.6476(5)	7.5770(6)	7.5152(5)
α **(°)**	119.405(4)	119.551(5)	119.528(5)
β **(°)**	103.905(5)	104.602(6)	105.149(5)
γ **(°)**	91.505(7)	91.469(8)	91.513(8)
V **(Å^3)**	632.49(8)	603.26(10)	584.61(8)
Z	2	2	2
T/K	298(2)	298(2)	298(2)

Table 3.6: Lattice parameters obtained from powder patterns up to 1.1 GPa.

In the next step the pressure was raised to 1.5 GPa. At this pressure new peaks were observed to grow in the pattern *e.g.* at *ca.* 6.2, 6.5 and 9.8° (shown by arrows in Figure 3.14), indicating a transition to a new form. The pattern at this pressure may represent a mixed phase as most of the peaks attributable to form I are still present in this pattern. Furthermore, it proved impossible to index this pattern suggesting a partial phase transition to a new form. The pressure was then increased further to 1.8 GPa. The powder pattern simplified somewhat and more new peaks emerged in the pattern. No further changes except shifting of peaks towards higher 2θ value were observed on raising the pressure to 2.8 GPa. Comparison with the calculated diffraction patterns of form I and form II or a mixture of these forms showed no similarity, suggesting that a new form (designated as form III) has been generated at 1.5 GPa. Further support for this hypothesis is provided by the appearance of the 2D-diffraction images (Figure 3.15). The image recorded at 1.5 GPa is noticeably more textured than at 1.1 GPa, indicating the appearance of larger crystallites. Such an observation is often characteristic of a solvent-mediated phase transition in which one form dissolves and recrystallises into another form. This is entirely possible since MA has a significant solubility in the methanol:ethanol mixture.

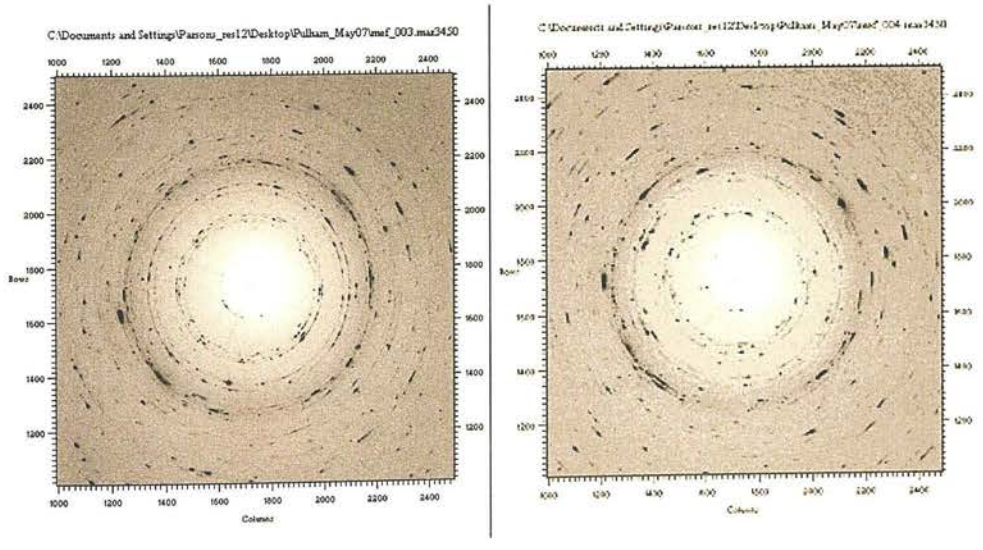

Figure 3.15: 2-D diffraction images of MA at 1.1 GPa (left) & 1.5 GPa (right).

There was some suspicion that the transition to the new form was incomplete as several peaks attributed to form I persisted. For this reason the pressure was cycled several times between 0.8 and 2.2 GPa. Figure 3.16 shows the comparison between patterns before and after this pressure cycling. It is evident from the results that the pattern has changed quite significantly, especially the low angle peak at *ca.* 1.8°, attributed to form I, which has completely disappeared. Moreover, broadening of the peaks was also observed with this pressure cycling. The pattern at 2.2 GPa after this cycling may represent the pure form III. However, all indexing attempts proved unsuccessful. The pressure was then increased to 3.2 GPa, but no significant changes were observed in the pattern.

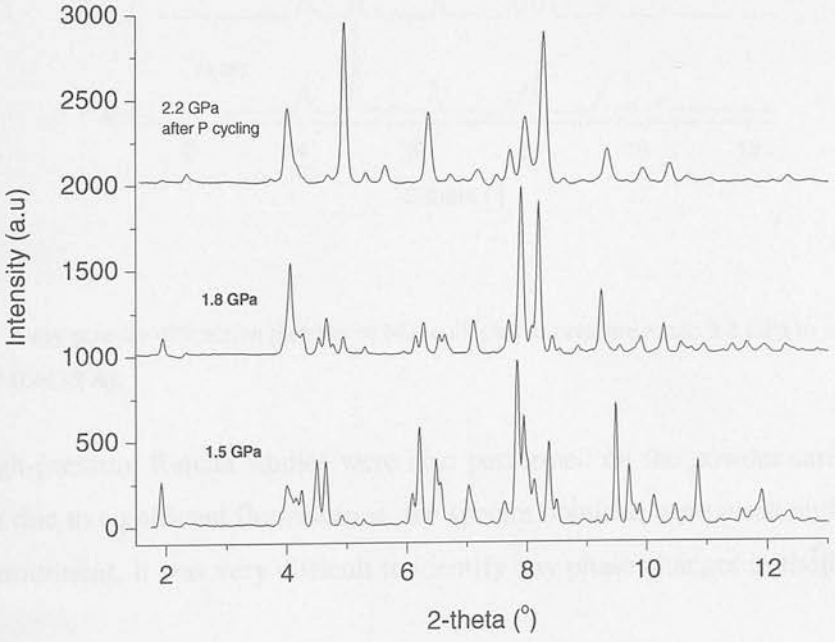

Figure 3.16: X-ray powder diffraction patterns of MA collected before and after pressure cycling (λ = 0.4439 Å).

In the next step the pressure was gradually reduced to ambient pressure. Figure 3.17 shows the powder patterns recorded after gradually releasing the pressure down to ambient pressure. There were no significant changes observed in

the powder patterns except for the movement of peaks towards lower 2θ values with the release of pressure, indicating that the new high-pressure form (form III) persisted on decompression.

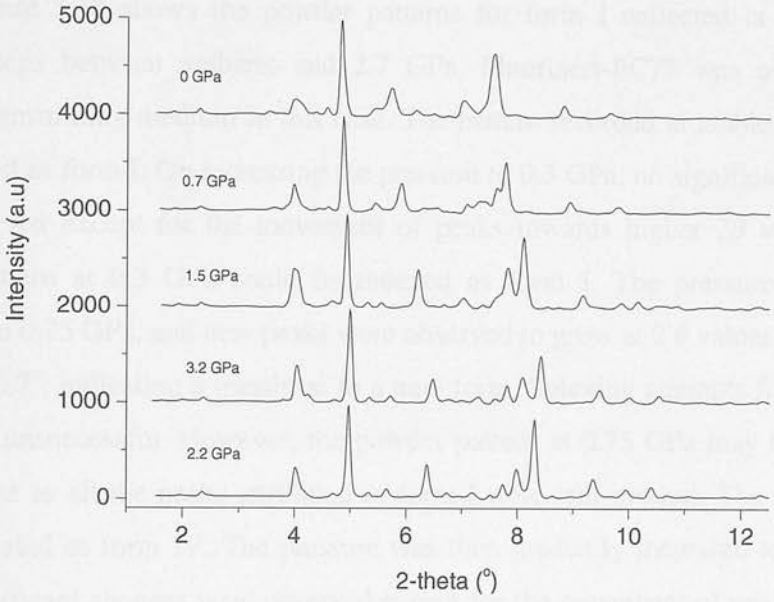

Figure 3.17: X-ray powder diffraction patterns of MA collected at pressure range 3.2 GPa to ambient-pressure ($\lambda = 0.4439$ Å).

High-pressure Raman studies were also performed on the powder sample of form I, but due to significant fluorescence, the spectra obtained were weak and peaks were not prominent. It was very difficult to identify any phase changes in the Raman spectra.

3.2.6.2. Powder compression using Fluorinert-FC75 as a pressure-transmitting medium

To avoid solvent-mediated effects on possible phase transitions it was decided to perform compression studies on powder samples of MA in the presence of a pressure-transmitting medium in which MA has a low solubility. Fluorinert-FC77, a fluorinated hydrocarbon, was selected for this purpose. For powder-compression

experiments in Fluorinert, the DAC was loaded with finely ground powder of either form I or form II in separate experiments.

Direct compression of powder sample of form I

Figure 3.18 shows the powder patterns for form I collected in increasing pressure steps between ambient and 2.7 GPa. Fluorinert-FC77 was used as the pressure-transmitting medium in this case. The pattern recorded at ambient pressure was indexed as form I. On increasing the pressure to 0.3 GPa, no significant changes were observed except for the movement of peaks towards higher 2θ values. The powder pattern at 0.3 GPa could be indexed as form I. The pressure was then increased to 0.75 GPa, and new peaks were observed to grow at 2 θ values of *ca.* 2.2, 10.5 and 10.7°, indicating a transition to a new form. Indexing attempts for this new form were unsuccessful. However, the powder pattern at 0.75 GPa may represent a mixed phase as all the peaks attributed to form I were still present. The new phase was designated as form IV. The pressure was then gradually increased to 2.7 GPa, but no significant changes were observed except for the movement of peaks towards higher 2θ values. However, broadening of the peaks with increasing pressure occurred on account of non-hydrostatic conditions associated with the pressure-transmitting medium.

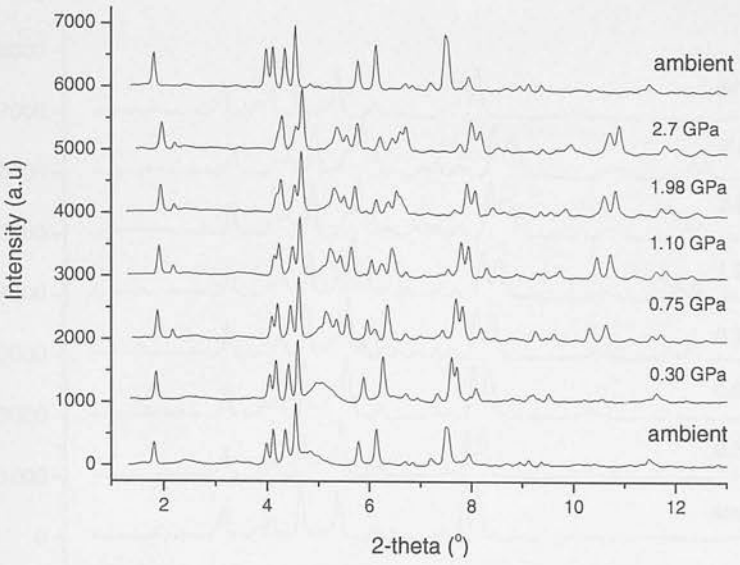

Figure 3.18: X-ray powder diffraction patterns of MA form I in Fluorinert-FC77 collected at pressures up to 2.7 GPa. The upper pattern represents the powder pattern obtained after reducing the pressure to ambient.

In the next step, the pressure was reduced to ambient. The powder pattern collected at ambient pressure (Figure 3.18) showed that the sample had transformed back to form I, indicating that the phase transition to form IV at 0.75 GPa was reversible.

Direct compression of powder sample of form II

Direct compression studies using Fluorinert-FC77 were also performed on the powder samples of form II. A DAC was loaded with powder samples of form II along with a ruby chip. Figure 3.19 shows the powder patterns for form II collected at increasing pressure steps between ambient and 2.8 GPa. The powder pattern at ambient pressure was successfully indexed as form II indicating no solvent mediated transition to form I. On increasing the pressure to 0.30 GPa and then to 0.57 GPa, no significant changes were observed. All the powder patterns up to 0.57 GPa could be indexed as form II.

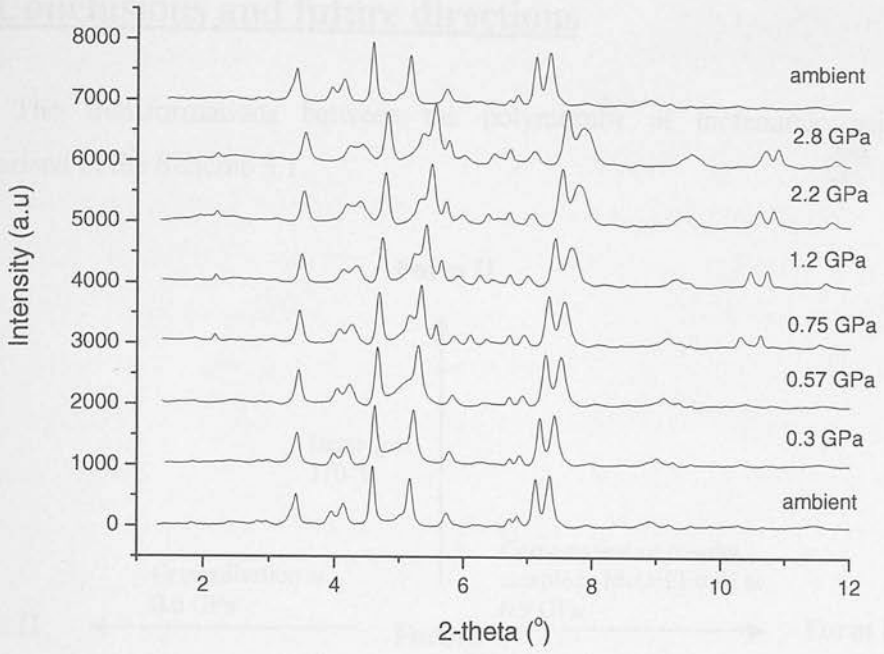

Figure 3.19: X-ray powder diffraction patterns of MA form II in Fluorinert-FC77 collected at pressures up to 2.8 GPa. The upper pattern represents the powder pattern obtained after gradually reducing the pressure to ambient.

At 0.75 GPa, new peaks appeared in the powder pattern at 2 θ values of *ca.* 2.2, 10.5 and 10.7°, indicating a transition to a new phase. This new phase was identified as form IV, by comparison with the results of compression of form I in Fluorinert-FC77. All indexing attempts were unsuccessful. However, the powder pattern at 0.75 GPa may also represent a mixed phase as all the peaks attributed to form II were still present. The pressure was then gradually increased to 2.8 GPa, but no significant changes were observed except for the movement of peaks towards higher 2θ values. However, broadening of the peaks with increasing pressure occurred on account of non-hydrostatic conditions associated with the pressure-transmitting medium.

In the next step, the pressure was reduced to ambient. The powder pattern collected at ambient pressure (Figure 3.19) showed that the sample had transformed back to form II, indicating that the phase transition to form IV at 0.75 GPa was reversible.

3.3. Conclusions and future directions

The transformations between the polymorphs of mefenamic acid are summarised in the Scheme 3.1.

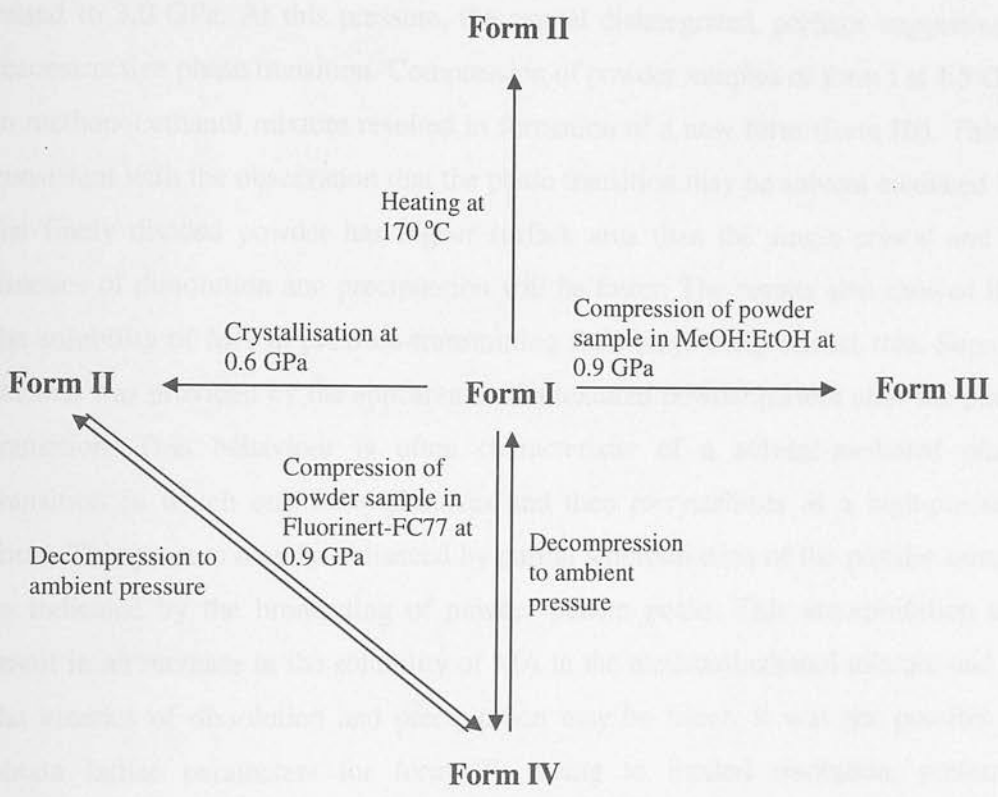

Scheme 3.1: Transformations between polymorphs of MA.

High-pressure crystallisation of a solution of mefenamic acid in ethanol contained in a diamond-anvil cell at a pressure of 0.6 GPa resulted in the reproducible formation of elusive form II. These results are of great significance as they demonstrate that form II can be obtained reproducibly at high pressure and recovered successfully to ambient pressure. Furthermore, no additives were required like in the study by Lee *et al.*, [18]. This may suggest that the form II is more thermodynamically stable form at high pressure. Furthermore, dry and cold milling results have shown that form II can also be produced by milling of form I, and that the pressure rather than temperature may be responsible for this transition. Milling of

pharmaceutical materials is an area that merits further explanation, particularly in relation to the possible effects of localised pressure.

Direct compression studies have shown that by compressing a single crystal of form I, no phase transition was observed up to 2.5 GPa. The pressure was then raised to 3.0 GPa. At this pressure, the crystal disintegrated, perhaps suggesting a reconstructive phase transition. Compression of powder samples of form I at 1.5 GPa in methanol:ethanol mixture resulted in formation of a new form (form III). This is consistent with the observation that the phase transition may be solvent mediated *i.e.* the finely divided powder has higher surface area than the single crystal and so kinetics of dissolution and precipitation will be faster. The results also showed that the solubility of MA in pressure-transmitting fluid plays a significant role. Support for this was provided by the appearance of a textured powder pattern after the phase transition. This behaviour is often characteristic of a solvent-mediated phase transition in which one form dissolves and then recrystallises as a high-pressure form. This process may be enhanced by partial amorphisation of the powder sample as indicated by the broadening of powder pattern peaks. This amorphisation can result in an increase in the solubility of MA in the methanol:ethanol mixture and so the kinetics of dissolution and precipitation may be faster. It was not possible to obtain lattice parameters for form III, owing to limited resolution, preferred orientation, and problems with texture. Decompression studies showed that form III can be recovered to ambient pressure and so future structural studies should perhaps focus on this aspect. It proved impossible to compress form II whilst using a methanol:ethanol mixture because of solvent-mediated conversion of form II to I. To reduce the effect of solubility, Fluorinert-FC77 was also used as pressure-transmitting medium. This allowed compression of powder samples of both forms I and II. The results from these experiments were different from the compression of form I in methanol:ethanol mixture. In this case a new polymorph, designated as form IV, was obtained at 0.75 GPa by compressing forms I and II. However the transition to form IV was incomplete. High-pressure crystallisation is a potential route to obtain this form and would be an area for future exploration. The high-

pressure recrystallisation attempts at relative low pressure in this study always resulted in the formation of form II.

3.4. References

1. R. J. Flower, *Pharmacol. Rev.,* 1974, **26**, 33-67.
2. V. Dokorou, M. A. Demertzis and D. Kovala-Demertzi, *Pharmakeutike.*, 2008, **21**, 1-9.
3. S. Avram, D. M. Duda-Seiman, I. Svab, S. Mancas, C. Duda-Seiman and D. F. Mihailescu, *Curr. Comput. Aided Drug Des.*, 2009, **5**, 1-12.
4. F. A. Aly, S. A. Al-Tamimi and A. A. Alwarthan, *Anal. Chim. Acta*, 2000, **416**, 87-96.
5. P. C. Ioannou, N. V. Rusakova, D. A. Andrikopoulou, K. M. Glynou and G. M. Tzompanaki, *Analyst.*, 1998, **123**, 2839-2843.
6. Y. Joo, H. S. Kim, R. S. Woo, C. H. Park, K. Y. Shin, J. P. Lee, K. A. Chang, S. Kim and Y. H. Suh, *Mol. Pharmacol.*, 2006, **69**, 76-84.
7. V. Dhanaraj and M. Vijayan, *Acta Crystallogr., Sect. B: Struct. Sci.*,1988, **44 (Pt 4)**, 406-412.
8. A. O. Surov, I. V. Terekhova, A. Bauer-Brandl and G. L. Perlovich, *Cryst. Growth Des*, 2009, **9**, 3265-3272.
9. K. Park, J. M. B. Evans and A. S. Myerson, *Cryst. Growth Des.*, 2003, **3**, 991-995.
10. L. D. Hughes, D. S. Palmer, F. Nigsch and J. B. O. Mitchell, *J. Chem. Inf. Model.*, 2008, **48**, 220-232.
11. A. J. Aguiar and J. E. Zelmer, *J. Pharm. Sci.*, 1969, **58**, 983-987.
12. S. Romero, B. Escalera and P. Bustamante, *Int. J. Pharm.*, 1999, **178**, 193-202.
13. K. Urakami, Y. Shono, A. Higashi, K. Umemoto and M. Godo, *Bull. Chem. Soc. Jpn.*, 2002, **75**, 1241-1245.
14. R. K. Gilpin and W. Zhou, *Vib. Spectrosc.*, 2005, **37**, 53-59.
15. S. Cesur and S. Gokbel, *Cryst. Res. Technol.*, 2008, **43**, 720-728.
16. J. F. McConnell and F. Z. Company, *Cryst. Struct. Commun.*, 1976, **5**, 861-864.
17. S. L. A. Munro and D. J. Craik, *Magn. Reson. Chem.*, 1994, **32**, 335-342.
18. E. H. Lee, S. R. Byrn and M. T. Carvajal, *Pharm. Res.*, 2006, **23**, 2375-2380.
19. S. Byrn and E. Lee, *Abstracts of Papers, 235th ACS National Meeting, New Orleans, LA, United States, April 6-10*, 2008, IEC-059.
20. I. S. Lee, A. Y. Lee and A. S. Myerson, *Pharm. Res.*, 2008, **25**, 960-968.
21. N. Mizuno, D. Shinkuma and T. Hamaguchi, *Yakugaku Zasshi*, 2003, **123**, 477-493.
22. A. Adam, L. Schrimpl and P. C. Schmidt, *Drug Dev. Ind. Pharm.*, 2000, **26**, 477-487.
23. F. Kato, M. Otsuka and Y. Matsuda, *Int. J. Pharm.*, 2006, **321**, 18-26.

24. M. M. Pop, K. Goubitz, G. Borodi, M. Bogdan, D. J. A. De Ridder, R. Peschar and H. Schenk, *Acta Crystallogr., Sect. B: Struct. Sci.*, 2002, **B58**, 1036-1043.
25. L. Fang, S. Numajiri, D. Kobayashi, H. Ueda, K. Nakayama, H. Miyamae and Y. Morimoto, *J. Pharm. Sci.*, 2004, **93**, 144-154.
26. A. Topacli and S. Ide, *J. Pharm. Biomed. Anal*, 1999, **21**, 975-982.
27. V. Dokorou, Z. Ciunik, U. Russo and D. Kovala-Demertzi, *J. Organomet. Chem.*, 2001, **630**, 205-214.
28. T. Iwasaki, M. Takahara, R. Sonoda and S. Watano, *Part. Part. Syst. Charact.*, 2007, **24**, 236-241.
29. A. J. Alvarez, A. Singh and A. S. Myerson, *Cryst. Growth Des.*, 2009, **9**, 4181-4188.
30. L. Merrill and W. A. Bassett, *Rev. Sci. Instrum.*, 1974, **45**, 290-294.
31. G. J. Piermarini, S. Block and J. D. Barnett, *J. Appl. Phys.*, 1973, **44**, 5377-5382.
32. G. J. Piermarini, S. Block, J. D. Barnett and R. A. Forman , *J. Appl. Phys.*, 1975, **46**, 2774-2780.
33. S. A. Moggach, D. R. Allan, S. Parsons, L. Sawyer and J. E. Warren, *J. Synchrotron Radiat.*, 2005, **12**, 598-607.
34. G. M. Sheldrick, *CELL_NOW*, University of Gottingen, Germany, 2002.
35. A. Dawson, D. R. Allan, S. Parsons and M. Ruf, *J. Appl. Crystallogr.*, 2004, **37**, 410-416.
36. B. AXS, *SAINT*, Bruker-AXS, Madison, Wisconsin, USA, 2003.
37. S. Parsons, *SHADE*, University of Edinburgh, Scotland, UK, 2004.
38. G. M. Sheldrick, *SADABS*, University of Göttingen, Germany, 2006.
39. P. W. Betteridge, J. R. Carruthers, R. I. Cooper, K. Prout and D. J. Watkin, *J. Appl. Crystallogr.*, 2003, **36**, 1487.
40. F. P. A. Fabbiani, D. R. Allan, W. I. F. David, S. A. Moggach, S. Parsons and C. R. Pulham, *CrystEngComm*, 2004, **6**, 504-511.
41. C. F. Macrae, P. R. Edgington, P. McCabe, E. Pidcock, G. P. Shields, R. Taylor, M. Towler and J. van de Streek, *J. Appl. Crystallogr.*, 2006, **39**, 453-457.
42. J. Bernstein, R. E. Davis, L. Shimoni and N. L. Chang, *Angew. Chem., Int. Ed. Engl.*, 1995, **34**, 1555-1573.
43. W. D. S. Motherwell, G. P. Shields and F. H. Allen, *Acta Crystallogr., Sect. B: Struct. Sci.*, 1999, **B55**, 1044-1056.
44. V. Dhanaraj and M. Vijayan, *Acta Crystallogr., Sect. B: Struct. Sci.*, 1988, **B44**, 406-412.
45. D. M. Adams and S. K. Sharma, *J. Chem. Soc., Faraday Trans. 2*, 1976, **72**, 2069-2074.
46. A. P. Hammersley, S. O. Svensson, M. H. and, A. N. Fitch and D. Hausermann, *High Pressure Res.*, 1996, **14**, 235-248.
47. W. Kraus and G. Nolze, *Powder Cell*, Berlin, Germany.
48. A. C. Larson and R. B. V. Dreele, *General Structure Analysis System (GSAS)*, Los Alamos National Laboratory, 2000.
49. B. H. Toby, *J. Appl. Crystallogr.*, 2001, **34**, 210-213.

Chapter 4

High-Pressure Studies of N,N'-dimethylurea

Chapter 4: High-Pressure Studies of N,N'-dimethylurea (DMU)

4.1. Background

Urea, $(NH_2)_2CO$, and related compounds have been the subject of extensive theoretical and experimental studies in the past four decades, mainly because of their interesting physical and chemical properties [1-5]. Urea is one of the most common and renowned chemical and biological compounds. It is the main nitrogen-containing end product of animal metabolism and is widely used in industry, mainly for the production of fertilisers, pharmaceuticals, and urea-formaldehyde plastics. Its crystal structure at ambient conditions, form I, consists of ribbons of molecules in which each carbonyl oxygen atom accepts four N-H...O hydrogen bonds [6, 7]. The overall structure that results from the optimisation of these bonds is relatively open [8]. Urea shows rich high-pressure behaviour, and at least four polymorphs exist at elevated pressures. In 1916, Bridgman discovered that urea transforms to form II above 373 K and 0.60 GPa, and to form III at 293 K above 0.48 GPa [9, 10]. Neutron powder diffraction studies of deuterated urea $(ND_2)_2CO$ identified form IV (stable between 2.80-7.20 GPa) and form V (stable above 7.20 GPa) [11, 12]. Most recently, single crystals of forms I, II and IV were grown *in situ* in a diamond-anvil cell (DAC), and their structures were determined by X-ray diffraction [13].

The work described in this chapter has focused on the high-pressure behaviour of N,N'-dimethylurea (DMU) also known as 1,3-dimethylurea, which represents one of the simplest examples of a disubstituted urea. DMU exists as a white crystalline powder with a melting point in the range 101-105 °C and a density of about 1.14 g/cm^3 at ambient temperature. DMU is widely used in a variety of scientific and industrial processes, *e.g.* as an intermediate in many pharmaceutical preparations [14], in membrane transport within red blood cells [15], and as a stabiliser in hydrated lubricating oil [16]. It has shown some protective effect against

streptozotocin-induced diabetes in mice, but has not been studied as a drug in humans [17].

The molecular structure of DMU with the numbering scheme used in this work is shown in the Figure 4.1.

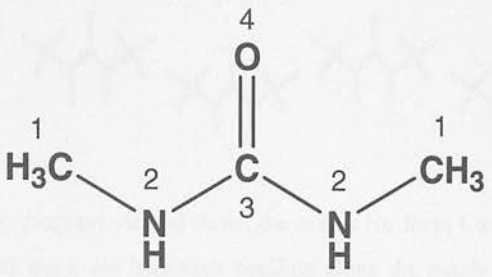

Figure 4.1: Molecular structure of N, N'-dimethylurea

Until recently, DMU was known to exist in only one crystalline modification denoted as form I. The crystal structure of this form was determined by Perez-Folch *et al.* in 1997 and was assigned the space group *Cc* [18]. This crystal structure was unexpected for it indicated a polar lattice, in contrast to that of urea (Figure 4.2). The authors also attempted a refinement in the space group *Fdd*2, but dismissed it on the basis that it led to larger thermal parameters and higher *R*-factors. Various crystallisation techniques were applied in an effort to obtain a polymorph with packing more like that observed in urea, but these were all unsuccessful [18]. The space group of DMU was subsequently reassigned to *Fdd*2 by Marsh during a survey of the crystal structure database [19].

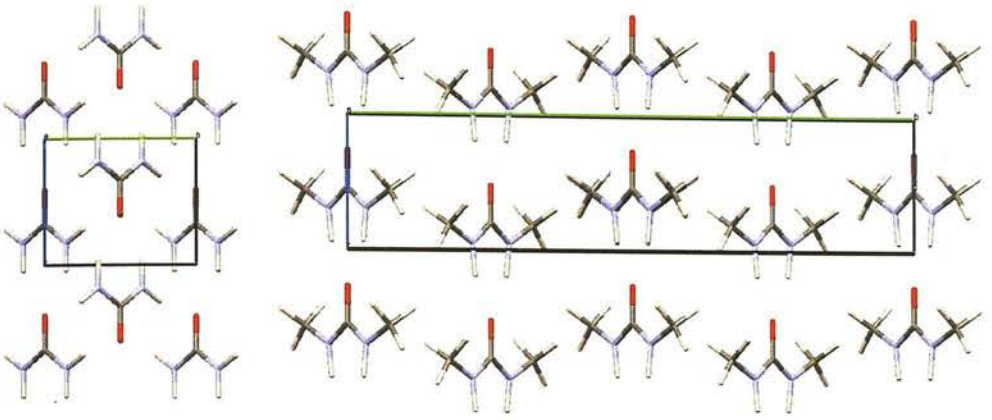

Figure 4.2: Crystal packing diagram viewed down the *a*-axis for form I urea (left) and form I DMU (right). Note that molecules stack *via* hydrogen bonding along the *c*-axis to create one-dimensional chains; for form I urea, neighbouring chains pack in opposite directions, giving rise to a nonpolar lattice, whilst DMU form I shows single chains oriented in only one direction.

More recently, another polymorph of DMU has been obtained at ambient pressure (denoted as form II) by Martins *et al.* [20]. Form II is an orthorhombic form with $P2_12_12$ space group, and was obtained accidentally from the slow crystallisation (more than 6 months) of a solution of DMU in phosphoric acid. Crystals of this phase were subsequently identified in samples of DMU purchased directly from Sigma-Aldrich. Figure 4.3 shows the comparison of X-ray powder patterns simulated from the crystal structures of form I (blue) and form II (red).

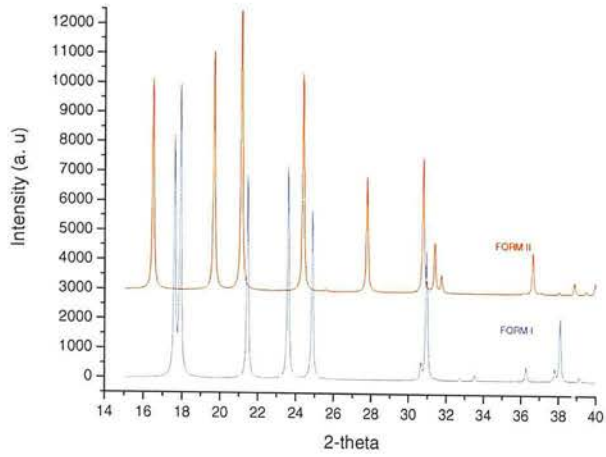

Figure 4.3: Comparison of simulated X-ray powder pattern for form I and II of DMU. These patterns were calculated using the program *MERCURY* [21] ($\lambda = 1.541$ Å).

The molecules in the crystal structure of form II pack in a slightly more efficient arrangement, and so the density of form II at room temperature exceeds that of form I by about 2 %. As a consequence, the authors suggested that this polymorph could be obtained by high-pressure techniques [20]. Furthermore, first order energy calculations performed on both forms suggested that form II is more stable below 100 K and form I is more stable above 100 K [20]. Based on these calculations along with computed thermodynamical values, the authors also suggested that form II should be considered a readily accessible polymorph. The aim of the current investigation was therefore to explore whether high-pressure methods could be used to obtain form II or other new forms. The results also stimulated crystal structure prediction (CSP) calculations on DMU performed separately at the University of Cambridge by Dr Graeme Day and the experimental and computational results are compared in this chapter.

4.2. Experimental

4.2.1. Material

N,N´-dimethylurea was purchased from Sigma Aldrich, UK and used as received. The supplied form was studied by collecting X-ray powder diffraction patterns and comparing them with the patterns calculated from the single crystal structure. Analytical grade solvents were used for the recrystallisation experiments.

All high-pressure experiments were carried out using Merrill-Bassett diamond-anvil cell (DAC) (half-opening angle 40°) [22], equipped with a pre-indented tungsten gasket of thickness 250 μm and a 300 μm diameter hole. For high-pressure crystallisation experiments, diamond-anvil cells using tungsten carbide backing disc [23] were used.

4.2.2. Methods

4.2.2.1. Variable temperature X-ray powder diffraction

Variable temperature X-ray powder diffraction (XRPD) experiments were performed using an Anton Parr TTK450 heating and cooling stage over the temperature ranges 20 -100 °C. XRPD data were collected on a Bruker AXS D8 diffractometer, using Cu-Kα radiation (λ = 1.5418 Å at 40 kV and 40 mA), equipped with a PSD detector. Each sample was analysed between 2θ = 2-40° with a step size of *ca.* 0.02°. Experimental powder patterns were compared to simulated powder patterns obtained from the single crystal structures of forms I and II of DMU.

4.2.2.2. Milling experiments

Milling of DMU form I was carried out in a Retsch MM301 Ball Mill. 0.5 g of sample was loaded into the milling vessel along with a steel ball (mass *ca.* 30 g and diameter *ca.* 20 mm). Milling was performed at rate of 5 Hz. XRPD was used to analyse powder samples obtained after different periods of milling.

4.2.2.3. High-pressure crystallisation from solution

About 1M solution of DMU was prepared in a methanol:ethanol (4:1) mixture. The solution was then loaded along with a few crystallites of DMU at 293 K into a DAC. A small piece of ruby was also added in order to allow the determination of the pressure by laser fluorescence spectroscopy as described in chapter 2 [24]. The pressure was increased to a minimum to form a sealed system and the cell was then subjected to gentle heating to dissolve all of the solid material. The pressure was then applied by tightening the screws of the DAC to induce precipitation. Crystallisation was achieved at *ca.* 0.7 GPa. The temperature was then cycled near 353 K in order to dissolve all but one of the crystallites. On slow cooling to 293 K a single crystal grew, which filled almost 50% of the gasket hole. The pressure within the gasket hole was determined to be *ca.* 0.7 GPa.

In another loading of the DAC with the same solution, a similar procedure was used to grow a single crystal at high pressure, but this time the pressure was increased to *ca.* 1.1 GPa before crystallisation occurred. The temperature was then cycled near 353 K at this pressure to dissolve all of the crystallites except one; this was allowed to grow by slow cooling to 293 K and filled almost all of the gasket hole.

4.2.2.4. Single crystal X-ray diffraction

Diffraction data were collected on a Bruker APEX CCD diffractometer at 293(2) K using Mo-Kα radiation (λ = 0.71073). Data collection and processing was performed according to procedures described by Dawson *et al.* [25]. Integrations were performed using the program *SAINT* [26], and absorption corrections used the programs *SHADE* [27] and *SADABS* [28]. In the case of single crystal grown at 0.7 GPa, diffraction data were collected with the diamond-anvil cell in two orientations (glued on the goniometer head by two different sides of the cell) to improve data completeness. Both data-sets were treated separately up to the absorption correction step. The two unmerged reflection data sets were then scaled and merged in *SORTAV* [29].

4.2.2.5. X-ray powder diffraction at high pressure

High-pressure powder diffraction experiments were carried out using a Merrill-Bassett diamond-anvil cell (half-opening angle 40°) [22], A pre-indented tungsten gasket of thickness 250 μm with a 300 μm diameter hole was used. To improve the uniformity of polycrystalline material, the powder was ground using a mortar and pestle prior to loading into the cell. The powder was loaded with a small ruby chip to measure pressure by the line shift in ruby fluorescence. The pressure-transmitting medium used in these experiments was either Fluorinert-FC77 or a methanol:ethanol (4:1) mixture.

Powder diffraction patterns were collected with synchrotron X-ray radiation using Station 9.5HPT (λ= 0.444 Å) at the SRS, Daresbury Laboratory and Beamline I15 (λ= 0.485 Å) at the Diamond Light Source, Oxfordshire. To improve the uniformity of the cones of diffracted radiation, the sample was continuously rastered over a range of $\pm$100 μm transverse to the incident X-ray beam in order to illuminate as many individual crystallites as possible. The scattered radiation was then collected on an image-plate area detector (Mar345). Any intense diffraction peaks due to diamonds were masked and the remaining two-dimensional pattern was then integrated to obtain a one dimensional powder-diffraction pattern with the help of *FIT2D* software [30].

4.3. Results and discussion

4.3.1. Variable temperature X-ray powder diffraction

X-ray powder diffraction studies were performed in the range 20-100 °C in order to explore the effect of temperature on the polymorphism of DMU. The sample received from the supplier was identified as a mixture of forms I and II, and is represented by the lower powder pattern in Figure 4.4. To improve the quality of the powder and to reduce the effects of preferred orientation the powder was lightly ground with a mortar and pestle. After this treatment, the X-ray powder pattern

showed only the presence of form I, indicating that a phase transition had occurred on grinding. The ease of this transition suggests that form II is metastable with respect to form I under these conditions in which localised shear forces and elevated temperatures may arise. Similar results were obtained by mechanical milling in the absence of any solvent. Figure 4.5 shows that the mixture of forms I and II rapidly transformed to form I after only 1 min of milling. For this reason, variable temperature experiments used the supplied powder with no prior grinding. The powder pattern at 30 °C represents a mixture of forms I and II. On raising the temperature to 40 °C, the powder pattern still showed a mixture of forms I and II, but the intensity of peaks due to form II had decreased and the intensity of peaks due to form I had increased. With further increase in temperature up to 50 °C all the peaks attributed to form II disappeared. The pattern at this temperature therefore represents pure form I. No further changes in the patterns were observed up to the melting point at 105 °C. After melting and subsequent cooling to 293 K the sample crystallised as form I.

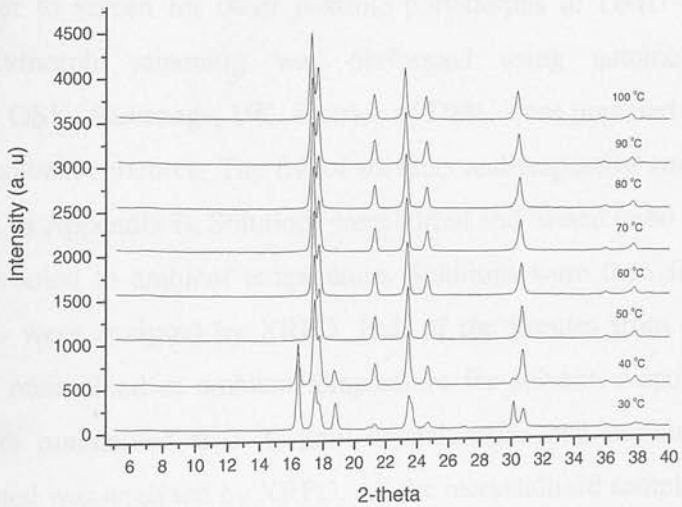

Figure 4.4: X-ray powder diffraction patterns of DMU recorded at temperature range 30°-100°C (λ = 1.541 Å).

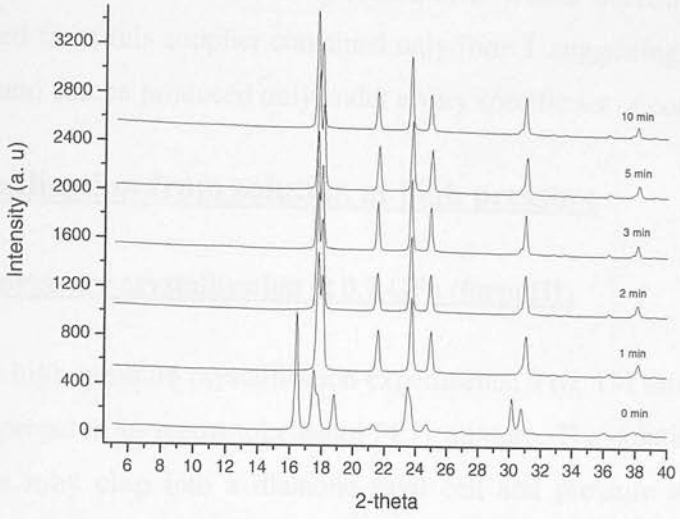

Figure 4.5: X-ray powder diffraction patterns of DMU recorded after different times of milling. The 0 min pattern represents the untreated sample and shows the presence of form II ($\lambda = 1.541$ Å).

4.3.2. Polymorph screening at ambient pressure

In order to screen for other possible polymorphs of DMU under ambient pressure, polymorph screening was performed using automated screening instruments at GSK, Stevenage, UK. Slurries of DMU were prepared in 48 different solvents and solvent mixtures. The list of solvents and respective concentrations of solute is given in Appendix B. Solutions were stirred and heated to 60 °C for *ca.* 24 h before being cooled to ambient temperature. Solutions were then filtered and the solid materials were analysed by XRPD. Half of the filtrates from all the solvent systems were maintained at ambient temperature for solvent evaporation and the other half were maintained at 0 °C until crystallisation had occoured. Any solid material obtained was analysed by XRPD. All the recrystallised samples from slurry, evaporation and cooling experiments were identified as form I. Recrystallisations from saturated solutions in a variety of solvents were also performed at high and low cooling rates, but all attempts resulted in form I. As the sample obtained from Sigma-Aldrich contained a mixture of form I and II, Sigma-Aldrich was also consulted to obtain the preparative scheme for their synthesis of DMU, but due to proprietary

reasons they were unwilling to give any information. Rather interestingly a second sample obtained from this supplier contained only form I, suggesting that form II is rather elusive and can be produced only under a very specific set of conditions.

4.3.3. Crystallisation from solution at high pressure

4.3.3.1. High-pressure crystallisation at 0.7 GPa (form III)

For the high-pressure crystallisation experiments, a *ca.* 1M saturated solution of DMU was prepared in methanol:ethanol (4:1) mixture. The solution was loaded along with the ruby chip into a diamond-anvil cell and pressure was applied to induce crystallisation at 0.7 GPa. All of the crystallites except one were dissolved by gentle heating. On cooling, a single crystal grew slowly to fill almost all of the gasket hole (Figure 4.6). Single crystal X-ray diffraction data were then collected. The data were indexed to give a monoclinic unit cell with lattice parameters shown in Table 4.1.

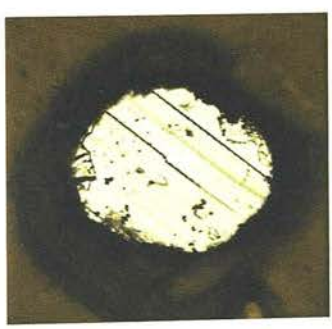

Figure 4.6: Optical image of single crystal of DMU (form III) in a diamond-anvil cell at 0.7 GPa.

	Form III
Crystal System	Monoclinic
Space group	*P2/c*
a **(Å)**	5.0888(10)
b **(Å)**	4.5563(3)
c **(Å)**	10.2891(7)
α **(°)**	90
β **(°)**	98.081(10)
γ **(°)**	90
V (Å^3)	263.20(5)
Z	2
D$_c$ **(g cm^{-3})**	1.24
P (GPa)	0.70(5)
T(K)	298(2)

Table 4.1: Unit cell parameters for crystal grown at 0.7 GPa (form III).

To improve the degree of completeness, diffraction data were collected with the diamond-anvil cell in two orientations. Both data sets were treated separately up to the absorption correction step. The two unmerged reflection files were then scaled and merged in *SORTAV* [29] in the manner described in experimental section.

Data processing was performed according to the procedure described in chapter 2, up to the absorption correction step. The structure was solved in *P2/c* using direct methods (SIR 97) [31]. Full-matrix least-squares structure refinement was then performed using *CRYSTALS* [32]. Hydrogen atoms were placed in calculated positions and allowed to ride on their parent atom. Full structural refinement details are tabulated in Appendix A. Crystallographic data in CIF format are available on the attached CD. This high-pressure polymorph of DMU was designated as form III.

4.3.3.2. High-pressure crystallisation at 1.1 GPa (form IV)

A second high-pressure form (designated as form IV) was also obtained from the same 1M solution as above (section 4.3.3.1), but this time the pressure was increased in a single step up to 1.1 GPa to give a polycrystalline solid. It proved difficult to grow a single crystal by gentle heating and cooling cycles at this pressure

and so the pressure was decreased to 0.9 GPa. On warming to *ca.* 393 K all of the crystallites dissolved except for one, which was allowed to grow by slow cooling to 293 K. On cooling the crystal grew to almost fill the gasket hole (Figure 4.7). After *ca.* 5 minute another small single crystal also started to grow. These two crystals are shown in Figure 4.7.

Figure 4.7: Optical image of two single crystals of DMU (form IV) in a diamond-anvil cell at 0.9 GPa

Single crystal X-ray diffraction data from both crystals were then collected. Data indexing was performed using the indexing programme *CELL_NOW* [33]. This gave a new orthorhombic unit cell with lattice parameters shown in Table 4.2. Reflections from both single crystals were integrated and treated separately up to the absorption correction step. The two unmerged reflection files were then scaled and merged in *SORTAV* [29] in the manner described in the experimental section. After this procedure, a data completeness of 61% was achieved. Data processing was performed according to the procedure described by Dawson *et al.* (2004) [34] and detailed in chapter 2. The structure was solved in space group *Pbcn* using direct methods (*SIR*) [31]. Data were refined using the same refinement strategy employed for the structure obtained at 0.7 GPa. Hydrogen atoms were placed in calculated positions and allowed to ride on their parent atoms. Full structural refinement details are tabulated in Appendix A. Crystallographic data in CIF format are available on the attached CD.

	Form IV
Crystal System	Orthorhombic
Space group	*Pbcn*
a **(Å)**	4.3175(13)
b **(Å)**	8.488(6)
c **(Å)**	11.752(4)
α **(°)**	90
β **(°)**	90
γ **(°)**	90
V (Å^3)	430.7(4)
Z	4
D_c **(g cm^{-3})**	1.36
P (GPa)	0.90(5)
T(K)	298(2)

Table 4.2: Unit cell parameters for the crystal grown at 0.9 GPa (form IV).

4.3.4. Description of crystal structures

Crystallographic data for the two new high-pressure polymorphs along with two ambient forms of DMU are summarised in Table 4.3. In the case of form II, both low-temperature (150 K) and ambient-temperature cell parameters are reported. The structures of forms I and II have been previously described by Marsh *et al.*, [19] and Martins *et al.*, respectively [20].

	[a]Form I	[b]Form II	[b]Form II	Form III	Form IV
CSD reference code	NIJHUJ01	--	--	--	--
Crystal system	Orthorhombic	Orthorhombic	Orthorhombic	Monoclinic	Orthorhombic
Space group	*Fdd*2	$P2_12_12$	$P2_12_12$	*P2/c*	*Pbcn*
a **(Å)**	11.4	5.2202(15)	4.9790(10)	5.0888(10)	4.3175(13)
b **(Å)**	20.186	10.769(3)	10.769(2)	4.5563(3)	8.488(6)
c **(Å)**	4.594	4.5952(3)	4.5764(9)	10.2891(7)	11.752(4)
β **(°)**	90.00	90.00	90.00	98.081(10)	90.00
V (Å^3)	1051.42	258.325(13)	245.518(12)	236.20(5)	430.7(4)
Z	8	2	2	2	4
D_c **(g cm^{-3})**	1.14	1.17	1.19	1.24	1.36
P (GPa)	0.0	0.0	0.0	0.70(5)	0.90(5)
T(K)	298(2)	298(2)	150(2)	298(2)	298(2)

[a]Ref 19. [b]Ref. 20

Table 4.3: Comparison of cell parameters of all four known polymorphs of DMU by different studies. In case of form II both 150 K and ambient temperature cell-parameters are presented.

In the crystal structure of all four polymorphs, DMU molecules adopt the Z-Z' conformation (Figure 4.8). The structures of all the polymorphs except form I show similar features compared to previously published structures of some N, N'-disubstituted symmetric and asymmetric ureas [35-37]. In all of these structures the DMU molecule always adopts the Z-Z' conformation. However, the formation of chains in the crystal structure is only present in the symmetrically substituted molecules and all of them show alternate hydrogen bonds from one row to the immediate neighbouring row. In the case of form I, the structure does not show this alternate hydrogen bonding scheme; neighbouring chains adopt the same orientation that runs along the *c*-axis of unit cell resulting in the polar structure. The crystal structures of all four forms are described in the following section.

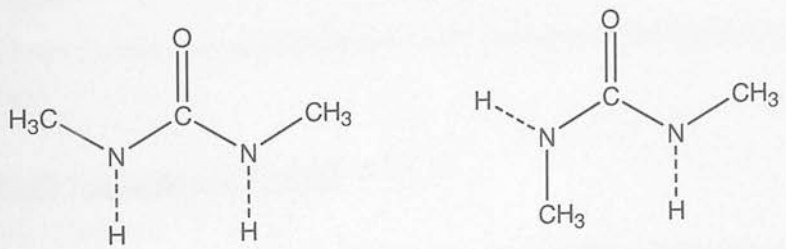

Figure 4.8: Two conformations of DMU molecules; one with two methyl groups on the same side with C=O (Z-Z') (left) and second with methyl groups on opposite direction (E-Z') (right).

4.3.4.1. Crystal structure of form I

The crystal packing and space-filling diagrams are shown in Figure 4.9. There are eight DMU molecules in the unit cell and all the non-hydrogen atoms are coplanar. DMU molecules are arranged in a head-to-tail fashion making bifurcated hydrogen bonds along the *c*-axis. Both nitrogen atoms of one molecule are hydrogen bonded to the oxygen atom of a neighbouring molecule, which combine to form one dimensional chains with an intermolecular distance of *ca.* 4.6 Å. The angle between the molecular planes of neighbouring chains is 70.2°. The hydrogen bond angles are *ca.* 145° because the same oxygen atom from the C=O group is hydrogen bonded to two parallel N-H groups.

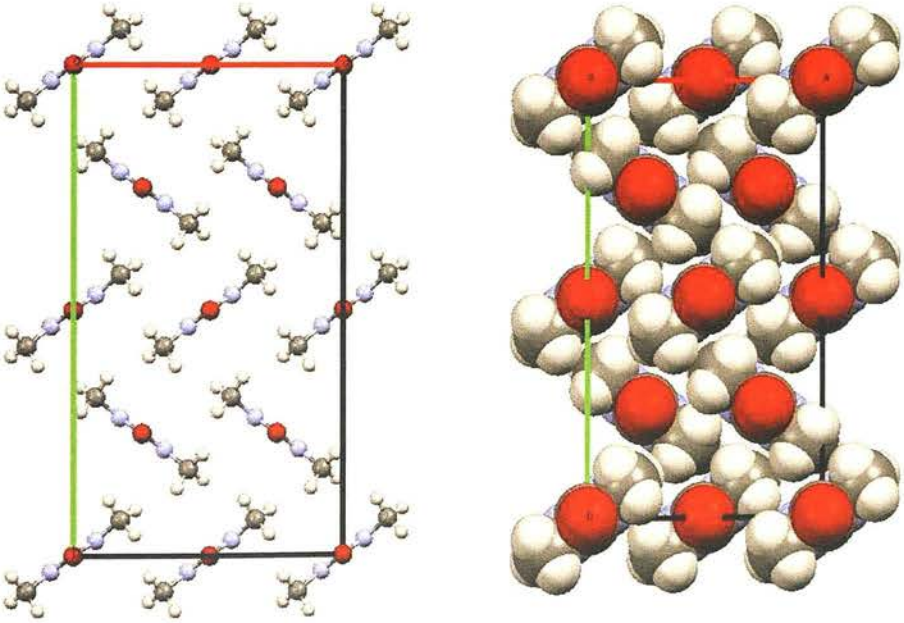

Figure 4.9: Crystal packing diagram of DMU form I (left) viewed down the *b*-axis and space-fill ing diagram (right).

4.3.4.2. Crystal structure of form II

The crystal packing and space-filling diagrams of form II are shown in Figure 4.10. The DMU molecules are planar and maintain the Z-Z' conformation. It is also evident from the structure that the similar strong interactions observed in form I are

found in form II, resulting in the same repeating structural unit *i.e.* chains of bifurcated hydrogen bond linked in a head-to-tail fashion with neighbouring chains repeating along the *c*-axis. However, in form II neighbouring chains adopt alternating orientations leading to a non-polar lattice that is characteristic of symmetrically disubstituted ureas in general and of urea form I itself [5]. The density of form II at room temperature exceeds that of form I by *ca.* 2%. Moreover, this form becomes significantly denser (5 %) at low temperature (150 K), which may be attributed to the structural flexibility along the *a*–axis direction, the cohesion along which is largely dominated by van der Waals' interactions. This observation supports the suggestion that form II might be accessible *via* crystallisation at pressure.

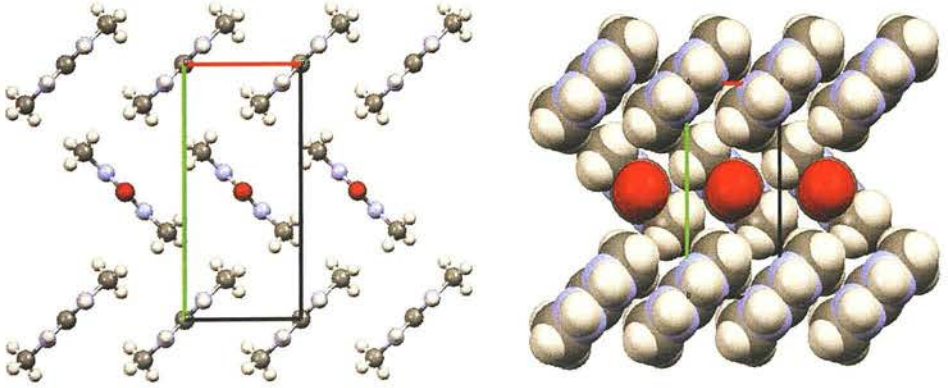

Figure 4.10: Crystal packing diagram of DMU form II (left) viewed down the *b*-axis and space fill diagram (right).

4.3.4.3. Crystal structure of form III

The crystal packing and space-filling diagrams of the high-pressure form III are shown in Figure 4.11. There are two DMU molecules in the unit cell. These molecules are arranged in a head-to-tail fashion linked by bifurcated hydrogen bonds along the *b*-axis: nitrogen atoms of one molecule are hydrogen bonded to the oxygen atom of a neighbouring molecule, which combine to form one dimensional chains with an intermolecular distance of *ca.* 4.56 Å. These infinite hydrogen-bonded chains adopt alternating orientations leading to a non-polar lattice. The difference between

form III and the ambient-pressure forms arises from the direction of these repeating units. In form III, DMU molecules repeat along the *b*-axis of the unit cell instead of along the *c*-axis. The space-filling diagram (Figure 4.11) shows efficient packing of DMU molecules in the form of layers. The calculated density of form III at 0.7 GPa is 1.24 g cm^{-3}.

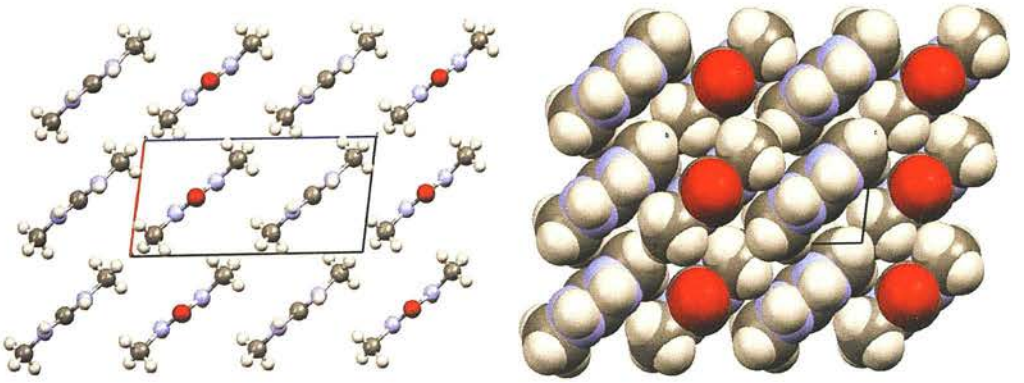

Figure 4.11: Crystal structure of DMU form III grown at 0.7 GPa viewed down the *b*-axis; the packing diagram shows an alternative arrangement of DMU chains (left) and the space-filling diagram showing packing of DMU in the form of layers (right).

4.3.4.4. Crystal structure of form IV

Crystal packing diagrams of form IV obtained at 0.9 GPa are shown in Figure 4.12. All the non-hydrogen atoms are coplanar and maintain the Z-Z' conformation. There are four molecules in the unit cell. As in the form III structure, molecules pack as infinite chains. These infinite hydrogen-bonded chains of DMU molecules run parallel to the *b*-axis. The neighbouring chains of DMU molecules adopt alternating orientations, leading tc a non-polar lattice. The structure of form IV is dominated by a two dimensional hydrogen-bonded network, where each DMU molecule accepts and donates two hydrogen bonds. Each molecule shows bifurcated hydrogen bonding with neighbouring molecules, but in this case a hydrogen bond is formed between an oxygen atom of one molecule with two nitrogen atoms of two adjacent molecules, resulting in a zig-zag arrangement of chains as shown in Figure 4.12(c). These infinite hydrogen-bonded chains of DMU molecules run parallel to the *b*-axis. The intermolecular distance between DMU molecules in adjacent chains is *ca.* 4.76 Å.

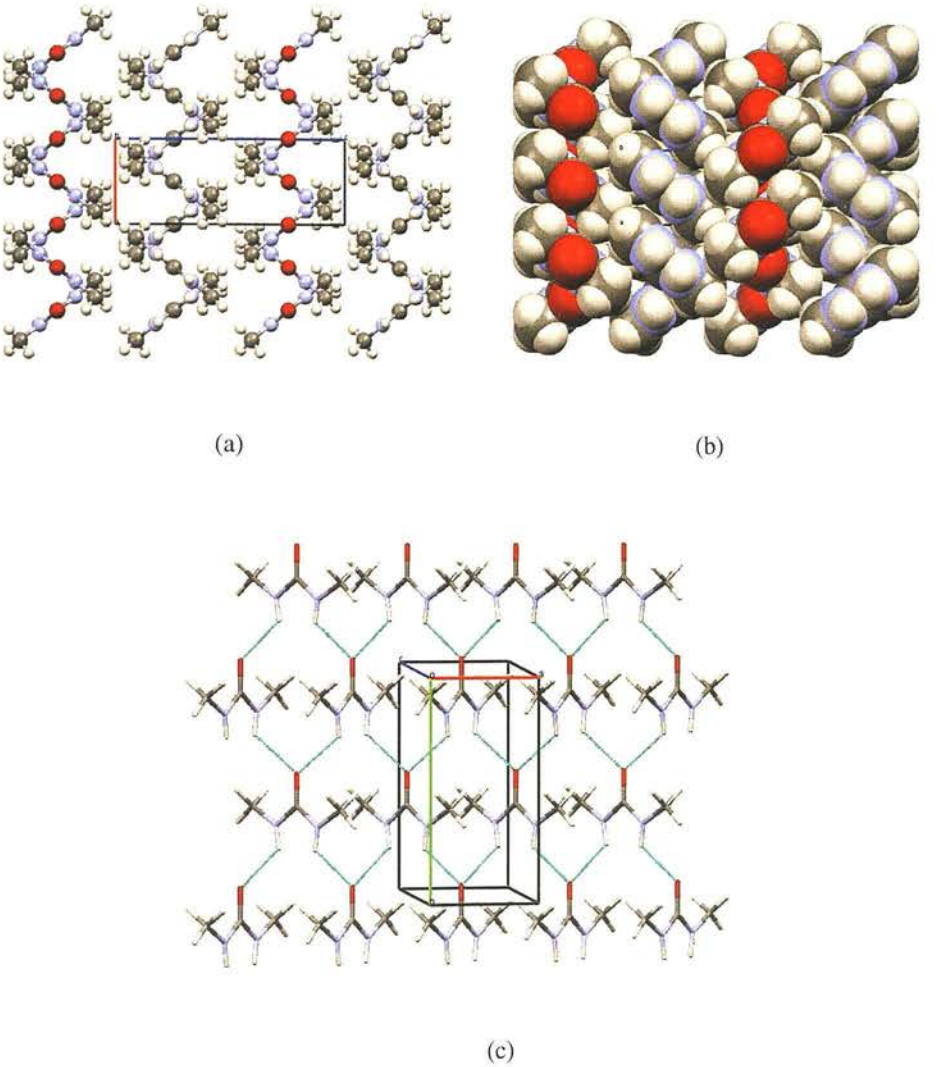

Figure 4.12: Crystal structure of DMU form IV grown at 1.1 GPa viewed down the *b*-axis. (a) Packing diagrams of crystal structure shows an alternative arrangement of DMU chains, (b) the space-filling diagram showing efficient packing of DMU and (c) hydrogen bonding network showing each DMU molecule forming hydrogen bonds with two neighbouring molecules.

4.3.4.5. Hydrogen bonding (graph-set analysis)

The hydrogen bonding in DMU can be best described with the aid of graph set analysis. Graph-set analysis is a very useful tool to reduce complicated networks to combinations of simple patterns. The graph-set notations are assigned by the method described by Bernstein *et al.* [38] and obtained by *PLUTO* [39] and *MERCURY* [21].

Forms I, II and III show similar types of hydrogen bonding to form infinite chains of DMU molecules. As described in section 4.3.3 the difference between the packing of DMU molecules in these polymorphs arises from the relative orientation of these chains in their respective crystal structure. Since there is no hydrogen bond between the neighbouring chains, all these polymorphs can be represented by the same graph-set notation. The description of the hydrogen-bond pattern in these forms according to the graph-set notation at the first level graph set is N_1 = C(4)R^1_2(6) . Graph-set motifs for these two modifications are illustrated in Figure 4.13.

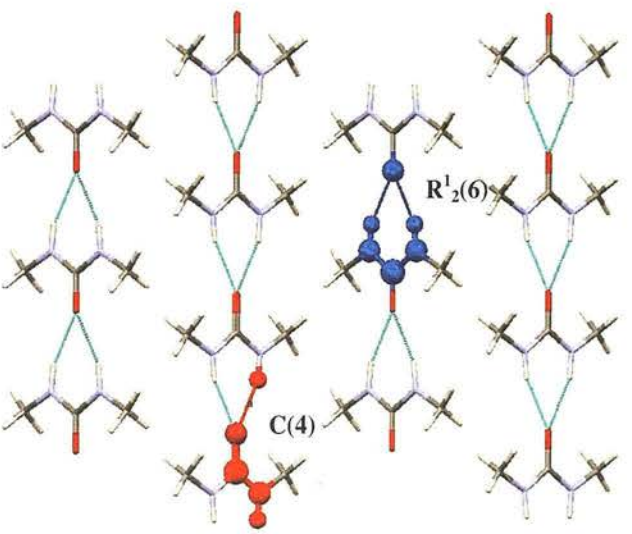

Figure 4.13: Hydrogen-bonding arrangements together with graph-set assignments of the structure of form II of DMU. Since forms I, II and III all shows similar arrangements of DMU molecules only the form II structure is shown. Atoms highlighted in blue show the ring motif whilst atoms in red show the chain motif of DMU molecules.

The crystal structure of form IV is dominated by the hydrogen-bonding pattern, which is different from all of the other forms. The description of the hydrogen-bonding patterns for form IV according to graph-set notation at a first level graph set is N_1 = C(4)C^1_2(6)R^3_4(14)R^5_6(22). Graph-set motifs for these four modifications are illustrated in Figure 4.14.

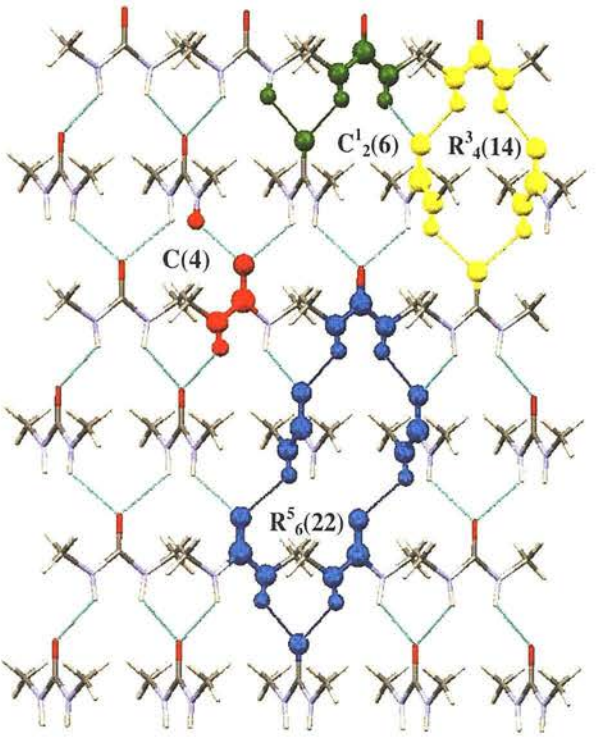

Figure 4.14: Hydrogen bonding pattern, with graph-set assignments, of the structure of form IV. Atoms highlighted in blue and yellow shows two different ring motifs whilst atoms in red and green show two chain motifs of DMU molecules.

Analysis of the local environment around a central molecule is also a useful tool to illustrate the packing of molecules in a crystal structure. Figures 4.15a and 4.15b show local environments of the centroids within a sphere of radius 6.5 Å for forms I and II, respectively. Centroids shown in pink and green correspond to molecules related to the central molecule *via* 2-fold screw rotation and glide symmetry, respectively. There are four and eight molecules associated with 2-fold screw rotations in forms I and II, respectively. Centroids shown in red correspond to DMU molecules related by translation symmetry. In the case of form I, each molecule has two nearest neighbours below 5 Å and eight further neighbours at distances in the range 5 - 6.5 Å. In form II, there are four nearest neighbours below 5 Å and eight neighbours at distances in the range 5 -6.5 Å. This illustrates the better packing of DMU molecules in form II. The distance between the molecules involved in hydrogen bonding (D...A = 2.86 Å) is the same in both forms I and II and so the

better packing in form II may be attributed to the alternative arrangements of these chains.

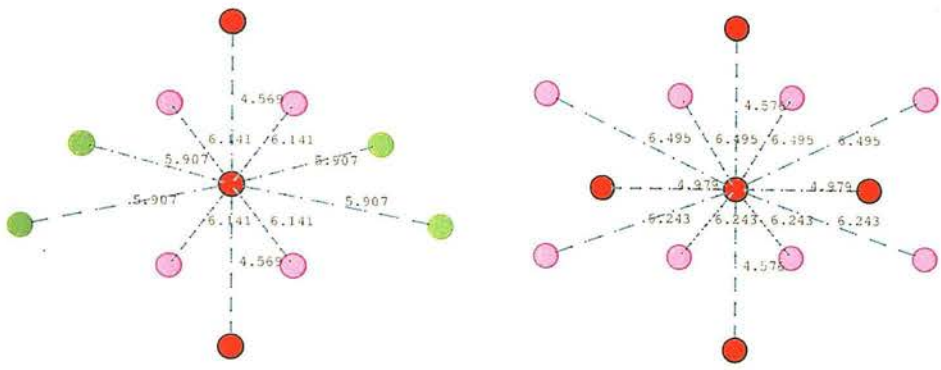

(a) (b)

Figure 4.15: The environment of a DMU molecule (centroid) in the crystal structures of (a) form I (b) form II (distance in Å).

The local environment of DMU molecules within a sphere radius of 6.5 Å for forms III and IV are compared in Figure 4.16. The centroids shown in red and green correspond to the DMU molecules related by translation and glide symmetry, respectively. There are four nearest neighbours from the middle centroid at distances in the range 4-5 Å in both forms III and IV. However, two and four molecules lie within the range of 5-6.5 Å in forms III and IV, respectively. This highlights the close packing of DMU molecules in form IV.

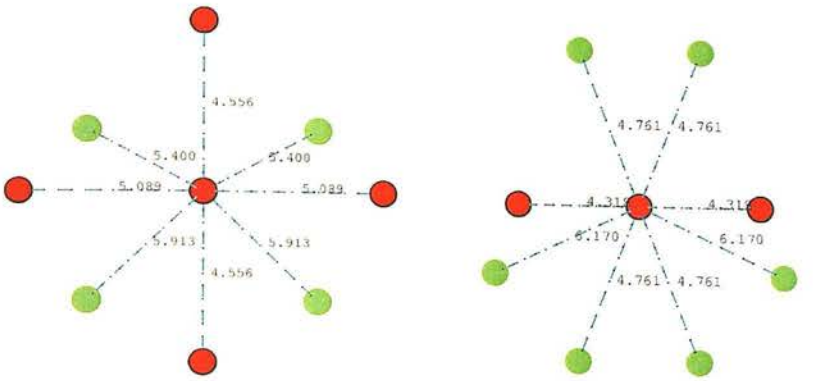

(a) (b)

Figure 4.16: The environment of a DMU molecule (centroid) in the crystal structures of (a) form III (b) form IV (distances in Å).

4.3.5. High-pressure powder diffraction experiments

4.3.5.1. High-pressure crystallisation from melt

Form III was also obtained by *in situ* crystallisation from the melt at high pressure. In this experiment, a DAC was loaded with finely ground powder of form I with no pressure transmitting medium and the pressure was then increased to 0.6 ± 0.05 GPa. At this pressure, the DAC was heated to melt the sample and on cooling a polycrystalline powder was formed. The powder diffraction pattern obtained from this sample along with the calculated pattern from single crystal data of form III (grown at 0.7 GPa) is shown in Figure 4.17. Compared to the calculated pattern, the peaks in the experimental pattern were at lower 2θ values, which is consistent with the lower pressure at which these measurements were made. The peaks were also noticeably broadened on account of the non-hydrostatic nature of the experiments.

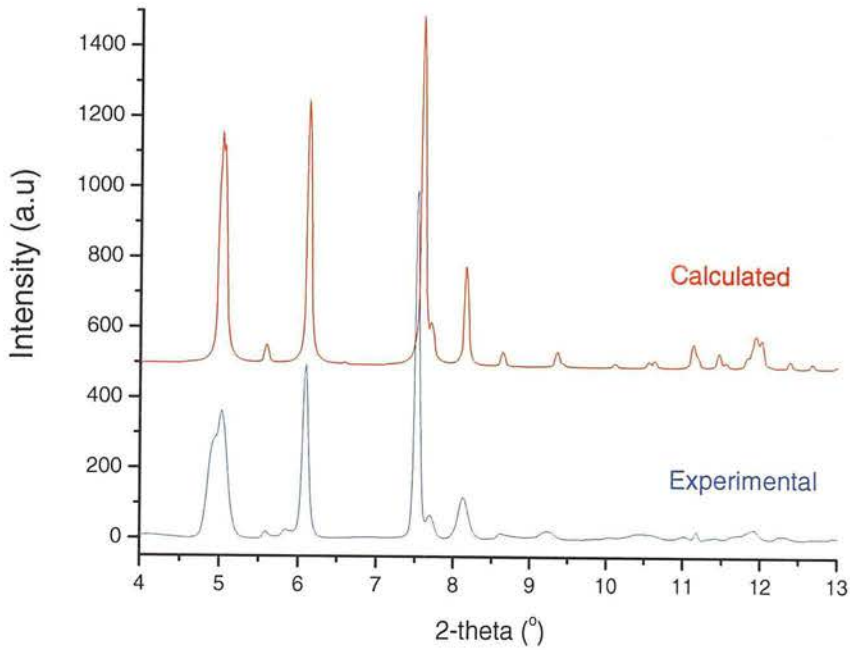

Figure 4.17: Comparison of X-ray powder diffraction patterns of DMU recorded at 0.6 GPa after recrystallisation from the melt (blue) with the simulated powder pattern of form III (red) calculated from single crystal data at 0.7 GPa (λ = 0.44397 Å).

4.3.5.2. Powder compression using methanol:ethanol (4:1) as pressure-transmitting medium

Figure 4.18 shows powder diffraction patterns of DMU collected at pressures between ambient and 0.38 GPa. Methanol:ethanol (4:1) mixture was used as the pressure-transmitting medium. The pattern recorded at ambient pressure was indexed as form I. On increasing the pressure to 0.16 GPa, all peaks attributable to form I completely disappeared and a new pattern was observed which could be indexed as form III (lattice parameters are shown in Table 4.4). On further compression to 0.25 GPa and then to 0.38 GPa, no significant changes were observed in the powder patterns except for the movement of peaks towards higher 2θ values.

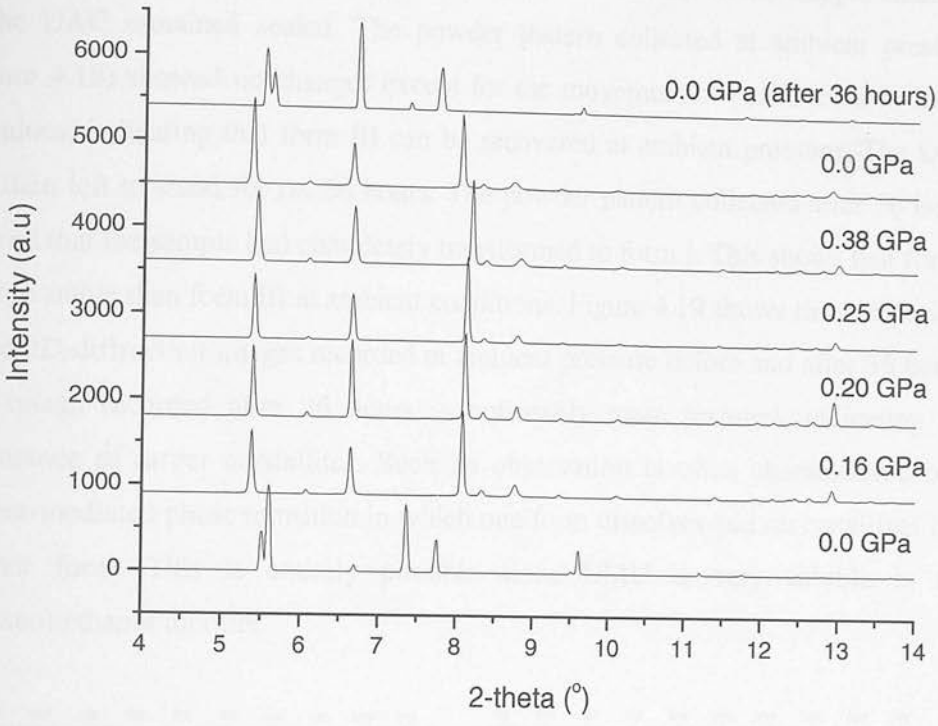

Figure 4.18: X-ray powder diffraction patterns of DMU with methanol:ethanol (4:1) as pressure-transmitting medium. Powder diffraction patterns were collected with synchrotron X-ray radiation (λ = 0.485 Å) using Beamline I15 at the Diamond Light Source, Oxfordshire.

Pressure	**0.0 GPa**	**0.16 GPa**	**0.20 GPa**	**0.25 GPa**	**0.38 Gpa**	**0.0 GPa[a]**	**0.0 GPa[b]**
Polymorph	Form I	Form III	Form III	Form III	Form III	Form III	Form I
Crystal System	Orthorhombic	Monoclinic	Monoclinic	Monoclinic	Monoclinic	Monoclinic	Orthorhombic
Space group	*Fdd*2	*P*2/*c*	*P*2/*c*	*P*2/*c*	*P*2/*c*	*P*2/*c*	*Fdd*2
a **(Å)**	11.4023(10)	5.2116(8)	5.1998(6)	5.1925(6)	5.1469(6)	5.3098(11)	11.4015(19)
b **(Å)**	20.1516(14)	4.5794(4)	4.5771(25)	4.5762(29)	4.5741(4)	4.5764(7)	20.1762(29)
c **(Å)**	4.5695(4)	10.4268(12)	10.4095(12)	10.4011(11)	10.3684(12)	10.4404(18)	4.5700(5)
β **(°)**	90	97.304(7)	97.430(4)	97.494(5)	97.657(12)	96.974(20)	90
V (Å^3)	1049.94(14)	246.82(5)	245.67(4)	245.04(4)	241.92(5)	251.82(8)	1051.28(25)
V/molecule (Å^3)	131.24(3)	123.41(2)	122.83(5)	122.52(2)	120.96(3)	125.91(4)	131.41(3)
Z	8	2	2	2	2	2	8
T (K)	293(2)	293(2)	293(2)	293(2)	293(2)	293(2)	293(2)

Table 4.4: Lattice parameters for DMU at different pressures (using MeOH/EtOH as pressure-transmitting medium). [a] Pressure was released to ambient. [b] Powder pattern was collected after 36 hours at ambient pressure.

In the next step the pressure was reduced to ambient, but the sample chamber of the DAC remained sealed. The powder pattern collected at ambient pressure (Figure 4.18) showed no changes except for the movement of peaks towards lower 2θ values, indicating that form III can be recovered at ambient pressure. The DAC was then left to stand for *ca.* 36 hours. The powder pattern collected after 36 hours showed that the sample had completely transformed to form I. This shows that form I is more stable than form III at ambient conditions. Figure 4.19 shows the comparison of the 2D-diffraction images recorded at ambient pressure before and after 36 hours. The image recorded after 36 hours is noticeably more textured, indicating the appearance of larger crystallites. Such an observation is often characteristic of a solvent-mediated phase transition in which one form dissolves and recrystallises into another form. This is entirely possible since DMU is very soluble in the methanol:ethanol mixture.

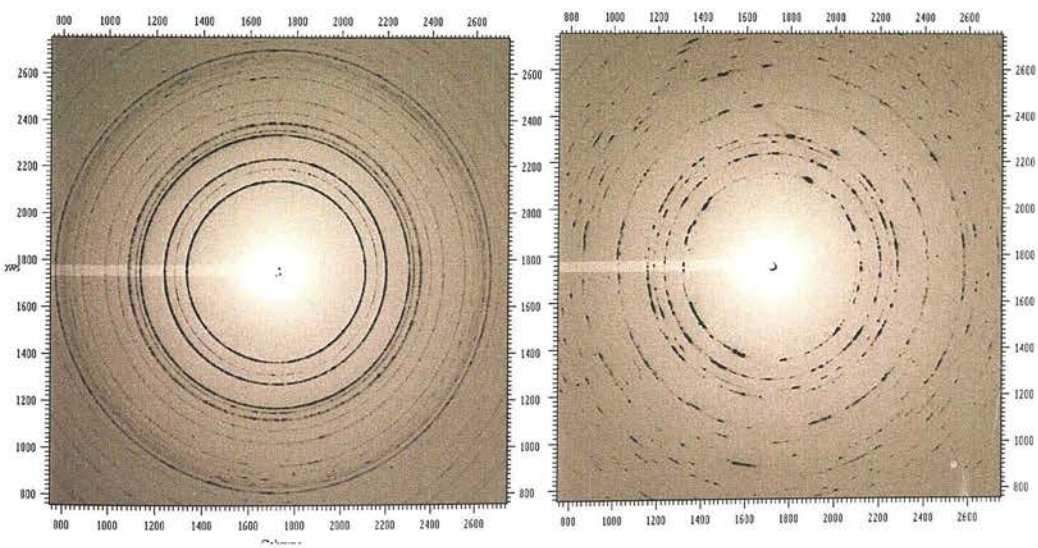

Figure 4.19: 2-D diffraction images of DMU at ambient pressure before (left) and after (right) 36 hours.

4.3.5.3. Powder compression using Fluorinert-FC77 as pressure-transmitting medium

Figure 4.20 shows the powder patterns for DMU collected at increasing pressure steps between ambient and 1.75 GPa. Fluorinert-FC77 was used as pressure-

transmitting medium in this case. The pattern recorded at ambient pressure was indexed as form I. On increasing pressure to 0.1 GPa all peaks attributable to form I disappeared and new peaks appeared in the pattern, indicating a phase transition. The pattern at 0.1 GPa was identified as a mixture of forms II and III. Figure 4.21 shows a Le Bail fit of the experimental pattern at 0.1 GPa to the lattice parameters of forms II and III. The pressure was then increased in small steps to 1.75 GPa. No further phase transition was observed and all the patterns were indexed as a mixture of form II and III, showing that both forms persist up to 1.75 GPa. However, broadening of peaks with pressure suggests either non-hydrostatic conditions associated with the pressure-transmitting medium or strain in the sample, perhaps indicating the onset of a phase transition. Unit cell parameters obtained with increasing pressures for form II and III are shown in Tables 4.5 and 4.6, respectively. The derived lattice parameters for forms II and III are highly correlated and therefore show rather similar values for volume/molecule.

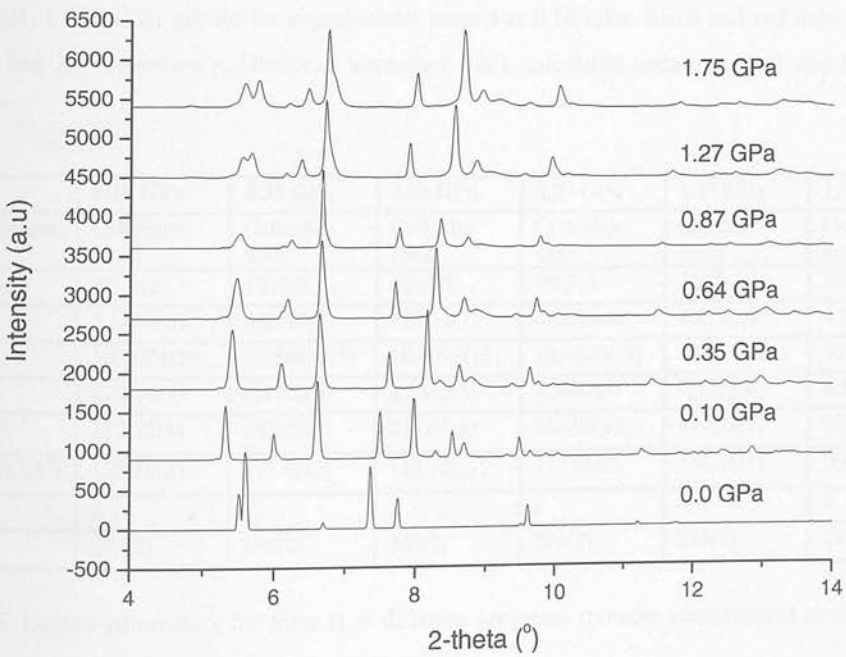

Figure 4.20: X-ray powder patterns of DMU with Fluorinert FC-77 as pressure-transmitting medium. Patterns were recorded at pressures up to 1.75 GPa. Powder diffraction patterns were collected with synchrotron X-ray radiation (λ = 0.485Å) using Beamline I15 at the Diamond Light Source, Oxfordshire.

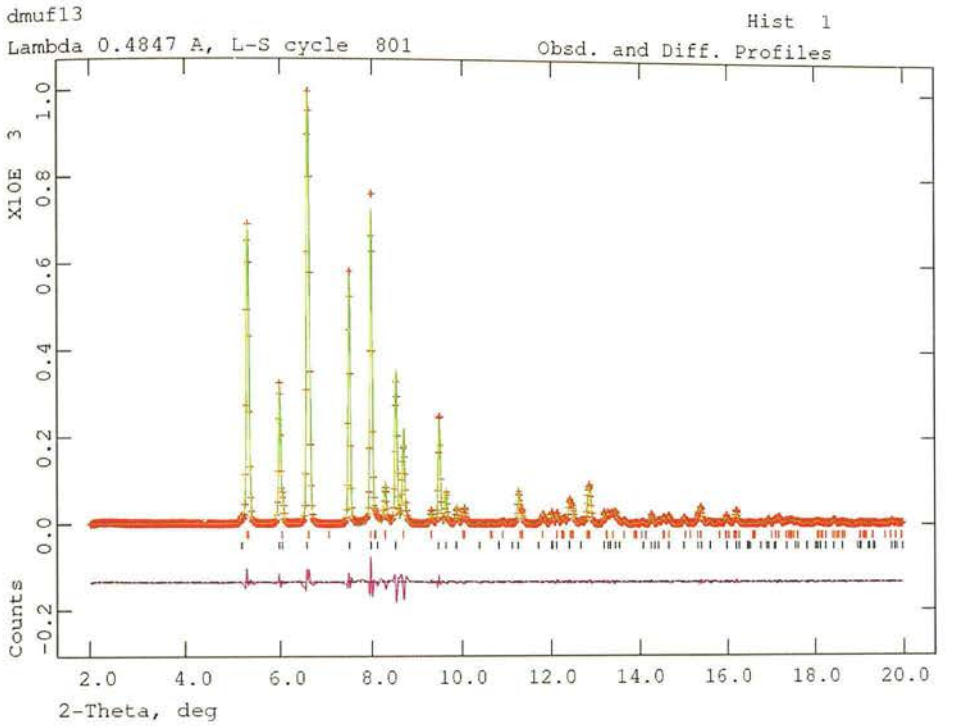

Figure 4.21: Le Bail fit profile for experimental pattern at 0.10 GPa. Black and red ticks represent forms II and III respectively. Observed intensities (red), calculated pattern (green) and difference (pink).

Pressure	**0.10 GPa**	**0.35 GPa**	**0.64 GPa**	**0.87 GPa**	**1.27 GPa**	**1.75 GPa**
Crystal System	Orthorho-mbic	Orthorho-mbic	Orthorho-mbic	Orthorho-mbic	Orthorho-mbic	Orthorho-mbic
Space group	$P2_12_12$	$P2_12_12$	$P2_12_12$	$P2_12_12$	$P2_12_12$	$P2_12_12$
***a* (Å)**	5.1428(6)	5.0377(8)	4.9679(7)	4.9285(8)	4.8130(9)	4.7674(9)
***b* (Å)**	10.7074(10)	10.5689(15)	10.4903(16)	10.4400(18)	10.3117(20)	10.2113(26)
***c* (Å)**	4.5893(4)	4.5762(6)	4.5562(5)	4.5477(4)	4.5239(6)	4.5066(8)
V (Å^3)	252.72(4)	243.65(6)	237.44(5)	234.00(6)	224.52(7)	218.46(8)
V/molecule (Å^3)	126.36(2)	121.83(3)	118.72(2)	117.01(2)	110.48(1)	109.23(4)
Z	2	2	2	2	2	2
T (K)	293(2)	293(2)	293(2)	293(2)	293(2)	293(2)

Table 4.5: Lattice parameters for form II at different pressures (powder compression studies using Fluorinert FC-77 as pressure-transmitting medium).

Pressure	0.10 GPa	0.35 GPa	0.64 GPa	0.87 Gpa	1.27 GPa	1.75 GPa
Crystal System	Monoclinic	Monoclinic	Monoclinic	Monoclinic	Monoclinic	Monoclinic
Space group	*P*2/c	*P*2/c	*P*2/c	*P*2/c	*P*2/c	*P*2/c
a (Å)	5.2559(5)	5.1659(6)	5.1153(7)	5.0751(8)	4.9742(8)	4.8691(11)
b (Å)	4.5873(32)	4.5654(5)	4.5391(8)	4.5229(8)	4.4925(8)	4.4630(10)
c (Å)	10.5216(8)	10.4184(15)	10.3535(19)	10.2804(18)	10.1565(20)	10.0855(23)
β (°)	96.948(6)	97.520(13)	97.985(15)	98.657(12)	98.912(18)	98.397(24)
V (Å^3)	251.81(4)	243.60(5)	238.07(7)	233.29(5)	224.22(7)	216.82(9)
V/molecule (Å^3)	140.90(5)	121.65(3)	119.03(8)	116.64(7)	112.11(3)	108.26(4)
Z	2	2	2	2	2	2
T (K)	293(2)	293(2)	293(2)	293(2)	293(2)	293(2)

Table 4.6: Lattice parameters for form III at different pressures (powder compression studies using Fluorinert FC-77 as pressure-transmitting medium).

In the next step the sample was heated to 150 °C for 10 minutes in order to overcome any kinetic barriers to potential phase transitions. The powder pattern recorded after heating (Figure 4.22) was completely different and could be successfully indexed to form IV (lattice parameters are shown in Table 4.7). The sharp peaks of the powder pattern combined with the excellent powder averaging (Figure 4.23) strongly suggest a reconstructive phase transition that has greatly increased the degree of powder averaging.

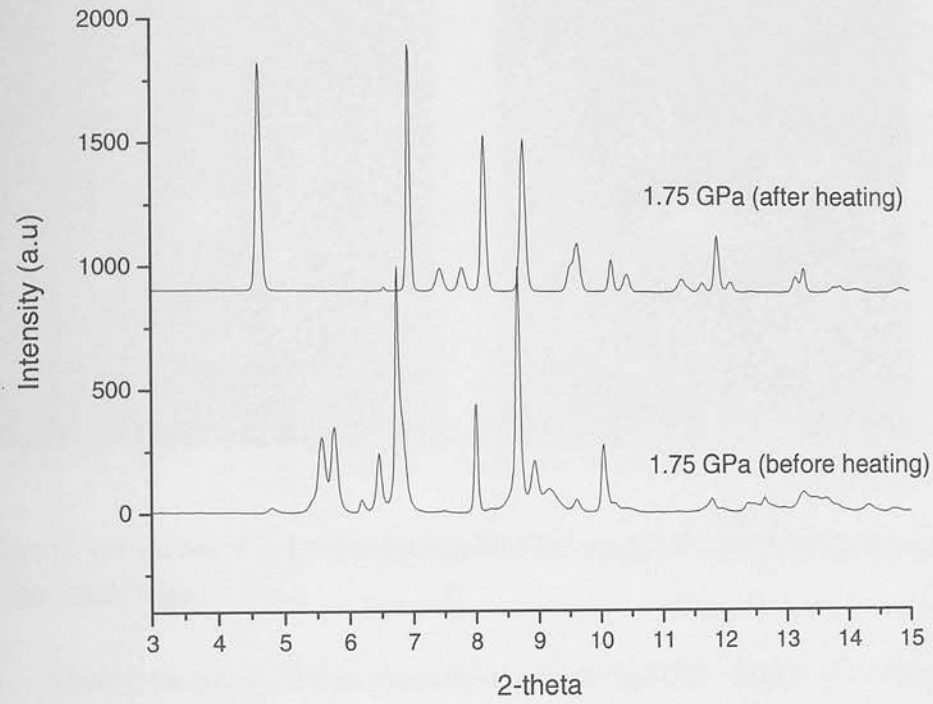

Figure 4.22: Comparison of powder patterns recorded before (lower) and after (upper) heating the sample at 1.75 GP to 100 °C for 10 minutes. Upper pattern was indexed as form IV ($\lambda = 0.485$Å).

Pressure	**Form IV**
Crystal System	Orthorhombic
Space group	*Pbcn*
***a* (Å)**	4.1529(4)
***b* (Å)**	8.4968(8)
***c* (Å)**	12.0074(8)
V (Å^3)	423.70(8)
Z	4
P (GPa)	1.75(5)
T (K)	293(2)

Table 4.7: Lattice parameters for form IV at 1.75 GPa.

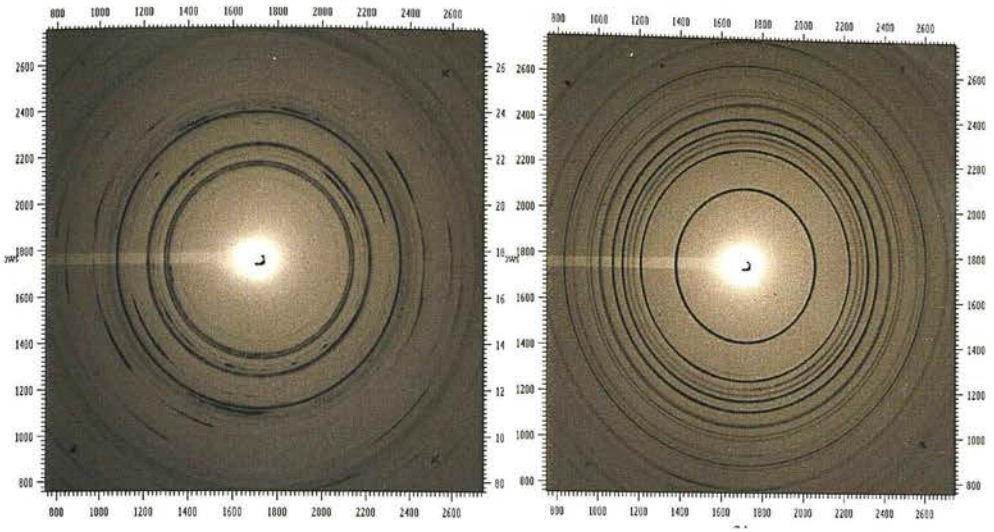

Figure 4.23: Comparison of 2-D diffraction image for DMU samples at 1.75 GPa before heating (left) and after heating (right).

Finally the pressure was released to ambient and this resulted in a very poor quality powder pattern (Figure 4.24). The diffuse rings suggest that the sample has become amorphous, perhaps indicating a potential phase transition that is kinetically hindered. For this reason the sample was heated to 80 °C for 5 minutes in order to overcome any kinetic barrier, and this greatly improved the quality of the powder pattern (Figure 4.24). Figure 4.25 shows the powder pattern recorded at ambient pressure after heating. It is evident from the comparison of powder patterns (Figure 4.25) that all the peaks attributed to form IV have completely disappeared and the sample has transformed to a new form. The powder pattern does not correspond to forms I, II and III or any mixture of the three. Unfortunately all indexing attempts for this form were unsuccessful; perhaps suggesting it may be a mixed phase. The DAC was then left for 2 hours at ambient pressure. The powder pattern recorded after 2 hours (Figure 4.14) shows partial transformation of the sample to form I.

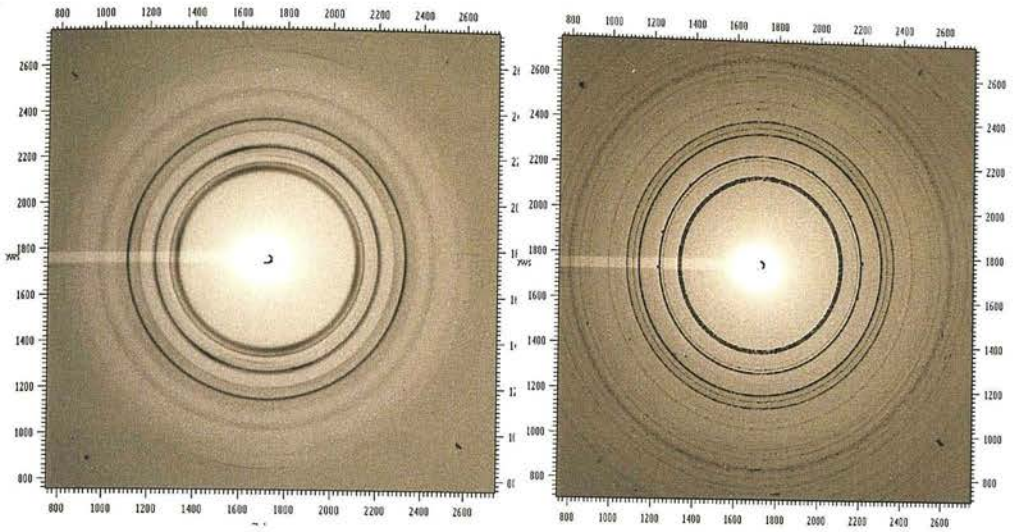

Figure 4.24: Comparison of 2-D diffraction image for DMU samples at ambient pressure before heating (left) and after heating (right).

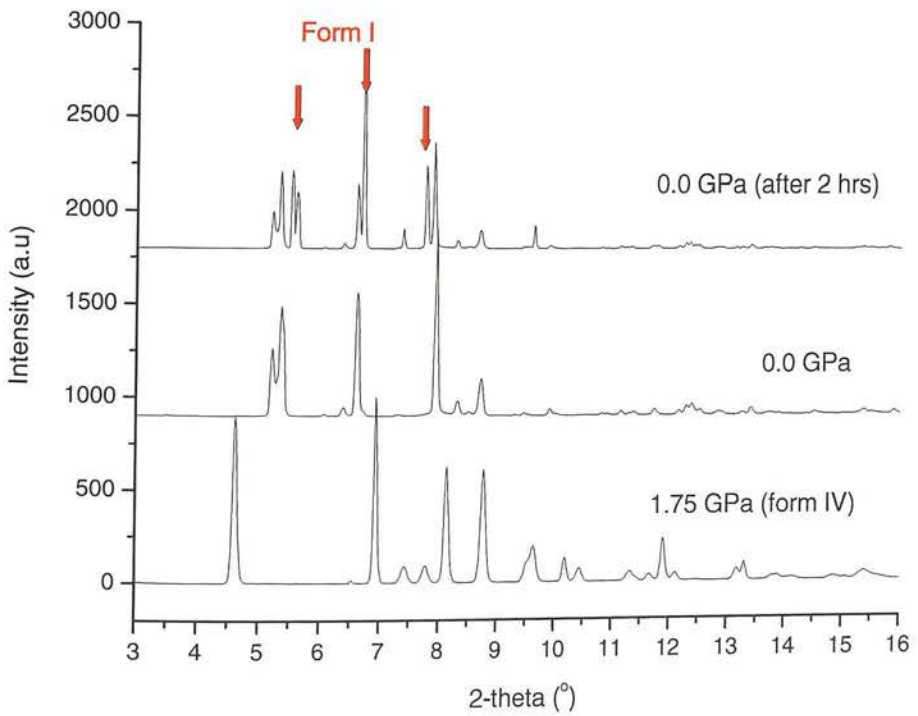

Figure 4.25: X-ray powder diffraction patterns of DMU recorded after releasing pressure to ambient ($\lambda = 0.485$ Å).

4.3.6. Stability and decompression studies

The transformations between the polymorphs of N, N'-dimethylurea are summarised in Scheme 4.1.

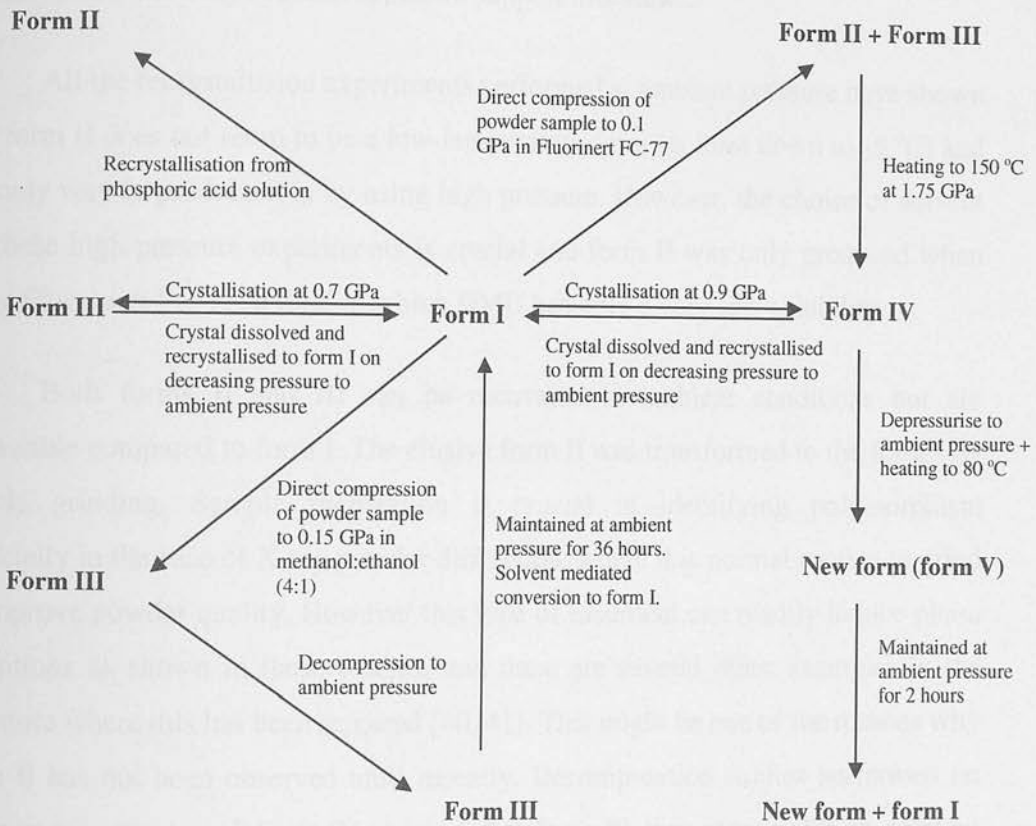

Scheme 4.1: Transformations of polymorphs of DMU

The question as to whether such high-pressure forms are sufficiently metastable that they can be recovered at ambient conditions is naturally of great importance. All the above experiments show that form I is the most stable polymorph under ambient conditions. Compression of the powder samples of form I using Fluorinert FC-77 as a pressure-transmitting medium produced a mixture of forms II and III at 0.1 GPa. Once produced, these forms were stable up to 1.75 GPa. Form III was rather persistent and was also produced by the compression of the powder samples of form I at 0.15 GPa in methanol:ethanol mixture and through the crystallisation from methanol:ethanol solution at 0.7 GPa. Comparison of the crystal

structures of forms I, II and III, suggests that direct compression of form I is unlikely to initiate a transition to form II or III, as this would involve the concerted reorientation of DMU molecules in alternate chains. This would be expected to give rise to a significant kinetic barrier, and so such phase transitions are likely to be solvent-mediated. These results appear to support this view.

All the recrystallision experiments performed at ambient pressure have shown that form II does not seem to be a low-temperature form (at least down to -5 °C) and the only way to produce it is by using high pressure. However, the choice of solvent for these high-pressure experiments is crucial and form II was only produced when using Fluorinert FC-77, a fluid in which DMU has only a very low solubility.

Both forms II and III can be recovered at ambient conditions but are metastable compared to form I. The elusive form II was transformed to the form I by simple grinding. Sample preparation is crucial in identifying polymorphism especially in the case of X-ray powder diffraction, where it is normal routine to grind to improve powder quality. However this type of treatment can readily induce phase transitions as shown in these studies, and there are several other examples in the literature where this has been reported [40, 41]. This might be one of the reasons why form II has not been observed until recently. Decompression studies performed on the powder samples of form III showed that form III was recoverable at ambient conditions, but converted back to form I through a solvent-mediated phase transition within 36 hours.

Form IV was produced by heating a mixture of forms II and III to 150 °C at 1.75 GPa. It was also produced through crystallisation of a DMU solution in methanol:ethanol at 0.9 GPa. Both these experiments strongly suggest that the transition to form IV is reconstructive, heat or solvation energy is needed to overcome any kinetic barrier to a phase transition. This is also evident from the crystal structure of form IV where an entirely different packing arrangement is observed. Optical observation of a single crystal during progressive decompression from *ca.* 0.9 GPa at 293 K, showed that the single crystal gradually dissolved.

Decompression of the powder sample of form IV to ambient pressure resulted in an amorphous form which on heating converted to a new form, again suggesting a reconstructive phase transition. This new form was recovered to ambient conditions; but after 2 hours it partially converted to form I. The choice of liquid as pressure-transmitting fluid is also very important in high-pressure experiments, presumably reflecting the solubilities of the substrates in the respective media. In this case, compression using methanol:ethanol mixture resulted in form III whilst compression using Fluorinert FC-77 resulted in a mixture of forms II and III.

4.4. Crystal structure prediction (CSP)

4.4.1. Introduction

The studies on DMU stimulated crystal structure prediction (CSP) calculations by Dr. Graeme Day at the University of Cambridge. DMU is a small and fairly rigid molecule and so should be a very good candidate for such calculations. The aims of these studies were to discover whether CSP methods were effective in identifying the experimentally observed forms and also to discover whether any of the predicted forms could be accessed experimentally.

4.4.2. Result and Discussion

Crystal structure predictions were performed assuming a rigid molecular geometry. In keeping the predictions blind from the experimental results, the only information about the observed crystal known in advance of computational work was that four polymorphs had been isolated experimentally; two of them were obtained at ambient conditions whilst the other two were generated at high-pressure. The structure of the DMU molecule shows the possibility of conformational changes around the C-N bond. Furthermore, a search of the CSD [42] on DMU and similar molecules indicated that the conformation around one of the nitrogen atoms may change. Therefore, calculations based on DFT (density functional theory) were

performed on the isolated molecule with the four molecular geometries shown in Figure 4.26.

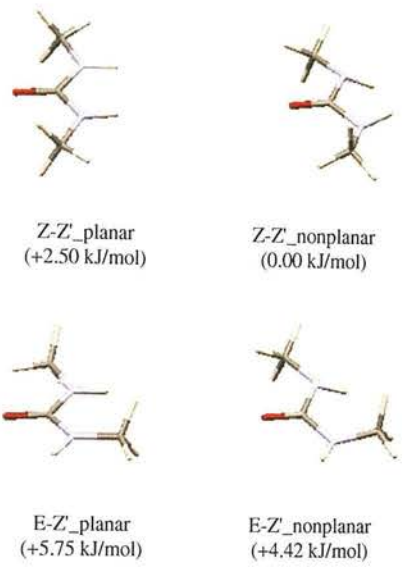

Figure 4.26: Four geometries of DMU molecule employed in CSP search. "Z-Z" represents the *trans* conformation of methyl groups whilst "E-Z" represents the *cis* conformation of methyl group around C=O bond.

Initial energy calculations showed that the Z-Z' conformations were the two lowest energy modifications. Furthermore, with the Z-Z' conformation two sets of predictions were performed; these differed only in the orientation of the hydrogen atoms on the methyl groups. The two geometries that were considered had a C-H bond either eclipsed with the C=O or a C-H eclipsed with the neighbouring N-H bond. These are related by a 60° rotation about the N-C bond. The two geometries of DMU molecules used in CSP are shown in Figure 4.27.

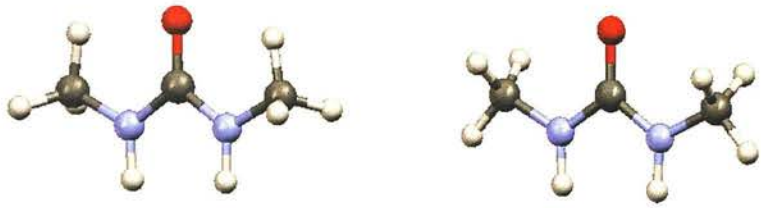

Figure 4.27: Two geometries of DMU molecule used in CSP; one with C-H of methyl group eclipsed with C=O bond (left) and second with C-H bond eclipsed with N-H bond (right)

Calculations were performed using a model described by T. G. Cooper *et al.*, [43]. Structures obtained from all these geometries were then combined and duplicate structures were removed by the program *PLATON* [44]. All four polymorphs were found in the set of low energy structures. Polymorphs II, III and IV were in the lowest five structures in the lattice energy. The CSP results are described in the following paragraphs.

Approximately 100 crystal structures of DMU were predicted within 5 kJ mol^{-1} of the global minimum in lattice energy. A plot of the energies and densities of the lowest energy calculated crystal structures, with the experimental structures highlighted, is shown in Figure 4.28. Unit cell parameters, space groups, volumes, densities and energies of the 50 lowest energy predictions are given in Table 4.8. As expected, all of the lowest energy structures contain N-H…O hydrogen bonds; the length of this bond (H...O) is within the range of 1.98-2.00 Å. Almost all of the 50 lowest energy structures show bifurcated hydrogen bonds to form infinite chains of DMU molecules that run parallel to one of unit cell axes. However, only two of these (nos. 4 and 11) form different arrangements of DMU molecule; structure no. 4 shows hydrogen bonding as depicted in one of the high-pressure forms of DMU (form IV) whilst structure no. 11 shows an unusual packing of molecules and can be excluded from the list. In all these predicted structures, DMU molecules are planar and adopt the Z-Z' conformation.

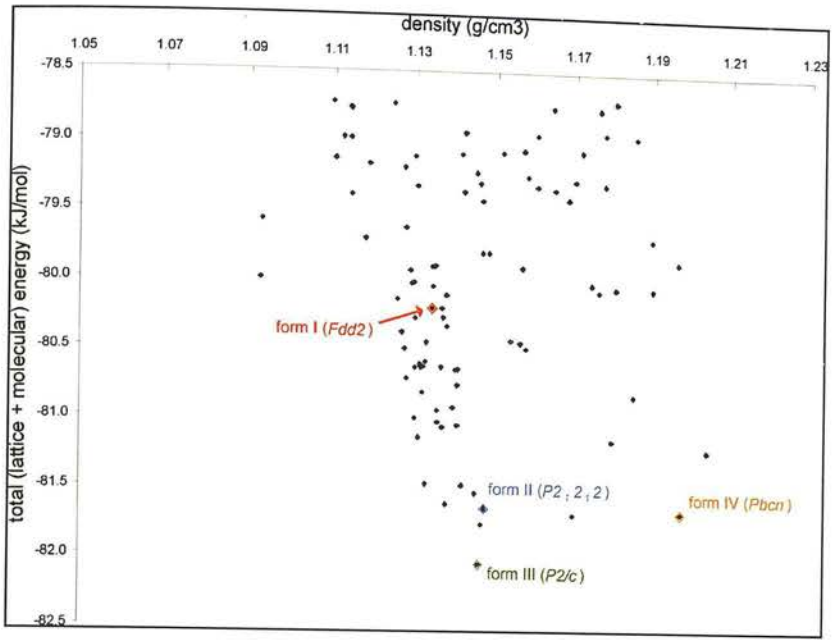

Figure 4.28: Plot of lattice energy against volume for the predicted structures of DMU within 5 kJ/mol of the global minimum. Experimental structures are highlighted as forms I, II, III and IV.

Rank on Energy	E lattice (kJ/mol)	Space Group	*a* (Å)	*b* (Å)	*c* (Å)	*α* (°)	*β* (°)	*γ* (°)	Volume (Å^3)	Density g/cm^3	notes
1	-82.06	*P2/c*	5.415	4.629	10.249	90	96.29	90	255	1.146	form III
2	-81.77	$P2_1/c$	4.632	5.415	20.352	90	90.45	90	510	1.147	
3	-81.70	$P2_1/c$	8.457	7.119	8.645	90	105.95	90	500	1.170	
4	-81.69	*Pbcn*	4.624	8.383	12.614	90	90	90	489	1.197	form IV
5	-81.66	$P2_12_12$	5.427	10.142	4.635	90	90	90	255	1.147	form II
6	-81.63	*P2/c*	10.962	4.63	10.582	90	106.71	90	514	1.138	
7	-81.55	*C2/c*	4.639	9.826	22.536	90	95.57	90	1022	1.145	
8	-81.49	*C2/c*	14.106	4.634	15.707	90	92.86	90	1025	1.142	
9	-81.48	*Pmmn*	6.45	8.646	4.633	90	90	90.01	258	1.133	
10	-81.23	$P2_1/c$	4.652	11.681	8.951	90	91.28	90	486	1.204	
11	-81.16	$P2_1/c$	4.899	11.314	9.042	90	97.96	90	496	1.179	
12	-81.15	*Pnma*	12.904	8.644	4.64	90	90	90	518	1.131	
13	-81.07	*C2/c*	10.338	4.637	10.8	90.03	96.05	90.02	515	1.137	
14	-81.06	*C2/c*	22.957	4.632	10.272	90	110	90	1026	1.140	
15	-81.03	*C2/c*	21.474	4.634	10.575	90	101.6	90	1031	1.136	

Table 4.8: Summary of the 50 lowest energy structures generated by CSP calculations. Crystal structures were generated with each of the 4 molecular geometries and then lattice energy minimised. The 1st , 4th ,5th and 41st ranked structures are a reasonable reproduction of forms III, IV, II and I of the DMU.

Rank on Energy	E lattice (kJ/mol)	Space Group	a (Å)	b (Å)	c (Å)	α (°)	β (°)	γ (°)	Volume (Å^3)	Density g/cm^3	notes
16	-81.00	$C2/c$	21.201	4.636	10.797	90	102.54	90	1036	1.130	
17	-80.95	$Pca2_1$	10.619	4.633	10.478	90	90	90	515	1.135	
18	-80.93	$P2_1/c$	5.418	4.635	20.583	90	96.43	90	514	1.139	
19	-80.84	$P2/c$	7.88	4.631	15.349	90	118.12	90	494	1.185	
20	-80.82	P-1	4.637	5.487	11.04	82.74	85.67	68.2	259	1.132	
21	-80.77	$P2_1/c$	4.635	20.365	7.113	90	130.16	90	513	1.140	
22	-80.72	$Imm2$	6.457	8.645	4.649	90	90	90	259	1.128	
23	-80.66	$P2_12_12_1$	4.638	5.418	20.434	90	90	90	513	1.140	
24	-80.65	$Pna2_1$	20.317	4.637	5.446	90	90	90	513	1.141	
25	-80.64	P-1	4.639	5.78	10.984	74.87	78.1	66.54	259	1.130	
26	-80.64	P-1	4.638	5.797	10.947	95.46	102.1	113.48	259	1.131	
27	-80.64	$P2_1/c$	11.108	4.636	10.848	90	112.78	90	515	1.136	
28	-80.63	$C2/c$	10.63	4.643	21.373	90	101.36	90	1034	1.132	
29	-80.62	P-1	4.638	5.796	10.947	95.47	102.09	113.44	259	1.131	
30	-80.60	$C2/c$	21.468	4.634	10.609	90	101.62	90	1034	1.132	
31	-80.50	$C2/c$	10.812	4.645	21.19	90	102.63	90	1038	1.127	
32	-80.50	$P2_1/c$	4.639	8.685	12.55	90	90.33	90	506	1.158	
33	-80.46	P-1	4.639	7	8.42	67.79	89.96	89.54	253	1.156	
34	-80.46	$Pbca$	7.524	8.616	15.942	90	90	90	1033	1.133	
35	-80.44	$P2_1/c$	8.331	7.421	8.447	90	103.72	90	507	1.154	
36	-80.39	$C2/c$	10.823	4.641	10.803	90	106.75	90	520	1.127	
37	-80.34	$Pna2_1$	4.639	10.167	10.908	90	90	90	514	1.138	
38	-80.28	$C2$	10.613	4.644	10.972	90	106.66	90	518	1.130	
39	-80.28	$C2/c$	10.093	4.602	11.301	90.16	101.23	90.04	515	1.137	
40	-80.21	$C2/c$	10.51	4.601	10.861	90.02	101.3	90.49	515	1.137	
41	-80.21	$Fdd2$	21.785	10.292	4.604	90.01	90	90	1032	1.134	form I (NIJHUJ01)
42	-80.15	$P2_1/c$	4.626	15.674	7.45	90	105.68	90	520	1.125	
43	-80.11	$C2/c$	10.695	4.603	10.656	89.16	101.21	89.83	514	1.138	
44	-80.08	$P2_1/c$	4.648	9.644	11.106	90	90.05	90	498	1.176	
45	-80.06	$P2_1/c$	13.325	4.564	8.344	90	104.16	90	492	1.190	
46	-80.06	$C2/c$	15.508	4.619	15.743	90	118.4	90	992	1.180	
47	-80.05	$C2/c$	15.805	4.638	14.099	90	93.12	90	1032	1.134	
48	-80.03	$P2_1$	4.641	10.493	5.792	90	113.23	90	259	1.129	
49	-80.03	$C2/c$	15.379	4.64	15.928	90	118.67	90	997	1.174	
50	-80.02	$P2_1/c$	10.984	4.637	10.612	90	106.55	90	518	1.130	

Table 4.8 (continued): Summary of the 50 lowest energy structures generated by CSP calculations.

To account for the lack of kinetic considerations in the structure prediction, as well as imperfections in the model potential, some observations from the Cambridge Structural Database (CSD) can be used to highlight some of the low energy predictions that are less likely. For example, some of the predicted polymorphs have

very long unit cell axes ranging up to 42.3 Å. A search of the CSD has shown that unit cell axes with dimensions over 30 Å are rare, even with two molecules in the asymmetric unit. The rarity of such structures in the CSD could reflect a kinetic disadvantage for such an elongated unit cell axis, perhaps because this can lead to extreme morphologies and uncompetitive overall growth rate. Five structures were therefore considered to be unlikely, though not impossible, based upon their unit cell axes. One of the useful parameters to evaluate predicted crystal structures is the frequency of space groups which occur in the CSD. A search of the CSD has shown that some space groups *e.g.* $P2_1/c$, are more common whilst some are very rare. In the 50 lowest energy predicted structure the most frequent space group was $C2/c$, with about 40% of structures showing this space group. A second common space group is $P2_1/c$, with about 20% of the structures belonging to this space group. Interestingly all of the four known polymorphs of DMU show different space groups. This might suggest that there are more DMU polymorphs which have not been experimentally observed yet. In our lowest energy predicted structure list, 4 out of 50 structures belonged to uncommon space groups and therefore were considered to be unlikely, though not impossible, and could be excluded from the list. Predicted structures were also viewed with *MERCURY* [21] and *PLATON* [44] in order to exclude any structures that have unusual intermolecular interactions.

The structure corresponding to a global minimum at -82.06 kJ mol^{-1} is a reasonable reproduction of the observed form III structure. This structure is denser than most of the predicted structures which is in agreement with the experimental observation that form III was obtained at high pressure (0.7 GPa).

The crystal structure with the second lowest lattice energy has a space group $P2_1/c$. It is just 0.29 kJ mol^{-1} above the global minimum. There are four molecules in the unit cell, and it shows a similar hydrogen bonding pattern to that found in forms I, II and III. However, in this case the DMU molecules are non-planar which results in slightly different hydrogen bond lengths from one another; one at 1.97 Å and a second at 1.99 Å. The difference in the two hydrogen bond lengths results in a different graph-set notation (N_1 = C(4)C(4)C^2_2(8)R^1_2(6)) in comparison to forms I, II and III. Crystal structure no. 3 is 0.29 kJ mol^{-1} higher in energy than the global minimum. This is also a $P2_1/c$ structure with four molecules in the unit cell, but the

density of this structure is significantly higher (~15%) than the previous one. However, the crystal structure shows corrugated chains of DMU molecules. This is rather unusual as all the reported disubstituted ureas with Z-Z' configurations show linear chains. On this basis, structure no. 3 can be excluded from this list.

The 4th ranked structure is a reasonable reproduction of the form IV structure. It is only 0.37 kJ mol^{-1} above the global minimum. The crystal structure representing form I was also one of the densest structures found in the CSP. The calculated density of this structure is 1.197 g cm^{-3}, *ca.* 4.5 % higher than for the global minimum structure. This result is in good agreement with the experimental results, as form IV was obtained by crystallisation at high pressure (0.9 GPa).

The 5th structure in the list of lowest energy structures (Table 4.8) corresponds to the observed form II structure. This crystal structure is 0.40 kJ mol^{-1} higher in lattice energy than the global minimum. Form I (one of the ambient pressure polymorphs) was also predicted by the calculations. This structure occurs low in the list and is represented by structure no. 41 in Table 4.8. However, this order can be improved, as some of structures (*e.g.* 8, 9 and 10) can be ruled out either by the presence of unreasonable packing or uncommon space group. This structure is only 2.39 kJ mol^{-1} higher in lattice energy than the global minimum structure. Furthermore these calculations were performed at 0 K, therefore stability of these forms may change. Results from these calculations show opportunities for experimentally obtaining other polymorphs.

4.5. Overall conclusions

High-pressure crystallisation of DMU solution in methanol:ethanol (4:1) mixture contained in a diamond-anvil cell at pressure 0.7 and 0.9 GPa resulted in formation of two new high-pressure polymorphs designated as forms III and IV, respectively. Crystal structures of these forms have been reported here. The molecular packing arrangement of the new forms is very different from forms I and II. However, DMU molecules adopt the same (Z-Z') conformation in all these forms.

Form II was finally produced at 0.1 GPa through compression of form I using Fluorinert FC-77 as a pressure-transmitting medium. This result shows that high-pressure techniques can be used to obtain elusive polymorphs particularly when the elusive polymorph is more dense. Form III was also produced by compression of powder samples of form I using methanol:ethanol mixture. It is clear from the results of this study that the role of the pressure-transmitting medium is very important; different pressure transmitting medium may result in different forms depending on the solubility of material. Decompression of form III immersed in methanol:ethanol showed that form III can be recovered to ambient pressure, but it was converted back to form I through a solvent mediated phase transition.

Form IV was produced by heating mixture of form II and III to 150 °C at 1.75 GPa. Decompression of form IV to ambient pressure resulted in formation of amorphous material which on heating converted to a new form. This new form was recoverable at ambient pressure, but partially converted to form I.

It is clear from this work that high-pressure techniques under a range of conditions allow one to obtain different polymorphs. Therefore pressure has the potential to add another valuable dimension to polymorph screening. Crystal structure prediction calculations have generated all four forms, and point towards more, as yet undiscovered, forms that may be accessible by experiment.

4.6. References

1. H. U. Lenne, *Zeitschrift fuer Kristallographie, Kristallgeometrie, Kristallphysik, Kristallchemie*, 1961, **115**, 297-302.
2. M. S. Miao, V. E. Van Doren, R. Keuleers, H. O. Desseyn, C. Van Alsenoy and J. L. Martins, *Chem. Phys. Lett.*, 2000, **316**, 297.
3. D. Gora and K. Parlinski, *J. Chem. Phys*, 2000, **113**, 8138-8141.
4. J. E. Worsham, H. A. Levy and S. W. Peterson, *Acta Crystallogr.*, 1957, **10**, 319-323.
5. S. Pal, A. K. Manna and S. K. Pati, *J. Chem. Phys.*, 2008, **129**, 204301-204307.
6. P. Vaughan and J. Donohue, *Acta Crystallogr.*, 1952, **5**, 530-535.
7. N. Sklar, M. E. Senko and B. Post, *Acta Crystallogr.*, 1961, **14**, 716-720.
8. F. J. Lamelas, Z. A. Dreger and Y. M. Gupta, *J. Phys. Chem. B*, 2005, **109**, 8206.
9. P. W. Bridgman, *Proc. Am. Acad. Arts Sci.*, 1916.
10. P. W. Bridgman, *Proc. Am. Acad. Arts Sci.*, 1938, **72**, 227-268.

11. M. M. Bonin, W. G. Weber, H.P. Toledano, ISIS Pulsed Neutron and Muon Source, Rutherford Appleton Laboratory, Didcot, UK, Annual report 1998.
12. H. P. Weber, W. G. Marshall and V. Dmitriev, *Acta Crystallogr., Sect. A*, 2002, **58**, c174.
13. A. Olejniczak, K. Ostrowska and A. Katrusiak, *J. Phys.Chem. C*, 2009, **113**, 15761.
14. Schay, E., W. Focke, and L. Walbrugh, Bayer Healthcare AG, Germany. *Application:WO Pat.*, 2006.
15. S. Ren, A. Das and E. J. Lien, *J. Drug Target.*, 1996, **4**, 103-107.
16. H. Dejima, J. Inokoshi and Y. Yoshida, Kao Corp, Japan. *Japan Pat.*, 1997.
17. S. Sandler, *Diabetologia*, 1984, **26**, 386-388.
18. J. Perez-Folch, J. A. Subirana and J. Aymami, *Journal. Chem. Crystallogr.*, 1997, **27**, 367-369.
19. R. Marsh, *Acta Crystallogr., Sect. B: Struct. Sci.*, 2004, **60**, 252-253.
20. D. M. S. Martins, C. K. Spanswick, D. S. Middlemiss, N. Abbas, C. R. Pulham and C. A. Morrison, *J. Phys. Chem. A*, 2009, **113**, 5998-6003.
21. C. F. Macrae, P. R. Edgington, P. McCabe, E. Pidcock, G. P. Shields, R. Taylor, M. Towler and J. van de Streek, *J. Appl. Crystallogr.*, 2006, **39**, 453-457.
22. L. Merrill and W. A. Bassett, *Rev. Sci. Instrum.*, 1974, **45**, 290-294.
23. S. A. Moggach, D. R. Allan, S. Parsons and J. E. Warren, *J. Appl. Crystallogr.*, 2008, **41**, 249-251.
24. G. J. Piermarini, S. Block, J. D. Barnett and R. A. Forman, *J. Appl. Phys.*, 1975, **46**, 2774-2780.
25. A. Dawson, D. R. Allan, S. Parsons and M. Ruf, *J. Appl. Crystallogr.*, 2004, **37**, 410-416.
26. B. AXS, *SAINT*, Bruker-AXS, Madison, Wisconsin, USA, 2003.
27. S. Parsons, *SHADE*, University of Edinburgh, Scotland, UK, 2004.
28. G. M. Sheldrick, *SADABS*, University of Göttingen, Germany, 2006.
29. R. Blessing, *Acta Crystallogr., Sect. A: Found. Crystallogr.*, 1995, **51**, 33-38.
30. A. P. Hammersley, S. O. Svensson, M. H. and, A. N. Fitch and D. Hausermann, *High Pressure Res.*, 1996, **14**, 235-248.
31. A. Altomare, G. Cascarano, C. Giacovazzo, A. Guagliardi, M. C. Burla, G. Polidori and M. Camalli, *J. Appl. Crystallogr.*, 1994, **27**, 435.
32. P. W. Betteridge, J. R. Carruthers, R. I. Cooper, K. Prout and D. J. Watkin, *J. Appl. Crystallogr.*, 2003, **36**, 1487.
33. G. M. Sheldrick, *CELL_NOW*, University of Gottingen, Germany, 2002.
34. A. Dawson, D. R. Allan, S. Parsons and M. Ruf, *J. Appl. Crystallogr.*, 2004, **37**, 410-416.
35. S. Stankovic and G. D. Andreetti, *Acta Crystallogr., Sect. B: Struct. Sci.*, 1978, **B34**, 3787-3790.
36. W. A. Brett, P. Rademacher and R. Boese, *Acta Crystallogr., Sect. C: Cryst. Struct. Commun.*, 1990, **C46**, 880-882.
37. A. M. Z. Slawin, J. Lawson, J. M. D. Storey and W. T. A. Harrison, *Acta Crystallogr., Sect. E: Struct. Rep. Online*, 2007, **63**, 2925-2927.
38. J. Bernstein, R. E. Davis, L. Shimoni and N. L. Chang, *Angew. Chem., Int. Ed. Engl.*, 1995, **34**, 1555-1573.
39. W. D. S. Motherwell, G. P. Shields and F. H. Allen, *Acta Crystallogr., Sect. B: Struct. Sci.*, 1999, **B55**, 1044-1056.

40. S. Y. Lin, *Asian J.Pharm. Sci.*, 2007, **2**, 211-219.
41. M. Otsuka, T. Matsumoto and N. Kaneniwa, *Chem. Pharm. Bull.*, 1986, **34**, 1784-1793.
42. F. H. Allen and W. D. S. Motherwell, *Acta Crystallogr., Sect. B: Struct. Sci.*, 2002, **58**, 407-422.
43. T. G. Cooper, K. E. Hejczyk, W. Jones and G. M. Day, *J. Chem. Theory Comput.*, 2008, **4**, 1795-1805.
44. A. Spek, *J. Appl. Crystallogr.*, 2003, **36**, 7-13.

Chapter 5

An Exploration of the Polymorphism of GSK Compound A

Chapter 5: An Exploration of the Polymorphism of GSK Compound A

5.1. Background

Compound A was received from GlaxoSmithKline (GSK). It is a GSK developmental compound known to have HM74A (a protein-coupled receptor) agonist activity and has shown some potential to treat dyslipidimia (a condition associated with elevation of lipids in blood). The molecular structure of compound A is shown in Figure 5.1.

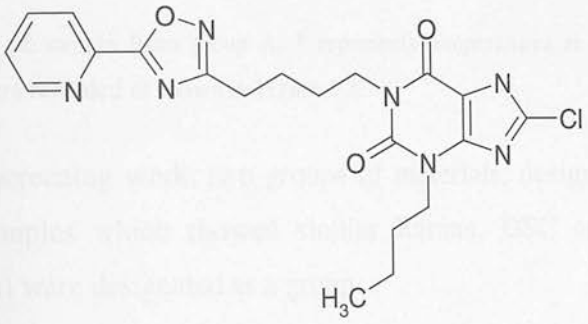

Figure 5.1: Molecular structure of compound A

Polymorph screening studies had previously been performed at GSK. Solid material used in these experiments (denoted as group A by GSK) was received after the first batch of synthesis and was identified as a mixture of two forms at ambient temperature. These forms were designated as unknowns 1 and 2. The DSC (Differential Scanning Calorimetry) plot obtained from group A (Figure 5.2) showed three endotherms. The peak at *ca.* 155 °C was the predominant form with a small amount of another form showing a small endotherm at *ca.* 148 °C. With increase in temperature the sample melted at *ca.* 156 °C and then recrystallised to give another form with a melting point of *ca.* 164 °C. The higher melting form was later designated as form I.

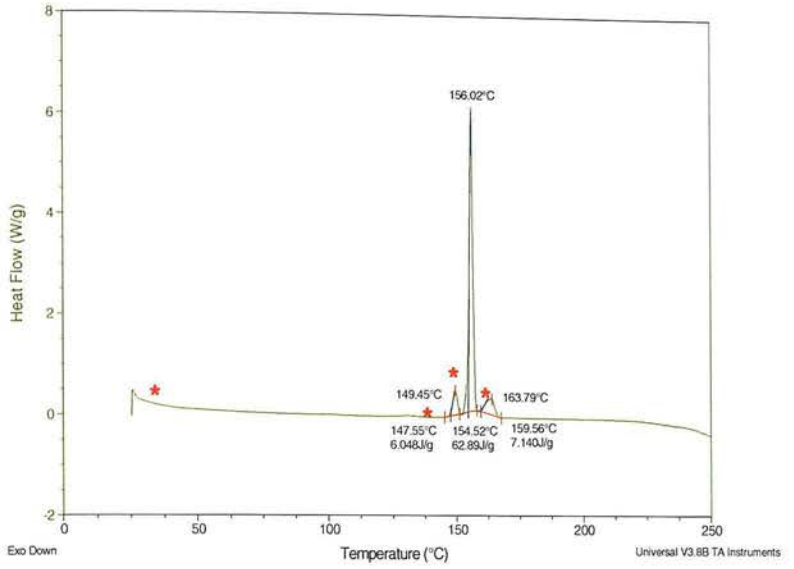

Figure 5.2: DSC plot of sample from group A. * represents temperatures at which X-ray powder diffraction patterns were recorded as shown in Figure 5.3.

From the screening work, two groups of materials, designated as B and C, were isolated. Samples which showed similar Raman, DSC and XRPD (X-ray powder diffraction) were designated as a group.

Figure 5.3 shows the DSC plot obtained from samples from group B. It showed a single endothermic melting event, which indicates the presence of a single form with a melting point of *ca.* 164 °C. This form was designated as form I. It was produced from a slurry of sample A maintained at > 5 °C for 24 hours. The XRPD pattern of form I is shown in Figure 5.7.

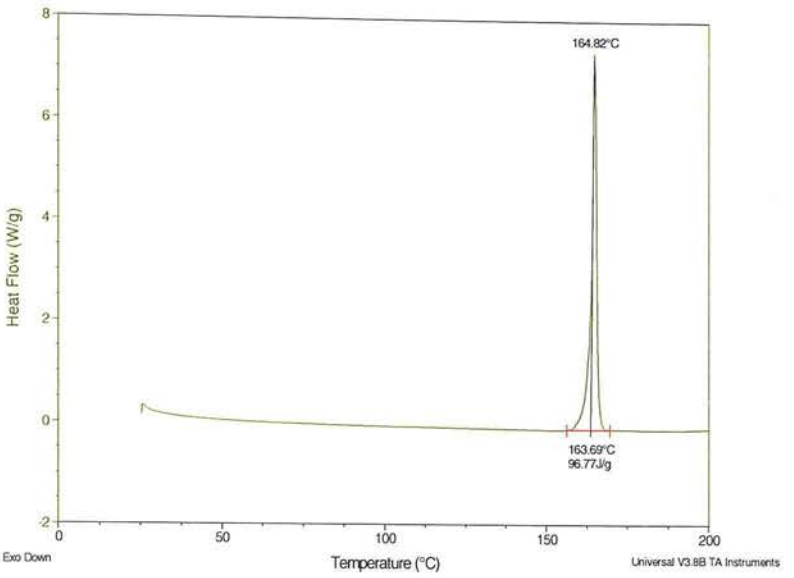

Figure 5.3: DSC plot of group B, indicating only a single endodermic peak at 164 °C.

From the samples of group C, another new form was identified by XRPD and was designated as form II. The XRPD pattern of form II is shown in Figure 5.7. It was produced from a slurry of sample A maintained at < 5 °C for more than 24 hours. Form II was also produced from a slurry of form I in 3 % aqueous acetone solution maintained at 0 °C for more than one week. The DSC plot obtained from form II (Figure 5.4) showed three endotherms. The first small peak at *ca.* 127 °C represents a solid to solid phase transition to a new form with melting point at *ca.* 149 °C, which ultimately converted to form I after melting and recrystallising events. The new form was identified as the same unknown 2 found for group A. XRPD patterns recorded before and after these events (highlighted by " * " in Figure 5.5) are shown in Figure 5.6. The XRPD pattern at ambient temperature (25 °C) represents pure form II, which converted to unknown 2 at *ca.* 135 °C.

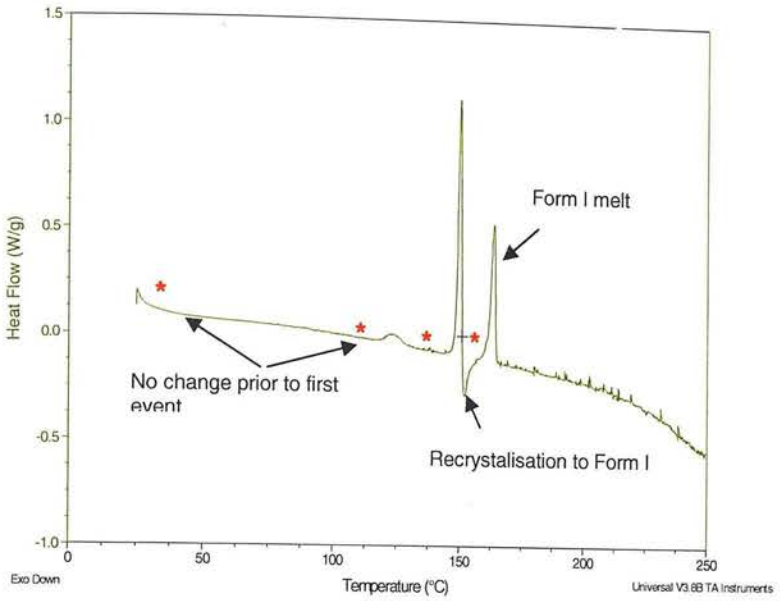

Figure 5.5: DSC plot of group C. * represents points where X-ray powder patterns were recorded as shown in Figure 5.6.

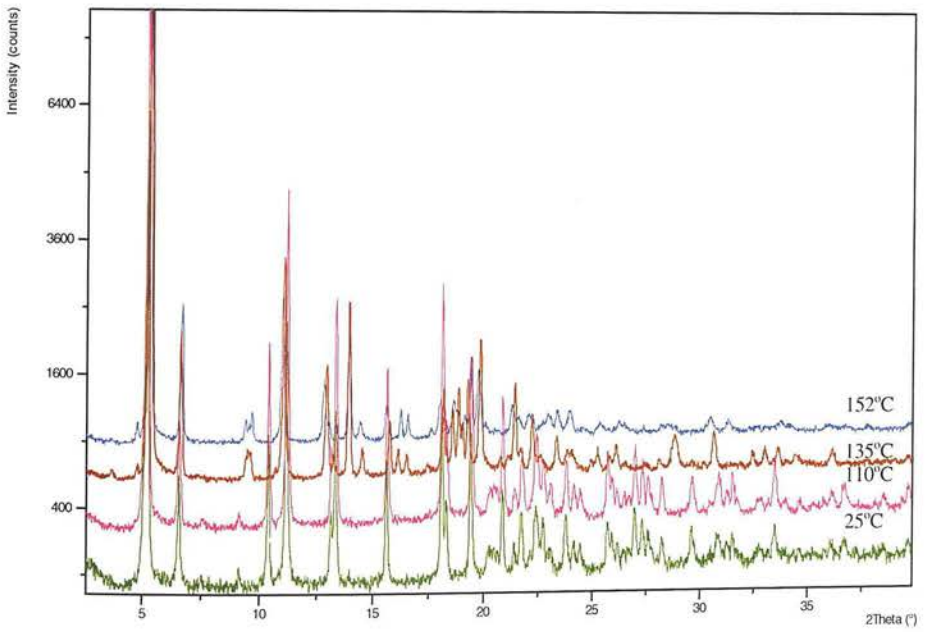

Figure 5.6: X-ray powder diffraction patterns for group C obtained at room temperature (green), 110 °C (pink), 135 °C (brown) and 152 °C (blue).

From the screening studies it can be summarised that compound A had four polymorphs; two of them (forms I and II) were identified from screening

experiments, whilst the other two (unknowns 1 and 2) were identified in initial samples from group A. Form I has the highest melting point (at *ca.* 164 °C) and for this reason is the most stable form. Form II is metastable with respect to form I and these forms are enantiotropically related. The transition temperature to produce form II from form I is *ca.* 5 °C. The polymorphism of compound A is summarised in Figure 5.8. Powder patterns (supplied by GSK) for forms I, II and unknown 2 are compared in Figure 5.7. No single crystal structure data were available for any of these forms.

The aims of the current investigation were therefore to obtain structural information for these polymorphs, to explore whether other polymorphs can be obtained at ambient pressure, and to explore whether high-pressure methods can be used to obtain new polymorphs.

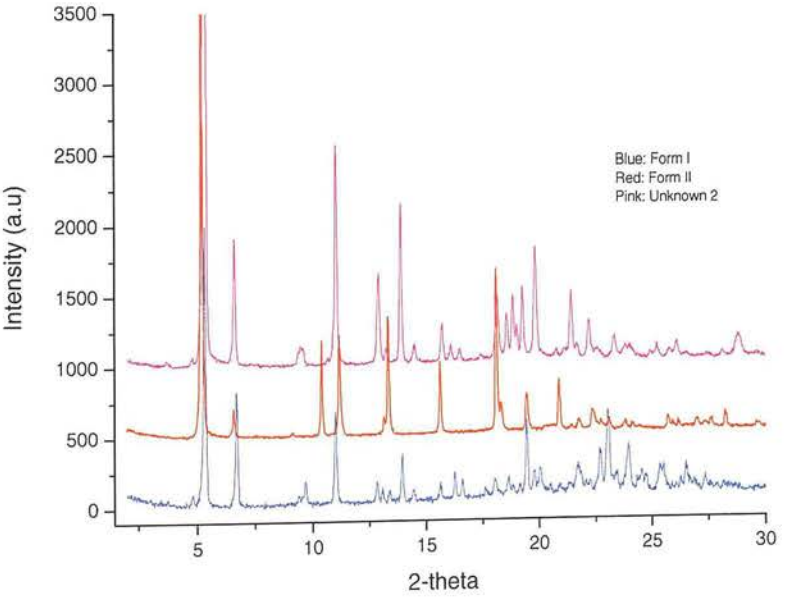

Figure 5.7: Experimental powder patterns of GSK form I, II and unknown 2 (λ = 1.5418 Å).

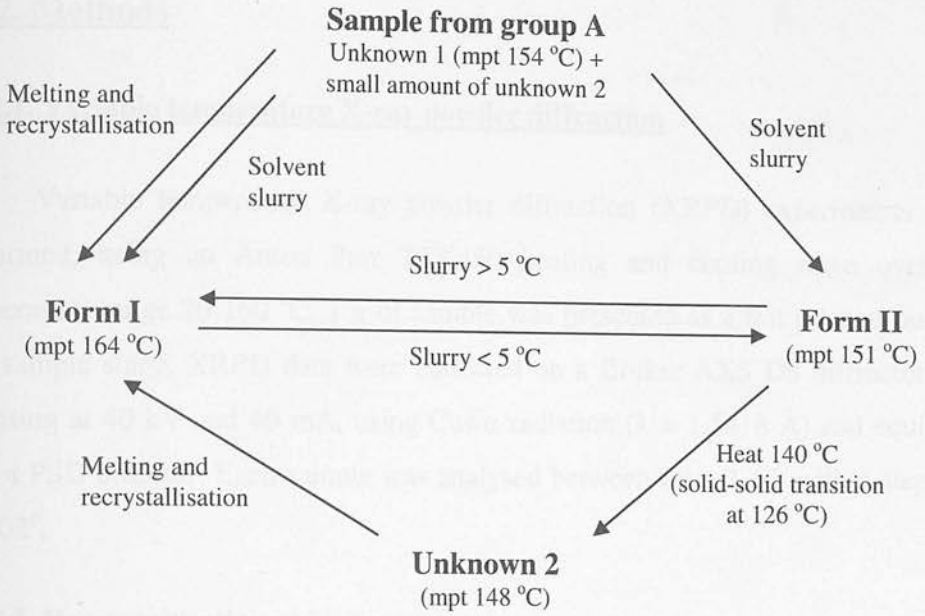

Figure 5.8: Polymorphism of compound A.

5.2. Experimental

5.2.1. Material

A powder sample of compound A was received from GSK. The supplied form was identified as form II by X-ray powder diffraction (XRPD). It was used without further modification for high-pressure X-ray powder compression studies. For the recrystallisation experiments analytical grade solvents were used. To obtain samples of form I, form II was heated to 160 °C for 12 hours.

All high-pressure experiments were carried out using a Merrill-Bassett diamond-anvil cell (DAC) (half-opening angle 40°), equipped with a pre-indented tungsten gasket of thickness 250 μm and a 300 μm diameter hole [1]. For high-pressure crystallisation experiments, a DAC with tungsten carbide backing discs was used [2].

5.2.2. Methods

5.2.2.1. Variable temperature X-ray powder diffraction

Variable temperature X-ray powder diffraction (XRPD) experiments were performed, using an Anton Parr TTK450 heating and cooling stage over the temperature range 20-160 °C. 1 g of sample was presented as a flat pressed powder in a sample stage. XRPD data were collected on a Bruker AXS D8 diffractometer operating at 40 kV and 40 mA, using Cu$K\alpha$ radiation (λ = 1.5418 Å) and equipped with a PSD detector. Each sample was analysed between 2θ = 2-40° with a step size of 0.02°.

5.2.2.2. Recrystallisation at high pressure

A *ca.* 0.1 M solution of compound A was prepared in methanol:ethanol (4:1) mixture. The solution was then loaded together with a few crystallites of the supplied form at 293 K into a DAC. A small piece of ruby was also added in order to allow the determination of the pressure [3]. After sealing the cell, it was then subjected to gentle heating to dissolve all of the solid material. The pressure was then applied by tightening the screws of the DAC to induce precipitation. Crystallisation was achieved at *ca.* 0.7 GPa. The temperature was then cycled near 353 K in order to dissolve all but one of the crystallites. Cooling to ambient temperature at this pressure always resulted in the formation of multiple crystallites. The pressure was then reduced to 0.4 GPa to facilitate growing of single crystal material. All of the crystallites except one were dissolved by gentle heating. A single crystal grew on slow cooling to 298 K.

5.2.2.3. Recrystallisation at ambient pressure

All recrystallisations were performed using the analytical grade solvents listed in Table 5.2. Saturated solutions were prepared by dissolving the supplied powder sample of form II and crystallisation was achieved by slow cooling to ambient temperature. Either powder or single crystal samples were obtained by these

crystallisations. Powder samples were analysed by XRPD. Single crystal data were collected at 298 and 150 K by using Bruker APEX CCD diffractometer using Mo-$K\alpha$ radiation ($\lambda = 0.71073$ Å). Further details are given in the subsequent sections.

Solvent	Solubility (mg/ml)[a] at 20 °C
Acetic acid	66
Acetic acid: water (50% v:v)	33
Acetone	66
Acetone: water (50% v:v)	33
$CHCl_3$	200
Cyclohexane	33
DMF	300
DMSO	133
EtOAc	66
Ethanol	-
IPA	33
MeCN	33
MeOH	33
Nitromethane	33
THF	100
1-butanol	100
Water	13

Table 5.2: Recrystallisation of compound A at ambient pressure. [a] Solubility data were provided by GSK.

5.2.2.4. Structure determination of form II from powder X-ray diffraction

A powder sample of form II (as supplied) was loaded into a 0.7 mm borosilicate glass capillary and mounted on a Bruker-AXS D8 diffractometer (at the University of Strathclyde, Glasgow). The diffractometer was equipped with a Bruker Lynxeye PSD. Data were collected at room temperature (298 K) in the range $2\theta = 2$-45° (6s per step, 0.016° step size; for indexing and structure determination) and $2\theta = 2$ –70° (variable count time scheme, 0.016° step size for Rietveld refinement [4, 5]). Indexing of the powder pattern was performed using *DICVOL*-04 [6]. Structure solution was performed using the global optimisation program *DASH* [7]. Data analysis was performed by the Rietveld method as implemented in *Topas* Academic V 4.1 [8]. *All structure refinements were carried out at The University of Strathclyde by Prof. Alastair Florence.*

5.2.2.5. X-ray powder diffraction at high pressure

High-pressure powder diffraction experiments were performed using a DAC. A pre-indented tungsten gasket of thickness 250 μm and a 300 μm diameter hole was used. To improve the uniformity of polycrystalline material, the powder was gently ground using a mortar and pestle prior to loading into the cell. The powder was loaded with a small ruby chip to measure the pressure. Methanol:ethanol mixture (4:1) was used as the pressure-transmitting medium in these experiments.

Powder diffraction patterns were collected with high flux synchrotron X-ray radiation (λ = 0.444 Å) using Beamline I15 at the Diamond Light Source, Oxfordshire. To improve the uniformity of the cones of diffracted radiation, the sample was continuously rastered over a range of $\pm$100 μm transverse to the incident X-ray beam in order to illuminate as many individual crystallites as possible. The scattered radiation was then collected on an image-plate area detector (Mar345). Any intense diffraction peaks due to diamonds were masked and the remaining two-dimensional pattern was then integrated to obtain a one dimensional powder-diffraction pattern using the program *FIT2D* [9].

5.3. Results

5.3.1. Variable temperature X-ray powder diffraction experiments

Figure 5.9 shows the X-ray powder diffraction patterns collected at increasing temperature, starting from 25 °C up to 160 °C. The powder pattern at 25 °C represents pure form II.

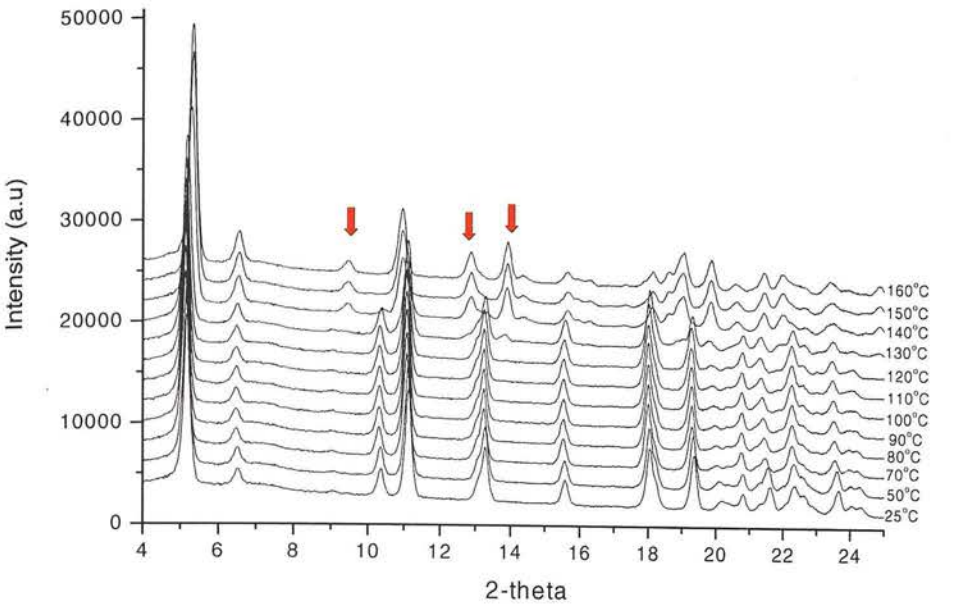

Figure 5.9: X-ray powder diffraction patterns of compound A recorded in the temperature ranges 25-160 °C (λ = 1.5418 Å).

It is evident from Figure 5.9 that the starting form II persisted up to 120 °C. On raising the temperature to 130 °C new peaks were observed to grow (2θ = 9.4, 12.7 and 13.7°) in the pattern. At 150 °C, the Bragg peaks at 2θ = 10.4 and 13.3° associated with form II completely disappeared. The pattern at 150 °C therefore represents a pure phase and was identified as form I by comparison with the powder pattern obtained for form I (Figure 5.10). No further changes in the patterns were observed up to the melting point at 163 °C. On cooling, the sequence of patterns shown in Figure 5.11 was obtained. There were no significant changes observed in the patterns down to -5 °C, indicating that form II is metastable and form I does not convert back to form II in the absence of a solvent. No evidence was observed for the formation of unknown 2 at 126 °C. This might be due to difference of purity of sample used in this experiment as compared to that used by GSK.

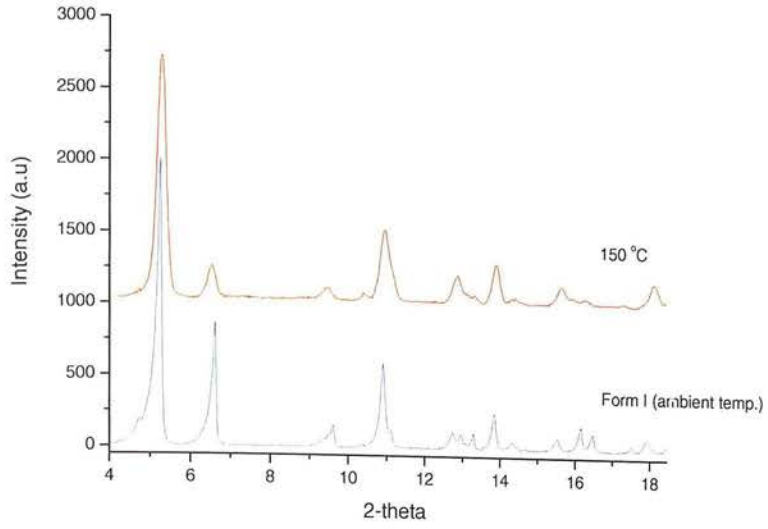

Figure 5.10: Comparison of XRPD pattern for form II at 150 °C (red) with experimental pattern of form I (blue) (λ = 1.5418 Å). Patterns were collected on different instruments.

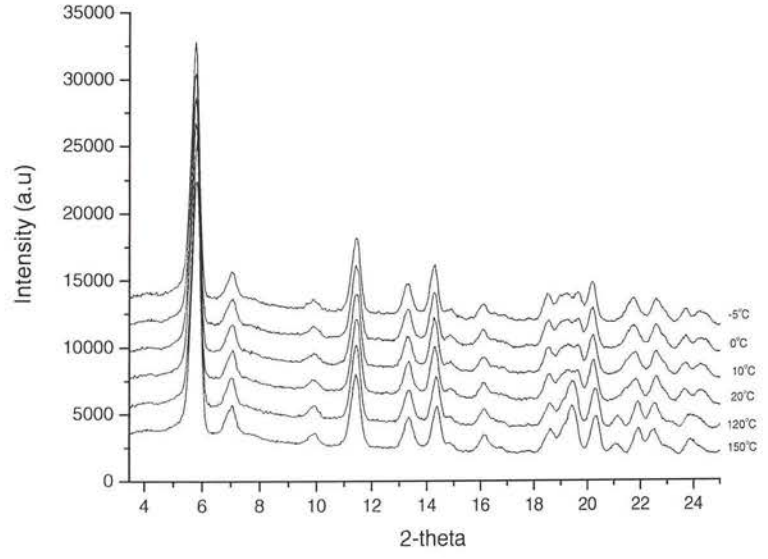

Figure 5.11: X-ray powder diffraction patterns recorded on cooling down to -5 °C (λ = 1.5418 Å).

5.3.2. Crystallisation from solution at high pressure

Pressure-induced crystallisation of a solution of compound A in methanol:ethanol mixture (4:1) was achieved at 0.7 GPa. Methanol:ethanol was selected as a solvent system because the compound is relatively soluble in this

mixture and it serves as a good pressure-transmitting medium. All of the crystallites except one were dissolved by gentle heating of the cell. Cooling to ambient temperature at this pressure always resulted in the formation of multiple crystallites. The pressure was then reduced to 0.4 GPa to facilitate growing of single crystal samples. All of the crystallites except one were dissolved by gentle heating. The sample was then allowed to cool until a single crystal had fully grown. Single crystal X-ray diffraction data were then collected. Data indexing was performed using the program *CELL_NOW* [10]. This gave a monoclinic unit cell, space group $P2_1/n$ with lattice parameters a = 5.111(3) Å, b = 16.399(11) Å c = 23.215(14) Å, β = 91.79(3)°, and V = 1945.2(2) Å^3. Comparison of the simulated peak positions (with arbitrary intensity) obtained from these lattice parameters with powder patterns of the known forms is shown in Figure 5.12. Peak positions with arbitrary intensity were generated by putting a hydrogen atom into unit cell using program *POWDER CELL* [11]. It is evident in Figure 5.12 that this form does not correspond to any of the known polymorphs observed by GSK, and so this new form was designated as form III.

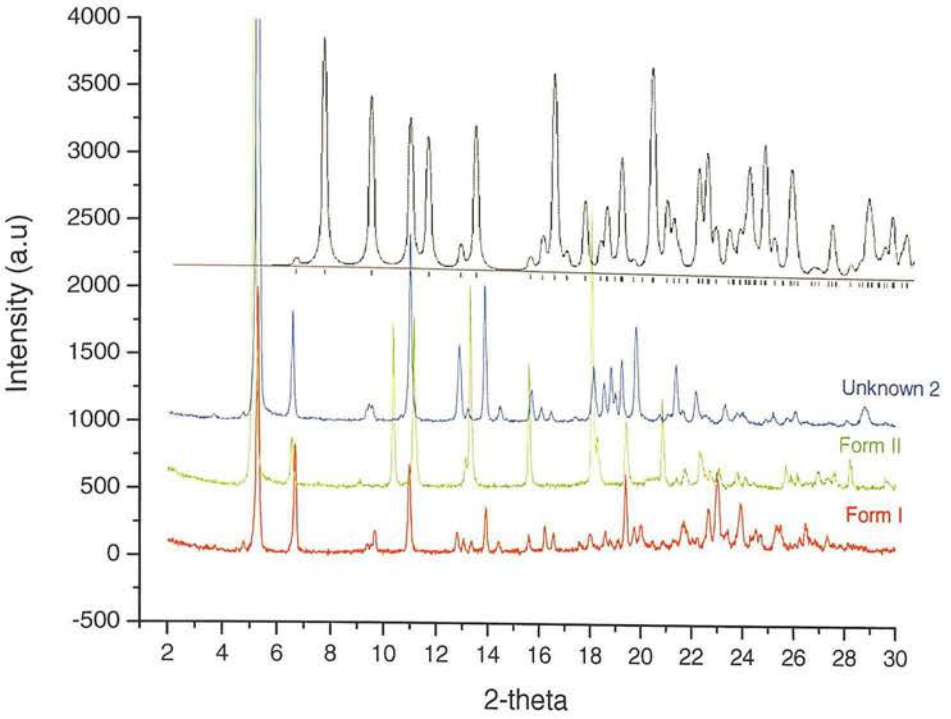

Figure 5.12 : Comparison of simulated peak positions (represented by tick marks) of form III (top) with experimental powder patterns of form I (red), form II (green) and unknown II (blue)(λ = 1.5418 Å).

Unfortunately the poor quality of the diffraction data caused by small sample size and low completeness of this dataset made it difficult to solve the structure from this data. Furthermore, optical observation of the crystal showed gradual growth of powder inside the DAC over a period of time (<10 minutes). Progressive decompression from 0.4 GPa at 298 K to ambient pressure allowed these crystallites to be recovered. These crystallites were then removed from the gasket and used as seeds to grow single crystals at ambient pressure from a saturated ethanol solution. This resulted in the production of needle-shaped crystals. These crystals proved to be highly metastable and optical observation showed that they started to transform to polycrystalline powder within 10 minutes. This powder was identified as form II by XRPD. These results prompted recrystallisation experiments at ambient pressure to see whether form III (obtained by high-pressure crystallisation) could be obtained at ambient pressure.

5.3.4. Recrystallisation at ambient pressure

Recrystallisation experiments at ambient pressure were performed in order to identify possible polymorphs of compound A and to obtain single crystals suitable for single-crystal diffraction studies. Saturated solutions were prepared by using common solvents shown in Table 5.2. Recrystallisation was achieved by slow cooling to ambient temperature. For all the solvents except ethanol and IPA, polycrystalline material was produced. Analysis of XRPD patterns showed that all of these powders comprised form II. Single crystals obtained from ethanol and IPA solution were subjected to single crystal X-ray diffraction. Results from these studies are described in the following sections.

5.3.4.1. Recrystallisation from ethanol solution

A saturated solution of compound A was prepared by dissolving *ca.* 0.5 g of material in 10 ml of hot ethanol. After 20 min of slow cooling to room temperature, needle shaped crystals started to grow along the walls of crystallisation vial. These needle-shaped crystals were highly metastable and optical observation showed that they started to transform to powder within 5-10 minutes. This powder was identified as form II by XRPD. To avoid this conversion, some crystals were isolated from solution at an early stage. Single crystal x-ray diffraction data were then collected. Data indexing was performed using the indexing programme *CELL_NOW* [10], and was successfully indexed in a monoclinic unit cell with lattice parameters shown in Table 5.3. Integration of data sets and global cell refinement were carried out using the program *SAINT* [12] and an absorption correction for the crystal was applied using *SADABS* [13]. The structure was solved in space group $P2_1/n$ using direct methods (SIR 97) [14]. Full-matrix least-squares structure refinement against $|F|^2$ was then performed using *CRYSTALS* [15]. Hydrogen atoms were placed in calculated positions and allowed to ride on their parent atom. Full structural refinement details are tabulated in appendix A. Crystallographic data in CIF format are available on the attached CD.

	Form III Obtained from ethanol solution	High pressure crystallisation (0.4 GPa)
Crystal System	Monoclinic	Monoclinic
Space group	$P2_1/n$	$P2_1/n$
a **(Å)**	5.2361(17)	5.111(3)
b **(Å)**	16.877(5)	16.399(11)
c **(Å)**	24.218(7)	23.215(14)
α (°)	90	90
β (°)	94.432(6)	91.79(3)
γ (°)	90	90
V **(Å^3)**	2133.7(11)	1945.2(2)
Z	4	4
P(GPa)	0.0	0.40(5)
T(K)	293(2)	293(2)

Table 5.3: Unit cell parameters for compound A form III obtained from ethanol and high pressure crystallisation.

Table 5.3 shows the close relationship between the lattice parameters for form III identified at high pressure and the form crystallised from ethanol at ambient pressure. This confirms that form III is distinct and is not the same as any of the unknown forms identified by GSK (Figure 5.13).

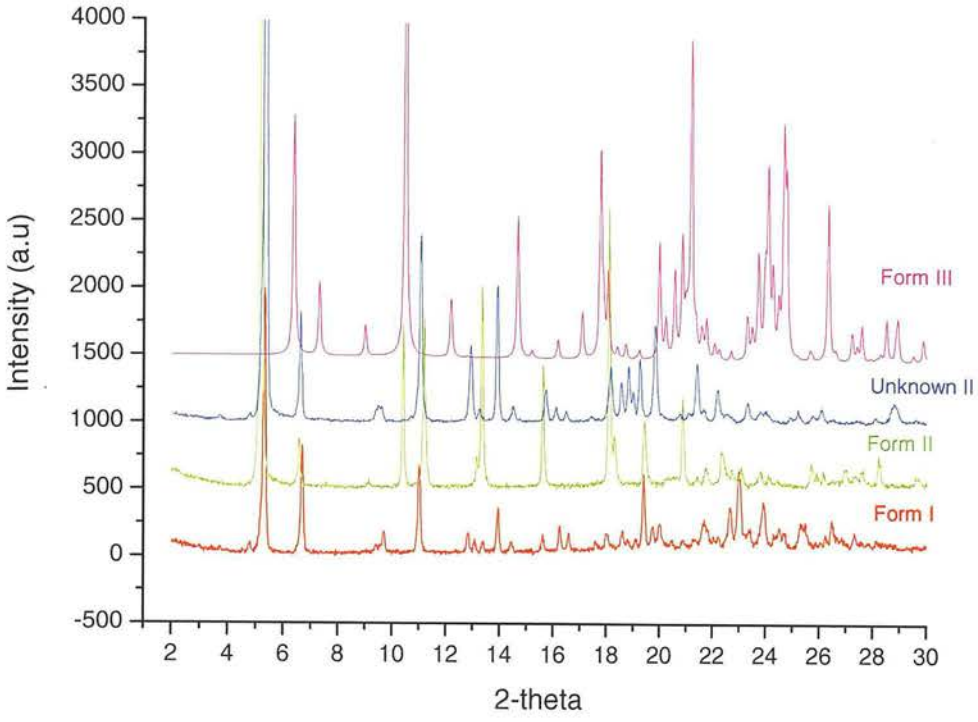

Figure 5.13 : Comparison of simulated powder pattern of form III (orange) with experimental powder patterns of form I (red), form II (blue), unknown I (brown) and unknown II (pink) (λ = 1.5418 Å).

5.3.4.2. Recrystallisation from IPA (isopropyl alcohol) solution

A saturated solution of compound A was prepared by dissolving *ca.* 0.5 g of solid material in 10 ml of hot IPA. On slow cooling over a period of 20 minutes block-shaped crystals were produced, which were then subjected to single crystal X-ray analysis. Diffraction data were collected at both 298 and 150 K. Data indexing was performed using the indexing programme *CELL_NOW* [10] and gave a triclinic unit cell with space group *P*-1. Lattice parameters at both temperatures are shown in Table 5.4. Integration of data sets and global cell refinements were performed using the program *SAINT* [12] and an absorption correction for the crystal was applied using *SADABS* [13]. The structure was solved in *P*-1 using direct methods (SIR 97) [14]. Full-matrix least-squares structure refinement against $|F|^2$ was then performed using *CRYSTALS* [15]. Hydrogen atoms were placed in calculated positions and allowed to ride on their parent atoms. Full structural refinement details

are tabulated in appendix A. Crystallographic data in CIF format are available on the attached CD.

	Form IV	Form IV
Crystal System	Triclinic	Triclinic
Space group	*P*-1	*P*-1
a **(Å)**	8.667(5)	8.9117(13)
b **(Å)**	10.2340(6)	10.2523(14)
c **(Å)**	13.2989(8)	13.3658(19)
α (°)	109.258(3)	108.744(7)
β (°)	98.285(3)	99.604(7)
γ (°)	107.830(3)	108.028(7)
V **(Å^3)**	1021.15(11)	1050.6(3)
Z	2	2
D$_c$ **(g cm^{-3})**	1.44	1.40
T(K)	150(2)	298(2)

Table 5.4: Unit cell parameters for form IV of compound A at 150 and 298 K.

Figure 5.14 shows the comparison between simulated powder pattern (calculated from single crystal structure) with all the other known forms. It is evident that this form does not correspond to any of the known forms and is therefore designated as form IV.

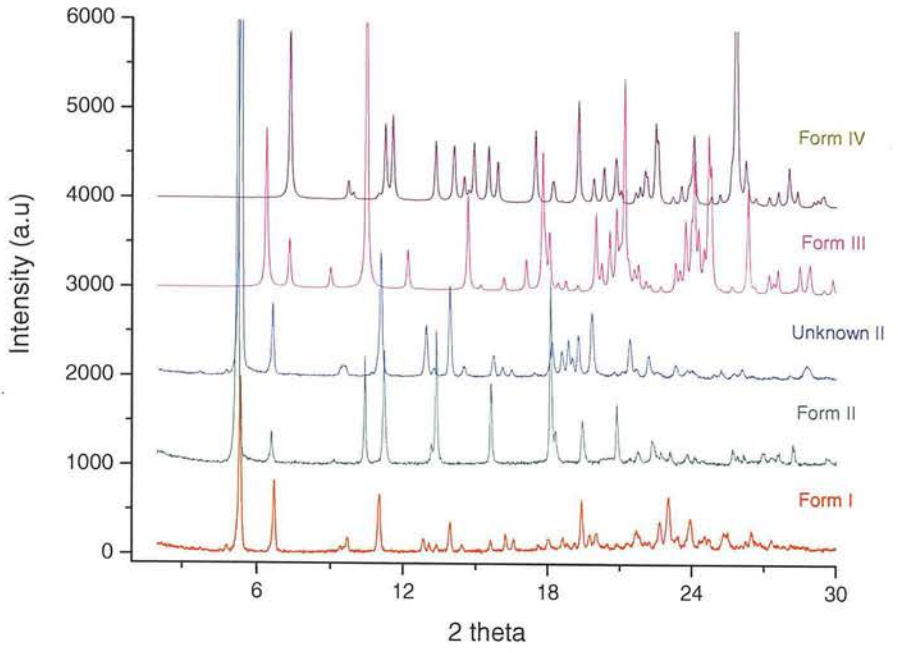

Figure 5.14: Comparison of X-ray powder diffraction patterns of polymorphs of compound A (λ = 1.5418 Å).

5.3.5. Structure determination of form II

The crystal structure of form II was solved *ab initio* from powder diffraction data. Fixed count time powder data sets were used for indexing attempts using *DICVOL-04* [6] and resulted a triclinic unit cell, space group *P*-1 with lattice parameter a = 4.4956 Å, b = 13.9295 Å, c = 17.4897 Å, α = 77.9990°, β = 83.2950°, γ = 81.2290° and V = 1054.665 Å^3.

The background was subtracted from the data prior to Pawley fitting (Pawley χ^2 = 6.39). The simulated annealing (SA) component of *DASH* [7] (0.02 cooling rate, 1.5 x 10^7 moves per run, 500 runs) was used to solve the crystal structure of form II. The internal coordinate description of the molecule was derived from the single-crystal structure of form IV. 292/500 SA runs returned a profile χ^2 / Pawley χ^2 ratio of less than 10, with the lowest profile χ^2 value being 17.11 (Figure 5.15).

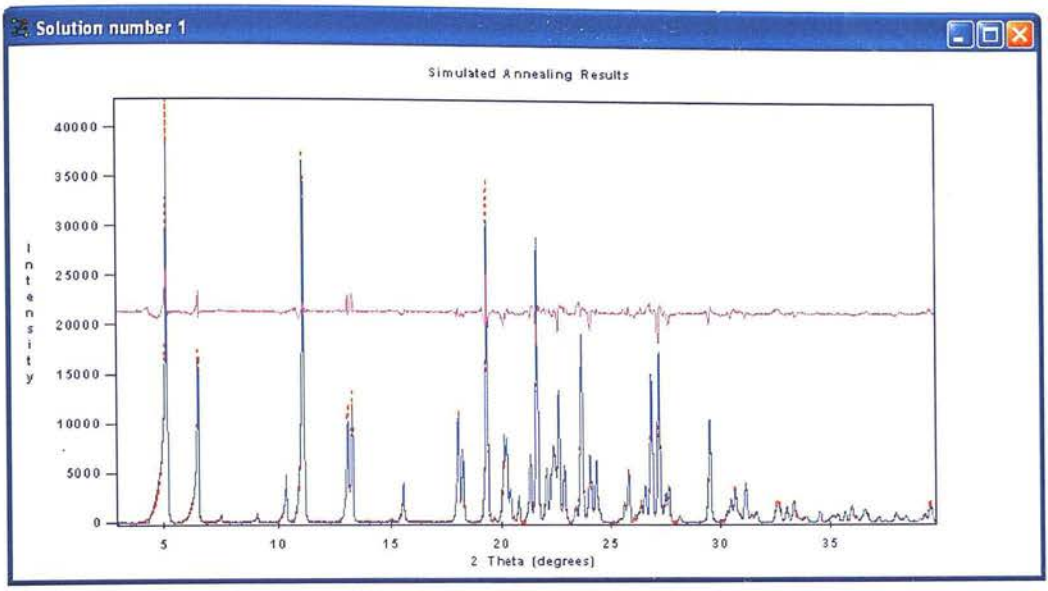

Figure 5.15: Observed (blue), calculated (red) and difference (pink) profiles from DASH for the best SA run for form II.

Inspection of the best 10 SA runs shows the excellent consistency of the global minimum returned by the search, with the position, orientation and conformation of the molecules essentially identical (Figure 5.16). A preliminary rigid body refinement in DASH confirmed a lack of significant preferred orientation effects in the data.

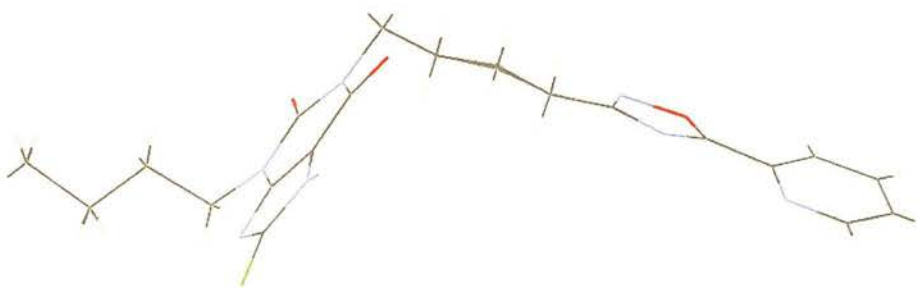

Figure 5.16: Overlay of the molecule taken from the top 10 solutions returned by the 500 DASH runs. The excellent reproducibility shows that the structure has been successfully solved, with no evidence of disorder or superposition of equal scattering groups.

The structure was refined against data in the range 2θ = 3.0-70° using a restrained Rietveld method as implemented in *TOPAS* Academic v 4.1 [8]. *All structure refinements were carried out at the University of Strathclyde by Prof. Alastair Florence.* A scale and background only refinement of the structure yielded an R_{wp} of 0.0564 which fell to 0.0403 during the refinement. Overlay of observed and calculated patterns with the difference profile is shown in Figure 5.17. All atomic positions (including H-atoms) for the structure were refined, subject to a series of restraints on bond lengths, bond angles and planarity. Isotropic temperature factors (U_{iso}) for non-H-atoms were constrained to be equal whilst the U_{iso} values of H-atoms constrained to be 1.2 times that for the parent atoms. Refined lattice parameters for the structure of form II are shown in Table 5.5

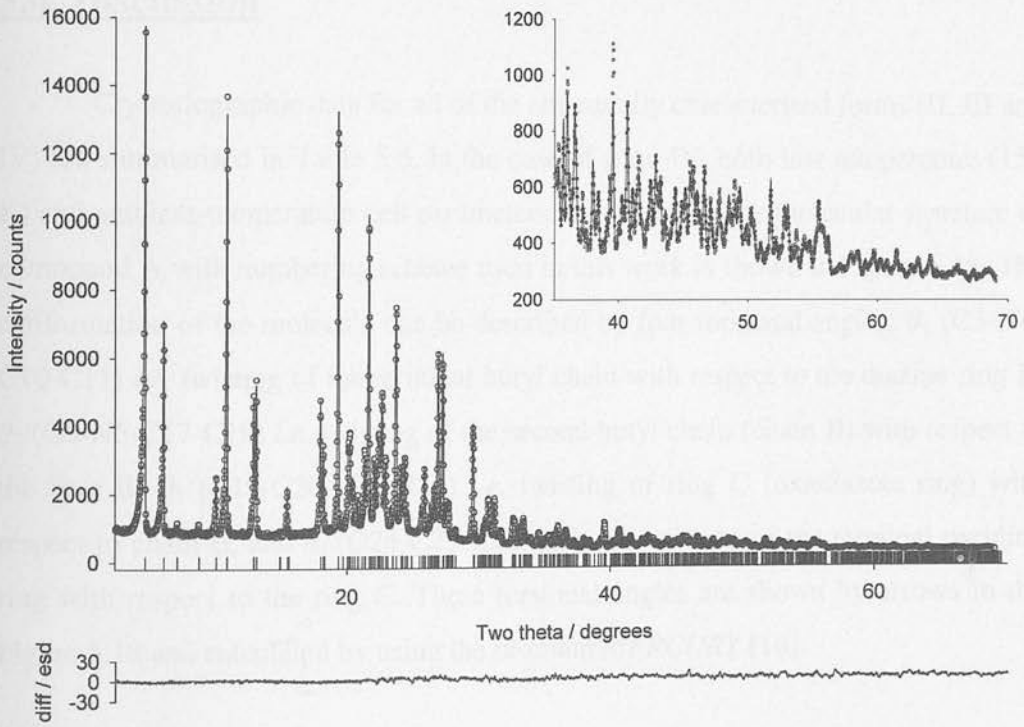

Figure 5.17: Final observed (points), calculated (line) and difference [(yobs - ycalc)/σ(yobs)] profiles for the Rietveld refinement of form II.

	Form II
Crystal System	Monoclinic
Space group	*P*-1
a **(Å)**	4.49519(6)
b **(Å)**	13.9284(2)
c **(Å)**	17.4895(3)
α (°)	77.9960(16)
β (°)	83.3233(11)
γ (°)	81.2257(16)
V **(Å^3)**	1054.49(3)
Z	2
D$_c$ **(g cm^{-3})**	1.398
T(K)	298(2)

Table 5.5: Unit cell parameters of GSK compound A form II.

5.4. Discussion

Crystallographic data for all of the structurally characterised forms (II, III and IV) are summarised in Table 5.6. In the case of form IV, both low temperature (150 K) and ambient-temperature cell parameters are reported. The molecular structure of compound A with numbering scheme used in this work is shown in Figure 5.18. The conformation of the molecule can be described by four torsional angles; θ_1 (C3-N4-C10-C11) *i.e.* twisting of the terminal butyl chain with respect to the diazine ring B, θ_2 (C5-N6-C17-C18) *i.e.* twisting of the second butyl chain (chain B) with respect to the ring B, θ_3 (C19-C20-C21-N25) *i.e.* twisting of ring C (oxadiazole ring) with respect to chain B, and θ_4 (O24-C23-C26-C27) *i.e.* twisting of the terminal pyridine ring with respect to the ring C. These torsional angles are shown by arrows in the Figure 5.18 and calculated by using the program *MERCURY* [16].

	Form II	Form III	Form IV	Form IV
Crystal system	Triclinic	Monoclinic	Triclinic	Triclinic
Space group	*P*-1	$P2_1/n$	*P*-1	*P*-1
***a* (Å)**	4.49519(6)	5.2361(17)	8.667(5)	8.9117(13)
***b* (Å)**	13.9284(2)	16.877(5)	10.2340(6)	10.2523(14)
***c* (Å)**	17.4895(3)	24.218(7)	13.2989(8)	13.3658(19)
α (°)	77.9660(16)	90.00	109.258(3)	108.744(7)
β (°)	83.3233(11)	94.432(6)	98.285(3)	99.604(7)
γ (°)	81.2257(16)	90.00	107.830(3)	108.028(7)
V (Å^3)	1054.49(3)	2133.7(11)	1021.15(11)	1050.6(3)
Z	2	4	2	2
D_c (g cm^{-3})	1.398	1.38	1.44	1.40
T(K)	293(2)	293(2)	150(2)	293(2)

Table 5.6: Comparison of unit cell parameters for forms II, III and IV of compound A.

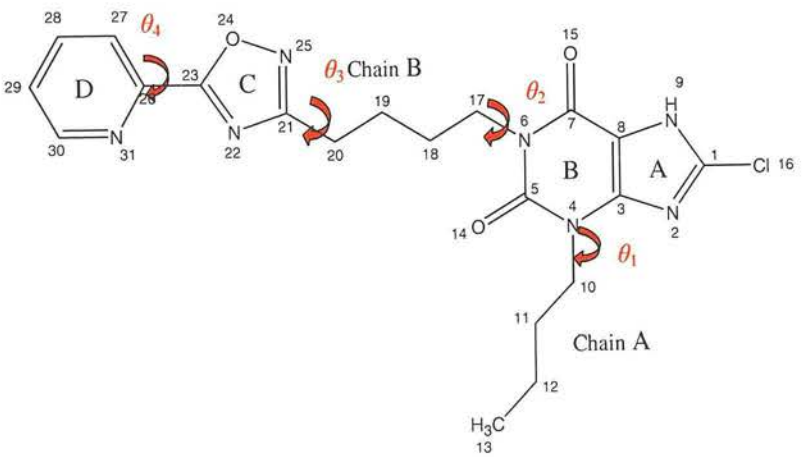

Figure 5.18: The molecular structure of GSK compound A with numbering scheme employed in this work. The molecule is divided into four rings designated A-D and two four carbon chains A and B. Torsional angles are shown by red arrows.

5.4.1. Description of crystal structure of form II

The crystal packing diagram for form II is shown in Figure 5.19. There are two molecules in the unit cell which form dimer units by making two hydrogen bonds between O15-H…N9 of each molecule. The O15...N9 distance is *ca.* 2.75 Å.

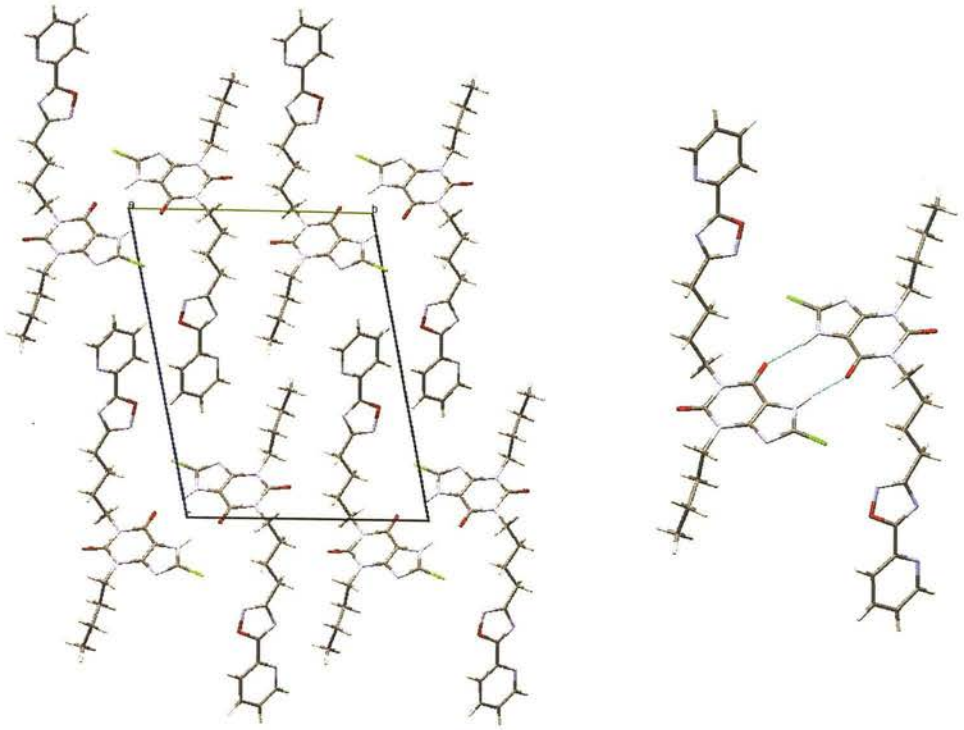

Figure 5.19: Crystal packing diagram of form II viewed down the *a*-axis (left) and the hydrogen bonded dimer unit (right).

The conformation of the molecules with respect to the four torsional angles is illustrated in Table 5.7.

5.4.2. Description of crystal structure of form III

The crystal packing diagram for form III is shown in Figure 5.20. There are four molecules in the unit cell. Similar to the crystal structure of form II, molecules pack as dimer units by making two hydrogen bonds between O15-H...N9 of each molecule. However the O15...N9 distance is *ca.* 2.66 Å, shorter than in form II (O15...N9 = 2.75 Å). The crystal structure shows disorder in the terminal butyl chain (Chain A) and the atoms of two sites at distribution with *ca.* 60:40 % occupancy. This is to be expected as the terminal chain is not involved in any intermolecular contacts and can move freely. Due to deterioration of crystals on cooling, diffraction data were not collected at lower temperatures.

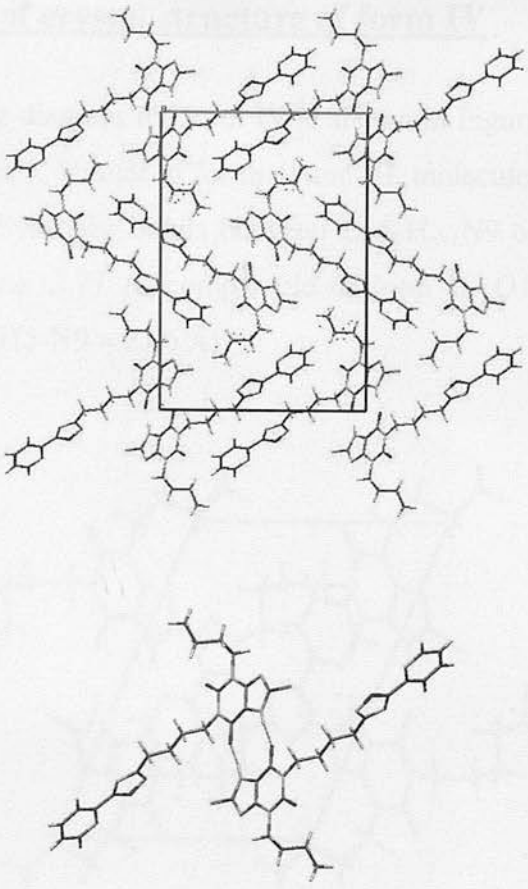

Figure 5.20: Crystal packing diagram of form III viewed down the *a*-axis (top) and hydrogen bonded dimer unit (bottom).

The conformations of molecules in the crystal structure of form III are entirely different compared to forms II and IV (see Table 5.7). The conformation of molecules in form III allows molecules to get close together through hydrogen bonding.

Torsional angle	Form II	Form III	Form IV
θ_1 (°)	97.6	78.7 & 109.1	-98.7
θ_2 (°)	-74.3	95.2	83.7
θ_3 (°)	0.4	3.6	-3.6
θ_4 (°)	-12.8	179.8	177.6

Table 5.7: Comparison of torsional angles for forms II, III and IV. The two values of θ_1 for form III arise because of disorder in the terminal butyl chain.

5.4.3. Description of crystal structure of form IV

Crystal packing diagram for form IV is shown in Figure 5.21. There are four molecules in the unit cell. Similar to forms II and III, molecules are packed as dimer units by making two hydrogen bonds between O15-H...N9 of each molecule. The O15...N9 distance is *ca.* 2.77 Å, comparable to form II (O15-N9 = 2.75 Å) and longer than form III (O15-N9 = 2.66 Å).

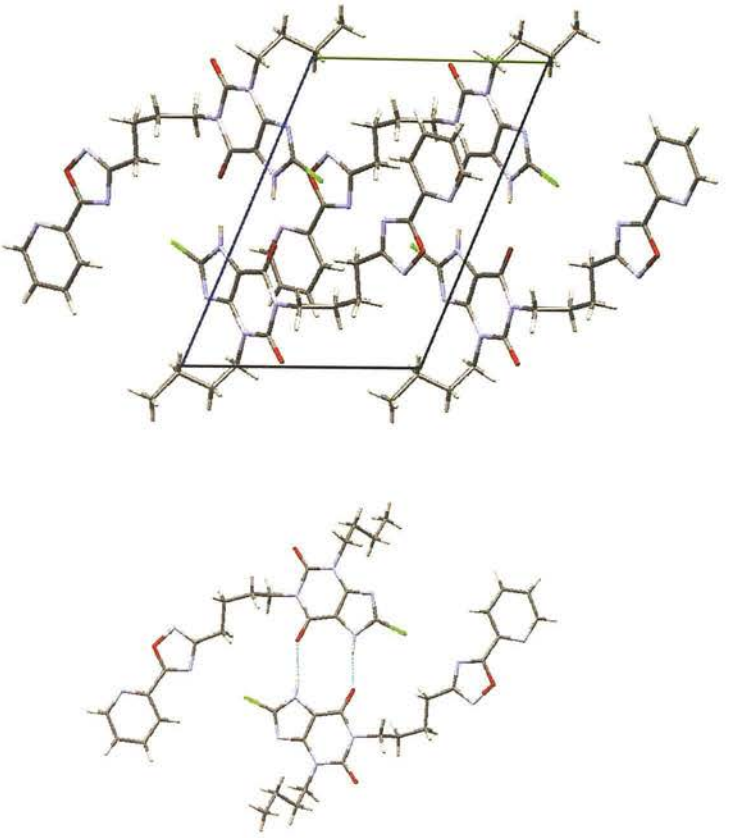

Figure 5.21: Crystal packing diagram of form IV viewed down the *a*-axis (top) and hydrogen bonded dimer unit bottom)

The conformation of molecules in the crystal structure of form IV is different from forms II and III (see Table 5.7). All three forms show differences in these torsional angles, indicating a high degree torsional flexibility of the molecule. The

difference in conformation among these forms is strikingly illustrated in the overlay diagram (Figure 5.22).

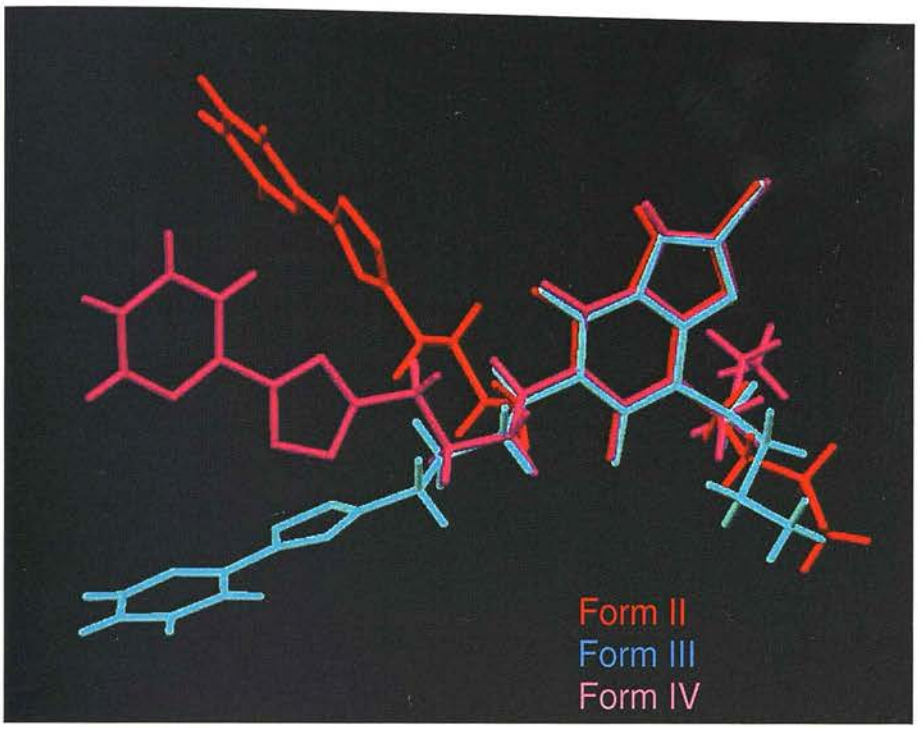

Figure 5.22: Overlay of compound A molecules as they pack in Forms II (red), III (blue) and IV (pink).

5.5. High-pressure powder diffraction experiments

X-ray powder patterns were collected at increasing pressure steps between ambient and 3.5 GPa (Figure 5.21). The pattern recorded at ambient pressure was indexed as form II. It is evident from Figure 5.21 that the starting form persisted up to 0.6 GPa. The only change observed was the movement of peaks towards higher 2θ values; this is more prominent at higher angles. In the next step pressure was increased to 0.9 GPa. At this pressure new peaks were observed to grow in the pattern *e.g.* at *ca.* 3.1° and 5.7° (indicated by arrows in Figure 5.21). Figure 5.22 shows that the powder pattern at 0.9 GPa does not correspond to any of the known forms even taking into account the possible effects of pressure on the patterns, and was therefore designated as form V. On further increase in pressure to 1.4 GPa more

new peaks emerged in the pattern. However, these peaks were at entirely different 2θ values and were not associated with either form V or form II and for this reason this new form was designated as form VI. Figure 5.22 shows the powder pattern of form VI compared with the other forms. However, the powder pattern at 1.4 GPa represents a mixed phase as Bragg peaks associated with form V were present in the pattern. All the indexing attempts were unsuccessful. On further increase in pressure up to 2.5 GPa the powder pattern simplifies somewhat, but not all the peaks attributed to form V disappeared. No further changes were observed in powder pattern by increasing pressure to 3.5 GPa.

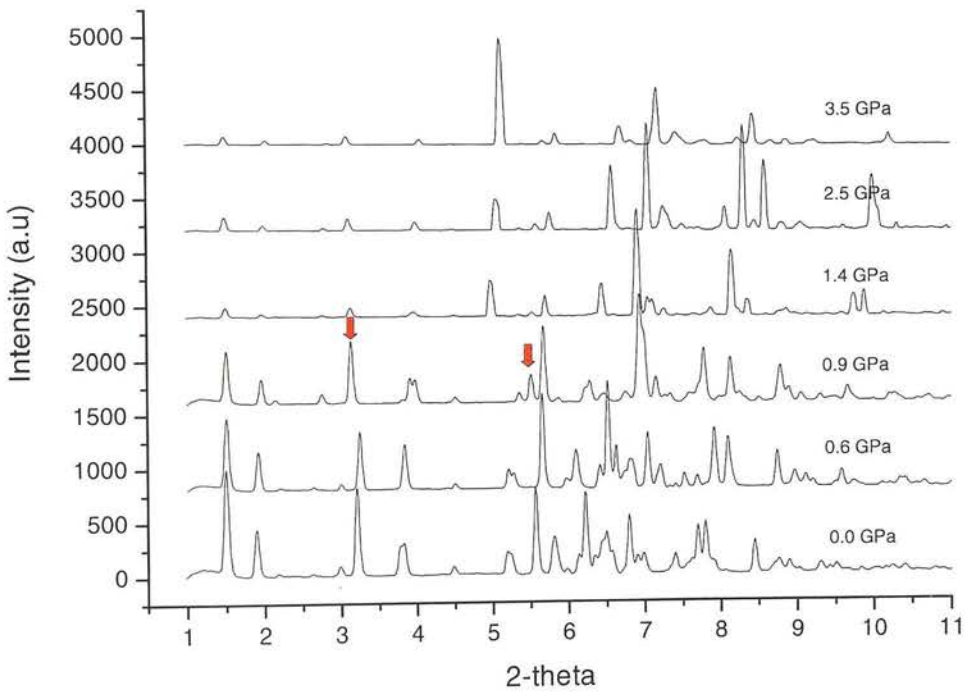

Figure 5.21: X-ray powder patterns of GSK compound A recorded at pressure up to 3.5 GPa (λ = 0.444 Å).

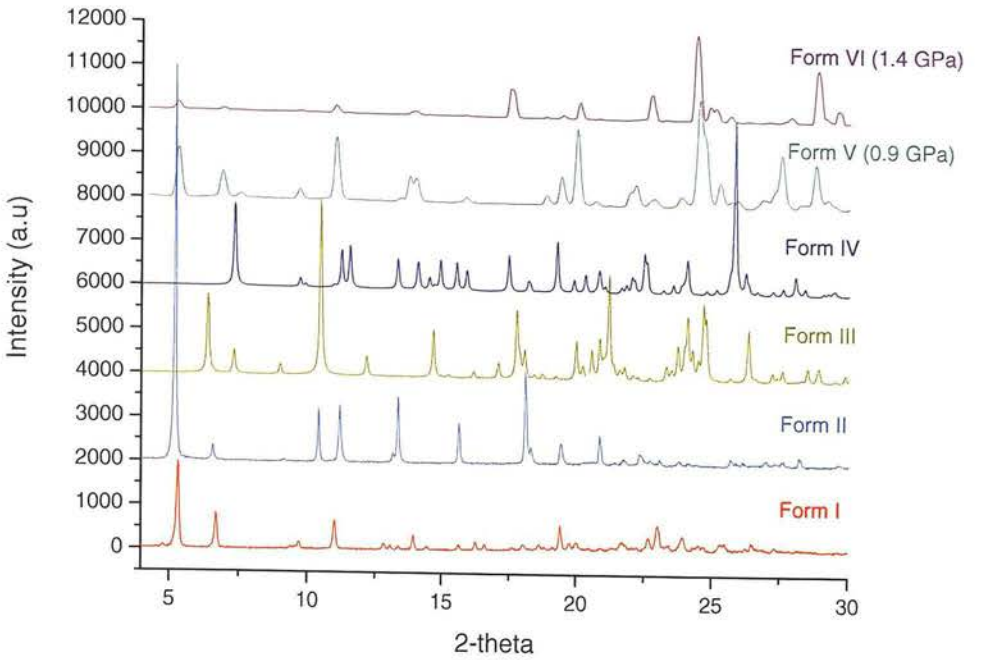

Figure 5.22: Comparison of polymorphs of compound A (λ = 1.5418 Å).

In an attempt to recover these high-pressure polymorphs, the pressure was gradually released. Powder patterns obtained by decreasing pressure in steps down to ambient are shown in Figure 5.23. In the first step the pressure was released to 1.0 GPa. From the powder pattern at 1.0 GPa it is evident that form VI persists down to this pressure, and the only change observed was movement of peaks towards lower 2θ values. On decreasing the pressure to 0.7 GPa peaks attributable to form V emerged in the pattern, indicating a reversible phase transition back to form V. On further decrease in pressure to ambient, the sample converted back to form II.

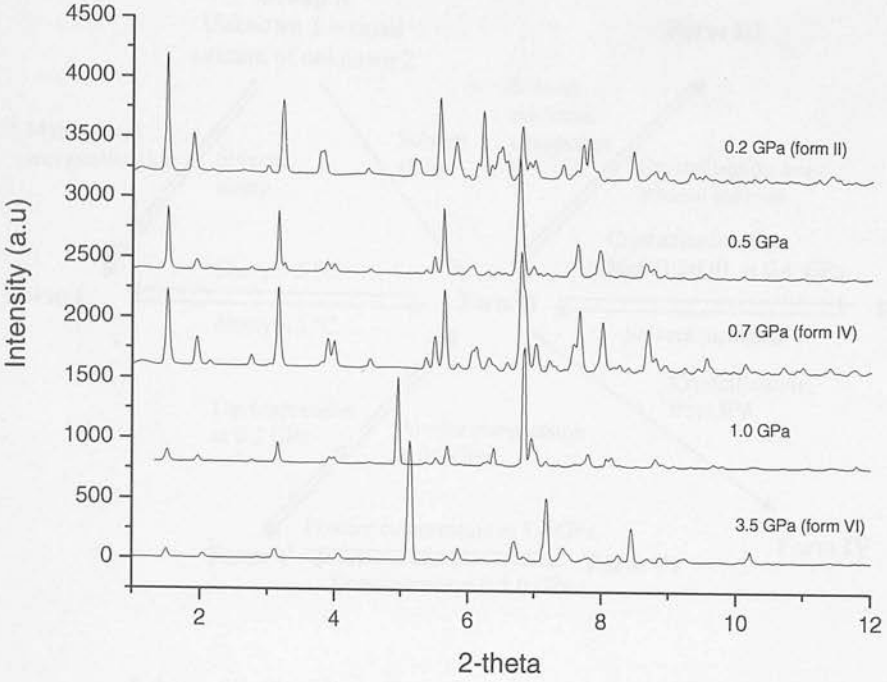

Figure 5.23: X-ray powder patterns of GSK compound A recorded after releasing pressure down to 0.2 GPa ($\lambda = 0.444$ Å).

5.6. Conclusions and future directions

The transformations between the polymorphs of compound A are summarised in Scheme 5.1.

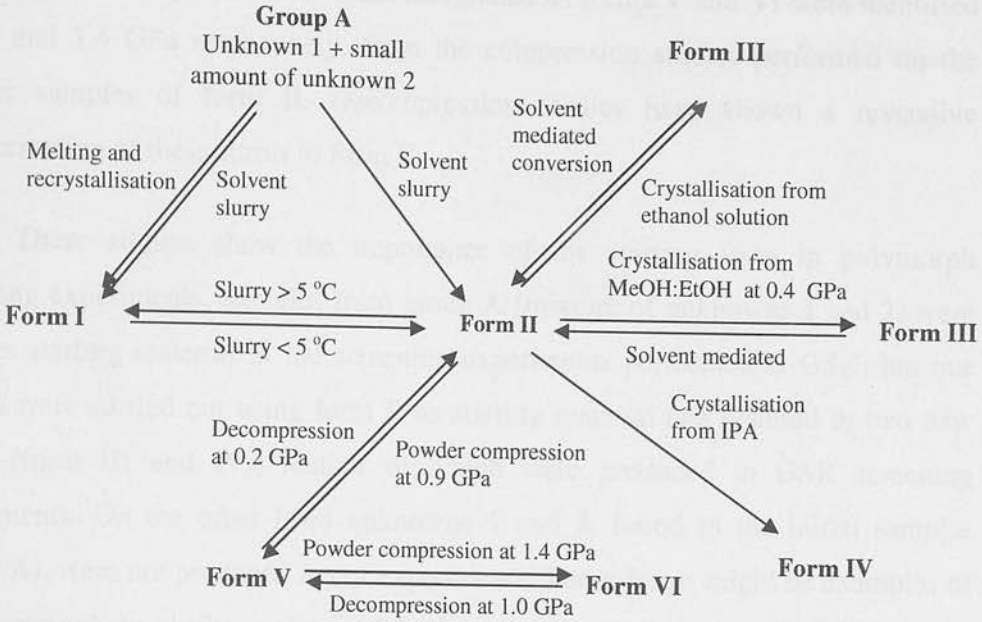

Scheme 5.1: Transformations of polymorphs of compound A.

The high-pressure recrystallisation of compound A in a methanol:ethanol (4:1) mixture contained in a diamond-anvil cell at a pressure of 0.4 GPa resulted in the formation of a new high-pressure polymorph designated as form III. Although it was not possible to obtain the crystal structure at high pressure, it was possible to recover this form to ambient pressure. The recovered sample was used as a seed to obtain single crystals of form III from ethanol solution at ambient pressure and the structure of form III was obtained by single crystal X-ray diffraction. Form III turns out to be highly metastable at ambient pressure and converted to form II within 10 minutes.

Another new polymorph (designated as form IV) was also obtained from crystallisation from IPA solution of form II at ambient condition and its crystal structure has been reported here. The crystal structure of form II was obtained for the first time from X-ray powder diffraction data. All these forms show similar hydrogen bonding motifs as molecules pack as dimer units through the formation of two hydrogen bonds. However, the main difference in the packing arrangement arises from the conformational flexibility of the molecule.

Two new high-pressure forms designated as forms V and VI were identified at 0.9 and 1.4 GPa respectively, from the compression studies performed on the powder samples of form II. Decompression studies have shown a reversible transformation of these forms to form II.

These studies show the importance of the starting form in polymorph screening experiments. Samples from group A (mixture of unknowns 1 and 2) were used as starting material in the screening experiments performed at GSK, but our studies were carried out using form II as starting material and resulted in two new forms (form III and IV), neither of which were produced in GSK screening experiments. On the other hand unknowns 1 and 2, found in the initial samples (group A), were not produced in our experiments. These forms might be examples of "disappearing" or elusive polymorphs where a polymorph may only be observed once before a new, more thermodynamically stable polymorph is crystallised. The crystallisation of the second form results in the 'disappearance' of the previous polymorph. Several examples of 'disappearing' polymorphs given in the literature have illustrated the importance of seed crystallites in the formation of the stable polymorph; once seed crystallites of the more stable form were present in the laboratory it proved impossible to obtain the other polymorphs [17].

Future work on this compound would focus on structural characterisation of form I and the high-pressure forms V and VI. It would also be of interest to investigate compression of forms I, III and IV.

5.7. References

1. L. Merrill and W. A. Bassett, *Rev. Sci. Instrum.*, 1974, **45**, 290-294.
2. S. A. Moggach, D. R. Allan, S. Parsons and J. E. Warren, *J. Appl. Crystallogr.*, 2008, **41**, 249-251.
3. G. J. Piermarini, S. Block, J. D. Barnett and R. A. Forman, *J. Appl. Phys.*, 1975, **46**, 2774-2780.
4. I. C. Madsen and R. J. Hill, *J. Appl. Crystallogr.*, 1994, **27**, 385-392.
5. K. Shankland, W. I. F. David and D. S. Sivia, *J. Mater. Chem.*, 1997, **7**, 569-572.
6. A. Boultif and D. Louer, *J. Appl. Crystallogr.*, 2004, **37**, 724-731.

7. W. I. F. David, K. Shankland, K. Shankland and N. Shankland, *Chem. Commun.*, 1998, 931-932.
8. A. Coelho, *TOPAS-Academic V. 4.1*, Brisbane, 2007.
9. A. P. Hammersley, S. O. Svensson, M. H. and, A. N. Fitch and D. Hausermann, *High Pressure Res.*, 1996, **14**, 235-248.
10. G. M. Sheldrick, *CELL_NOW*, University of Gottingen, Germany, 2002.
11. G. N. Werner Kraus, *Powder Cell*, Federal Institute for Material Research and Testing, Germany, 2001.
12. B. AXS, *SAINT*, Bruker-AXS, Madison, Wisconsin, USA, 2003.
13. G. M. Sheldrick, *SADABS*, University of Göttingen, Germany, 2006.
14. A. Altomare, G. Cascarano, C. Giacovazzo, A. Guagliardi, M. C. Burla, G. Polidori and M. Camalli, *J. Appl. Crystallogr.*, 1994, **27**, 435.
15. P. W. Betteridge, J. R. Carruthers, R. I. Cooper, K. Prout and D. J. Watkin, *J. Appl. Crystallogr.*, 2003, **36**, 1487.
16. C. F. Macrae, P. R. Edgington, P. McCabe, E. Pidcock, G. P. Shields, R. Taylor, M. Towler and J. van de Streek, *J. Appl. Crystallogr.*, 2006, **39**, 453-457.
17. J. D. Dunitz and J. Bernstein, *Acc. Chem. Res.*, 1995, **28**, 193-200.

Chapter 6

An Exploration of the Polymorphism of GSK Compound B

Chapter 6: An Exploration of the Polymorphism of GSK Compound B

6.1. Background

Compound B was received from GlaxoSmithKline (GSK), Stevenage, UK. It is a GSK developmental compound known to have pharmacological activity, but the details have not been disclosed by GSK. The molecular structure of compound B with the numbering scheme used in this work is shown in Figure 6.1.

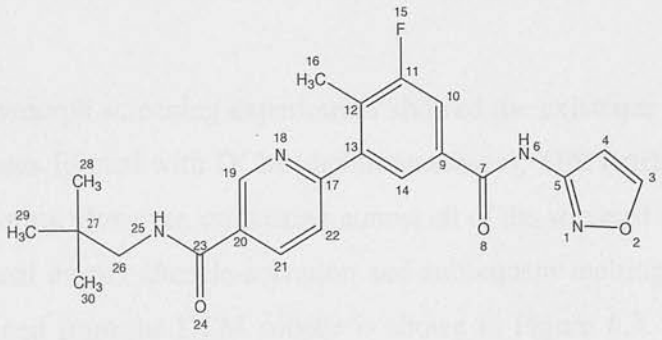

Figure 6.1: Molecular structure of compound B with numbering scheme.

Polymorph screening studies had previously been performed at GSK. Form I was the first form to be identified. Figure 6.2 shows the DSC plot obtained from a sample of form I, which shows only one endothermic event, representing melting of form I at *ca.* 188 °C.

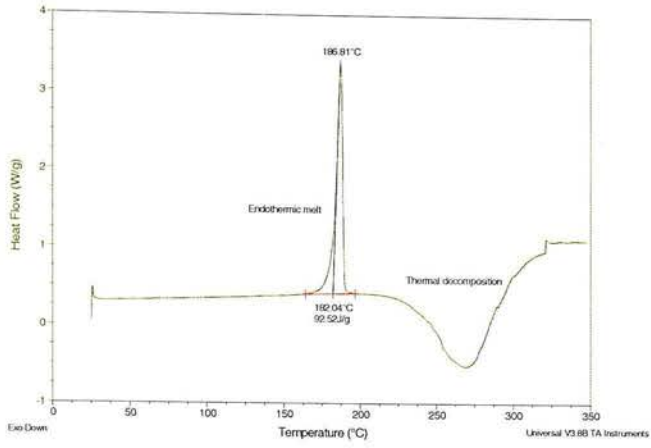

Figure 6.2: DSC plot obtained from form I sample. A single endothermic peak shows melting of form I at *ca.* 188 °C.

The polymorph screening experiments showed the existence of form I along with three solvates formed with DCM (dichloromethane), TFE (trifluoroethane) and $CHCl_3$ (chloroform). However, on heating almost all of the solvated samples showed additional thermal events after de-solvation and subsequent melting of form I. The DSC plot obtained from the DCM solvate is shown in Figure 6.3. It showed three endotherms representing three forms. The first peak at *ca.* 188 °C represents melting of form I which after recrystallisation resulted in a new form with a melting point of *ca.* 212 °C. On further increase in temperature this new form recrystallised into another form with a melting point of *ca.* 218 °C.

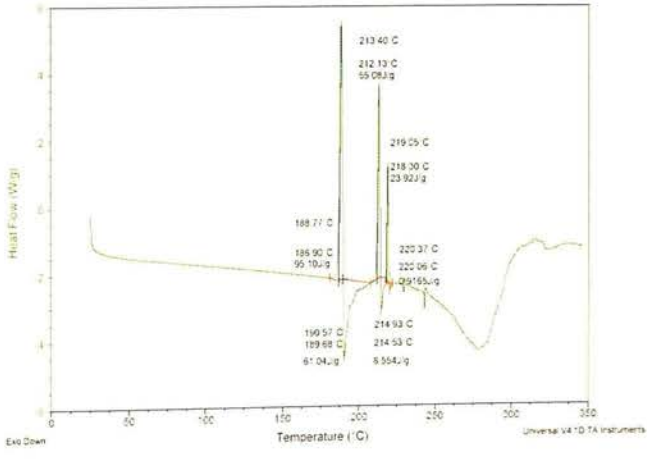

Figure 6.3: DSC plot of DCM solvate, showing three endotherms representing three forms.

A series of experiments was then performed at GSK in an attempt to isolate the suspected additional forms of compound B. In total, four additional anhydrous (unsolvated) forms (designated as form II-V) were obtained and characterised from this work. The preparation of these forms is described in the following section.

Form II

Form II was generated in a hot stage microscopy experiment performed on a sample of the solvate formed with $CHCl_3$. The sample was heated at 10 °C/min until it melted at 200 °C. On cooling, needle-shaped crystals started to grow from the melt (Figure 6.4). These crystals were then used to seed a slurry of form I held at 60 °C in ethyl acetate for 24 hours. The solid obtained was analysed by Raman spectroscopy, XRPD and DSC and identified as a new anhydrous form. This form was designated as form II. The DSC plot obtained from a sample of form II is shown in Figure 6.5.

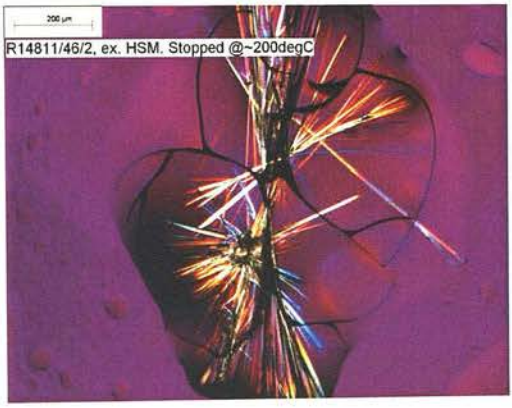

Figure 6.4: Image taken from hot stage microscope showing growth of needle shaped crystal from melt of form II on cooling.

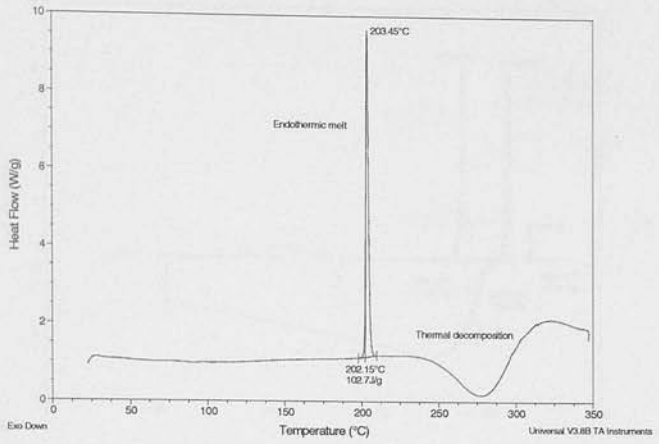

Figure 6.5: DSC plot obtained from samples of form II. Single endotherm represents melting of form II at *ca.* 203 °C.

Form III

Form III was generated in a DSC temperature cycling experiment performed on a sample of the $CHCl_3$ solvate. The sample was heated to 204 °C at 10 °C/min, cooled to ambient temperature and then heated to 250 °C at 10 °C/min. The resulting DSC plot (Figure 6.6) indicates the conversion of form I to a new form with a melting point at *ca.* 208 °C and is designated as form III. A second sample was also prepared in a similar manner, heated to 204 °C and then cooled to ambient to obtain samples for XRPD analysis. IR and Raman spectra were also recorded, and these data were deemed sufficient to designate this form as anhydrous form III. Numbers of experiments were performed in solution using the sample of form III produced in the DSC experiment as seeds. These were unsuccessful in producing form III, but instead generated form II and form IV (see below).

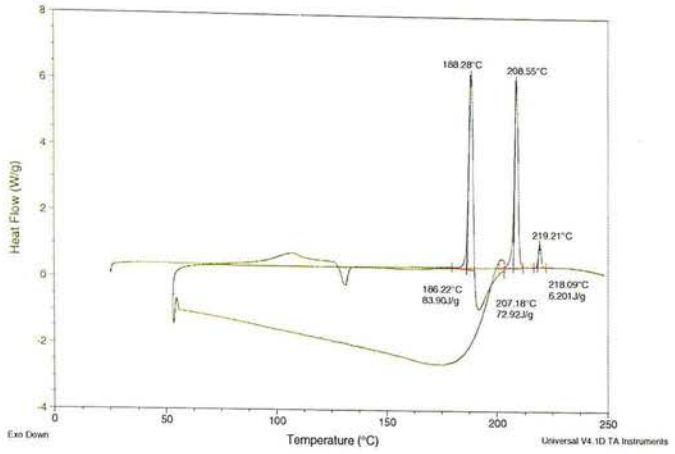

Figure 6.6: DSC plot obtained from samples of $CHCl_3$ solvate. The sample was first heated to 204 °C in order to the melt sample (first endotherm at *ca.* 188 °C represents melting of form I). The sample was then cooled to 50 °C and this resulted in recrystallisation of the melt to form III. A second endotherm at *ca.* 208 °C represents melting of form III. On further heating, form III converted to a new form with a melting point of *ca.* 219 °C (explained below).

Form IV

Form IV was produced from recrystallisation of compound A using form III as seeds. A thin slurry of form I was formed at 60 °C in EtOAc. This was heated to 70 °C, forming a clear solution and held at this temperature for 10 minutes. The solution was then cooled to 50 °C, and seeded with form III material obtained from thermal cycling experiments. The solution was then cooled to 30 °C. The resulting solid was then isolated by filtration and analysed by IR and Raman spectroscopy and XRPD. These data were deemed sufficient to designate this form as anhydrous form IV. The XRPD pattern of form IV is shown in Figure 6.8.

Form V

Form V was generated in DSC temperature cycling experiments performed on form IV. A sample of form IV was heated to 217 °C at 10 °C/min, cooled to 50 °C and then heated to 250 °C. The resulting DSC plot (Figure 6.7) shows the conversion of form IV into form V.

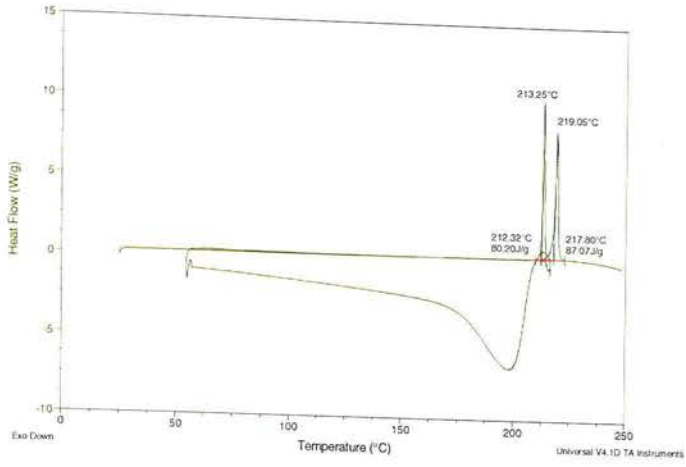

Figure 6.7: DSC plot obtained from samples of form IV. The sample was first heated to 217 °C in order to melt all form IV (first endotherm at ca. 213 °C represents melting of form IV) then cooled to 50 °C and this result in crystallisation to form V. Second endotherm at *ca.* 219 °C represents melting of form V.

A second sample of form V was also prepared in a similar manner and was used as seed to try to generate form V from saturated solution of compound B. However, this was unsuccessful, and form II was generated every time. Stability studies performed at GSK on all of the forms have shown that form II is the most stable form at ambient conditions and for this reason was the developmental form for further studies.

From all the above polymorph screening results it can be summarised that compound B has five anhydrous polymorphs. There are no single crystal data available for any of these forms. X-ray powder diffraction patterns of all these forms are compared in Figure 6.8 and the melting points for these forms are tabulated in Table 6.1.

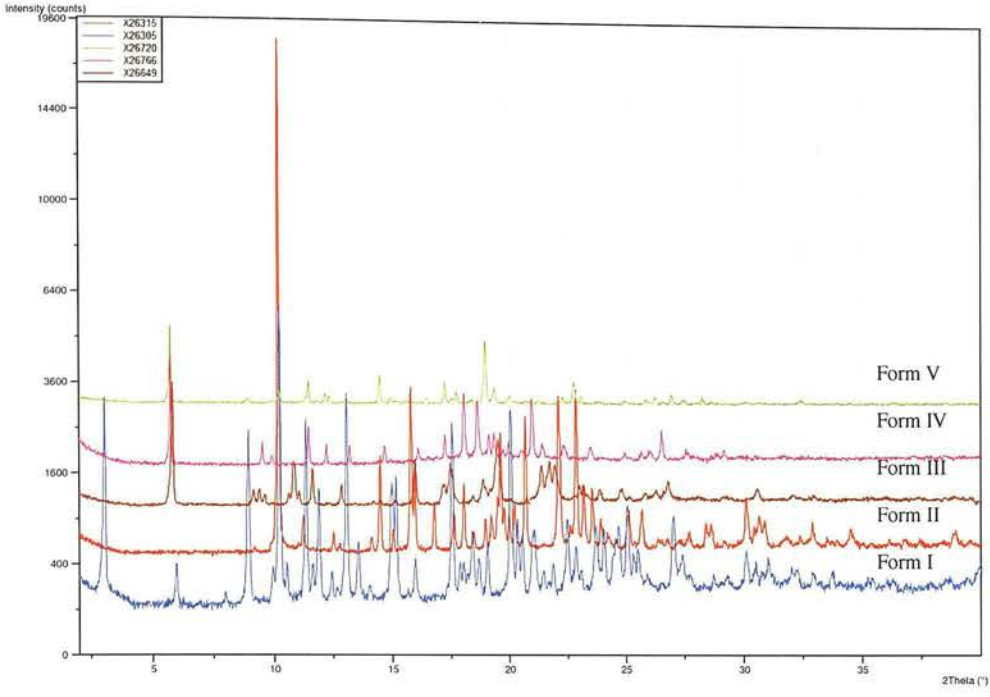

Figure 6.8: Comparison of experimental X-ray powder pattern of polymorphs of compound B (λ = 1.544 Å).

Form	Melting Onset (°C)
I	186
II	203
III	207
IV	212
V	218

Table 6.1: Melting points of polymorphs of compound B.

The high-pressure studies described in this chapter aimed to identify whether (a) any of the five forms could be obtained under pressure, and (b) any further polymorphs could be obtained at high pressure.

6.2. Experimental

6.2.1. Material

GSK compound B was received from GSK Stevenage, UK. The supplied form was identified as form II on the basis of X-ray powder diffraction measurements. For the recrystallisation experiments analytical grade solvents were used.

All high-pressure experiments were carried out using a Merrill-Bassett diamond anvil cell (DAC) (half-opening angle 40°) [1] and a pre-indented tungsten gasket of thickness 250 μm with 300 μm diameter hole.

6.3. Results and discussion

6.3.1. Recrystallisation from solution at ambient pressure (crystal structure of form II)

Single crystals of GSK compound B were obtained from slow cooling of a saturated solution (*ca.* 0.5 M) in ethanol. Single crystal X-ray diffraction data were collected at 150(2) K on a Bruker Smart CCD diffractometer employing Mo-$K\alpha$ radiation (λ = 0.71073). Indexing was performed using the indexing programme *CELL_NOW* [2] and identified a triclinic unit cell, space group *P*-1 with lattice parameters shown in Table 6.2. Integration of the data sets and global cell refinements were carried out using the program *SAINT* [3]. The intensity data were corrected for absorption by *SADABS* [4]. The structure was solved in *P*-1 using direct methods (SIR 97) [5]. Full-matrix least-squares structure refinement against $|F|^2$ was then performed using *CRYSTALS* [6]. Hydrogen atoms were placed in calculated positions and allowed to ride on their parent atom. Full structural refinement details are tabulated in appendix A. Crystallographic data in CIF format are available on the attached CD.

	Form II
Crystal System	Triclinic
Space group	*P*-1
a **(Å)**	9.2992(2)
b **(Å)**	10.0625(3)
c **(Å)**	12.0600(3)
α (°)	92.7920(10)
β (°)	102.9880(10)
γ (°)	106.1160(10)
V **(Å^3)**	1048.94(5)
Z	2
D$_c$ **(g cm^{-3})**	1.30
T (K)	150(2)

Table 6.2: Unit cell parameters for form II of compound B.

6.3.2. Description of crystal structure of form II

The crystal packing in form II, together with a space-filling diagram, is shown in Figure 6.9. There are two molecules in the unit cell which form dimer units *via* two hydrogen bonds between N6-H...O24 of each molecule (Figure 6.10). These dimer units are further linked with neighbouring dimer units by secondary hydrogen bonds formed between N25-H...N1 atoms. This results in infinite chains of dimer units parallel to the *b*-axis of the unit cell. Hydrogen bonding in form II can be best described with the aid of graph-set analysis. The graph-set notations are assigned by the method described by Bernstein *et al.* [7] and confirmed by *PLUTO* [8] and *MERCURY* [9]. The description of the hydrogen-bond pattern in form II according to the graph-set notation at the first level graph set is $N_1 = C(4)R^2_2(24)$. The C(4) motif represents chain arrangements of dimer unit as shown in Figure 6.10, whilst the R^2_2 motif represents ring of atoms formed by dimer unit. π-π interactions (shown by red arrows in Figure 6.10) are also present in molecules of the dimer unit. Distances between the molecules involved in these interactions are shown in Table 6.3.

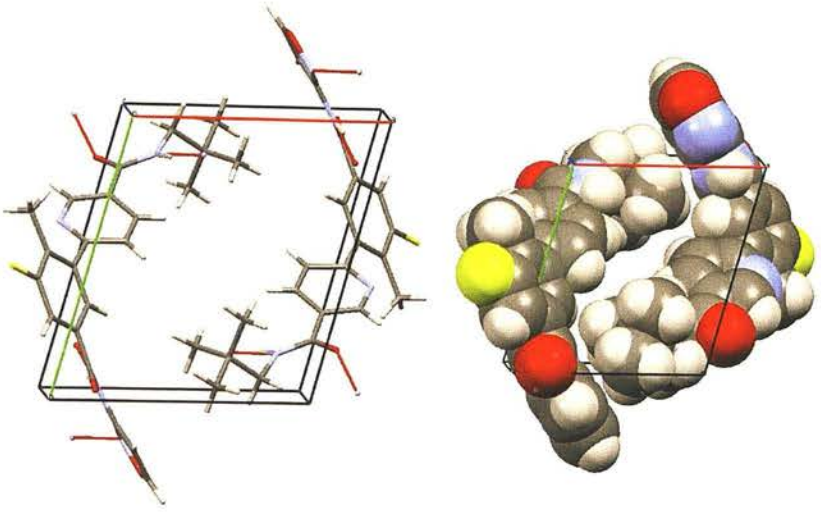

Figure 6.9: Crystal packing diagram viewed down *c*-axis (left) (hanging red contacts show hydrogen bonds) and space-filling diagram (right) for form II.

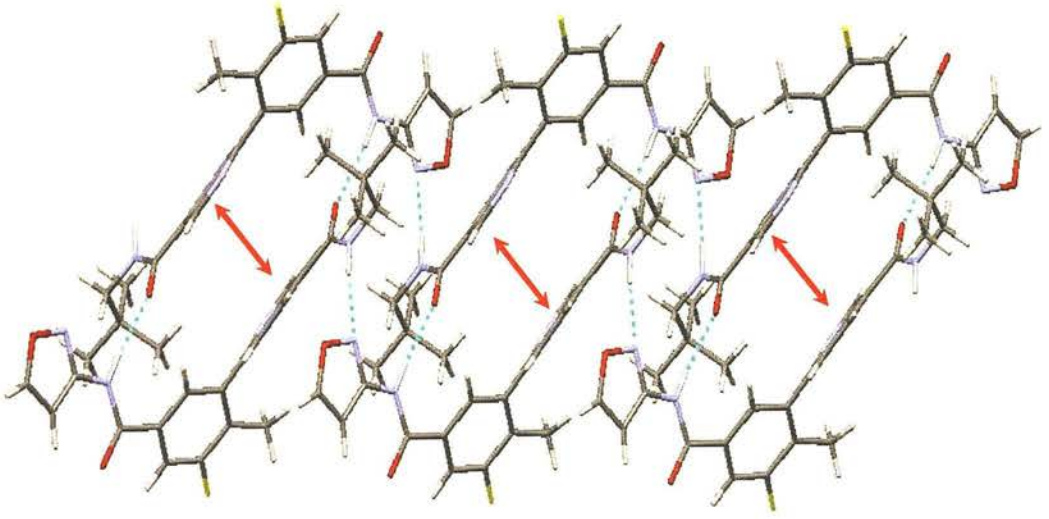

Figure 6.10: Hydrogen bonded chains of dimer units in form II. Red arrows show π-π interaction between aromatic rings of the molecules.

	Distance (Å)
N6...O24	2.90
N25...N1	3.05
π-π interaction	3.87

Table 6.3: Distance between molecules involved in hydrogen bonding and π-π interaction for form II.

The conformation of the molecule in the crystal structure can be described by three torsional angles (Figure 6.11); θ_1 (C14-C9-C7-N6) *i.e.* twisting of the terminal azole ring with respect to the phenyl ring, θ_2 (C14-C13-C17-C22) *i.e.* twisting of pyridine ring with respect to the phenyl ring and θ_3 (C19-C20-C23-O24) *i.e.* twisting of the terminal chain with respect to the pyridine group. These torsional angles are calculated using the program *MERCURY* [9] and are shown in Table 6.4.

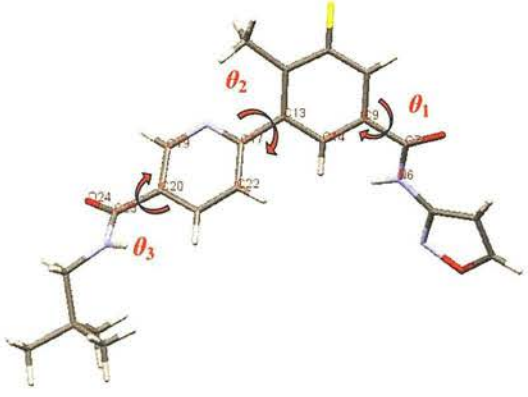

Figure 6.11: Compound B molecule with description of torsional angles, θ_1 = C14-C9-C7-N6, θ_2 = C14-C13-C17-C22 and θ_3 = C19-C20-C23-O24.

	Torsional angle
θ_1 (C14-C9-C7-N6)	31.2°
θ_2 (C14-C13-C17-C22)	46.2°
θ_3 (C19-C20-C23-O24)	23.1°

Table 6.4: Description of torsional angles for form II.

6.3.3. Direct compression of single crystal of form II

High pressures for single-crystal X-ray diffraction studies were generated using a Merrill-Bassett diamond anvil cell (DAC) [1] equipped with 600 μm culet diamonds and a tungsten gasket. A single-crystal of form II and a small ruby chip were loaded into the DAC (Figure 6.12), together with Fluorinert-FC77 as a pressure-transmitting medium. The pressure applied to the sample was determined by the ruby fluorescence method [10] using the 632.8 nm excitation line from a He-Ne laser. The fluorescence was detected by a Jobin-Yvon LabRam 300. High-pressure data sets were collected on a Bruker *APEX II* CCD diffractometer by using ω-scans in 12 settings of 2θ and φ with step size 0.3° for 40 s [11]. The first data set was collected at ambient pressure. Indexing of the reflections confirmed the known triclinic form II of compound B. Diffraction data were then collected at incremental steps of pressure up to 3.82 GPa. Data indexing from all the data sets were performed using the indexing programme *CELL_NOW* [2]. Lattice parameters at pressures up to 3.8 GPa are compared in Table 6.5. On raising the pressure to 4.2 GPa the crystal disintegrated, perhaps suggesting a reconstructive phase transition.

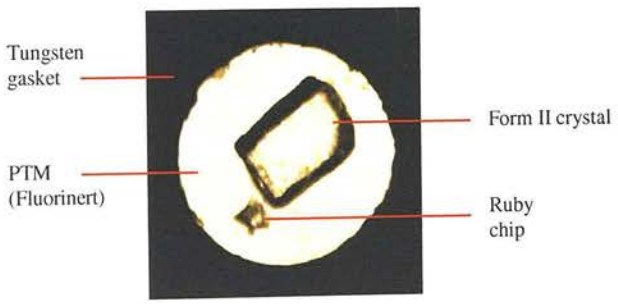

Figure 6.12: Single crystal of form II loaded with ruby and Fuorinert-FC77 as pressure-transmitting medium (PTM).

Pressure	ambient	0.3 GPa	0.5 GPa	1.2 GPa	1.4 GPa	2.0 GPa	2.5 GPa	3.2 GPa	3.8 GPa
Crystal System	Triclinic	Triclinic	Triclinic	Triclinic	Triclinic	Triclinic	Triclinic	Triclinic	Triclinic
Space group	*P*-1	*P*-1	*P*-1	*P*-1	*P*-1	*P*-1	*P*-1	*P*-1	*P*-1
a/Å	9.3942(17)	9.2468(17)	9.1676(6)	9.0310(15)	8.987(3)	8.8340(9)	8.6991(8)	8.6016(16)	8.567(5)
b/Å	10.1512(7)	9.8924(7)	9.7474(2)	9.4568(16)	9.4376(10)	9.3641(4)	9.3009(3)	9.1835(6)	9.171(2)
c/Å	12.1831(10)	12.0152(10)	11.9223(3)	11.746(5)	11.6995(13)	11.6485(5)	11.6154(4)	11.5244(8)	11.507(3)
α/	91.831(6)	93.246(6)	94.00(2)	95.30(2)	95.766(8)	96.043(3)	96.244(3)	97.146(6)	97.315(19)
β/	103.167(12)	102.971(12)	102.875(4)	102.42(6)	101.977(17)	101.851(7)	101.828(6)	101.138(11)	100.74(4)
γ/	107.468(12)	106.738(12)	106.530(4)	106.27(4)	106.011(17)	105.947(7)	105.808(6)	105.319(12)	105.07(4)
V/Å^3	1072.8(2)	1016.95(2)	985.51(8)	927.9(7)	919.8(3)	893.27(12)	871.43(10)	846.53(19)	842.8(6)
Z	2	2	2	2	2	2	2	2	2
T/K	293(2)	293(2)	293(2)	293(2)	293(2)	293(2)	293(2)	293(2)	293(2)

Table 6.5: Unit cell parameters for form II with increasing pressure up to 3.8 GPa

All single-crystal data sets up to 3.8 GPa were processed according to the procedure described by Dawson *et* al. [12]. Integration of data sets and global cell refinement were carried out using the program *SAINT* [3], in which 'dynamic masks' were used in order to prevent integration of areas of the detector shaded by the body of the DAC. An analytical correction for the absorption by the DAC component was then applied using *SHADE* [13] and an absorption correction for the crystal was applied using *SADABS* [4]. Known fractional coordinates were taken from the form II crystal structure and a full-matrix least-squares-refinement against |F| was performed using the program *CRYSTALS* [6]. Isotropic refinement of non-H atoms was used to ensure a high data:parameter ratio. Hydrogen atoms were placed in calculated positions and fixed during refinement. Because of high *R*-factor, the crystal structure at 3.8 GPa is not reported. Crystallographic data for all the other structures in CIF format are available on the attached CD.

Figure 6.13 illustrates the variation of unit cell parameters with increasing pressure. There is a continuous decrease in cell lengths *a*, *b* and *c*; the α-angle increases, whilst the β- and γ- angles decrease with increasing pressure. Figure 6.14 shows the variation of unit cell volume with increasing pressure. The unit cell volume decreases by *ca.* 20 % between ambient pressure and 3.8 GPa. This large decrease in volume suggests a high compressibility for form II. A continuous decrease in the volume also shows that there is no 1st or 2nd order phase transition associated with compression.

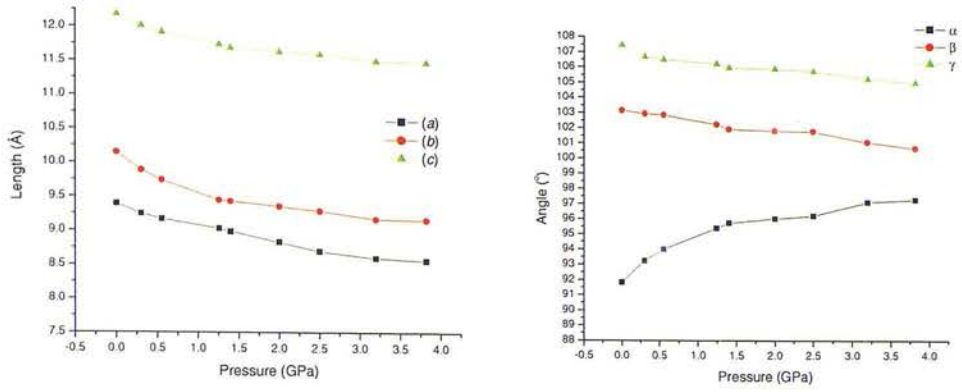

(a) (b)

Figure 6.13: Variation of lattice parameters of form II with increasing pressure (a) unit cell length (b) unit cell angles.

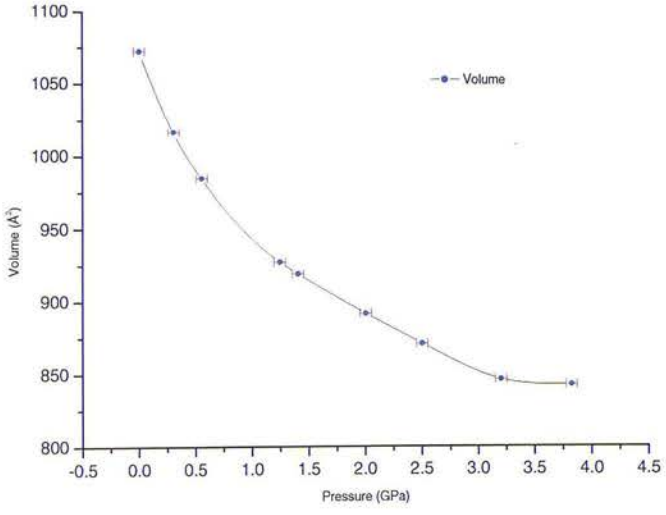

Figure 6.14: Variation of unit cell volume of form II with increasing pressure.

Compression studies were also performed on the powder samples of form II. Finely ground powder samples of form II along with a ruby chip were loaded into a DAC. Fluorinert-FC77 was used as the pressure transmitting medium. Raman spectroscopy was used to identify any structural transition with pressure.

Scans with acquisition times of 15 minutes were collected at incremental pressure steps between ambient pressure and 2.5 GPa. Figure 6.15 shows the Raman spectra plotted at selected pressures. From ambient pressure to 2.5 GPa, no significant changes were observed in the spectra, thus confirming that no pressure-induced phase transition occurs under these conditions.

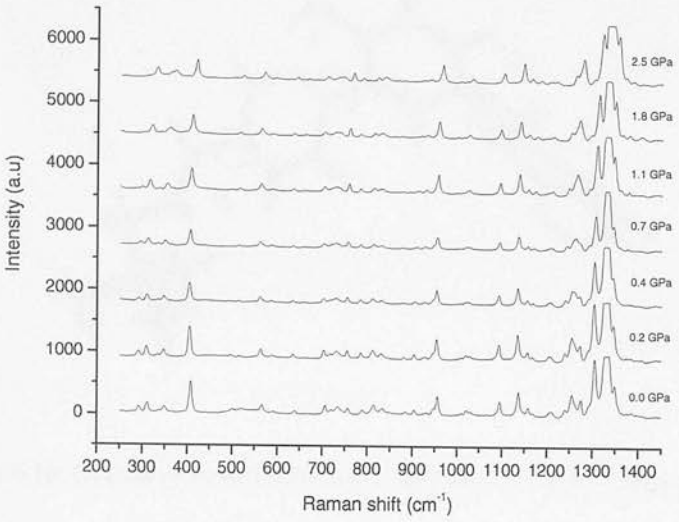

Figure 6.15: Raman spectra of form II with increasing pressure.

Over the studied pressure range, no significant changes were observed in the molecular conformation or in any of the primary bond lengths and angles of the molecule. The hydrogen bonding interactions N6…O24 and N25…N1 both become shorter, although rather surprisingly it is the shorter of the two that is the more compressible. It appears to be approaching a limiting value of 2.56 Å (at 3.2 GPa) which from our past experience indicates an onset of a phase transition. The π-π interactions also become shorter over this pressure range (see Table 6.6).

Distance (Å)	**0.0 GPa**	**0.3 GPa**	**0.5 GPa**	**1.4 GPa**	**2.0 GPa**	**2.5 GPa**	**3.2 GPa**
N6...O24	2.88	2.86	2.69	2.66	2.63	2.60	2.56
N25...N1	3.07	3.05	3.03	2.98	2.96	2.94	2.93
π-π interaction	3.91	3.69	3.57	3.35	3.29	3.25	3.18

Table 6.6: Variation of intermolecular distances for form II with increasing pressure.

Figure 6.16 shows the structural overlay of molecules at ambient and 3.2 GPa. The only changes observed were a *ca.* 8° twist in θ_1 and a *ca.* 5° twist in θ_2. The variation of the three torsional angles, θ_1, θ_2 *and* θ_3 with pressure are shown in Table 6.7.

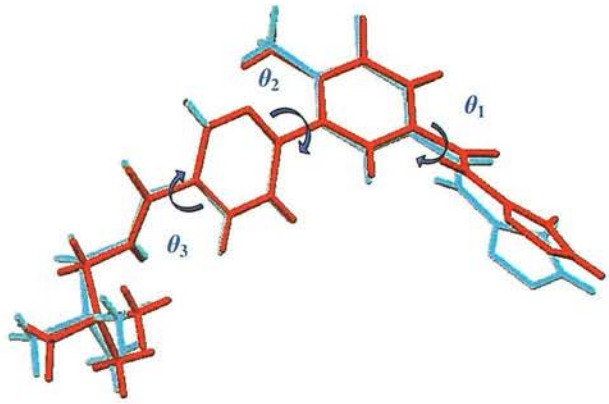

Figure 6.16: Overlay of form II structures at ambient (red) and 3.2 GPa (blue).

Torsional angle	0.0 GPa	0.3 GPa	0.5 GPa	1.4 GPa	2.0 GPa	2.5 GPa	3.2 GPa
θ_1 (°)	34.6	33.8	32.1	31.3	30.2	28.7	26.8
θ_2 (°)	46.1	43.9	42.9	42.3	42.8	41.8	40.9
θ_3 (°)	19.6	21.4	19.2	18.1	17.4	18.2	17.8

Table 6.7: Variation of torsional angles for form II with increasing pressure.

The apparent stability of form II structure with respect to pressure is presumably a result of the particular crystal structure of form II in which the molecules pack as dimer units by making two hydrogen bonds, locking the molecules into a specific conformation. This conformation is also stabilised by the π-π interaction between the pyridine rings of the two molecules involved in dimer formation. Application of pressure results in more dense packing, with loss of voids in the structure (as depicted in Figure 6.17) without a change in the geometry *i.e.* the barrier to molecular rearrangement is presumably high and cannot be achieved simply by compression. These observations therefore prompted a study using recrystallisation from solution at high pressure.

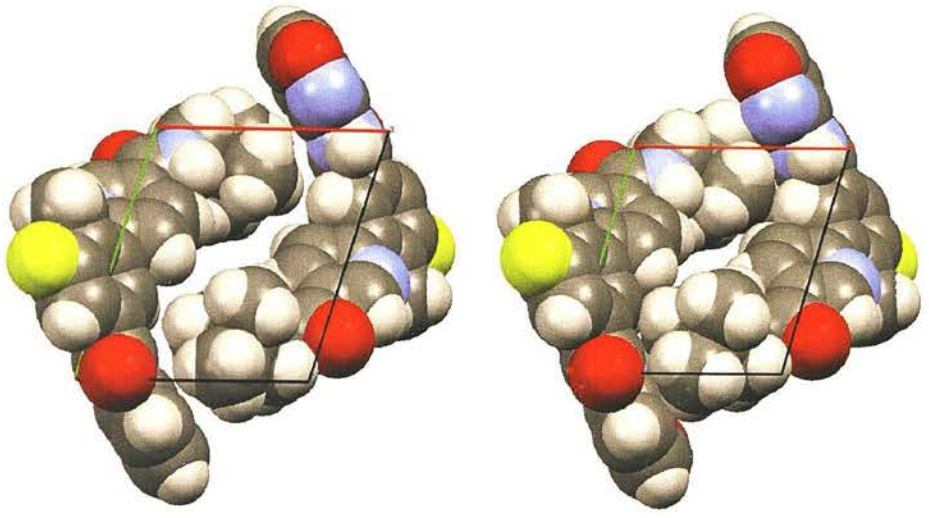

Figure 6.17: Comparison of space-filling diagrams for form II at ambient pressure (left) and 3.2 GPa (right).

6.3.4. Crystallisation from solution at high pressure

A *ca.* 1M solution of compound B was prepared in methanol:ethanol (4:1) mixture. The solution was then loaded along with a few crystallites of compound B (form II) at 293(2) K into a DAC. A small piece of ruby was also added in order to allow the determination of the pressure by laser fluorescence spectroscopy [10]. The pressure was increased to a minimum in order to form a sealed system and the cell was then subjected to gentle heating to dissolve all of the solid material. Pressure was then applied by tightening the screws of the DAC to induce precipitation. Crystallisation was achieved at *ca.* 0.6 GPa. The pressure was then reduced to 0.4 GPa in order to facilitate growth of a single crystal. The temperature was then cycled near 353(2) K in order to dissolve all but one of the crystallites. On slow cooling to 293(2) K a single crystal grew (Figure 6.18). The pressure within the gasket hole was determined to be *ca.* 0.4 GPa. Diffraction data were collected on a Bruker *APEX II* CCD diffractometer by using ω-scans in 12 settings of 2θ and φ with step size 0.3° for 40 s. Data indexing was performed using the indexing programme *CELL_NOW* [2]. This gave a monoclinic unit cell with space group $P2_1/n$. Lattice parameters are shown in Table 6.8.

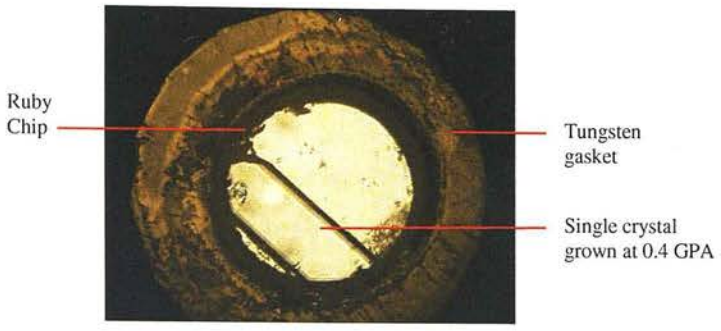

Figure 6.18: Optical image of single crystal of compound B in diamond-anvil cell grown at 0.4 GPa.

	0.4 GPa (form VI)
Crystal System	Monoclinic
Space group	$P2_1/n$
***a* (Å)**	9.9904(13)
***b* (Å)**	9.9041(6)
***c* (Å)**	21.3712(19)
***α* (°)**	90
***β* (°)**	102.987(8)
***γ* (°)**	90
***V* (Å^3)**	2060.5(4)
Z	4
***D*$_c$ (g cm^{-3})**	1.32
P (GPa)	0.40(5)
T (K)	293(2)

Table 6.8: Unit cell parameters for form VI of compound B.

Data processing was performed according to the procedure described by Dawson *et al.* (2004) [12]. Integration of data sets and global cell refinement were carried out using the program *SAINT* [3], in which 'dynamic masks' were used in order to prevent integration of areas of the detector shaded by the body of the DAC. An analytical correction for the absorption by the DAC component was then applied using *SHADE* [13] and an absorption correction for the crystal was applied using *SADABS* [4]. The structure was solved in space group $P2_1/n$ using direct methods (*SHELX*) [14]. Full-matrix least-squares structure refinement was then performed using *CRYSTALS* [6]. Isotropic refinement of non-H atoms was used to ensure a high data:parameter ratio. Hydrogen atoms were placed in calculated positions and

allowed to ride on their parent atom. Full structural refinement details are shown in Appendix C. Crystallographic data in CIF format are available in the attached CD.

Figure 6.19 shows the comparison between the calculated powder pattern from single crystal data for the high-pressure form with the experimental powder patterns of all the known forms of compound B. It is evident that the new high-pressure form does not correspond to any of the known form and so this new form is designated as form VI.

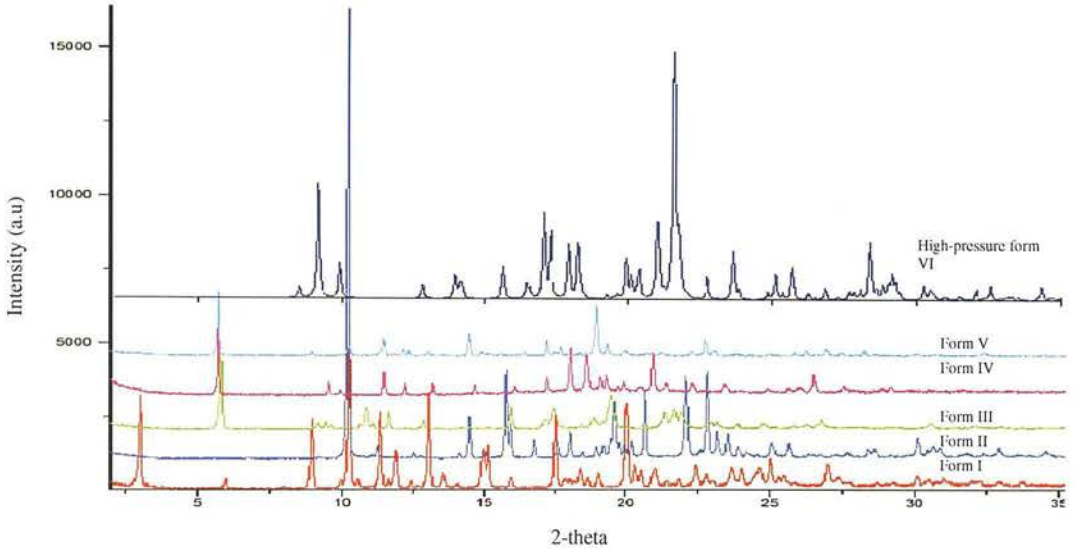

Figure 6.19: Comparison of simulated X-ray powder diffraction pattern calculated from single crystal data for high-pressure form (top) with the experimental X-ray powder patterns of all known polymorphs of compound B (λ = 1.544 Å).

6.3.5. Description of crystal structure of high-pressure form (form VI)

Figure 6.20 shows the packing and space-filling diagrams for form VI. There are four molecules in the unit cell. It shows different arrangements of molecules compared to form II. There is no dimer formation in the structure. In form VI, molecules are linked together by forming two hydrogen bonds between N25 and O24 atoms (N25-H...O24), with a N25...O24 distance = 2.93 Å. This results in infinite

chains of hydrogen-bonded molecules running parallel to the *b*-axis (Figure 6.21). These hydrogen-bonded chains adopt alternating orientations with respect to neighbouring chains. Molecules in the form VI crystal structure show different conformations compared to form II; the three torsional angles are compared in Table 6.9. All three torsional angles are different between these forms, indicating a high degree of torsional flexibility for the molecules. The differences in conformations for these forms can best be seen in the overlay diagram (Figure 6.22).

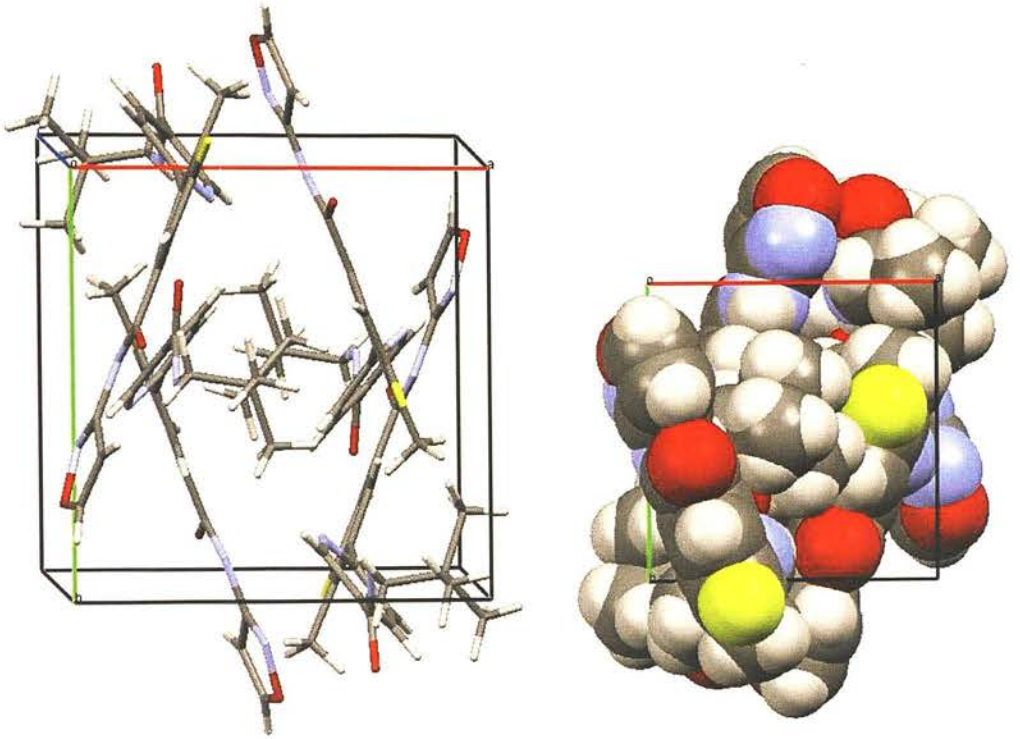

Figure 6.20: Crystal packing diagram viewed down *c*-axis (left) and space-filling diagram (right) of form VI.

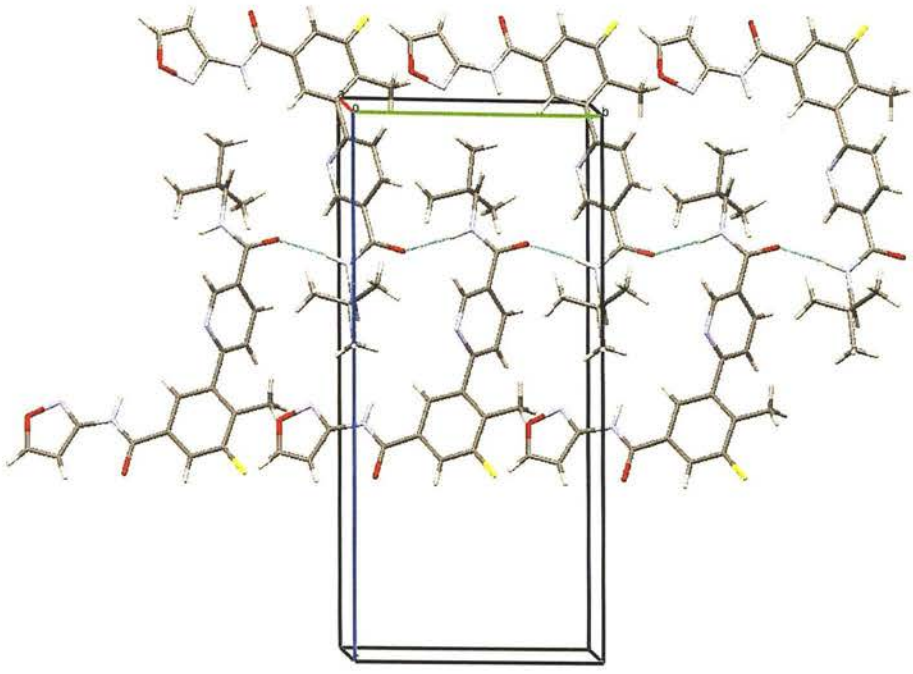

Figure 6.21: Hydrogen bonded chain of molecules in form VI. For simplicity only one chain is shown.

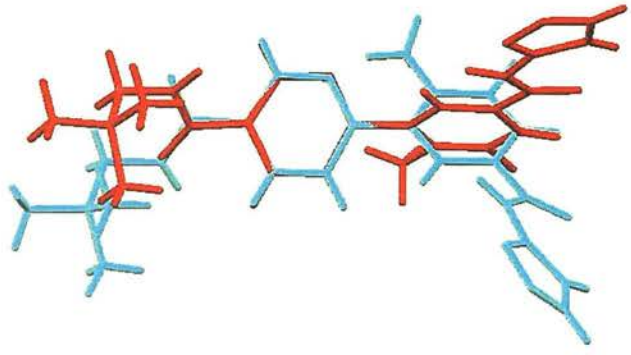

Figure 6.22: Comparison of molecular conformations for form II (blue) and VI (red).

Torsional angle	Form II	Form VI
θ_1	34.6°	8.1°
θ_2	46.1°	112.2°
θ_3	19.6°	137.7°

Table 6.9: Comparison of torsional angles between form II and VI.

6.3.6. Decompression studies

The question as to whether this high-pressure form can be recovered to ambient conditions was naturally of great importance. Pressure was gradually released from 0.4 GPa to ambient pressure at 293(2) K. Optical observation showed that the single crystal of form VI survived on decompression (Figure 6.23) showing no reconstructive phase transition. However, optical observation of the crystal does not rule out a non-reconstructive phase transition. Figure 6.24 shows the comparison between Raman spectra recorded at 0.4 GPa and ambient pressure. It is evident from the comparison that there is no phase transition; both spectra are identical and form VI has been recovered. This was confirmed by recording single crystal X-ray diffraction data of the recovered crystal at ambient pressure. A unit cell of a = 10.0199(6), b = 9.9211(4), c = 21.4471(9) and β = 102.939(4) was obtained, consistent with that of form VI.

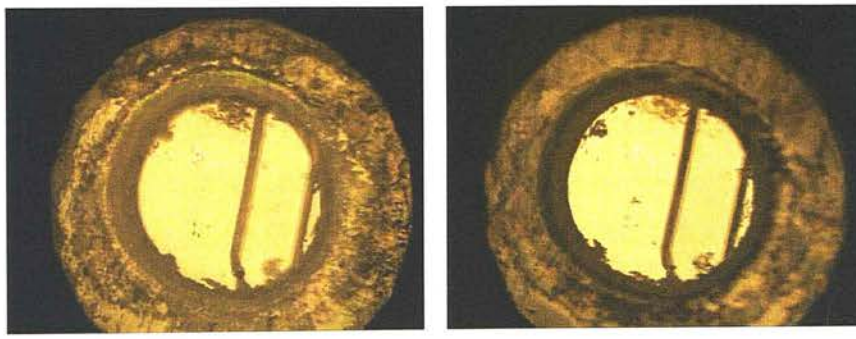

Figure 6.23: Optical image of form VI at ambient (left) and 0.4 GPa (right).

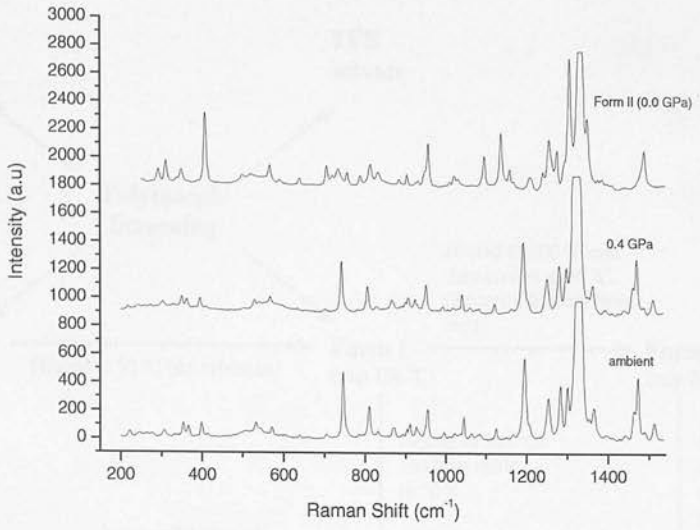

Figure 6.24: Comparison of Raman spectra of form VI collected at 0.4 GPa and ambient pressure. Raman spectrum for form II (top) is also shown for comparison.

6.4. Conclusions and future work

The polymorphism in compound B is summarised in scheme 6.1. Compound B has shown rich polymorph behaviour. This could probably have been predicted on the basis of its molecular structure, where conformational flexibility can result in different polymorphs. Six polymorphs along with three solvates of compound B have been identified; transformation between these forms is shown in scheme 6.1.

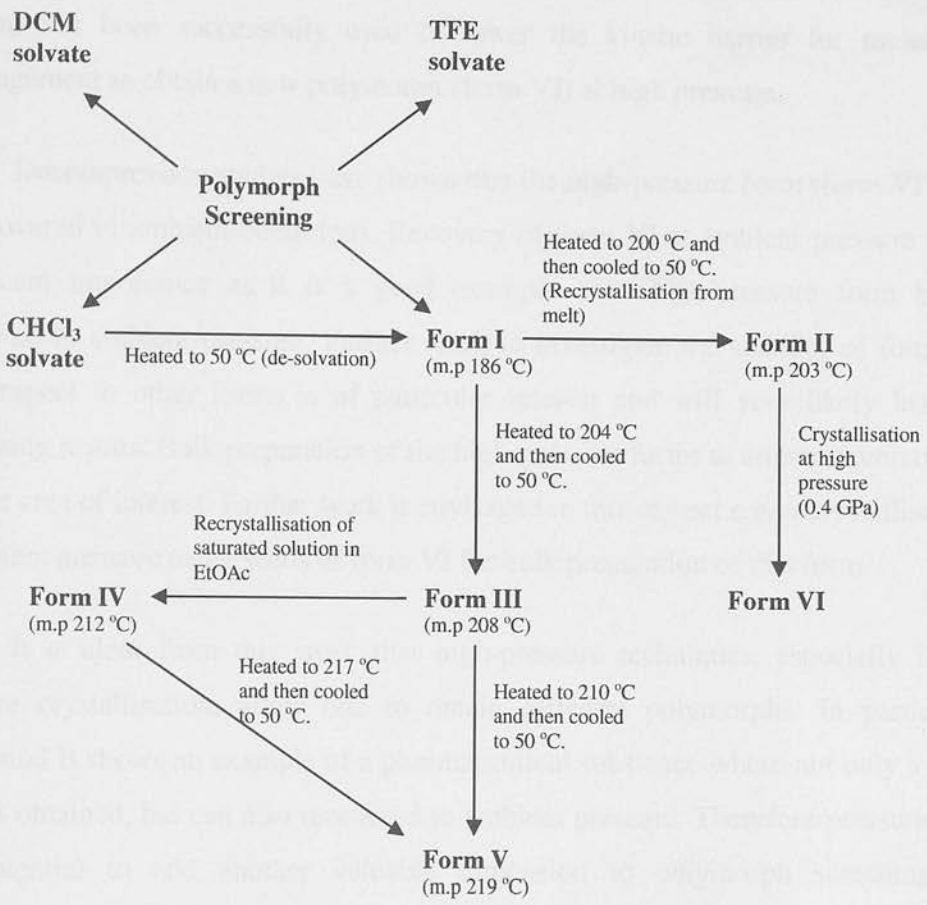

Scheme 4.1: Transformations of polymorphs of compound B.

The work presented in this chapter has demonstrated that high-pressure crystallisation can be used to prepare a new polymorph, designated as form VI. A single crystal was grown at 0.4 GPa and the structure was successfully solved.

The crystal structure of most stable form (form II) has been obtained for the first time. Direct compression of a single crystal of form II has shown an unusually high compressibility for the structure with no phase transition up to 3.8 GPa. By increasing pressure to 4.2 GPa the crystal disintegrated, suggesting a reconstructive phase transition. Form II is an example of a structure where molecules are locked into a specific conformation. This conformation is stabilised by hydrogen bonding and π-π interactions and suggests a high kinetic barrier towards molecular

rearrangement in the solid. It shows a good example where recrystallistion from solution has been successfully used to lower the kinetic barrier for molecular rearrangement to obtain a new polymorph (form VI) at high pressure.

Decompression studies have shown that the high-pressure form (form VI) can be recovered to ambient conditions. Recovery of form VI at ambient pressure is of significant importance as it is a good example of a high-pressure form being recovered to ambient pressure. Further work to investigate the stability of form VI with respect to other forms is of particular interest and will very likely lead to interesting results. Bulk preparation of the high-pressure forms at ambient pressure is another area of interest. Further work is envisaged in this respect *e.g.* recrystallisation at ambient pressure using seeds of form VI for bulk preparation of this form.

It is clear from this work that high-pressure techniques, especially high-pressure crystallisation, allow one to obtain different polymorphs. In particular compound B shows an example of a pharmaceutical substance where not only a new form is obtained, but can also recovered to ambient pressure. Therefore pressure has the potential to add another valuable dimension to polymorph screening of pharmaceuticals.

6.5. References

1. L. Merrill and W. A. Bassett, *Rev. Sci. Instrum.*, 1974, **45**, 290-294.
2. G. M. Sheldrick, *CELL_NOW*, University of Gottingen, Germany, 2002.
3. B. AXS, *SAINT*, Bruker-AXS, Madison, Wisconsin, USA, 2003.
4. G. M. Sheldrick, *SADABS*, University of Göttingen, Germany, 2006.
5. A. Altomare, G. Cascarano, C. Giacovazzo, A. Guagliardi, M. C. Burla, G. Polidori and M. Camalli, *J. Appl. Crystallogr.*, 1994, **27**, 435.
6. P. W. Betteridge, J. R. Carruthers, R. I. Cooper, K. Prout and D. J. Watkin, *J. Appl. Crystallogr.*, 2003, **36**, 1487.
7. J. Bernstein, R. E. Davis, L. Shimoni and N. L. Chang, *Angew. Chem., Int. Ed. Engl.*, 1995, **34**, 1555-1573.
8. W. D. S. Motherwell, G. P. Shields and F. H. Allen, *Acta Crystallogr., Sect. B: Struct. Sci.*, 1999, **B55**, 1044-1056.
9. C. F. Macrae, P. R. Edgington, P. McCabe, E. Pidcock, G. P. Shields, R. Taylor, M. Towler and J. van de Streek, *J. Appl. Crystallogr*, 2006, **39**, 453-457.

10. G. J. Piermarini, S. Block, J. D. Barnett and R. A. Forman, *J. Appl. Phys.*, 1975, **46**, 2774-2780.
11. S. A. Moggach, D. R. Allan, S. Parsons, L. Sawyer and J. E. Warren, *J. Synchrotron Radiat.*, 2005, **12**, 598-607.
12. A. Dawson, D. R. Allan, S. Parsons and M. Ruf, *J. Appl. Crystallogr.*, 2004, **37**, 410-416.
13. S. Parsons, *SHADE*, University of Edinburgh, Scotland, UK, 2004.
14. G. M. Sheldrick, *SHELXS86*, University of Gottingen, Germany, 1986.

Chapter 7

Conclusions, General Remarks and Future Directions

Chapter 7: Conclusions, General Remarks and Future Directions

7.1. Conclusions

The high-pressure techniques described in this thesis have been shown to be very successful means for the preparation of both new and elusive polymorphs of complex molecular compounds *e.g.* pharmaceuticals. Structural information has been obtained at elevated pressures, including structure solution and refinement of a variety of new high-pressure forms. A key factor contributing to this success has been the combination of techniques that include single-crystal X-ray diffraction, X-ray powder diffraction, and Raman spectroscopy.

An elusive polymorph of a potent analgesic drug substance, mefenamic acid, has been obtained from crystallisation of ethanol solution at 0.6 GPa and dry milling of powder samples. Two new polymorphs of mefenamic acid designated as form III and form IV have been obtained from compression studies on powder samples using methanol:ethanol and Fluorinert-FC77, respectively. Two new high-pressure polymorphs, designated as form III and form IV of N,N'-dimethylurea (DMU) have been obtained using the high-pressure recrystallisation technique at 0.7 and 0.9 GPa, respectively. These forms were also produced by compression of powder samples of DMU using methanol:ethanol mixture as pressure-transmitting medium. Decompression studies have shown that form III can be recovered to ambient pressure, but is metastable with respect to form I. Decompression of powder samples of form IV resulted in the formation of another new form. Powder compression studies using Fluorinert-FC77 as pressure-transmitting medium also revealed that the elusive form II of DMU could also be produced through high-pressure techniques, particularly when the elusive polymorph is more dense. These studies show that the choice of liquid as pressure-transmitting fluid is also very important in high-pressure experiments, reflecting the importance of solvent-mediated transitions.

High-pressure techniques have been shown to be an excellent tool for probing polymorphism in more complex pharmaceutical compounds. This is underlined by the high pressure studies of GSK developmental compounds A and B. New polymorphs for these compounds have been obtained at high pressure. Of particular importance are form III and form VI of compounds A and B, respectively, where these high-pressure forms were obtained through high-pressure crystallisation and can be recovered to ambient pressure. From the compression studies performed on the powder samples of compound A, two new high-pressure forms designated as forms V and VI were also identified. New polymorphs of these compounds were also produced from recrystallisation at ambient pressure. These studies show the importance of the starting form in polymorph screening experiments as these new forms were not produced in GSK screening experiments, where different starting polymorphic forms were used. In contrast, some of the forms obtained at GSK were not found during the course of the high pressure experiments, thus emphasising that high-pressure techniques are complementary rather than a direct replacement for conventional screening methods.

7.2. General remarks and future directions

There are several reasons why pressure is effective in the discovery of new polymorphs, particularly when combined with recrystallisation from solution. High-pressure conditions encourage structures in which molecules pack together more efficiently, leading to closure of voids in the structure. This means that changes in the relative orientations of molecules in a solid are very likely to occur, thereby giving rise to different motifs of intermolecular interactions. These interactions are themselves sensitive to distance, and hence to the effects of pressure. The strengths of these intermolecular interactions are susceptible to the relatively modest pressures used in these studies.

High-pressure crystallisation from solution removes the need for excessively high temperatures and overcomes the barrier to molecular rearrangement in the solid since the lattice energy is now overcome by solvation energy. Furthermore, the

interaction between solute and solvent molecules are also modified by pressure thereby changing the solubility of given polymorph. In some cases the solubility difference between two or more forms might also be expected to change, thereby encouraging recrystallisation of one polymorph at the expense of another. The changes in the solvent properties under pressure are still poorly understood, but clearly play a significant role in the high-pressure crystallisation process.

Further work to investigate the high-pressure behaviour of pharmaceutical materials will very likely lead to improvements in the scope of polymorph screening. Of particular interest could be recovery and bulk preparation of high-pressure polymorphs.

The work presented in this thesis also highlights the challenges associated with high-pressure single-crystal X-ray diffraction and powder X-ray diffraction, one of the most important being the restricted reciprocal space caused by the diamond-anvil cells. The design of high-pressure cells that will improve the access of X-ray to the sample chamber is therefore an area of current interest. New strategies for the collection of single-crystal high-pressure data are also expected to attract considerable attention *e.g.* data collection of multiple crystals within the cell to improve data completeness and the use of shorter X-ray wavelengths to improve coverage of reciprocal space.

Appendix

Appendix A: Crystallographic Data

Crystallographic Information Files for the structures described in Chapters 3, 4, 5 and 6 are on the attached CD.

Chapter 3: Mefenamic acid form II

Form II	
Crystal data	
Chemical formula	$C_{15}H_{15}NO_2$
Mr	241.29
Cell setting, space group	Triclinic, *P*-1
a, *b*, *c* (Å)	7.7900(15), 9.1890(18), 9.4120(19)
α, β, γ (°)	106.751(10), 92.287(12)°, 101.337(11)
V(Å^3)	629.1(2)
Z	2
D_x(Mg m^{-3})	1.27
Radiation type	Mo$K\alpha$
No. of reflections for cell parameters	418
θ range (°)	2.272-20.870
μ (mm-1)	0.085
Temperature (K)	298(2)
Pressure (GPa)	0.30(5)
Crystal form, colour	Block, colourless
Crystal size (mm)	0.1 × 0.1 ×0.15
Data collection	
Diffractometer	Bruker *SMART*
Data collection method	ω scans
Absorption correction	multi-scan (SADABS)
*T*min	0.630
*T*max	1.000
No. of measured, independent and observed reflection	4003, 1210
Criterion for observed reflection	$I > 2\sigma(I)$
*R*int	0.0269
Θmax (°)	20.87
Range of h, k, l	$-7 \rightarrow h \rightarrow 7$ $-9 \rightarrow k \rightarrow 9$ $-9 \rightarrow l \rightarrow 9$
Refinement	
Refinement on	*F*
R factor, *wR* factor, S	0.0953, 0.0942, 1.23
No. of reflection	418
No. of parameters	73
H-atom treatment	Riding
Weighting scheme	$w' \times [1 - (\Delta F_{obs} / 6 \times \Delta F_{est})^2]^2$ $w' = [P_0T_0'(x) + P_1T_1'(x) + ...P_{n-1}T_{n-1}'(x)]^{-1}$,

	where P_i are the coefficients of a Chebychev series in $t_i(x)$, and $x = F_{calc}/F_{calcmax}$. $P_0 - P_{n-1}$ = 3.28 -0.337 1.88
$(\Delta/\sigma)_{max}$	<0.0001
$\Delta\rho_{max}$, $\Delta\rho_{min}$ (eÅ^{-3})	0.50, -0.46
Extinction method	none

Table 1: Crystal, collection and refinement details for MA form III at 0.3 GPa

Chapter 4: N, N-dimethylurea (form III and form IV)

	Form III	Form IV
Crystal data		
Chemical formula	$C_3H_8N_2O$	$C_3H_8N_2O$
Mr	88.10	86.10
Cell setting, space group	Monoclinic, *P2/c*	Orthorhombic, *Pbcn*
a, b, c (Å)	5.0888(10), 4.5563(3), 10.2891(7)	4.3178(12), 8.490(6), 11.757(4)
α, β, γ (°)	90, 98.081(10), 90	90, 90, 90
V(Å^3)	236.20(5)	430.7(4)
Z	2	4
D_x(Mg m^{-3})	1.24	1.36
Radiation type	Mo*K*α	Mo*K*α
No. of reflections for cell parameters	137 and 140	385 and 159
θ range (°)	4.001-23.053	3-23
μ (mm^{-1})	0.094	0.103
Temperature (K)	298(2)	298(2)
Pressure (GPa)	0.70(5)	0.90(5)
Crystal form, colour	Block, colourless	Block, colourless
Crystal size (mm)	0.12 x 0.16 x 0.30	0.10 x 0.10 x 0.15
Data collection		
Diffractometer	Bruker SMART	Bruker SMART
Data collection method	ω scans	ω scans
Absorption correction	Empirical & multi-scan (*SADABS*)	Empirical & multi-scan (*SADABS*)
T_{min}	0.87	0.76
T_{max}	0.99	0.99
No. of measured and independent reflections	150, 137	200, 200
Criterion for observed reflection	$I > 2\sigma(I)$	$I > 2\sigma(I)$
R_{int}	0.000	0.0359
θ_{max} (°)	23.05	23.3457
Range of h, k, l	$-2 \rightarrow h \rightarrow 1$ $0 \rightarrow k \rightarrow 5$ $0 \rightarrow l \rightarrow 11$	$-4 \rightarrow h \rightarrow 4$ $-6 \rightarrow k \rightarrow 6$ $-12 \rightarrow l \rightarrow 12$
Refinement		
Refinement on	*F*	*F*
R-factor, *wR*-factor, S	0.050, 0.055, 1.20	0.05, 0.049, 1.10

No. of reflection	111	124
No. of parameters	29	29
H-atom treatment	Riding	Riding
Weighting scheme	$w' \times [1 - (\Delta F_{obs} / 6 \times \Delta F_{est})^2]^2$ $w' = [P_0T_0'(x) + P_1T_1'(x) + ...P_{n-1}T_{n-1}'(x)]^{-1}$, where P_i are the coefficients of a Chebychev series in $t_i(x)$, and $x = F_{calc}/F_{calcmax}$. $P_0 - P_{n-1} = 6.46\ -2.45\ 4.37$	$w' \times [1 - (\Delta F_{obs} / 6 \times \Delta F_{est})^2]^2$ $w' = [P_0T_0'(x) + P_1T_1'(x) + ...P_{n-1}T_{n-1}'(x)]^{-1}$, where P_i are the coefficients of a Chebychev series in $t_i(x)$, and $x = F_{calc}/F_{calcmax}$. $P_0 - P_{n-1} = 6.42\ -3.77\ 3.79$
$(\Delta/\sigma)_{max}$	<0.0001	<0.0001
$\Delta\rho_{max}$, $\Delta\rho_{min}$ (eÅ^{-3})	-0.12, -0.14	-0.19, -0.19
Extinction method	none	none

Table 2: Crystal, collection and refinement details for DMU form III and form IV

Chapter 5: GSK Compound A

GSK Compound A (form III)	
Crystal data	
Chemical formula	$C_{20}\ H_{22}\ C_{l1}\ N_7\ O_3$
Mr	443.89
Cell setting, space group	Monoclinic, $P2_1/n$
a, b, c (Å)	5.2361(17), 16.877(5), 24.218(7)
α, β, γ (°)	90, 94.432(6), 90
V(Å3)	2133.7(11)
Z	4
D_x(Mg m^{-3})	1.38
Radiation type	MoKα (0.71073 Å)
No. of reflections for cell parameters	425
θ range (°)	3.92-13.635
μ (mm-1)	0.217
Temperature (K)	298(2)
Pressure (GPa)	0.0
Crystal form, colour	Needles, colourless
Crystal size (mm)	0.10 x 0.10 x 0.5
Data Collection	
Diffractometer	Bruker *SMART*
Data collection method	φ and ω scans
Absorption correction	Empirical & multi-scan (SADABS)
T_{min}	0.6651
T_{max}	0.7449
No. of measured and independent reflections	6142, 3056
Criterion for observed reflections	$I > 2\sigma(I)$
R_{int}	0.0394
θ_{max} (°)	23.53
Range of h, k, l	-5 → h → 5 -15 → k → 18 -27 → l → 22
Refinement	
Refinement on	*F*

R-factor, *wR*-factor, S	0.0063, 0.025, 1.20
No. of reflection	805
No. of parameters	276
H-atom treatment	Riding
Weighting scheme	$w' \times [1 - (\Delta F_{obs} / 6 \times \Delta F_{est})^2]^2$ $w' = [P_0T_0'(x) + P_1T_1'(x) + ...P_{n-1}T_{n-1}'(x)]^{-1}$, where P_i are the coefficients of a Chebychev series in $t_i(x)$, and $x = F_{calc}/F_{calcmax}$. $P_0 - P_{n-1} = 2.73\ -2.91\ 1.97$
(Δ/σ)max	<0.0001
$\Delta\rho_{max}$, $\Delta\rho_{min}$ (eÅ^{-3})	0.29, -0.26
Extinction method	none

Table 3: Crystal, collection and refinement details for GSK compound A form III

	GSK Compound A form IV (298 K)	**GSK Compound A form IV (150 K)**
Crystal data		
Chemical formula	$C_{20}\ H_{22}\ Cl_1\ N_7\ O_3$	$C_{20}\ H_{22}\ Cl_1\ N_7\ O_3$
Mr	443.89	443.98
Cell setting, space group	Triclinic *P*-1	Triclinic *P*-1
a, b, c (Å)	8.9117(13), 10.2533(14), 13.3658(19)	8.6775(5), 10.2340(6), 13.2989(8)
α, β, γ (°)	108.744(7), 99.604(7), 108.028(7)	109.258(3), 98.285(3), 107.830(3)
V(Å^3)	1050.6(3)	1021.15(3)
Z	2	2
D_x(Mg m^{-3})	1.40	1.44
Radiation type	Mo*K*α	Mo*K*α
No. of reflections for cell parameters	1944	1944
θ range (°)	3-22	3-22
μ (mm^{-1})	0.220	0.226
Temperature (K)	298(2)	150(2)
Crystal form, colour	Block, colourless	Block, colourless
Crystal size (mm)	0.11 x 0.21 x 0.24	0.11 x 0.21 x 0.24
Data collection		
Diffractometer	Bruker SMART	Bruker SMART
Data collection method	φ and ω scans	ω scans
Absorption correction	Empirical & multi-scan (*SADABS*)	Empirical & multi-scan (*SADABS*)
T_{min}	0.6603	0.6379
T_{max}	0.7454	0.7454
No. of measured and independent reflections	13900, 4291	12433, 4155
Criterion for observed reflections	$I > 2\sigma(I)$	$I > 2\sigma(I)$
R_{int}	0.0400	0.0442
θ_{max} (°)	26.4889	26.3867
Range of *h, k, l*	$-11 \rightarrow h \rightarrow 11$ $-12 \rightarrow k \rightarrow 12$ $-15 \rightarrow l \rightarrow 16$	$-10 \rightarrow h \rightarrow 10$ $-12 \rightarrow k \rightarrow 12$ $-16 \rightarrow l \rightarrow 16$
Refinement		
Refinement on	*F*	F^2
R-factor, *wR*-factor, S	0.056, 0.167, 1.01	0.047, 0.127, 1.000

No. of reflection	4021	4155
No. of parameters	280	280
H-atom treatment	Riding	Riding
Weighting scheme	$w' \times [1 - (\Delta F_{obs} / 6 \times \Delta F_{est})^2]^2$ $w' = [P_0T_0'(x) + P_1T_1'(x) + ...P_{n-1}T_{n-1}'(x)]^{-1}$, where P_i are the coefficients of a Chebychev series in $t_i(x)$, and $x = F_{calc}/F_{calcmax}$. $P_0 - P_{n-1}$ = 0.280 0.294 0.963E-01	Calculated = $1/[\sigma^2(F_o^2) + (0.072P)^2 + 0.650P]$ where $P = (F_o^2 + F_c^2)/3$
$(\Delta/\sigma)_{max}$	<0.0001	<0.0001
$\Delta\rho_{max}$, $\Delta\rho_{min}$ (eÅ^{-3})	0.36, -0.27	-0.25, 0.51
Extinction method	none	none

Table 4: Crystal, collection and refinement details for GSK compound A form IV

Chapter 6: GSK compound B

	Form II	Form VI (high-pressure form)
Crystal data		
Chemical formula	$C_{22}H_{23}F_1N_4O_3$	$C_{22}H_{23}F_1N_4O_3$
Mr	410.45	410.45
Cell setting, space group	Triclinic, P-1	Monoclinic, $P2_1/n$
a, b, c (Å)	9.2992(2), 10.0625(3), 12.0600(3)	9.9904(13), 9.9041(6), 21.3712(19)
α, β, γ (°)	92.7920(10), 102.9880(10), 106.1160(10)	90, 102.987(8), 90
V(Å^3)	1048.94(5)	2060.5(4)
Z	2	4
D_x(Mg m^{-3})	1.30	1.32
Radiation type	Mo*K*α	Mo*K*α
No. of reflections for cell parameters	9176	1766
θ range (°)	5-61	3-20
μ (mm^{-1})	0.094	0.096
Temperature (K)	150(2)	298(2)
Pressure (GPa)	0.00	0.40(5)
Crystal form, colour	Block, colourless	Block, colourless
Crystal size (mm)	0.12 x 0.27 x 0.55	0.10 x 0.10 x 0.15
Data collection		
Diffractometer	Bruker SMART	Bruker SMART
Data collection method	ω scans	ω scans
Absorption correction	multi-scan (*SADABS*)	multi-scan (*SADABS*)
T_{min}	0.86	0.87
T_{max}	0.89	0.99
No. of measured, independent and observed reflection	16977, 5854	1357, 1294
Criterion for observed reflection	$I > 2\sigma(I)$	$I > 2\sigma(I)$
R_{int}	0.0298	0.0921

θ_{max} (°)	30.5242	26.487
Range of h, k, l	$-12 \rightarrow h \rightarrow 12$ $-14 \rightarrow k \rightarrow 13$ $-15 \rightarrow l \rightarrow 16$	$-5 \rightarrow h \rightarrow 5$ $-11 \rightarrow k \rightarrow 11$ $-25 \rightarrow l \rightarrow 25$
Refinement		
Refinement on	*F*	*F*
R-factor, *wR*-factor, S	0.0502, 0.0523, 1.10	0.0871, 0.0891, 0.98
No. of reflection	5040	686
No. of parameters	271	121
H-atom treatment	Riding	Riding
Weighting scheme	$w' \times [1 - (\Delta F_{obs} / 6 \times \Delta F_{est})^2]^2$ $w' = [P_0T_0'(x) + P_1T_1'(x) + ...P_{n-1}T_{n-1}'(x)]^{-1}$, where P_i are the coefficients of a Chebychev series in $t_i(x)$, and x = $F_{calc}/F_{calcmax}$. $P_0 - P_{n-1}$ = 0.870 0.640 0.534 3	$w' \times [1 - (\Delta F_{obs} / 6 \times \Delta F_{est})^2]^2$ $w' = [P_0T_0'(x) + P_1T_1'(x) + ...P_{n-1}T_{n-1}'(x)]^{-1}$, where P_i are the coefficients of a Chebychev series in $t_i(x)$, and x = $F_{calc}/F_{calcmax}$. $P_0 - P_{n-1}$ = 7.68 -3.21 3.92
$(\Delta/\sigma)_{max}$	0.0006	0.0001
$\Delta\rho_{max}$, $\Delta\rho_{min}$ (eÅ^{-3})	0.41, -0.26	0.24, -0.25
Extinction method	none	none

Table 5: Crystal, collection and refinement details for GSK compound B form II and form VI.

Appendix B:

Chapter 4: Polymorph Screening of N,N'-dimethylurea

No.	Solvent	Drug substance (mg)	Solvent (ml)
1	1, 4-Dioxane	100	0.75
2	1-Butnol	75	0.75
3	1-Propanalol	75	0.75
4	Acetic acid	100	0.75
5	AcOH:Water (50 %)	100	0.75
6	Acetone	100	0.75
7	Acetone:Water (1%)	75	0.75
8	Acetone:Water (50%)	100	0.75
9	Benzonitrile	75	0.75
10	Trichloromethane	75	0.75
11	Chlorobenzene	50	0.75
12	Cyclohexane	50	0.75
13	Cyclohexanone	75	0.75
14	Dichloromethane	100	0.75
15	DEGDME	50	0.75
16	Dimethycarbonate	50	0.75
17	Dioxane:Water (1%)	50	0.75
18	DMSO	175	0.75
19	Ethylacetate	75	0.75
20	Ethylacetate:Cyclohexane (1:2)	50	0.75
21	Ethylacetate:Toluene (1:2)	75	0.75
22	Heptane	35	0.75
23	Isopropylalcohol	50	0.75
24	Isopropylalcohol:iPrOAc (1:2)	75	0.75
25	Isopropylalcohol:Water (1%)	50	0.75
26	Isopropylether	50	0.75
27	Isopropyl acetate	75	0.75
28	Acetonitrile	50	0.75
29	Acetonitrile:Water (1%)	50	0.75
30	MEK	50	0.75
31	Methylacetate	75	0.75
32	Methanol	75	0.75
33	Methanol:Water (1%)	75	0.75
34	Methanol:Water (20%)	75	0.75
35	Methanol:Water (50%)	75	0.75
36	MIBK	50	0.75
37	Nitromethane	50	0.75
38	NMP	175	0.75
39	Polyethyleneglycol	100	0.75
40	TBME	50	0.75
41	Trifluoroethanol	100	0.75
42	Tetrahydrofuran	75	0.75
43	Tetrahydrofuran:Water (1%)	75	0.75
44	Toluene	75	0.75
45	Water	100	0.75
46	Ethanol	100	0.75
47	Methanol:Ethanol (4:1)	100	0.75
48	DMF	75	0.75

Table 6: Solvent used in automated polymorph screening of N,N'-dimethylurea.

Appendix C: Conferences and Lecture Courses Attended

Year 1

Poster presentations:

Nasir Abbas, Iain D. H. Oswald, Colin R. Pulham, Clare Anderton, Alistair Lennie, and Timothy J. Prior. **Exploring polymorphism and solvate formation of urea using high pressure.** British Crystallographic Association Spring Meeting. Canterbury, UK, April 2007.

Lecture courses:

11th BCA-CCG Intensive Course on X-ray Structural Analysis, Durham, UK, March 2007. Organised by the British Crystallographic Association.

Science Communication in Action and Presentations Skills. Organised by the University of Edinburgh.

Participated in Summer Science Exhibition 2007, **The Big Squeeze**. Organised by The Royal Society, UK.

Year 2

Oral presentations:

Nasir Abbas, Colin R. Pulham and Clare Anderton. **Exploring polymorphism in pharmaceuticals using high-pressure techniques.** GlaxoSmithKline, Stevenage UK, March 2008.

Poster presentations:

Nasir Abbas, Iain D. H. Oswald, Colin R. Pulham, Clare L. Anderton, Alistair Lennie, and John E Warren. **Exploring polymorphism and solvate formation in pharmaceuticals using high pressure techniques**. British Crystallographic Association Spring Meeting. York, UK, April 2008.

Nasir Abbas, Iain D. H. Oswald, Colin R. Pulham, Clare L. Anderton, Alistair Lennie, and John E Warren. **Exploring polymorphism and solvate Formation in pharmaceuticals using high pressure**. Erskine Williamson day. CSEC, Edinburgh, 2008.

Lecture courses:

Summer school on Application of Synchrotron techniques. Oxford, August 2008.

Academic Paper Writing. Organised by EastChem. St Andrews, UK, July 2007

Year 3

Oral presentations:

Nasir Abbas, Colin R. Pulham and Clare Anderton. **Exploring polymorphism in pharmaceuticals using high-pressure techniques.** GlaxoSmithKline, Stevenage, UK, October, 2009.

Nasir Abbas, Colin R. Pulham, Clare Anderton, Graeme Day, Alistair Lennie, Timothy J. Prior and Annette Kleppe. **Exploring polymorphism and solvate formation using high pressure**. Edinburgh University Postgraduate Meeting, Firbush, Scotland, March 2009.

Poster presentation:

Nasir Abbas, Iain D. H. Oswald, Graeme Day, Colin R. Pulham, Clare L. Anderton, Alistair Lennie, and John E Warren. **Exploring polymorphism of N,N'-dimethylurea using high pressure techniques.** CPOSS open day, University College London, UK, March 2009.

Nasir Abbas, Iain D. H. Oswald, Graeme Day, Colin R. Pulham, Clare L. Anderton, Alistair Lennie, and John E Warren. **Exploring polymorphism and solvate formation in N,N'-dimethylurea using high pressure techniques.** British Crystallographic Association Spring Meeting, Loughborough, UK, April 2009.

Nasir Abbas, Iain D. H. Oswald, Graeme Day, Colin R. Pulham, Clare L. Anderton, Alistair Lennie, and John E Warren. **Exploring Polymorphism using High Pressure (a case study of N,N'-dimethylurea).** Erice Summer School on High-pressure crystallography, Erice, Italy, June 2009.

Lecture course:

Erice Summer School on High-pressure crystallography, Erice, Italy, June 2009

Publications

D. M. S. Martins, C. K. Spanswick, D. S. Middlemiss, N. Abbas, C. R. Pulham and C. A. Morrison, *J. Phys. Chem. A*, 2009, **113**, 5998-6003.

N. Abbas, I. D. H. Oswald, M. G. Day, C. R. Pulham, C. Anderton, A. Lennie and A. Kleppe, *Manuscript in Preparation*. High-Pressure Studies of N,N,-dimethylurea.

Appendix D: Abbreviations

CSD	**Cambridge Structural Database**
CIF	**Crystallographic Information File**
DSC	**Differential Scanning Calorimetry**
DMU	**N,N'-dimethylurea**
D...A	**Hydrogen-bond Donor...Hydrogen-bond Acceptor**
FDA	**Food and Drug Administration**
IR	**Infrared**
MA	**Mefenamic acid**
NMR	**Nuclear Magnetic Resonance**
2-D	**Two-Dimensional**
3-D	**Three-Dimensional**